ANALYSIS OF NATURALLY OCCURRING RADIO SIGNALS RECEIVED DURING A SOLAR ECLIPSE AND A NEW MECHANISM FOR THE GENERATION OF WHISTLER PRECURSORS

by

C. D. REEVE, B.Sc.

A thesis submitted for the

degree of Doctor of Philosophy

Department of Physics
University of Southampton

September 1972

To Anne and Suzy.

ABSTRACT

FACULTY OF SCIENCE

PHYSICS

Doctor of Philosophy

ANALYSIS OF NATURALLY OCCURRING VLF RADIO SIGNALS RECEIVED DURING A SOLAR ECLIPSE AND A NEW MECHANISM FOR THE GENERATION OF WHISTLER PRECURSORS

by Christopher Deal Reeve

Naturally occurring VLF radio signals received during the solar eclipse of 7 March 1970 at St. John's, Newfoundland, Canada and Norwich, Vermont, U.S.A. have been analysed. A correlation between solar obscuration and the low frequency cutoff of tweeks, energy from lightning discharges, is found in the signals from St. John's from which it is calculated that the phase height of reflection of the ionospheric D-region increases by 7 ± 1 km at totality. An estimate of the position of the thunderstorm generating the tweeks is made from meteorological records. It is calculated that the maximum eclipse effect in the D-region occurs 4 ± 3 min after eclipse totality. The absence of a similar effect at Norwich is explained in terms of the differences in the propagation characteristics of the paths from the thunderstorm to the two receiving stations. The reception of discrete VLF emissions at both stations close to eclipse totality is attributed to the eclipse induced modification to the ionospheric electron density distribution, allowing the emissions to propagate to the ground whereas under normal daytime conditions they would have been absorbed in or reflected by the lower ionosphere.

Whistlers received at St. John's shortly after the eclipse are accompanied by precursors, rising frequency emissions which precede the whistler with which they are associated. Previous work on the

whistler-precursor is discussed. The triggering time and frequency of the precursors are found to be in reasonable agreement with the theory of Dowden (1972). Noting some apparent shortcomings of this theory alternative mechanisms for the generation of precursors are considered. A mechanism in which the precursor is triggered by two frequency components of the whistler having the same group delay interacting to give energy at the difference of their frequencies is found not to give agreement with the observed data.

The possibility of the precursor being triggered by unducted energy from the same source as the precursed whistler is investigated using a ray tracing computer program developed by Alexander (1971). It is found that an unducted path in which energy from the lightning discharge is first magnetospherically reflected and then refracted from the inner edge of the plasmapause allows the energy to arrive in the equatorial plane with the correct wave normal angle to be able to trigger an emission by transverse resonance with energetic electrons. It is shown that the locus of precursor trigger points, in the frequency-time plane, predicted by the unducted model is in reasonably good agreement with the observed data. A comparison is made between this mechanism and the theory of Dowden (1972).

Some implications of the unducted model are considered. It is shown that energy from lightning discharges at latitudes too low to generate whistlers may be directed preferentially to the equatorial plane at an L value just inside the plasmapause arriving with the correct wave normal angle to resonate with energetic electrons by transverse resonance. It is suggested that such a mechanism might be responsible for the appearance of apparently spontaneously generated VLF discrete emissions and should result in an enhanced precipitation of energetic electrons into the atmosphere at latitudes just inside the plasmapause.

ACKNOWLEDGEMENTS

I wish to thank my supervisor, Dr. M.J. Rycroft, for introducing me to this fascinating subject and for his guidance and advice throughout the course of my research. I am also very grateful to Dr. and Mrs. Rycroft for their kindness to my wife and me during the past three years.

I would like to thank the Professors of Physics, in particular Prof. G.W. Hutchinson for the use of the facilities of the department. I am very grateful to Dr. G.J. Daniell and Mr. F.M. Kenny for many useful discussions on the more mathematical aspects of VLF propagation.

I am very grateful to Prof. S.W. Breckon and members of the Physics Department, Memorial University of Newfoundland for their help during my stay in St. John's.

I wish to thank Prof. M.G. Morgan for supplying the VLF data from the station at Norwich, Vermont and Prof. T.R. Kaiser and Dr. K. Bullough for the data from Halley Bay. I am also indebted to Prof. T. Laaspere, Prof. R.L. Dowden and Dr. D.L. Carpenter for supplying extra data for my study of precursors.

I would also like to thank Messrs. Smith, Grey and Kirk, of the Meteorological Office, for their assistance and Miss J. Duncombe for computing the eclipse parameters for the two stations.

I wish to express my thanks to all the members of the radio physics group at Southampton University for helping to make my time with the group so enjoyable. In particular I must thank Mr. M. Jarvis for the precursor data from South Uist and for his help processing the photographs for this thesis.

I am glad to have this chance to thank my parents for all they have done for me during the past 24 years. I am also very grateful to my wife, Anne, for all her help and encouragement during

the course of my research and also for proof reading the script and preparing the diagrams. I must also thank my daughter, Suzy, for helping to keep me cheerful when things were going wrong.

Finally my thanks should also go to Mrs. S. Bayly for her careful preparation of the typescript.

CONTENTS

-oOo-

CHAPTER ONE

Introduction

This thesis is concerned with a study of naturally occurring radio signals in the very low frequency (VLF) 3 kHz - 30 kHz and extremely low frequency (ELF) 3 Hz - 3 kHz bands. Analysis of these signals yields much information about the regions, within 10 earth radii of the earth, through which the radiation has propagated. These regions fall under three main headings; the magnetosphere, the ionosphere and the earth-ionosphere cavity. By these means, using comparatively simple and relatively inexpensive apparatus a great deal may be learned of the earth's immediate environment, which would otherwise require complex instrumentation aboard highly expensive space vehicles.

In this chapter the subject is discussed in broad outline, defining the terms to be used in later chapters. More detailed reviews of the particularly relevant aspects are presented in chapters two, three and four.

1.1 History

Reports of what are now known to be naturally occurring radio signals date from as long ago as 1886 when British post office operators heard descending tones (whistlers) on a 22 km telephone line without amplification (Fuchs, 1938). During the following years there were several reports of similar phenomena (Preece, 1894; Barkhausen, 1919, 1930; Eckersley, 1925, 1928, 1929; Burton, 1930; Burton and Broadman, 1933a, b). Burton and Broadman (1933a) reported a positive correlation between the lower cut off frequency of musical atmospherics (tweeks) and solar obscuration during a solar eclipse. Eckersley (1935) showed that a sudden impulse would be dispersed such that its frequency f was proportional to the reciprocal of the square of its propagation time t

through an unpolarized medium such as the ionosphere, provided that the Lorentz polarization term was omitted. He demonstrated that his theoretical formulation was in good agreement with the observed characteristics of whistlers.

The most important step in the study of VLF phenomena was the application of the sound spectrograph to their analysis. This device produced a dynamic (frequency-time) spectrum of the VLF signal and for the first time enabled precise measurements to be made. Using such an analyzer Storey (1953) provided the basis for current VLF studies by proposing that whistlers were produced by energy from lightning discharges echoing back and forth along the lines of force of the earth's magnetic field. His theory required an unexpectedly high electron density in the outer ionosphere thus providing the first evidence for the existence of the magnetosphere. Storey (1957 a, b) confirmed Eckersley's dispersion law, showing that the dispersion D, defined to be $1/tf^{\frac{1}{2}}$, was proportional to the weighted electron density content of the tube of force along which the whistler had propagated.

Helliwell et al (1956) reported a new type of whistler, exhibiting both rising and falling frequency characteristics, which they called the nose whistler. This was explained by removing the restriction, imposed by Eckersley and Storey, that the wave frequency should be small compared with the electron gyro frequency. It has been shown that the frequency that suffers minimum delay (nose frequency, f_n) is characteristic of propagation along a particular field line and that the time delay of the nose frequency t_n gives a measure of the electron density in the equatorial plane in the region through which the whistler has propagated (Angerami, 1966).

In recent years many types of VLF signals have been reported. These include discrete VLF emissions, having either or both rising and

falling frequency characteristics and hiss appearing as band limited thermal noise. Of these some have been satisfactorily explained; the origins of others remain obscure. These VLF emissions are discussed in more detail in section 1.3.2.

1.2 The Ionosphere

At altitudes greater than about 70 km the earth's atmosphere is appreciably ionized by solar radiation giving rise to the region of plasma known as the ionosphere. Lyman α (ultra violet) radiation is the main ionizing agent at the lower altitudes around 80 km, while at greater heights around 300 km it is solar ~~X~~ UV radiation that is responsible for the ionization. The electron density in the daytime ionosphere varies from typically around $10^3 cm^{-3}$ at 70 km to about $10^6 cm^{-3}$ at 300 km. While the density of neutral particles is orders of magnitude greater than such values at all ionospheric heights the electron density is sufficient to affect the propagation of VLF radio waves to a large extent.

1.2.1 The earth-ionosphere cavity

The region between the earth's surface and the lower edge of the ionosphere is known as the earth-ionosphere cavity or earth-ionosphere waveguide. Both the surface of the earth and the sharp electron density gradient at the base of the ionosphere form sharply ~~b~~ou~~n~~ded good conductors so that to a first order approximation the cavity may be considered as a parallel plate waveguide with infinitely conducting walls. When the wavelength of the radiation is approximately equal to the circumference of the earth standing waves are set up in the cavity; these earth-ionosphere cavity resonances have been observed at the fundamental frequency around 8 Hz and also at harmonics around 14, 20 and 26 Hz (Schumann, 1952, Galejs, 1965, Rycroft, 1965).

1.2.2 Waveguide mode propagation

The mode of propagation whereby a wave is constrained to propagate within certain boundaries is termed waveguide mode propagation. Reducing the earth-ionosphere waveguide to its simplest approximation one can consider a set of Cartesian coordinates (x, y, z) with infinitely conducting, perfectly reflecting planes at z = 0 and z = a (Fig. 1.1). Radiation propagating within the waveguide may be considered as a sum of two plane waves, since waves initially propagating with their wave vectors (wave normals, $\underline{k}$) in the xz plane making an angle ϕ with the x axis will be reflected off the conducting plane at z = 0 as waves whose wave vectors make an angle ϕ with the minus x axis. After a second reflection from the plane z = a they again become waves of the first type. There are two possible polarizations for such waves; if E is parallel to the y axis they are known as transverse electric (TE) waves, whereas if H is parallel to the y axis they are called transverse magnetic waves (TM). Of these the TM modes are the more relevant to the study of natural radiation since the lightning discharge, which is the predominant source of energy, consists of a vertical current, which excites only the TM modes. Considering only TM modes the field components for the two plane waves described above are, omitting the time factor $\exp(i\omega t)$,

i) $$E_x = E_1 \sin\phi \exp\left[-ik(x\cos\phi - z\sin\phi)\right],$$
$$E_z = E_1 \cos\phi \exp\left[-ik(x\cos\phi - z\sin\phi)\right],$$
$$H_y = -E_1 \exp\left[-ik(x\cos\phi - z\sin\phi)\right].$$

ii) $$E_x = E_2 \sin\phi \exp\left[-ik(x\cos\phi + z\sin\phi)\right],$$
$$E_z = -E_2 \cos\phi \exp\left[-ik(x\cos\phi + z\sin\phi)\right],$$
$$H_y = E_2 \exp\left[-ik(x\cos\phi + z\sin\phi)\right].$$

The components of the resultant wave are obtained by summing the components of the constituents. By imposing the boundary condition that E_x

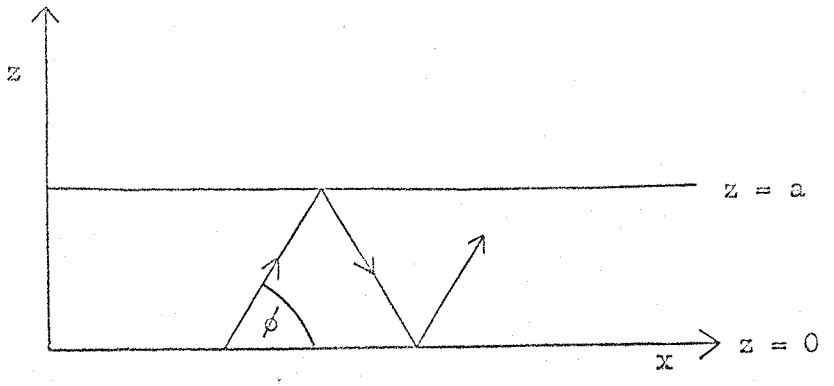

Fig. 1/1. Parallel sided waveguide.

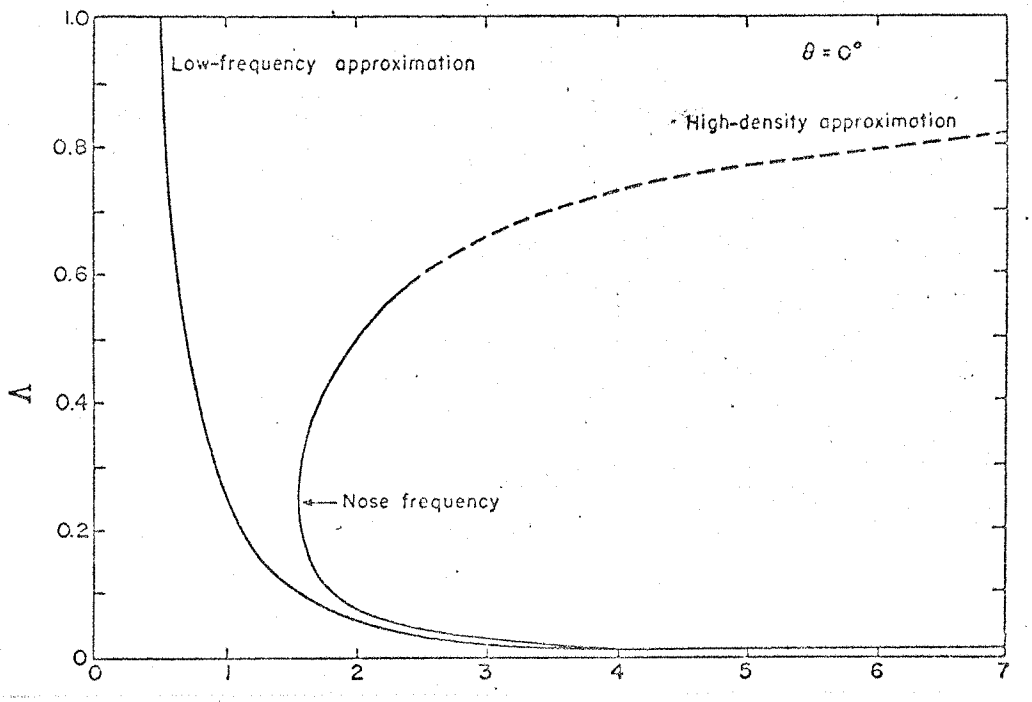

Normalized frequency versus group delay for longitudinal propagation

Fig. 1/2

vanishes at z = 0 it is found that $E_2 = -E_1 = E$ say. Hence the components of the resultant wave are

$$E_x = 2i\ E \sin\phi \sin(k\ z \sin\phi) \exp(-ikx \cos\phi),$$
$$E_z = 2\ E \cos\phi \cos(k\ z \sin\phi) \exp(-ikx \cos\phi), \quad (1.2/1)$$
$$H_y = -2E \cos(k\ z \sin\phi) \exp(-ikx \cos\phi).$$

Since H_y does not vanish at z = 0 and there can be no time varying H_y within the conductor it follows that a surface current must flow in the conductor parallel to the x axis. E_x must also vanish at z = a; hence, for any integer n, $k\ a \sin\phi = n\pi$ (1.2/2)

Since $k = \omega/c$ this equation fixes the angle ϕ for a given angular frequency ω and corresponds to constructive interference between the component plane waves.

The wavelength of the disturbance in the waveguide is

$$\lambda_g = \lambda/\cos\phi \quad (1.2/3)$$

where $\lambda = 2\pi/k$. Thus, combining equations 1.2/2 and 1.2/3,

$$1/\lambda_g^2 = 1/\lambda^2 - \left(\frac{n}{2a}\right)^2 \quad (1.2/4)$$

Hence if $n\lambda > 2a$ then λ_g is imaginary and the wave is evanescent. Therefore the frequency $f_c = n\ c/2a$ corresponds to a cut off frequency below which radiation will not propagate in the waveguide; n is termed the mode number. For the TM_1 mode, the cut off frequency will be

$$f_c = c/2a. \quad (1.2/5)$$

1.2.3 Atmospherics

Atmospherics, or sferics, are energy from lightning discharges which has propagated in the earth-ionosphere waveguide. They are identified aurally as clicks. At night when the base of the ionosphere is sharp and well defined at around 75 km the parallel plate waveguide approximation is moderately good and the sferics are observed to exhibit a cut off frequency at around 2 kHz in agreement with Eq. 1.2/5. They

are also slightly dispersed in the frequency time plane at frequencies just above the cut off frequency. This type of sferic is called onomatopaeically a tweek (Helliwell, 1965).

1.3 The Magnetosphere

Above the ionosphere there exists a region of plasma, whose motion is constrained by the earth's magnetic field; this region is known as the magnetosphere. The main constituents of the magnetospheric plasma are protons and electrons, unlike the ionosphere which contains a high percentage of heavy molecular and atomic ions (Oxygen and Nitric Oxide). On the daytime side of the earth the boundary of the magnetosphere is at about 10 R_E (1 R_E = one earth radius $\simeq$ 6370 km.) while on the nighttime side the magnetosphere extends to a much greater distance ($\sim$100 R_E). This asymmetry is caused by the solar wind, a flux of plasma emanating from the sun, which compresses the earth's magnetic field on the solar side, the day side. The magnetosphere acts as a barrier to the solar wind as the plasma flows around the magnetosphere the geomagnetic field lines are drawn out into a long geomagnetic tail on the nighttime side.

1.3.1 Whistler mode propagation

The whistler mode describes that mode of propagation wereby VLF radiation travels through the magnetosphere and is guided along the earth's geomagnetic field lines. Most of the known properties of the whistler mode can be explained with the aid of the magneto-ionic theory (Ratcliffe, 1959). In this theory the plasma, which is permeated by a static magnetic field, is assumed homogeneous, consisting of neutrals and equal numbers of electrons and positive ions. Because of their large mass relative to that of electrons, the effect of ions is usually negligible at whistler frequencies. It is also assumed that the angle

between the wave normal direction and the direction of the earth's magnetic field $\theta \simeq 0$; this is the quasi-longitudinal (QL) approximation (Ratcliffe, 1959). It may be shown (Helliwell, 1965) that at whistler frequencies the QL approximation is valid for values of θ up to 45^{o} or more. It is further assumed that collisions between electrons and neutrals may be neglected. This is a reasonable assumption since the most important dispersive effects take place in regions of very low collision frequency.

Having made these approximations the expression for the square of the refractive index becomes

$$\mu^2 = \frac{f_N^{\,2}}{f(f_{B_e}\cos\theta - f)} \qquad 1.3/1$$

where f_N is the plasma frequency,

f_{B_e} is the electron gyrofrequency, and

f is the wave frequency.

The dispersive characteristics of the whistler mode are found by evaluating the group velocity $v_g = c/\mu'$, where $\mu' = \frac{d}{df}(\mu f)$ is the group refractive index. Hence

$$v_g = 2c\,\frac{f^{\frac{1}{2}}(f_{B_e}\cos\theta - f)^{3/2}}{f_N f_{B_e}\cos\theta} \qquad 1.3/2$$

By imposing the condition that $f \ll f_{B_e}\cos\theta$, the Eckersley expression for the group velocity is obtained;

$$v_g = 2c\,\frac{\sqrt{f\, f_{B_e}\cos\theta}}{f_N} \qquad 1.3/3$$

The group delay for longitudinal propagation ($\theta = 0$) is found by evaluating the integral

$$t = \int_{path} \frac{ds}{v_g} \qquad 1.3/4$$

Using 1.3/2 this reduces to

$$t = \frac{1}{2^{\frac{1}{2}} (1 - \Lambda)^{3/2}} \quad \text{sec,} \qquad 1.3/5$$

or using 1.3/3

$$t = \frac{1}{2\Lambda^{\frac{1}{2}}} \text{ sec,} \qquad 1.3/6$$

where $\Lambda = \frac{f}{f_{B_e}}$.

Equation 1.3/6 is similar to the expression derived by Eckersley (1935) and is only valid in the low frequency limit. The expression 1.3/5 has a minimum value at $\Lambda = 0.25$. This corresponds to the nose frequency as observed by Helliwell et al (1956). The two expressions for group delay are plotted in Fig. 1/2.

1.3.2 Whistlers and VLF emissions

At mid latitudes (between 30° and 50° magnetic latitude), the most common naturally occurring VLF signal propagating through the magnetosphere is the whistler. Energy from a lightning flash penetrates the ionosphere and propagates in the whistler mode, being dispersed as described in the preceding section. Under certain circumstances the whistler may propagate through the ionosphere at the other end of the field line and be received at a ground station. (The two ends of a geomagnetic field line are known as conjugate points.) This type of whistler is known as a one hop whistler. Part of the whistler energy may be reflected from the ionosphere and propagate back along the field line to be received as a two hop whistler in the initial hemisphere, exhibiting twice the dispersion of the one hop whistler. Similarly 3, 4, 5 etc. hop whistlers may be produced (Fig. 1/3). Electron density values for the path of propagation may be deduced from whistler data because of the dependence of the refractive index upon the plasma frequency, f_o, which is proportional to the square root of the electron density. This topic will be discussed in greater detail in Chapter ~~Three~~ Four.

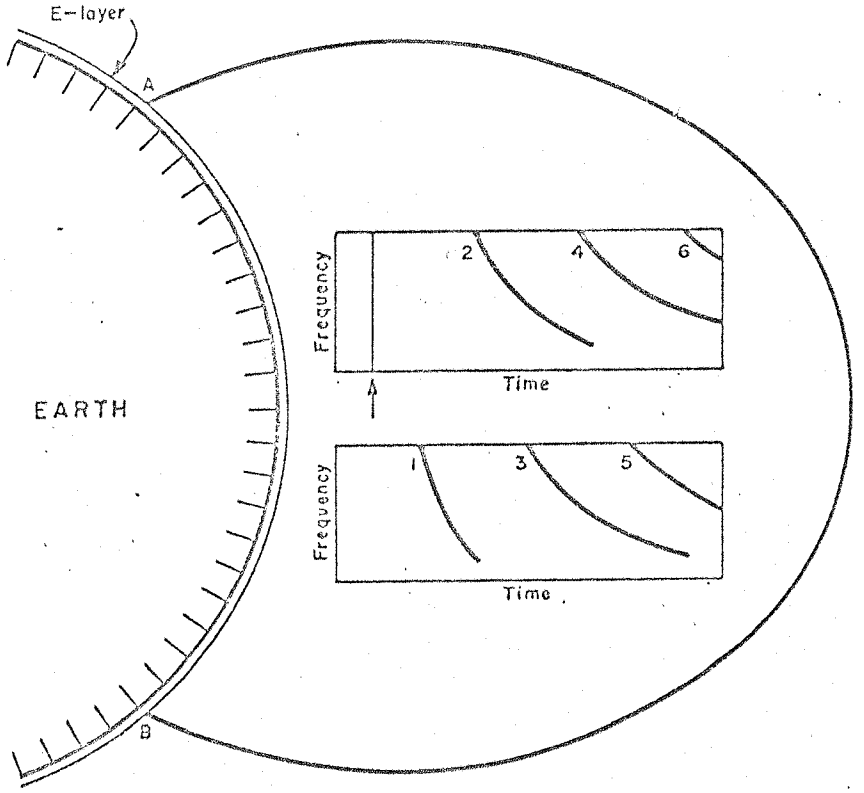

Field-line path followed by a ducted whistler. Inset diagrams show idealized spectra of whistler echo trains at conjugate points A and B.

Fig. 1/3

The term VLF emission covers any naturally occurring VLF signal of magnetospheric origin. There are many types of emission, but broadly speaking they fall into two main categories. Firstly, there are those signals that are apparently spontaneously generated, which include

(i) Hiss: a broad band emission, appearing as band limited thermal noise. It can appear anywhere in a wide range of frequencies from 500 Hz to frequencies higher than the upper limit of the VLF band.

(ii) Discrete emissions: transient signals with a duration of up to a few seconds. They can be rising tones (risers), falling tones or any combination of the two. A falling tone followed by a rising tone is called a hook; a rising tone followed by a falling tone is known as an inverted hook. More complicated combinations have also been observed as well as quasi-sinusoidal tones, which can last for many seconds.

(iii) Chorus: a series of overlapping rising tones, often accompanied by or superimposed on a band of hiss. At geomagnetic latitudes between around 50° and 60°, it is generally confined to the frequency range 2 - 4 kHz and is known as dawn chorus. At higher latitudes the range 0.5 - 2 kHz is more typical; here it is known as polar chorus.

(iv) Periodic Emissions: a sequence of discrete emissions which repeats at regular intervals. This interval is usually the two hop whistler delay but the emissions do not always exhibit the corresponding two hop whistler dispersion.

The second category includes the so-called triggered emissions, which appear, in the frequency-time domain, to branch out from other events and can thus be said to have been triggered by them. Whistlers, discrete emissions and signals from VLF transmitters have been observed to trigger emissions. One particularly interesting emission which could be a triggered emission is the precursor, which appears before the whistler with which it is associated.

VLF emissions are thought to be generated close to the equatorial plane by an interaction between VLF radiation and streams of energetic electrons in which energy is transferred from the electron beam to the VLF waves. This mechanism will be discussed in detail in Chapter ~~Three~~ Four.

Fig. 1/4 shows examples of a number of whistlers and VLF emissions.

1.4 Outline of Research

The analysis of VLF signals can produce much information about the ionosphere and magnetosphere. However, by their very nature, experiments on naturally occurring VLF signals are completely uncontrolled. This fact has important consequences, especially for short term projects; being subject to the vagaries of Nature these do not always follow their planned course. This tendency has been amply demonstrated during the course of this research.

It was first planned to study VLF signals recorded simultaneously at three stations spaced in latitude but on the same line of geomagnetic longitude. To this end, VLF receivers were set up in Central Iceland, on South Uist in the Outer Hebrides, and in Southern England, at Chilbolton near Winchester. The time was chosen carefully, 1969 being a year of maximum solar activity and thus geomagnetic activity, but although many interesting phenomena were recorded in Iceland there was nothing corresponding to them at the other stations (Case et al, 1970).

A solar eclipse presents a unique opportunity to study the structure of the daytime ionosphere and magnetosphere under known conditions. A decrease in electron density in the lower ionosphere is expected during the eclipse (Bowhill, 1970). From consideration of the diffusive equilibrium model of the magnetosphere (Angerami and Thomas, 1964), it has been proposed that this decrease might be reflected in the electron content of the magnetospheric tube of force whose foot existed in the eclipsed ionosphere (Rycroft and Reeve, 1970). A study of whistler dis-

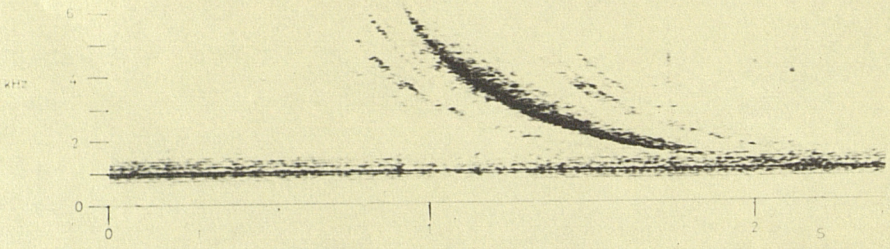

Whistler: Chilbolton, England 1702 U.T. 8 March 1970

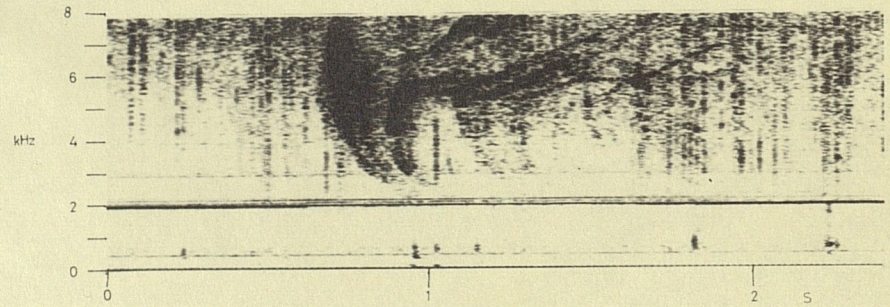

Triggered Emissions: South Uist, Outer Hebrides 2012 U.T. 1 July 1971

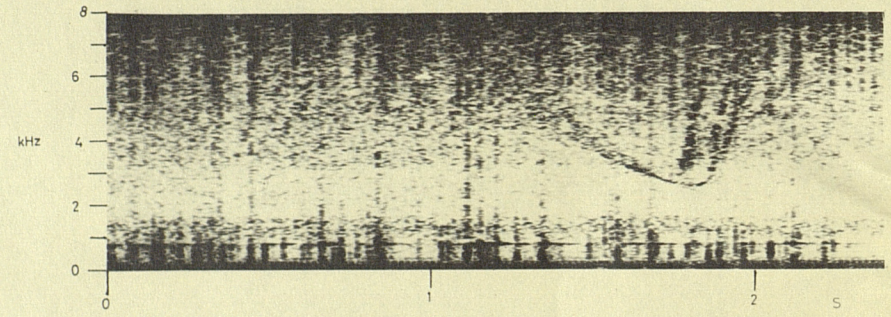

Spontaneous Emission (Hook): South Uist, Outer Hebrides
1912 U.T. 9 July 1970

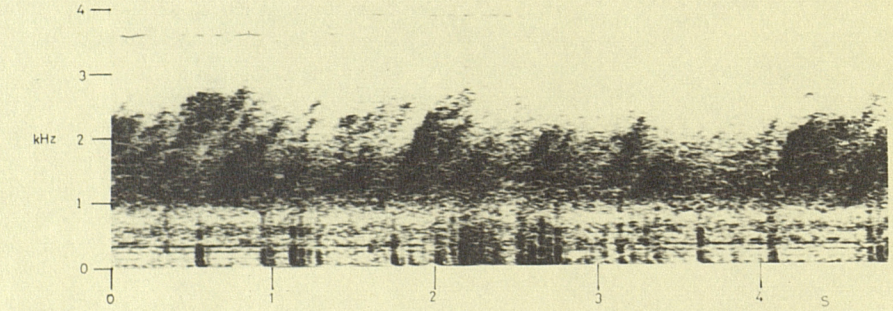

Chorus: South Uist, Outer Hebrides 0650 U.T. 10 October 1969

Fig. 1/4 VLF Emissions

persion during an eclipse should confirm this. During the solar eclipse of March 7, 1970, VLF observations were made at St. John's, Newfoundland, close to the path of totality; at Norwich, Vermont, U.S.A. in the partially eclipsed region and at Halley Bay, Antarctica, which is close to the magnetic conjugate of St. John's. Again Nature did not cooperate to the extent of providing whistlers at the correct time; however the period March 6 - 10, 1970, was one of exceptional magnetic activity and many interesting VLF emissions were recorded. These included a series of risers lasting about three minutes very close to the time of totality at St. John's, and a series of whistler precursors soon after the eclipse had ended. Also a study of the data showed that the eclipse had had a very marked effect on some of the atmospherics received at St. John's.

The first part of this research has been concerned with the analysis of the risers and sferics recorded in Newfoundland, and associated data from Norwich, and their interpretation in terms of the effect of the eclipse upon the ionosphere. The latter part of this research has been concerned with the whistler precursor. An attempt is made to explain this phenomenon in terms of the accepted properties of the magnetospheric plasma using ray tracing techniques. A comparison is made between the observed properties of the precursor and the predictions of the theory.

CHAPTER TWO

The Lower Ionosphere: Review

The first part of the research described in this thesis is concerned with the deduction of ionospheric parameters from observations of natural VLF signals made during a total solar eclipse. Because of its importance in the field of worldwide communications the ionosphere has been the subject of much research in recent years. In this chapter previous work on the ionosphere is reviewed, discussing the more important techniques employed and the results obtained.

The natural VLF signals in question have propagated in the earth-ionosphere waveguide; therefore it is the lower regions of the ionosphere that have the predominant effect upon them and hence the information obtained is mainly concerned with these lower regions.

2.1 The structure of the ionosphere as a whole

The ionisation of the earth's atmosphere which produces the ionosphere is caused by a variety of sources. Of these the most important is the sun, solar X rays and ultra violet radiation being responsible for a large proportion of the ionisation processes in the ionosphere. Other sources include cosmic rays, and energetic protons and electrons.

The rate of ionisation at any altitude depends upon the composition of the atmosphere at that height as well as the characteristics of the incident radiation. As the solar radiation propagates down through the neutral atmosphere at ionospheric heights the various components are attenuated by different amounts. At the same time the composition of the atmosphere alters with altitude. Consequently different ionisation processes become predominant at the different heights. Thus the ionosphere

is divided into four main layers which are designated the D, E, F1 and F2 layers, each layer being characteristic of a different set of ionisation processes. An electron density profile of the ionosphere representative of daytime conditions is shown in fig. 2/1.

2.2 The D region

The D region is the lowest layer in the ionosphere, extending from about 50 km to 90 km. Sometimes the term C layer is used to describe the region between 50 km and 70 km where cosmic rays are the main ionising agents (Rishbeth and Garriott, 1969). It is probably the most complex and least understood region of the ionosphere. Being the lowest lying region it is produced by the most penetrating of the ionising radiations incident on the earth. It is characteristically a region of very weakly ionised plasma, the neutral density exceeding the electron and ion density by several orders of magnitude (Whitten and Popoff, 1971).

2.2.1 The chemistry of the D region; production and loss mechanisms

The detailed chemistry of the D region is lengthy and complex. It has been described by Keneshea (1968) in terms of 87 photochemical reactions. These reactions fall under the following headings:

(i) Photoionisation: $X + h\nu \rightarrow X^+ + e$

(ii) Ion-ion recombination: $X^+ + Y^- \rightarrow X + Y$

(iii) Electron-ion recombination:

$X^+ + e + M \rightarrow X + M$ (three body)

$X^+ + e \rightarrow X^* \rightarrow X + h\nu$ (radiative)

$XY^+ + e \rightarrow X^* + Y^*$ (dissociative)

(iv) Ion-atom interchange: $X^+ + YZ \rightarrow XY^+ + Z$

(v) Collisional detachment: $X^- + M \rightarrow X + e + M$

(Three body attachment in reverse direction)

(vi) Associative detachment: $X^- + Y \rightleftharpoons XY + e$

(Dissociative attachment in reverse)

(vii) Photodetachment: $X^- + h\nu \rightleftharpoons X + e$

(Radiative attachment in reverse)

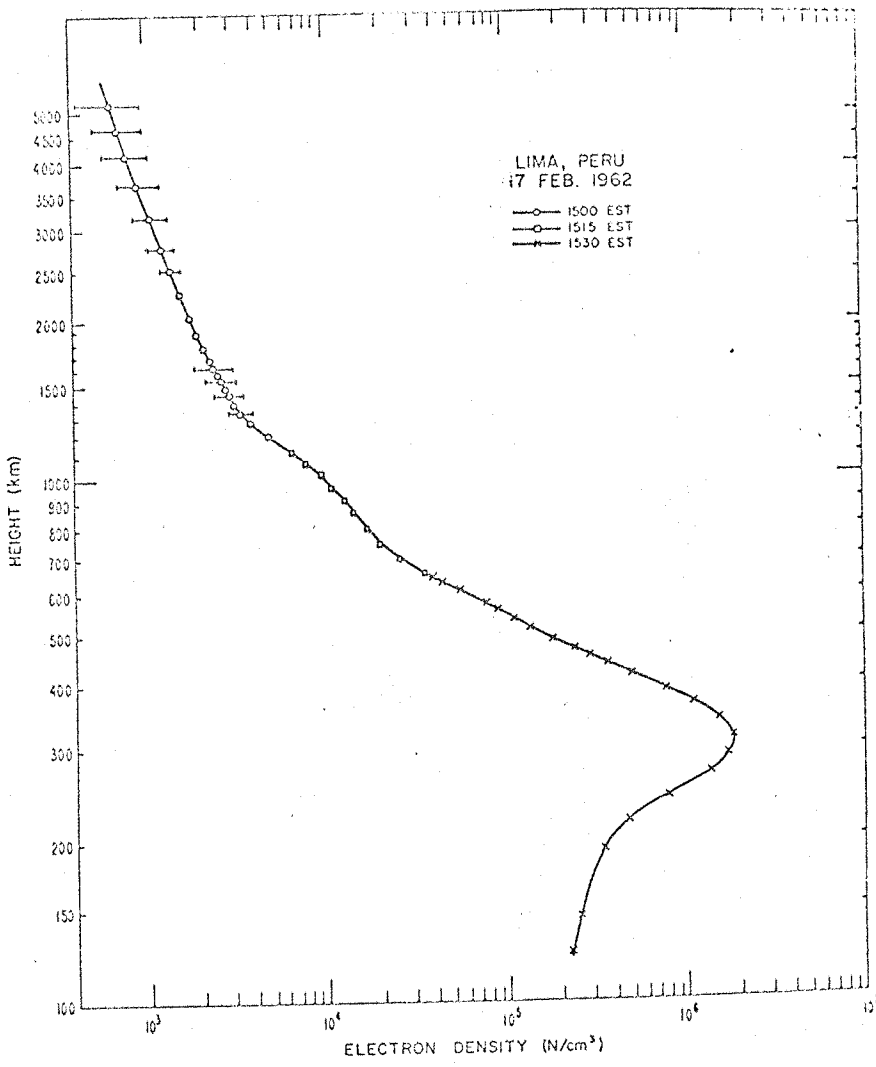

Electron-density profile obtained from incoherent scatter measurements.

(After K. L. Bowles, Mar. 1963, NBS Tech. Note 169.)

Fig. 2/1. Electron density profile typical of daytime conditions.

Four main production sources may be considered for the ionosphere between 60 km and 100 km;

the ultraviolet component is important above 95 km, X rays between 85 and 95 km, Lyman α between 75 and 85 km and cosmic rays below 70 km (Sales, 1967). The importance of Lyman α (1216 Å) as an ionising agent in the D region is due to the fact that an atmospheric (molecular oxygen) window exists near 1216 Å, allowing this radiation to penetrate more deeply into the atmosphere than neighbouring wavelengths. However the energy of a Lyman α photon is only 10.14 eV, which is less than the ionisation potentials of all the major atmospheric constituents. Of the minor atmospheric species several are subject to ionisation by Lyman α, including nitric oxide (NO), the methyl radical (CH_3) and various metallic meteor atoms (Swider, 1967). Nitric oxide is probably produced in the D region as follows: (Nicolet, 1965)

$$\left.\begin{array}{l} N + O + M \rightarrow NO + M \\ N + O_2 \rightarrow NO + O \end{array}\right\} \quad NO + N \rightarrow N_2 + O$$

(M is a neutral particle)

The rates of both production and loss of NO are thus proportional to the concentration of atomic nitrogen; consequently the equilibrium concentration of NO is independent of the concentration of N. It is, however, dependent on temperature because the rates of the two reactions are temperature dependent, especially the latter (Rishbeth and Garriott, 1969). Results from a rocket-borne spectrometer experiment (Barth, 1966) show that the NO concentration at 70 km is around 10^3 greater than that calculated from this model Sechrist (1967) suggests that this discrepancy may be explained by the temperature dependence of the NO concentration.

All the atmospheric constituents may be ionised by cosmic radia-

tion and X rays; one would thus expect primarily NO^+, O_2^+ and N_2^+ ions as the positive ions constituents of the D region. However reactions such as:

$$N_2^+ + O_2 \rightarrow NO^+ + NO$$

and

$$O_2^+ + N_2 \rightarrow NO^+ + NO$$

should lead to NO^+ as the predominant positive ion (Aitkin, 1967). Narcisi and Bailey (1965) have shown using a rocket-borne mass spectrometer experiment that NO^+ comprises only 10% of the total ions, and that the major positive ions have masses of 19 and 37 AMU and higher. They attribute these ions to reactions involving water vapour, which lead to the production of H_3O^+ (mass 19) and $H_5O_2^+$ (mass 37). Swider (1967) has suggested that the presence of these ions might be related to the ionisation of CH_3 by Lyman α.

The negative ion composition of the D region is not well understood. Nitrogen does not form stable negative ions and the O^- and O_2^- ions can be destroyed by visible light; Reid (1961, 1964) has suggested that the O_3^- and NO_2^- ions may be dominant since they require ultraviolet light for electron detachment, most of which is absorbed in the E region.

Production and loss processes for the whole ionosphere have been summarised by Rishbeth and Garriott (1969). In the D region the most important loss processes are: ion-ion recombination, three body and dissociative electron-ion recombination, three body attachment, collisional detachment and photodetachment. For each reaction in the D region there is a reaction rate, which can differ by up to 35 orders of magnitude from one reaction to another (Keneshea, 1968). Crain (1967) discusses a "lumped parameter" approach in which individual reactions are not considered explicitly but rates are attributed to each type of reaction. Thus the following equations are obtained:

$$\frac{dN}{dt} = P - AN - BNN^{+} + C(N^{+} - N^{-})$$

$$\frac{dN^{+}}{dt} = P - BNN^{+} - EN^{+}(N^{+} - N^{-})$$

where P is the electron production rate

N is the electron density

N^{+} is the positive ion density

N^{-} is the negative ion density

A is the electron attachment coefficient

B is the electron-ion recombination coefficient

C is the electron detachment coefficient

E is the ion-ion recombination coefficient.

By using realistic values for the coefficients, derived from consideration of the reactions which are believed to be most important, simple models may be evolved which give good agreement with observations. Each of the parameters must be altitude dependent and so these models contain a large number of unknown and adjustable parameters. It is therefore possible for different combinations of coefficients to give similar results for a given situation. It is necessary to form models that give good agreement with a wide range of situations. Crain (1967) gives the following values for the lumped parameters:

$A = 10^{8}Z^{2} + 10^{2}Z \text{ sec}^{-1}$ Z is the density in atmospheres.

$B = 10^{-7} \text{cm}^{3} \text{ sec}^{-1}$

$C = 0.4 \text{ sec}^{-1}$

$E = 10^{-7} \text{cm}^{3} \text{ sec}^{-1}$.

The other approach requires consideration of each individual reaction. Because of the large number of reactions thought to be involved such analysis is difficult.

2.2.2 Diurnal variations in the D region

Since the sun is the major source of ionising radiation it is reasonable to expect the electron density in the D region to change gradually with solar zenith angle during the day and to show a sharp change over the sunrise and sunset periods. At night the major source of ionisation is cosmic rays. There is a small flux of scattered Lyman α, around 10^{-2} erg $cm^{-2}sec^{-1}$ compared with around 4 erg $cm^{2}sec^{-1}$ during the day (Aikin, 1967). By observing the changes in the D region over the sunrise and sunset periods information may be obtained about the processes which take place and their reaction rates. Aikin (1967) has calculated theoretical values for the diurnal variation in electron density at various heights (Fig. 2/2). These calculations assume NO^{+} as the major positive ion and the dissociative recombination of NO^{+} as the major loss process. At 80 km the maximum ionisation occurs 45 min after local noon in agreement with the observations of Rao et al. (1962).

Several authors have discussed the changes in electron density over the sunrise or sunset period (Deeks, 1966; Smith et al., 1966; Mechtly and Smith, 1968). Fig. 2/3 shows the profiles derived by Deeks (1966). Other observations confirm these profiles, the major feature being that over the sunrise period a small peak in electron density appears at around 65 km, with a minimum at around 70 km and a sharp gradient between 70 and 75 km. The nighttime profiles show a sharp gradient between 80 and 90 km. Fig. 2/4 (Bowhill et al., 1966) shows in detail how the change takes place over the sunrise period.

2.2.3 Solar eclipse effects on the D region

The value of observations of electron densities over sunrise and sunset periods is somewhat limited because the change is, by its nature, gradual. The flux of solar radiation, and hence the ionisation rate, decreases smoothly between local noon and sunset. However, a

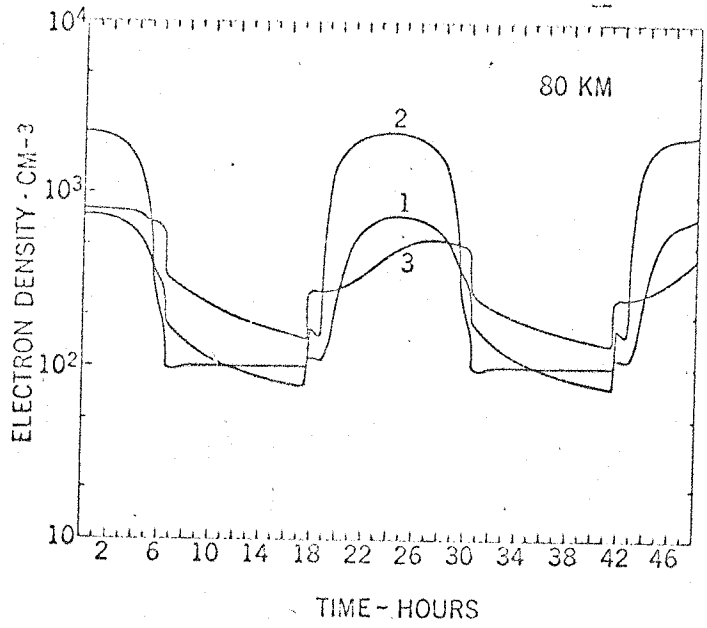

Diurnal variation of electron density at 80 km. for:

(1) $a_{DNO} = 3 \times 10^{-7}$ *c.c./sec.*

(2) $a_{DNO} = 1.6 \times 10^{-6}$ *c.c./sec.*

(3) $a_{DNO} = 3 \times 10^{-8}$ *c.c./sec.*

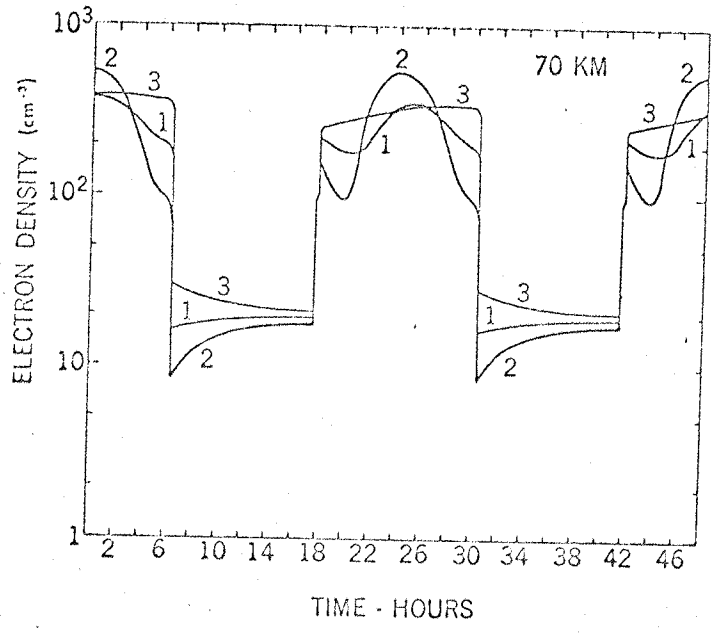

Diurnal variation of electron density at 70 km. for:

(1) $a_{DNO} = 3 \times 10^{-7}$ *c.c./sec.*

(2) $a_{DNO} = 1.6 \times 10^{-6}$ *c.c./sec.*

(3) $a_{DNO} = 3 \times 10^{-8}$ *c.c./sec.*

A daytime atomic oxygen profile is employed.

Fig. 2/2

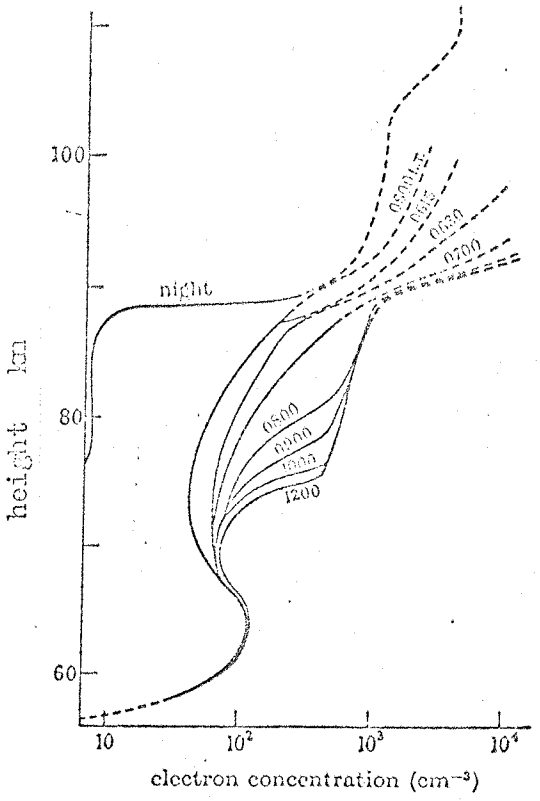

. The local-time variation of electron concentration at March equinox, sunspot minimum, at middle latitudes. The dashed parts of the curve are inserted to complete the calculations, but their precise form is not well determined.

Fig. 2/3

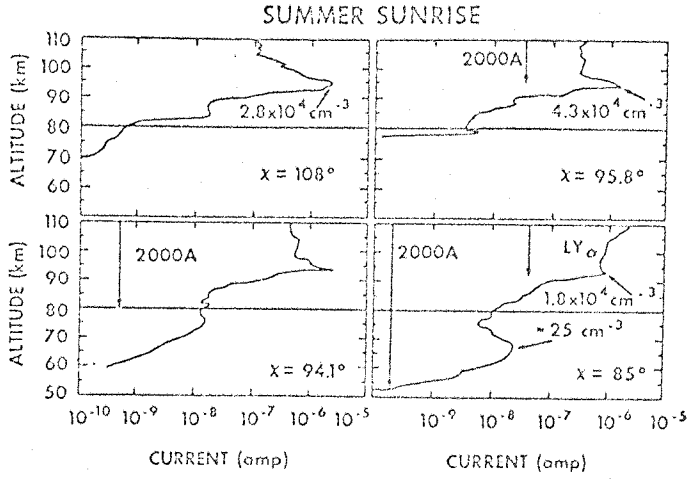

Rocket measurements of the lower ionosphere during sunrise.

Fig. 2/4

solar eclipse, especially a total eclipse occurring close to local noon, presents the opportunity to observe the D region while the ionising flux of radiation changes from a maximum to a nighttime value and back to a maximum in a period of around two hours. On the other hand eclipses are very rare compared to sunsets and they do not always occur at convenient times or places. In recent years a number of experiments have been carried out during solar eclipses, in particular during the February 15th 1961 eclipse over Europe, the May 20th 1966 eclipse over N. Africa and S. Europe, the November 12th 1966 eclipse over S. America and the March 7th 1970 eclipse over Mexico and N. America.

Fig. 2/5 shows how electron density in the D region varies with solar obscuration, as calculated by Deeks (1966), and Fig. 2/6 shows measurements of D region electron density made using four rockets during the 1966 eclipse by Mechtly et al. (1969). These results are in generally good agreement with those made by other observers (Smith et al., 1965; Mechtly et al., 1972; Kane, 1969) and obtained theoretically by Sales (1967). The important features are the complete decay of the lower D region and the smaller loss around 80 km. It may be possible to calculate the recombination coefficient B from the observed time lag between maximum obscuration and minimum electron density. For example Smith et al. (1965) deduce a recombination coefficient of around $2 \times 10^{-6} cm^3 sec^{-1}$ from an observed time lag of 5 minutes at 90 km. Further discussion of eclipse results will be presented in Chapters 6 and 7 with special reference to the March 7th 1970 eclipse.

2.2.4 Experimental techniques for D region studies

There are a number of techniques employed to study the D region. A brief description of each is presented, as is a comparison between the results obtained from them.

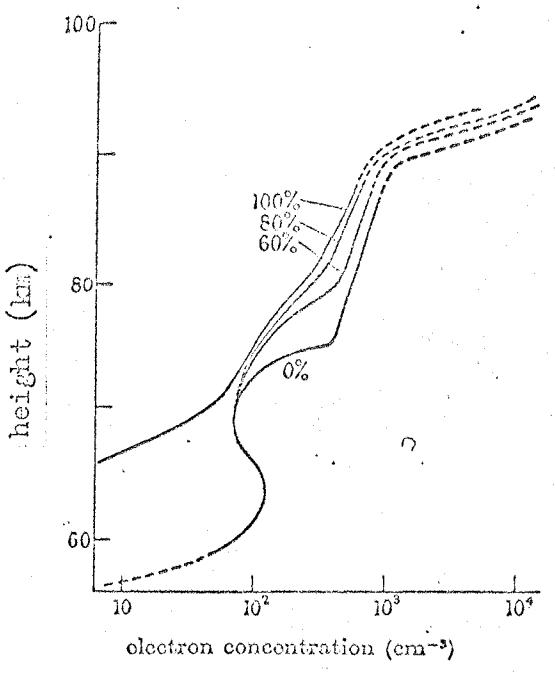

. The height distribution of electrons at different stages of a solar eclipse during mid-day, March equinox, sunspot minimum at middle latitudes. The figures on the curves represent the percentage obscuration of the solar disk. The dashed parts of the curve are inserted to complete the calculations, but their precise form is not well determined.

Fig. 2/5

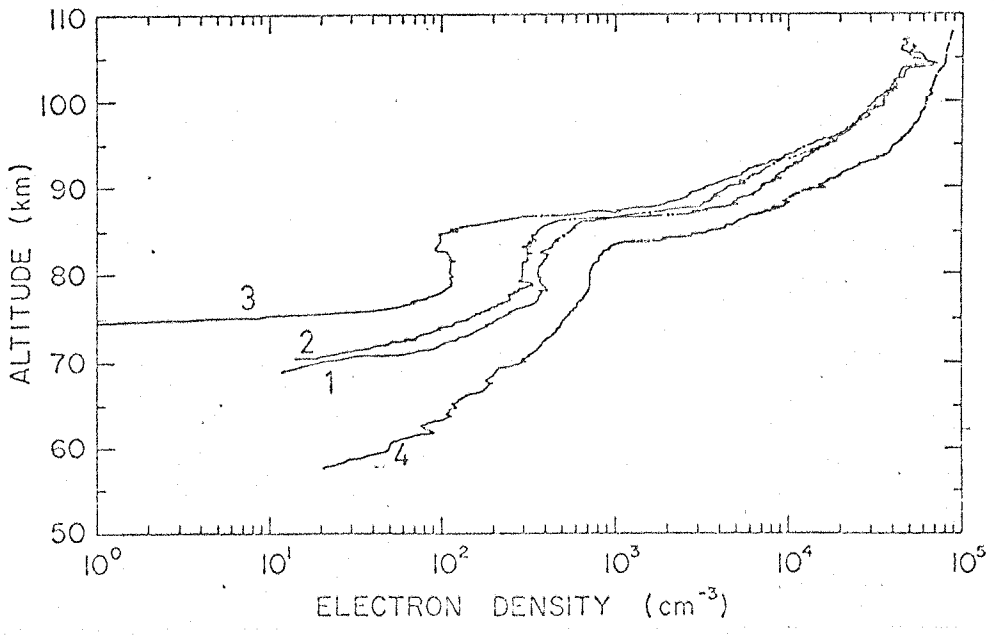

Rocket-borne measurements of electron density during a solar eclipse. 1 and 2, partial eclipse; 3, total eclipse; 4, full sun.(Mechtly et al, 1969)

Fig. 2/6

(i) The Ionosonde

A radio wave of frequency f transmitted vertically into the ionosphere is reflected when:

$$\frac{f_o^2}{f^2} = 1 \pm \frac{f_{B_e}}{f}$$

f_o is plasma frequency $= \sqrt{\frac{Ne^2}{4\pi^2 \varepsilon_o m}}$

f_{B_e} is gyro frequency $= \frac{eB}{2\pi m}$

provided that $f_o \gg f$. Therefore the height of reflection, and hence the delay time between transmitted and received signal, depends on the electron density. The ionosonde consists of a transmitter which sweeps in frequency between 1 and 25 MHz, a receiver which measures the time delay between transmission and echo reception and a means of displaying delay time against frequency. Because of the small electron density the ionosonde is of limited value in D region studies.

(ii) The Riometer

The riometer (Relative Ionospheric Opacity meter) (Little and Leinbach, 1959) is an instrument which records changes in the intensity of cosmic noise, most of which are due to absorption in the D and F_2 regions. From these records it is possible to deduce information about the regions where the absorption takes place.

(iii) Cross Modulation

This technique, originated by Fejer (1955), consists of transmitting 'wanted' and 'disturbing' pulses and observing the interaction between them by means of a suitable receiver. Both signals are pulsed, the repetition rate of the disturbing pulses being half that of the wanted pulses. Alternate wanted pulses encounter a disturbing pulse in the D region at a known height that can be varied; by comparing the amplitudes of the disturbed and undisturbed pulses the electron density, collision frequency and energy transfer coefficient of the D region may be deduced.

(iv) Partial Reflection

The partial reflection method (Gardner and Pawsey, 1953) relies on weak reflections from discontinuities of refractive index in the D region. Short pulses at a wave frequency of around 3 MHz are transmitted vertically and the amplitude of the echoes of the extraordinary and ordinary waves measured as a function of delay time. The electron density may be deduced from the differential absorption of the two modes. The method is strongly dependent on the collision frequency profile, which must be assumed in order to deduce electron densities. By measuring the differential phase of the partial reflections of the two components the collision frequency in the lower D region may be deduced. Simultaneous measurements of differential amplitude and phase provide a means of investigating the nature of the irregularities causing the partial reflections (Belrose et al., 1972).

(v) Faraday Rotation

A wave propagating through the ionosphere may be considered as a superposition of two circularly polarised components, one clockwise the other anticlockwise. Because the two components have different phase velocities, the plane of polarisation of the resultant appears to rotate. By measuring the rate of rotation information may be obtained about the electron content, weighted by the earth's magnetic field, integrated along the path of propagation. This experiment is used extensively aboard ionospheric sounding rockets (e.g. Bauer and Jackson, 1962).

(vi) Differential Doppler Shift

In this method two harmonically related frequencies are transmitted from a rocket travelling nearly vertically. Seddon (1953) used 4.3 MHz and its sixth harmonic. In free space the phase path lengths of the two frequencies would be in the harmonic ratio but the ionosphere lowers the phase path length of the lower frequency. The two

frequencies are received at the ground and the lower is multiplied by the harmonic ratio. From the difference in the path lengths the electron density profile may be obtained.

(vii) Differential Absorption

Because of the high density of neutral particles in the D region the collisions between electrons and neutrals may not be neglected in the treatment of wave propagating in the D region. Their effect is to make the D region an absorbing medium, the absorption being a frequency dependent quantity. By measuring the differential absorption of a pair of radio waves of different frequency the electron density or collision frequency in the D region may be deduced (Sen and Wyller, 1960). A variation of this method measures the differential absorption of the ordinary and extraordinary components of a single frequency close to the gyro frequency.

(viii) The Full Wave Approach

In this method D region parameters are deduced from observations of reflections of VLF waves from the lower ionosphere. The solutions of the complete wave equations are employed (Gibbons and Nertney, 1952). The full wave approach has been developed for computer use by Barron and Budden (1960) and Pitteway (1965). An iterative method is used; model distributions are postulated, their reflecting properties are computed and compared with the observed data. By adjusting the models a best fit solution may be obtained. This method has been used extensively to compute D region electron density distributions (e.g. Deeks, 1966).

(ix) The Langmuir Probe

The Langmuir Probe (Langmuir and Mott-Smith, 1924) consists of a small metal electrode which is inserted into the ionospheric plasma. If the probe is operated at a few volts negative it repels all electrons and attracts ions; the probe current then gives a measure of the ion

number density By making the probe potential a few volts positive the electron number density may be determined.

(x) Thomson Scatter Radar

The Thomson Scatter Radar Techniques utilizes the classical Thomson scattering of high power radio waves by individual ionospheric electrons (Gordon, 1958). The power returned is directly proportional to the electron concentration. This method may also be used to determine electron and ion temperatures although the results obtained do not agree with measurements made using rocket and satellite probes under similar conditions (Whitten and Poppoff, 1971).

CHAPTER THREE

Waveguide mode propagation in a realistic model of the earth-ionosphere cavity

The simple theory presented in 1.2.2 considered the earth-ionosphere cavity as being bounded by a pair of flat, perfectly reflecting parallel planes. To obtain a more realistic model the following amendments must be made:

(i) The ionosphere must be considered as an imperfect reflector;

(ii) The curvature of the earth must be considered;

(iii) The effect of the earth's magnetic field must be included.

The mode theory of the earth-ionosphere waveguide has been described in detail by Budden (1961) and Wait (1962). It is not proposed to present a detailed mathematical analysis here; the simple theory will be considered in a more general way and the effect of each amendment will be discussed.

3.1.1 General formulation and waveguide mode theory

In Fig. 3/1 the earth is represented by the plane $z = 0$ and the ionosphere by the plane $z = h$ in a cylindrical coordinate system (ρ, ϕ, z). Both planes are assumed to be perfect reflectors. A vertical dipole source is located at the origin. To an observer on the ground the signal appears to come from the source and a series of identical images, one located just below the ground and at $\pm 2h$, $\pm 4h$ etc. For a wavelength λ the waves emanating from the ionosphere interfere constructively in a direction making an angle Θ with the vertical such that

$$2hC = n\lambda \qquad 3.1/1$$

where $C = \cos \Theta$

and n is an integer.

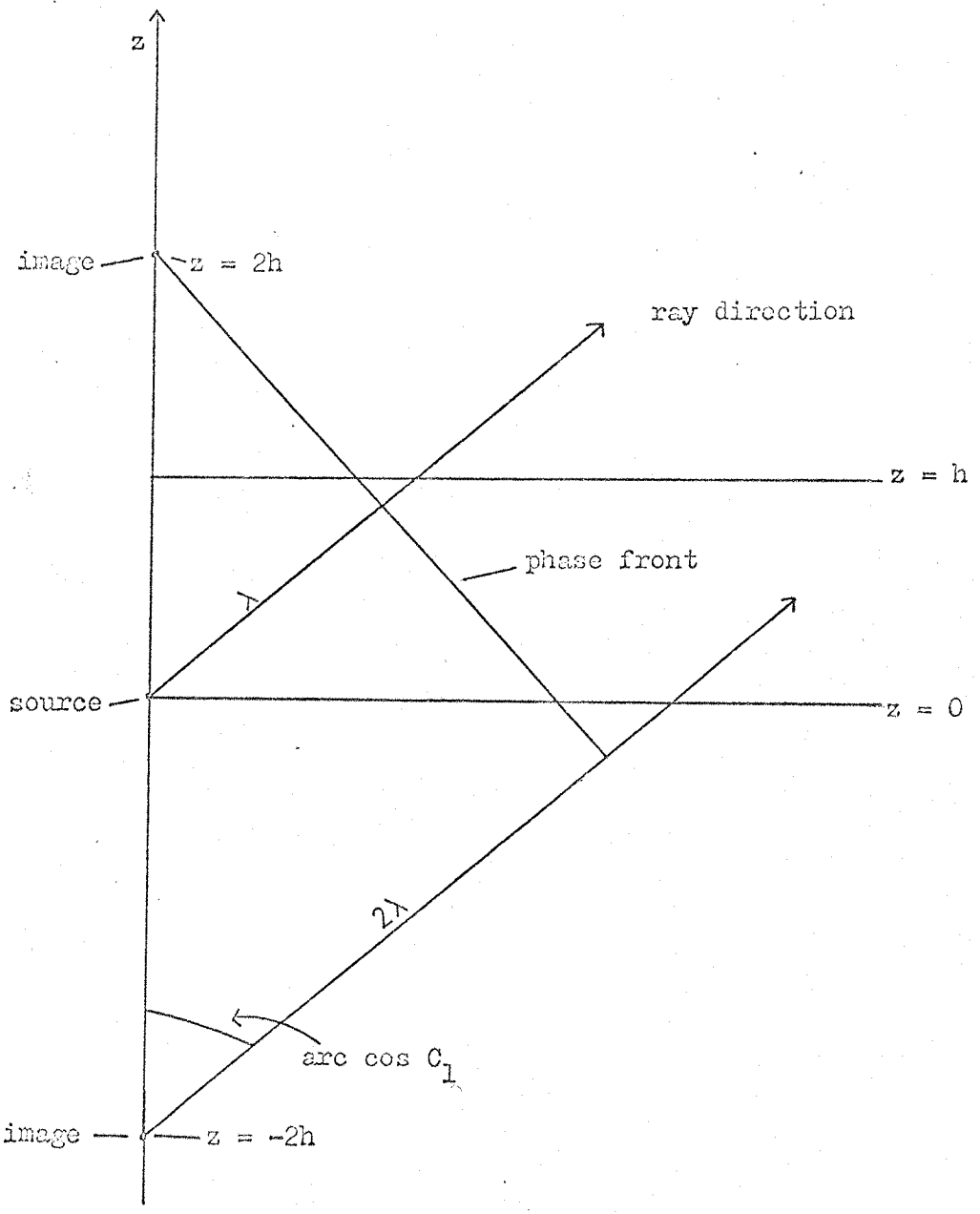

Fig. 3/1. Earth-ionosphere waveguide - ray geometry for first mode.

Thus for a given value of n

$$C_n = \frac{n\lambda}{2h} \qquad 3.1/2$$

The images from the ground interfere constructively at an angle $\pi-\theta$ with the vertical. Therefore for a given value of n there are two families of waves having the same horizontal component of velocity c/S_n but opposing vertical components, where

$$S_n = \sin\theta \text{ and} \qquad 3.1/3$$
$$S_n^2 = 1 - C^2$$

The resultant wave may be considered as a single wave propagating in the horizontal direction with phase velocity $v_p = c/S_n$ (see section 1.2.2). Each value of n corresponds to a mode; hence it is termed the mode number. For the mode 0, $\theta = \pi/2$ and both families of waves are directed in a horizontal direction. This wave may be considered to originate in line source carrying current I_a. If s is the length of the source dipole and I is its current (Wait, 1962), then

$$I_a = \frac{s}{h} I \qquad 3.1/4$$

since all the image dipoles are of equal strength (because of the perfect reflectors).

The field produced by such a source is given by Wait (1960). It is

$$E_z = \frac{1}{4}\mu_o\omega I_a H_o^{(2)}(k\rho) = \frac{\frac{1}{4}\mu_o\omega I s H_o^{(2)}(k\rho)}{h} \qquad 3.1/5$$

where $H_o^{(2)}$ is the Hankel function of the second kind of argument $k\rho$

and $k = 2\pi/\lambda$.

Considering the nth order mode (i.e. the mode produced by nth pair of images) the line current of the source is now $I \sin\theta = IS_n$ because of the obliquity of the rays. Also the electric field at a

given point will be perpendicular to the ray direction so that to obtain E_z the field must be multiplied by S_n.

Hence

$$E_{zn} = 2\frac{\mu_o \omega I s}{4h} \; S_n^2 H_o^{(2)}(k\rho S_n) \qquad 3.1/6$$

the factor 2 arising from the 2 sets of images. The total field is obtained by summing over all modes from 0 to ∞ giving:

$$E_z = \frac{\mu_o \omega I s}{4h} \; H_o^{(2)}(k\rho) + \sum_{n=1}^{\infty} 2S_n^2 \, H_o^{(2)}(k\rho S_n) \qquad 3.1/7$$

For $\rho \gg \lambda$ this reduces to

$$E_z = \tfrac{1}{2}\left(\frac{\mu_o}{\varepsilon_o}\right) \frac{Is}{h(\lambda\rho)^{\frac{1}{2}}} \exp(i\,\pi/4) \quad \exp(-ik\rho) + \sum_{n=1}^{\infty} 2\, S_n^{3/2} \exp(-ik\rho S_n) \qquad 3.1/8$$

taking only the first terms of the asymptotic expansion of the Hankel function.

By considering λ_g as the wavelength in the z direction

$$\lambda_g = \lambda / S_n \qquad 3.1/9$$

Combining 3.1/9 and 3.1/2 the cut off frequency for a given mode (f_n) may be obtained as in section 1.2.2

$$f_n = \frac{nc}{2h} \qquad 3.1/10$$

3.1.2 Modification for imperfect reflection

The reflection coefficient for a wave incident on the ground at an angle whose cosine is C is denoted by $R_g(C)$; the corresponding reflection coefficient for the ionosphere is $R_i(C)$. In general R_g and R_i may be complex. For constructive interference a wave must traverse the waveguide being reflected off each boundary, suffering a net phase change of $2n\pi$ radians. This condition may be written as:

$$R_g(C)\, R_i(C) \exp(-i2khC) = \exp(-i2\pi n) = 1 \qquad 3.1/11$$

where n is an integer.

To determine the resultant field, it is necessary to solve 3.1/11 for C_n for each mode. Hence S_n is determined for substitution in expressions such as 2.3/8. S_n is, in general, complex; therefore S_n may be written as

$$S_n = \text{Re } S_n + i \text{ Im } S_n \qquad 3.1/12$$

The resultant wave field, which contains a term $\exp(-ik\rho S_n)$, will thus contain a term $\exp(k\rho \text{ Im } S_n)$ as well as the term $\exp(-ik\rho \text{ Re } S_n)$. This implies an attenuated travelling wave. The imaginary part of S_n is called the absorption coefficient (K) and is usually given in units of db/Mm. The guide wavelength and phase velocity are given by:

$$\lambda_g = \frac{\lambda}{\text{Re } S_n} \qquad 3.1/13$$

$$v_p = \frac{c}{\text{Re } S_n} \qquad 3.1/14$$

In general the solution of 3.1/11 is complicated. Some solutions have been given by Wait (1957, 1962).

For example if the walls are highly conducting the reflection coefficients may be approximated to

$$R_g(C) = \frac{\mu_g C - C_g}{\mu_g C + C_g} \simeq 1 - \frac{2 C_g}{\mu_g} \simeq \exp\left(\frac{-2}{\mu_g C}\right) \qquad 3.1/15$$

$$R_i(C) = \frac{\mu_i C - C_i}{\mu_i C + C_i} \simeq 1 - \frac{2 C_i}{\mu_i} \simeq \exp\left(\frac{-2}{\mu_i C}\right) \qquad 3.1/16$$

assuming $|C|^2 \gg |\mu_g|^{-2} \gg |\mu_i|^{-2}$

where $\mu_g(1 - C_g^2)^{\frac{1}{2}} = (1 - C^2)^{\frac{1}{2}} = \mu_i(1 - C_i^2)^{\frac{1}{2}}$ 3.1/17

and $\mu_g = \left(\frac{\sigma_g + i \varepsilon_g \omega}{i \varepsilon \omega}\right)^{\frac{1}{2}}$, $\mu_i = \left(\frac{\sigma_i + i \varepsilon_i \omega}{i \varepsilon \omega}\right)^{\frac{1}{2}}$

where σ is the conductivity and ε the permittivity.

The resonance equation 3.1/11 may then be simplified to

$$k\,h\,C = n\pi + \frac{i\,\Delta}{C} \qquad 3.1/18$$

where $$\Delta = \left(\frac{1}{\mu_i} + \frac{1}{\mu_g}\right) \qquad 3.1/19$$

if $\frac{\Delta}{C}$ is assumed to be a small quantity. 3.1/18 may be solved giving

$$S_n \simeq \left[1 - \left(\frac{\pi n}{kh}\right)^2\right]^{\frac{1}{2}} - i\,\frac{\delta_n}{2kh}\,\Delta\left[1 - \left(\frac{\pi n}{kh}\right)^2\right]^{\frac{1}{2}}$$

where $\delta_o = 1$, and $\delta_n = 2$ for $n = 1, 2, \ldots$ 3.1/20

This perturbation method is valid only if the magnitude of the second term is small. This restriction and the previous one may be satisfied simultaneously if

$$k\,h\,|\Delta| \ll 1 \qquad 3.1/21$$

and

$$\frac{|\Delta|}{k\,h} \ll 1 - \left(\frac{\pi n}{kh}\right)^2 \qquad 3.1/22$$

Since the walls are assumed highly conducting

$$\sigma_g \gg \varepsilon_g\omega \text{ and } \sigma_i \gg \varepsilon_i\omega$$

Hence

$$\Delta \simeq \sqrt{i} \quad |\Delta| \simeq \sqrt{i}\left[\left(\frac{\varepsilon\omega}{\sigma_g}\right)^{\frac{1}{2}} + \left(\frac{\varepsilon\omega}{\sigma_i}\right)^{\frac{1}{2}}\right] \qquad 3.1/23$$

Therefore

$$R_e S_n \simeq \left[1 - \left(\frac{n\pi}{kh}\right)^2\right]^{\frac{1}{2}} + \frac{\delta_n\,|\Delta|}{2\sqrt{2}\,kh}\left[1 - \left(\frac{\pi n}{kh}\right)^2\right]^{-\frac{1}{2}} \qquad 3.1/24$$

$$I_m S_n \simeq -\frac{\delta_n\,|\Delta|}{2\sqrt{2}\,kh}\left[1 - \left(\frac{n\pi}{kh}\right)^2\right]^{-\frac{1}{2}} \qquad 3.1/25$$

From 3.1/24 it may be seen that a non-infinite conductivity increases the real part of S_n and hence decreases the phase velocity (see 3.1/14).

The above expressions are not valid however for a mode near cut off because of 3.1/22. This may be overcome by solving 3.1/18 (valid for $|\Delta|\,kh \ll 1$) as a quadratic in C. This gives (Wait, 1962):

$$S_n = 1 - \frac{i\,\Delta}{2kh} \qquad n = 0 \qquad 3.1/26$$

$$S_n \simeq \left[1 - \left(\frac{\pi n}{kh}\right)^2 - i\,\frac{2\Delta}{kh} \right]^{\frac{1}{2}} \qquad n = 1,\ 2,\ 3,\ \ldots \qquad 3.1/27$$

This approximate solution would appear to indicate that the attenuation increases indefinitely as the conductivity decreases. However for low conductivity the condition $|\Delta| \ll 1$ becomes violated. It may be shown that for a given value of n the attenuation reaches a maximum value as $|\Delta|$ is increased and then decreases to a broad minimum (Wait, 1962). This may be illustrated by solving the resonance equation 3.1/11 under the condition that $|N_i C| \ll 1$, $|N_g C| \gg 1$ which is a reasonable assumption for the earth- ionosphere waveguide. At very low frequencies the solution is found to be: (Wait, 1962)

$$R_e\, S_n = \overline{S}_n + \frac{1}{2\sqrt{2}\pi(h/\lambda)\overline{S}_n} \left[(\overline{C}_n)^2 \left(\sqrt{L} - \frac{1}{\sqrt{L}} \right) + \sqrt{G} \right] \qquad 3.1/28$$

$$I_m\, S_n = \frac{-1}{2\sqrt{2}\pi(h/\lambda)\overline{S}_n} \left[(\overline{C}_n)^2 \left(\sqrt{L} + \frac{1}{\sqrt{L}} \right) + \sqrt{G} \right] \qquad 3.1/29$$

where $\mu_i^{\,2} = 1 - \frac{i}{L}$

$$\overline{C}_n = \frac{\pi\left(n - \frac{1}{2}\right)}{kh} = \frac{n - \frac{1}{2}}{2\,h/\lambda}$$

$$\overline{S}_n = \left[1 - (\overline{C}_n)^2 \right]^{\frac{1}{2}}$$

$$G = \frac{\varepsilon_o \omega}{\sigma_g}$$

It may be seen that for a fixed value of h/λ and $\sqrt{G}$ the Imaginary part of S_n has a broad minimum when $L = 1$; when L is less than 1 the attenuation factor varies as $L^{-\frac{1}{2}}$ or as $\sigma_i^{\frac{1}{2}}$; when L is greater than 1

the attenuation factor varies as $L^{\frac{1}{2}}$ or as $\sigma_i^{-\frac{1}{2}}$.

3.1.3 Effect of the earth's curvature

The curvature of the earth tends to prevent the angle of incidence of the ray from becoming grazing at the ionosphere while allowing it to be grazing at the earth; both these effects tend to reduce the reflection coefficients of the earth and ionosphere. If the radius of the earth is R_E, the height of the ionosphere h and the angles of incidence at the ionosphere and earth are ϕ' and ϕ respectively, then from Snell's law

$$R_E \sin\phi = (R_E + h) \sin\phi' \qquad 3.1/30$$

Wait (1960) has calculated a modified resonance equation taking the earth's curvature into consideration. It is

$$R_g(C)R_i(C')\exp\left[-2ik\int_0^h \left[C^2 + \frac{2z}{R_E}S^2\right]^{\frac{1}{2}} dz\right] = \exp(-2i\pi n) \qquad 3.1/31$$

where $C = \cos\phi$ and $C' = \cos\phi'$

Numerical results by Wait and Spies (1960) show that the curvature of the earth may increase the attenuation by a factor of three (see Fig. 3/2).

The curvature of the earth also has the effect of reducing the phase velocity to less than c in most cases on interest (Wait and Spies, 1960). The curvature has greatest effect on the lowest order modes since these modes involve rays with angles of incidence which are nearest grazing.

3.1.4 Effect of the earth's magnetic field

The effect of the earth's magnetic field is to make the ionosphere an anisotropic medium. The magneto-ionic theory (Ratcliffe, 1959) shows that the refractive index of the ionosphere, when permeated by a static magnetic field, becomes double valued. Hence a transverse magnetic wave incident on the ionosphere will give rise

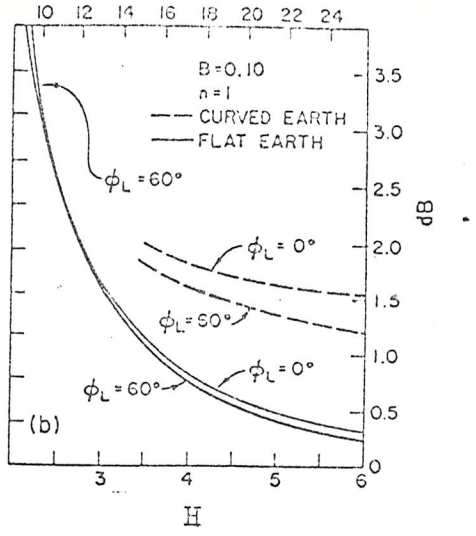

The upper and right-hand scales are specifically for h=70 km, which is a typical daytime height ($B=\lambda L/h$)
(After J. R. Wait and K. Spies, 1960, Influence of earth curvature and terrestrial magnetic field on VLF propagation, J. Geophys. Res. 65, 2325.)

Fig. 3/2 Effect of earth curvature on waveguide mode attenuation.

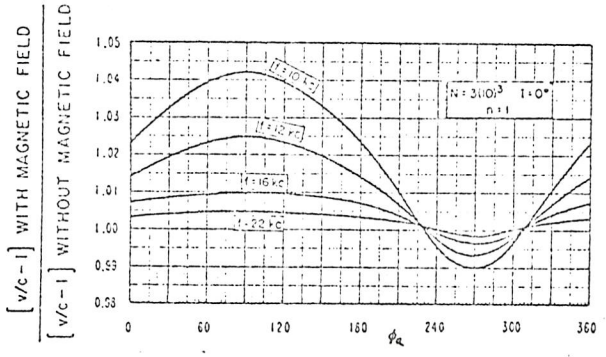

Differences between phase velocities (with and without the magnetic field).

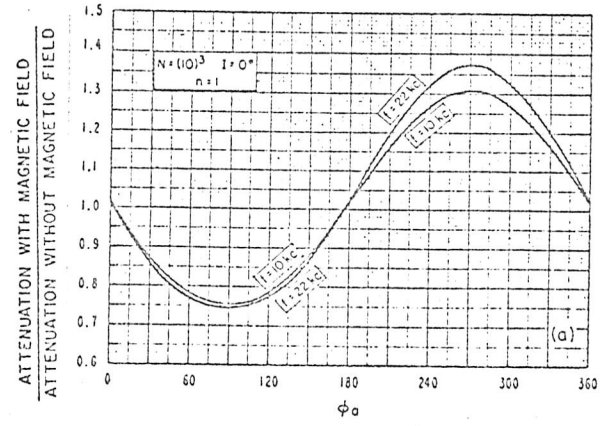

Ratios of attenuation (with and without the magnetic field) as a function of azimuth.

(After J. R. Wait and K. Spies, 1960, Influence of earth curvature and terrestrial magnetic field on VLF propagation, J. Geophys. Res. 65, 2325.)

Fig. 3/3

to two reflected waves (one TM and one TE) and two transmitted waves (one TM and one TE). In general there will be a coupling between these TE and TM waves but this is usually negligibly small (Wait, 1962). This double refraction in the ionosphere is described mathematically by two reflection coefficients $_{//}R_{//}$ and $_{\perp}R_{\perp}$ together with two conversion coefficients $_{//}R_{\perp}$ and $_{\perp}R_{//}$ where the first subscript refers to the polarization of the electric field of the incident wave relative to the plane of incidence and the second subscript to that of the reflected wave. A detailed mathematical analysis of the effect is given by Wait (1962). The main result is that, when the magnetic field is included the phase velocity and attenuation become dependent upon the direction of propagation (Fig. 3/3).

3.1.5 Further refinements

So far the ionosphere has been considered to be a sharply bounded medium. Experimental evidence tends to indicate that this is not so and that it should be considered a stratified medium, i.e. consisting of layers of different conductivity. It has also been assumed that the direction of the earth's magnetic field is constant. The effect of the stratified ionosphere and a dipping magnetic field have been discussed in a series of papers (Wait and Walters, 1963, 1964; Wait, 1963; Galejs, 1964a,b, 1965, 1966, 1968a,b). The results of these refinements do not alter the results already described to a great extent.

CHAPTER FOUR

The Magnetosphere: A Review

The second part of this thesis is concerned primarily with the whistler precursor, a rising tone which precedes the whistler with which it appears to be associated. No satisfactory explanation has yet been found for this phenomenon. It will be shown that the whistler precursor may be explained in terms of the accepted properties of the magnetosphere, and the transverse resonance instability (Helliwell, 1967, Rycroft, 1972) which is thought to be responsible for the generation of both spontaneous and the more obviously triggered emissions. In this chapter, present knowledge of the magnetosphere is reviewed with particular reference to those properties thought to be involved with the generation of precursors.

4.1 General properties of the magnetosphere

The magnetosphere is a region of plasma above the ionosphere where the motion of the charged particles is controlled primarily by the earth's magnetic field. The main constituents of the magnetospheric plasma are electrons, protons and helium ions. The density of neutrals is approximately equal to the density of ions at an altitude of $\sim$ 1000 km, the predominant neutral component being hydrogen. Fig. 4/1 shows a diagram of the magnetosphere. The areas marked 'stable trapping' are the Van Allen radiation belts of energetic charged particles trapped by the geomagnetic field, which extend out to a few earth radii. Electron energies range between a fraction of an eV (thermal electrons) and several MeV while proton energies extend from thermal values to several hundred MeV. The flux of the most energetic electrons has a maximum at equatorial radial

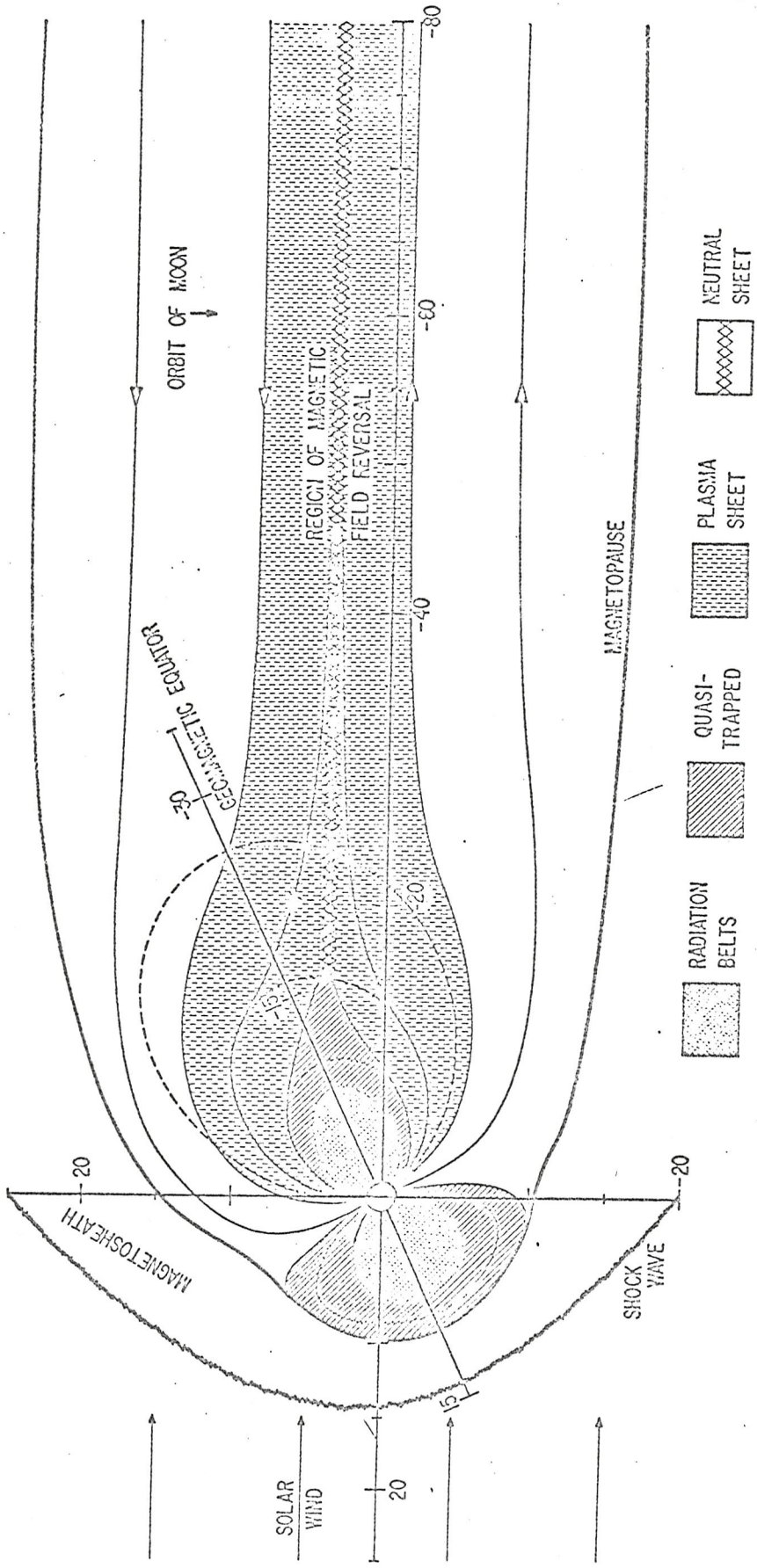

MAGNETOSPHERE AND TAIL

Fig. 4/1

distances of around 3 to 5 R_E while energetic protons tend to peak around 1.5 R_E; the lower energy particles are spread throughout the magnetosphere (Vette, 1970). Beyond the stable trapping region there exist large transient fluxes of pseudo-trapped particles.

The solar wind, a stream of plasma emanating from the sun, impinges upon the earth's magnetic field at a speed of around 300 - 500 km sec^{-1}. This is greater than the Alfven velocity, the magnetohydrodynamic equivalent of the speed of sound; therefore a standing shock wave or bow shock is produced upstream of the magnetosphere. The earth's magnetic field presents a barrier to the charged particles in the solar wind. The magnetopause marks the outer boundary of the magnetosphere beyond which the solar wind cannot penetrate directly; in it currents flow in such a way as to reinforce the magnetic field within the magnetosphere and to reduce the field outside. Between the bow shock and the magnetopause is the magnetosheath, a region of turbulence. The solar wind is made to flow around the magnetosphere; as it does so the geomagnetic field lines are drawn out into a long tail on the anti-solar side, a magnetic neutral sheet being formed near to the equatorial plane.

In the magnetosphere a trapped particle performs three kinds of motion:

(i) gyration about a magnetic field line;

(ii) motion along a magnetic field line, 'bouncing' back and forth between mirror points;

(iii) a drift motion in a direction transverse to the magnetic field lines.

Thus the motion of a charged particle in the magnetosphere is conveniently described in terms of three adiabatic invariants of motion (Northrop and Teller, 1960). These are:

(i) the magnetic moment, $\mu = \frac{p_\perp^2}{2m_o B}$, where $p_\perp$ is the component of the

relativistic momentum perpendicular to the magnetic field of magnitude B and m_o is the rest mass of the particle;

(ii) the longitudinal or integral invariant, $J = \oint p_{//}\, dl$, where $p_{//}$ is the component of relativistic momentum parallel to the magnetic field and the integration is taken along the guiding centre of the particles motion from one mirror point to the other and back;

(iii) the flux invariant, $\Phi = \oint \underline{A} \cdot d\underline{I}$ where $\underline{A}$ is the vector potential of the magnetic field, $\underline{I} = \underline{J} / 2p$, and the integration is taken along a closed curve lying on the surface defined by $\underline{J}$ = constant. The particle is thus constrained to drift around the earth on the shell defined by $\underline{J}$ = constant, μ = constant. An electron drifts eastwards, a proton westwards (Matsushita and Campbell, 1967). The shell is identified by its L parameter, defined to be I^3B, which is approximately equal to the radial distance to the shell in the equatorial plane, measured in earth radii (McIlwain, 1961). Each L shell is formed by rotating a magnetic field line about the earth. Thus any field line and the points on the earth at either end of it are labelled by the L parameter; it is often useful to refer to the L value of a field line or of a point on the earth's surface.

The electron density in the equatorial plane is found to decrease gradually with distance from the earth up to about 4 R_E, when there is an abrupt change from around 100 cm^{-3} to around 1 cm^{-3} within a distance as small as 0.15 R_E (Carpenter, 1966, Mathur and Rycroft, 1972). This region of rapid change is known as the plasmapause; its position depends on local time as well as the level of magnetic activity (Carpenter, 1966, Rycroft and Thomas, 1970). The plasmapause will be discussed in greater detail in a later section.

Page 44 was not included in the bound thesis.

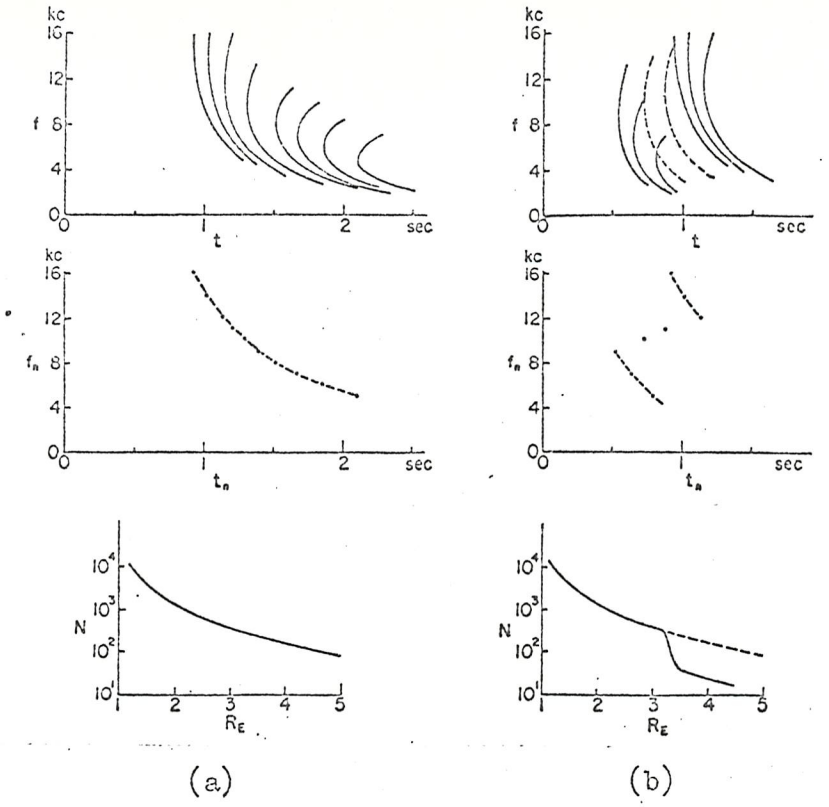

Whistler method for electron concentration (HELLIWELL, 1965).

Fig. 4/2

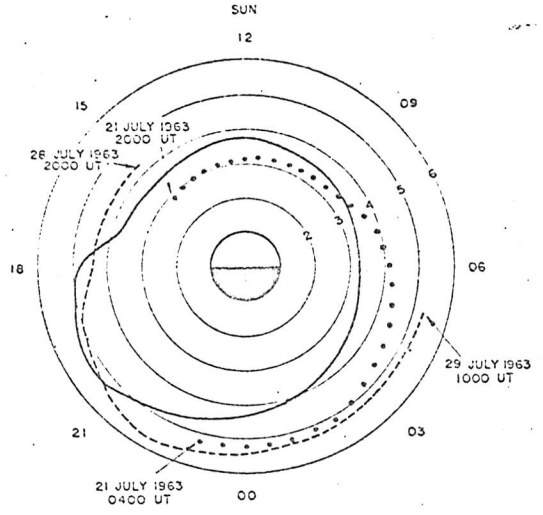

Equatorial radius of the knee versus local time. The solid curve represents average behavior during periods of moderate, steady geomagnetic agitation (K_p = 2–4). The observations were made in July and August 1963 at Eights, Antarctica. The dots show a particular example involving increasing magnetic agitation
; the dashes, an example of decreasing agitation

Carpenter (1966)

Fig. 4/3

Page 46 was not included in the bound thesis.

is a field aligned structure and that its position depends strongly on the level of magnetic activity as well as exhibiting a marked diurnal variation. The diurnal variation follows the following pattern and is found to be highly repeatable:

(i) a slow inward movement of the knee on the nightside, covering 1.5 R_E in around 10 hours,

(ii) a slight outward motion on the day side, covering around 0.5 R_E,

(iii) a rapid outward shift in the late afternoon, around 1800 LT, covering around 1 R_E in about 1 hour.

The pattern of the diurnal variation is shown in Fig. 4/3.

During periods of changing magnetic activity the position of the knee changes with at most a few hours delay, moving inwards with increasing magnetic activity. A statistical study by Rycroft and Thomas (1970) shows that during the local night the equatorial radial distance to the centre of the plasmapause is given by the relation:

$$R_p = 5.64 - (0.78 \pm 0.12)\, K_p^{\frac{1}{2}} \qquad 4.2/4$$

where K_p is the three-hourly index of magnetic activity, which takes values between zero, for extremely quiet conditions, and 9 for extremely disturbed conditions. During the intense magnetic storm of March 8th 1970 knee whistlers were observed at Chilbolton, Southern England (L = 2.4) giving a plasmapause position of L = 3.1 (Mathur and Rycroft, 1972). At extremely quiet times the plasmapause may move out as far as L = 8 or 9 (Helliwell, 1968).

The width of the plasmapause is found to be generally around 0.2 R_E in the equatorial plane although there is evidence to indicate that the width decreases at times of high magnetic activity (Chappell, Harris and Sharp, 1970).

A steep electron density gradient such as the plasmapause acts as a reflector for very low frequency radio signals. Alexander (1971), using

ray tracing techniques to be described in a later section, has shown that whistler mode radiation impinging on the plasmapause from within is generally reflected by it and thus remains inside.

4.2.2 Ray tracing in the magnetosphere

The magnetosphere, being a region of plasma permeated by a magnetic field, is an anisotropic medium, since the refractive index and hence the phase velocity are functions of the direction of propagation (equation 1.3/1). Therefore waves of a given frequency propagating in slightly different directions will have different phase velocities and hence different wavelengths in the medium. This is shown diagramatically in Fig. 4/4; AA and BB are plane wavefronts having slightly different directions to the magnetic field $\underline{B}_o$. BB is assumed the slower of the two. After 1 sec the point of constructive interference has moved from O to P and the wavefronts are at AA' and BB'. The locus of the points of constructive interference defines the direction of energy flow and is called the ray path. From the geometry of the figure

$$\left.\begin{aligned} \tan\alpha &= \frac{y}{c/\mu} \\ y\, d\Theta &= x \\ x &= (c/\mu) - \left(\frac{c}{\mu + d\mu}\right) \end{aligned}\right\} \qquad 4.2/5$$

where Θ is the angle between the wave normal and the earth's magnetic field,

where μ is the real part of the refractive index.

Hence the ray direction may be related to the anisotropy of the refractive index thus:

$$\tan\alpha = \mu^{-1}\frac{d\mu}{d\Theta} \qquad 4.2/6$$

If it is assumed that $f \ll f_{B\,e}$ then this relation reduces to the expression obtained by Storey (1953):

$$\tan\alpha = \tfrac{1}{2}\tan\Theta.$$

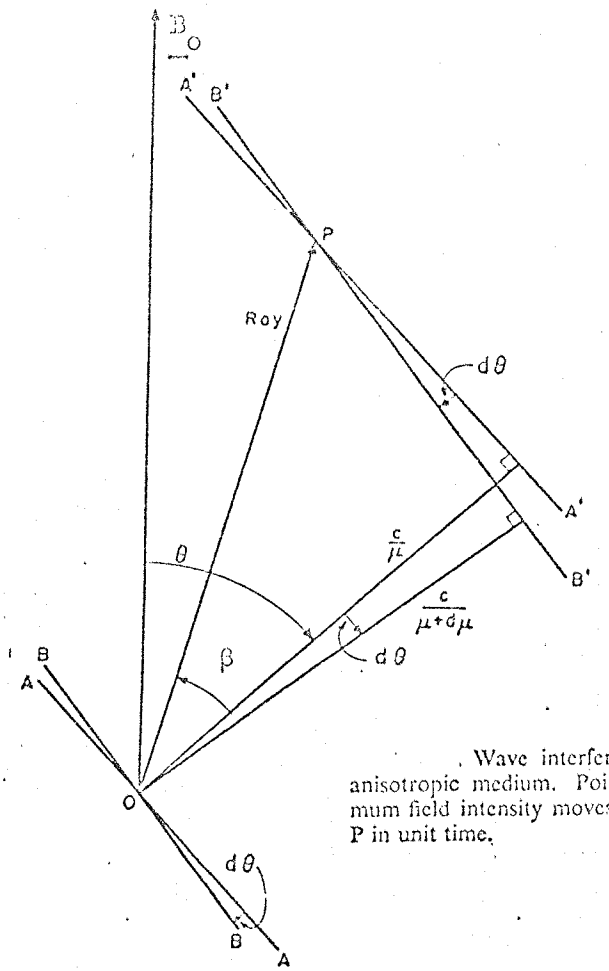

. Wave interference in an anisotropic medium. Point of maximum field intensity moves from 0 to P in unit time.

Fig. 4/4

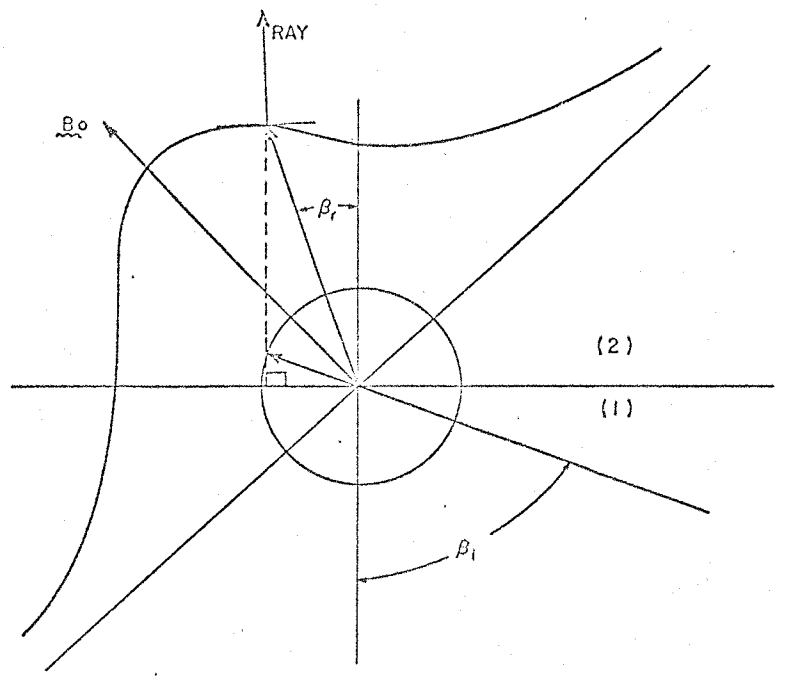

Graphical solution of Snell's law.

Fig. 4/5

This leads to the famous Storey limiting angle of $19^{\circ}29'$, i.e. the ray direction never departs from the geomagnetic field direction by more than $19^{\circ}29'$.

The refractive index surface is a very useful concept in ray tracing. It is formed by plotting the refractive index as a function of θ and rotating the resulting curve about the direction of the ambient magnetic field. Poeverlein (1948) has shown that the ray direction is the normal to the refractive index surface for a given value of θ. When calculating the time delay the expression 1.3/2 is not the correct one to use. It may be seen that, in Fig. 4/4, while the wavefronts have moved a distance v_g the point of constructive interference has moved a distance $v_g \sec \alpha$. This is the group ray velocity, v_{gr} and is the velocity at which the energy is propagated through the magnetosphere.

As a ray propagates through the magnetosphere the refractive index changes constantly, since the electron density, magnetic field strength collision frequency, and ion composition, which all affect the refractive index, are changing. A ray may be traced through the magnetosphere by dividing it up into regions in which the refractive index is assumed constant and using Snell's law at each boundary. The refractive index surface may be used to solve Snell's law graphically (Poeverlein, 1948). Snell's law requires that the tangential component of the refractive index vector be the same on both sides of the boundary, which is equivalent to matching the tangential components of $\underline{E}$ and $\underline{H}$. The graphical solution of Snell's law is illustrated in Fig. 4/5, where the boundary in question is between the atmosphere (medium 1), where the refractive index is unity, and the lower ionosphere (medium 2). The solution is obtained by extending a perpendicular from the boundary through the end of the refractive index vector for medium 1 until it meets the refractive index surface of medium 2. By drawing the refractive index vector

from this point back to the origin the matching condition is automatically fulfilled; the corresponding ray direction is obtained by drawing the normal to the refractive index surface.

The graphical method of ray tracing applied to the magnetosphere is obviously a very lengthy and tedious process. Haselgrove (1954) has derived a set of differential equations which describe the behaviour of a wave in an anisotropic medium These equations are in a suitable form for numerical integration using a computer. By using a realistic model of plasma distribution in the magnetosphere and a suitable expression for the refractive index, the ray paths may be calculated. Alexander (1971) has described a comprehensive ray tracing program, based on the Haselgrove equations, which takes account of all the main features of the magnetosphere. Two diffusive equilibrium models of plasma distribution are included, one describing the conditions for a summer day, the other for a winter night; a model plasmapause may be included as well as model ducts, (to be discussed in the following section). The results obtained using this program are in good agreement with the observed characteristics of VLF signals, which have propagated through the magnetosphere.

4.2.3 Ducts in the magnetosphere

Magnetospheric ducts consist of field aligned enhancements in the magnetospheric electron density Their effect on VLF propagation is to guide the ray along the magnetic field line keeping the angle between the wave normal and the magnetic field small This is a necessary condition for the signal to be received on the ground; waves whose wave normal angles are large may be totally internally reflected at the base of the ionosphere, since the large refractive index of the ionosphere relative to the atmosphere results in a small critical angle (Yabroff, 1961). The absorption of the ionosphere is also strongly dependent on this angle (Smith et al., 1960)

In order to understand the need for ducts it is necessary to examine the refractive index surface in the magnetosphere taking into account the presence of ions, mainly hydrogen, helium and oxygen. Fig. 4/6 shows the refractive index surfaces for frequencies (a) below 0.5 $f_{B\,e}$ and (b) between 0.5 $f_{B\,e}$ and $f_{B\,e}$; in both cases the frequency is assumed to be greater than the lower hybrid resonance frequency f_{LHR} given by:

$$f_{LHR}^2 = \left[\frac{f_o^2 \; f_{B\,e}^2}{f_o^2 + f_{B\,e}^2}\right] \frac{m_e}{m_p} \left(\alpha_{H^+} + \frac{\alpha_{He^+}}{4} + \frac{\alpha_{O^+}}{16}\right) \qquad 4.2/7$$

where m_e and m_p are the masses of the electron and proton respectively and α_{H^+} , α_{He^+} , and α_{O^+} are the fractional concentrations of H^+, He^+ and O^+. It may be seen that for both cases there is a limiting value for the angle between the wave normal and the magnetic field, at which the refractive index tends asymptotically to infinity. This limiting angle is given approximately by

$$\cos \Psi_{max} = f/f_{B\,e}$$

If the wave normal angle exceeds this value the wave becomes rapidly attenuated. Below the lower hybrid resonance frequency, however, the refractive index surface becomes closed as shown in Fig. 4/7, so that the wave normal may be in any direction, including perpendicular to the magnetic field. Unless the refractive index becomes very large (when the frequency is almost equal to f_{LHR} and the wave normal angle is close to 90°) the attenuation of the wave is not very great (Kimura, 1966). The value of f_{LHR} increases at low altitudes as the electron ~~density~~ gyrofrequency becomes greater. As the ray propagates down into a region where the wave frequency is less than the lower hybrid resonance frequency the wave normal approaches and passes through 90° to the field line. As it does so the ray refracts round, becoming transverse to

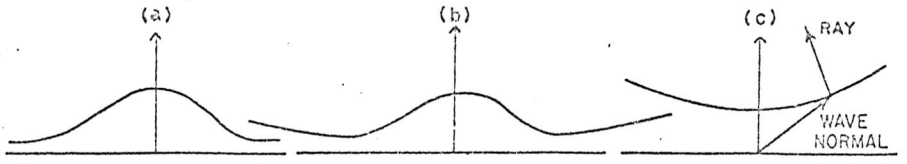

Refractive index surfaces. (a) $f < 0.1 f_{Be}$; (b) $f < 0.5 f_{Be}$; (c) $f > 0.5 f_{Be}$

Fig. 4/6

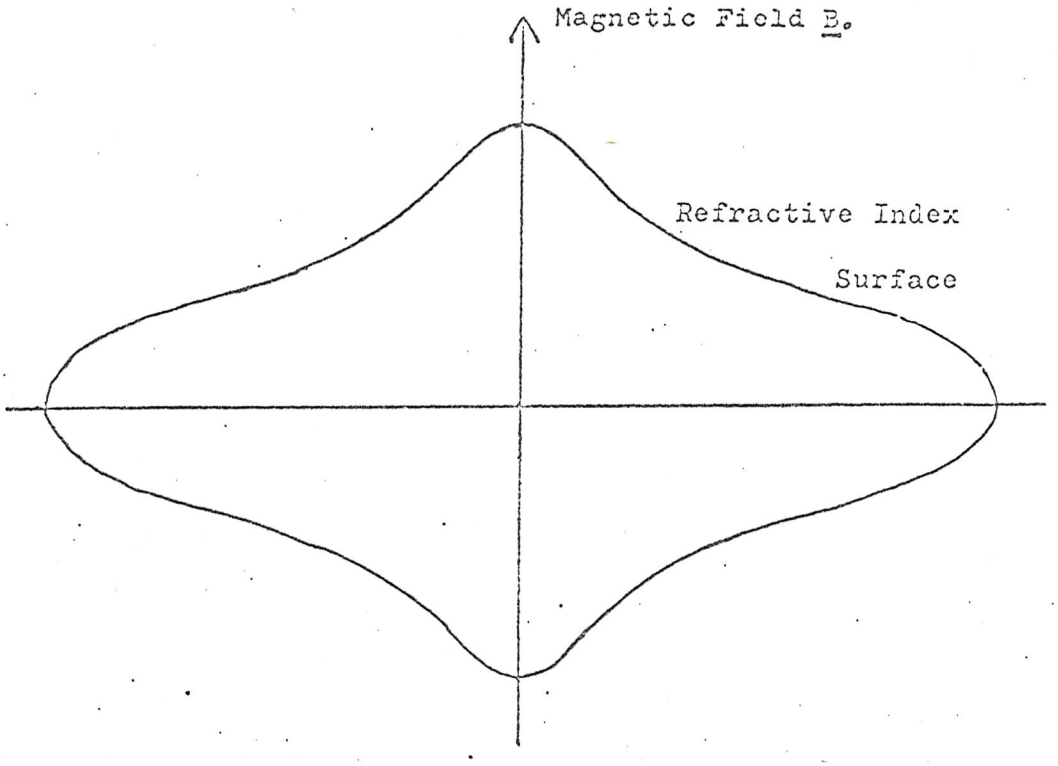

Fig. 4/7. Refractive index surface for $f < f_{LHR}$.

the field line when the wave normal angle is 90°, and thereafter propagates back upwards (Storey and Cerisier, 1968; Alexander, 1971). This phenomenon is often referred to as magnetospheric reflection, although refraction would be a more accurate term. Generally, a VLF ray launched into the magnetosphere at one end of a field line does not propagate round to the conjugate point, but is magnetospherically reflected one or more times until its energy is dissipated (Alexander, 1971) as shown in Fig. 4/8. Signals of this type have been received on satellites and are known as MR (magnetospherically reflected) whistlers (Smith and Angerami, 1968).

Fig. 4/9 shows the electron density profile across a duct; the profile shown is that used by Alexander (1971) and is Gaussian in shape. The corresponding refractive index surfaces are shown in Fig. 4/9(b). Using the Poeverlein construction it may be seen that, provided the wave normal angle is initially not too large, the ray zig-zags along the duct and is thus guided along the field line. At the same time the angle between the wave normal and the magnetic field varies by a small amount either side of zero. Since the magnitude of the wave normal angle always remains small the ray may be guided through the lower hybrid resonance region without being reflected and may thus be received in the lower ionosphere and hence on the ground. The refractive index surfaces shown in Fig. 4/10(b) are for the case when $f < 0.5\ f_{B\,e}$. If $f > 0.5\ f_{B\,e}$ then the refractive index surfaces are as in Fig. 4/10 and the ray is not trapped in the duct. It may be shown that in this case a depression in electron density is required for trapping rather than an enhancement (Alexander, 1971). Rays that are trapped in a duct at low altitudes where the gyrofrequency is large may escape from the duct at higher altitudes when the wave frequency becomes greater than or equal to half the gyrofrequency. This is demonstrated in

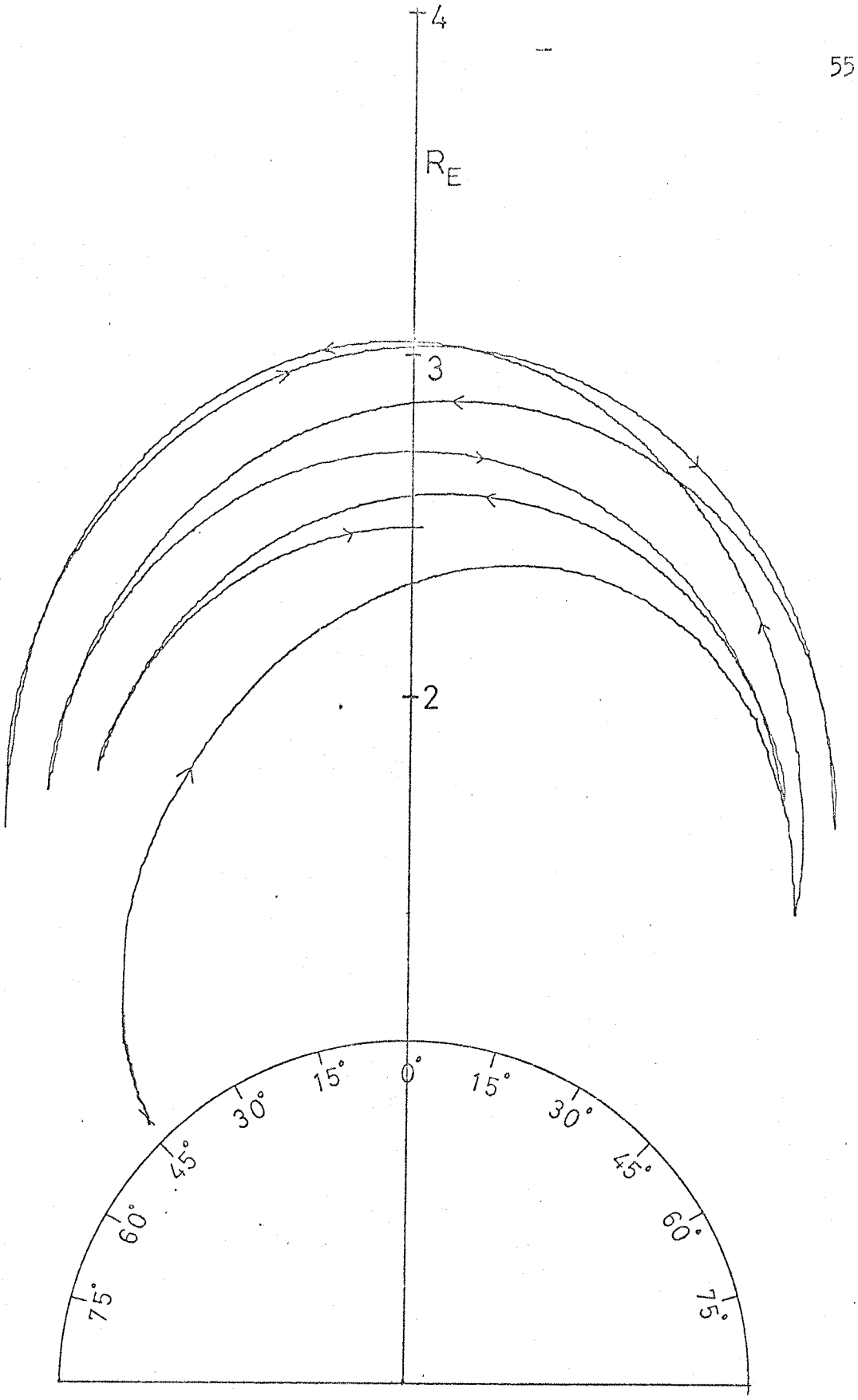

Fig. 4/8. 3 kHz ray undergoing many magnetospheric reflections.

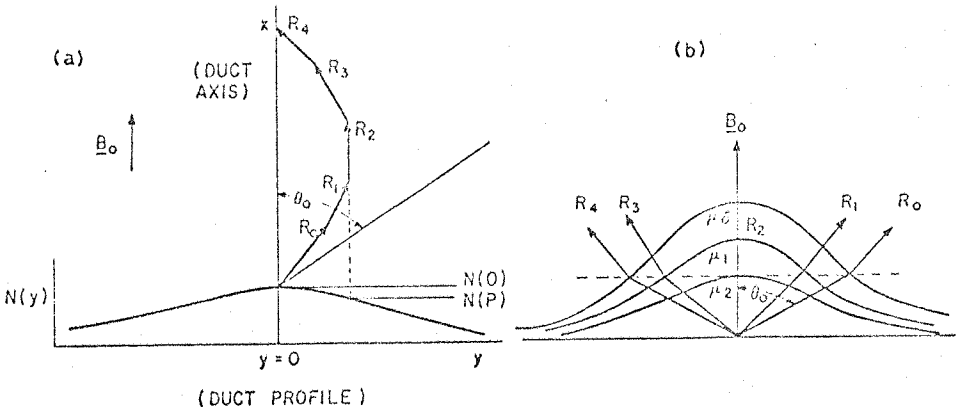

Duct propagation. (a) Density profile and ray path; (b) Refractive index surfaces.

Fig. 4/9

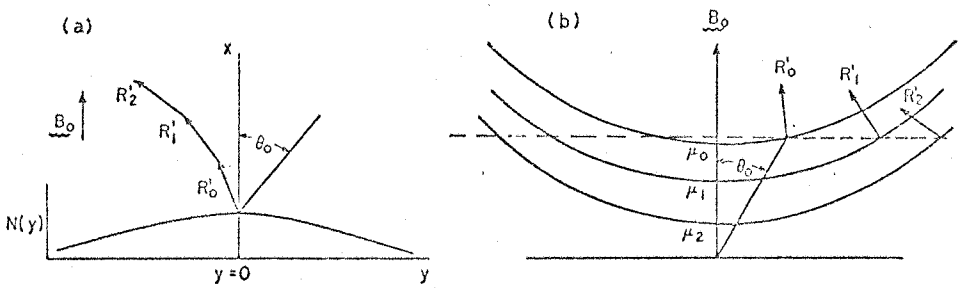

Untrapped propagation. (a) Density profile and ray path; (b) Refractive index surfaces.

Fig. 4/10

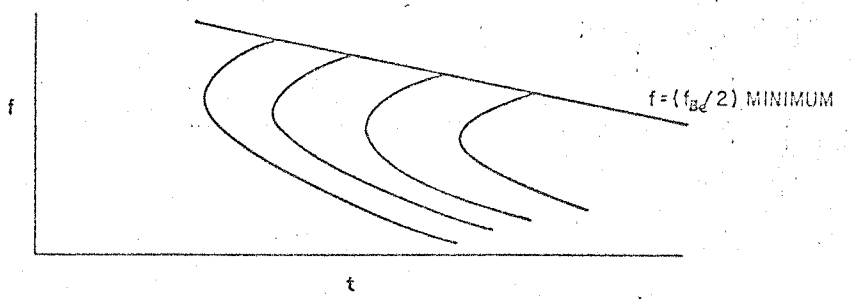

Multi-path whistlers with cutoff.

Fig. 4/11

Fig. 4/11, which shows a series of multi path whistlers from the same sferic exhibiting a sharp upper cut off at a frequency equal to half the minimum gyrofrequency on their path of propagation.

Experimental evidence for ducts is scarce. However simultaneous observations of whistlers on satellites and at the ground show that all the frequencies forming the whistler travel along the same path, which would not be the case for unducted propagation (Smith and Angerami, 1968). Direct measurement of magnetospheric electron density profiles (Angerami, 1970) tends to suggest that the magnetosphere is striated with more or less random troughs and enhancements and that the larger enhancements may act as ducts, a suggestion which is supported by the observation of multipath whistlers as shown in Fig. 4/11.

4.2.4 Models of the magnetosphere

In order to trace rays through the magnetosphere it is necessary to form a realistic model of the distribution of plasma in the magnetosphere. It is also desirable that this model should be in a convenient form for numerical computations. Angerami and Carpenter (1966), using whistler data, showed that inside the plasmapause ($L \leq 4$) a diffusive equilibrium model is a good approximation; outside the plasmapause where the equatorial electron density is of the order of 100 times less it was shown that an idealised collisionless model was a more realistic estimate. In this section these and some related models are discussed, outlining their theory.

(i) The diffusive equilibrium model

In this model it is assumed that the ions and electrons are constrained to move only along the earth's magnetic field lines under the influence of the earth's gravitational field of a charge separation electric field and of the centrifugal force arising from the rotation of the earth (Angerami and Thomas, 1963). It has been shown that the

most crucial factors governing the form of the plasma distributions are the temperature and ionic composition at the base level of the model, assumed to be at 500 km (Angerami and Thomas, 1963) or 1000 km (Angerami, 1966). The latter value of the base level is more convenient since electron density at 1000 km have been extensively studied using the Alouette I topside sounder data. Angerami (1966) gives the following formula for the electron density distribution under diffusive equilibrium conditions:

$$N = N_b \left[\sum_i \alpha_{i\,b} \exp\left(-\frac{z}{H_i}\right) \right]^{\frac{1}{2}} \qquad 4.2/8$$

with $$z = r_b - \frac{r_b^2}{r} - \frac{\Omega^2}{2g_b} \left(r^2 \cos^2 G - r_b^2 \cos^2 G_b\right)$$

and $$H_i = \frac{kT}{m_i\, g_b}$$

where α is the fractional concentration of each ionic species

r is the radial distance from the centre of the earth

Ω is the angular rotational speed of the earth

g is the acceleration due to gravity

G is the geomagnetic latitude

k is Boltzmann's constant

T is temperature

m is the mass

The subscript i refers to the ith ionic species, O^+, H^+ and He^+ being the species usually considered; the subscript b refers to the base level of the model. (It is assumed that $T = T_e = T_i$ and that T is independent of altitude) Angerami (1966) has shown that the centrifugal force term only becomes important for $L \geq 6$.

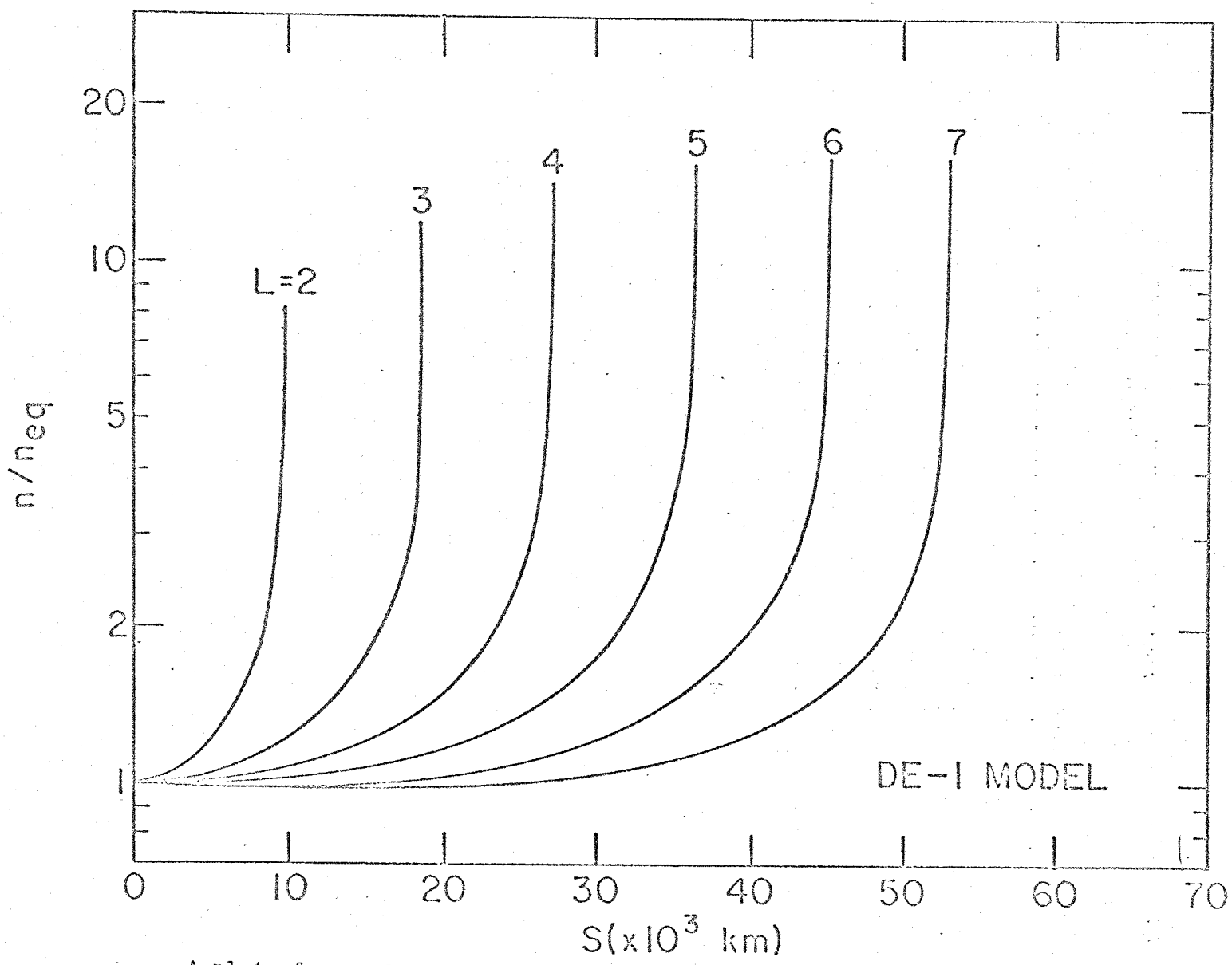

Fig. 4/12(a)

A plot of normalized electron concentration versus distance along field lines at several L values according to a diffusive equilibrium model. ($T_i = T_e = 1600^{\circ}K$, 90% O^+, 8% H^+ and 2% He^+ at 1000 km) the arc length is measured from the equator, and the end points of the curves correspond to 1000 km altitude.

(ii) The collisionless model

In this model the plasma is assumed to consist of electrons and protons only; the forces acting on the particles are assumed to be the same as for the diffusive equilibrium model but the effect of collisions between the particles is not considered (Angerami, 1966). The electron concentration is given by:

$$N = N_b \left\{ \exp(-\frac{z}{2H}) - (1 - \frac{B}{B_b})^{\frac{1}{2}} \exp \left[- \frac{z}{2H(1 - B/B_b)} \right] \right\} \quad 4.2/9$$

where B is the magnetic field strength and z and H are as for the diffusive equilibrium model (eq. 4.2/8).

Angerami (1966) has shown that this model approximates very closely to the r^{-4} model, the latter having the advantage of being much simpler to work with; the electron density is given by:

$$n = n_b \, r_b^4 \, r^{-4} \quad 4.2/10$$

(iii) The hybrid model

The hybrid model described by Park (1972) combines the diffusive equilibrium model with the collisionless model. A diffusive equilibrium model is applied from 1000 km altitude up to 30° dipole latitude and a collisionless model from 30° to the equator. The model attempts to recognize the fact that when the magnetospheric concentrations are low the plasma may not be in diffusive equilibrium whereas it is unrealistic to assume no collisions down to 1000 km as in the purely collisionless model. This model is, therefore, mainly applicable to the magnetosphere beyond the plasmapause.

(iv) The summer day (SD) and winter night (WN) models

These two models are essentially diffusive equilibrium models where the value of the various parameters at the base level (900 km in this case) have been put into a form suitable for digital computing

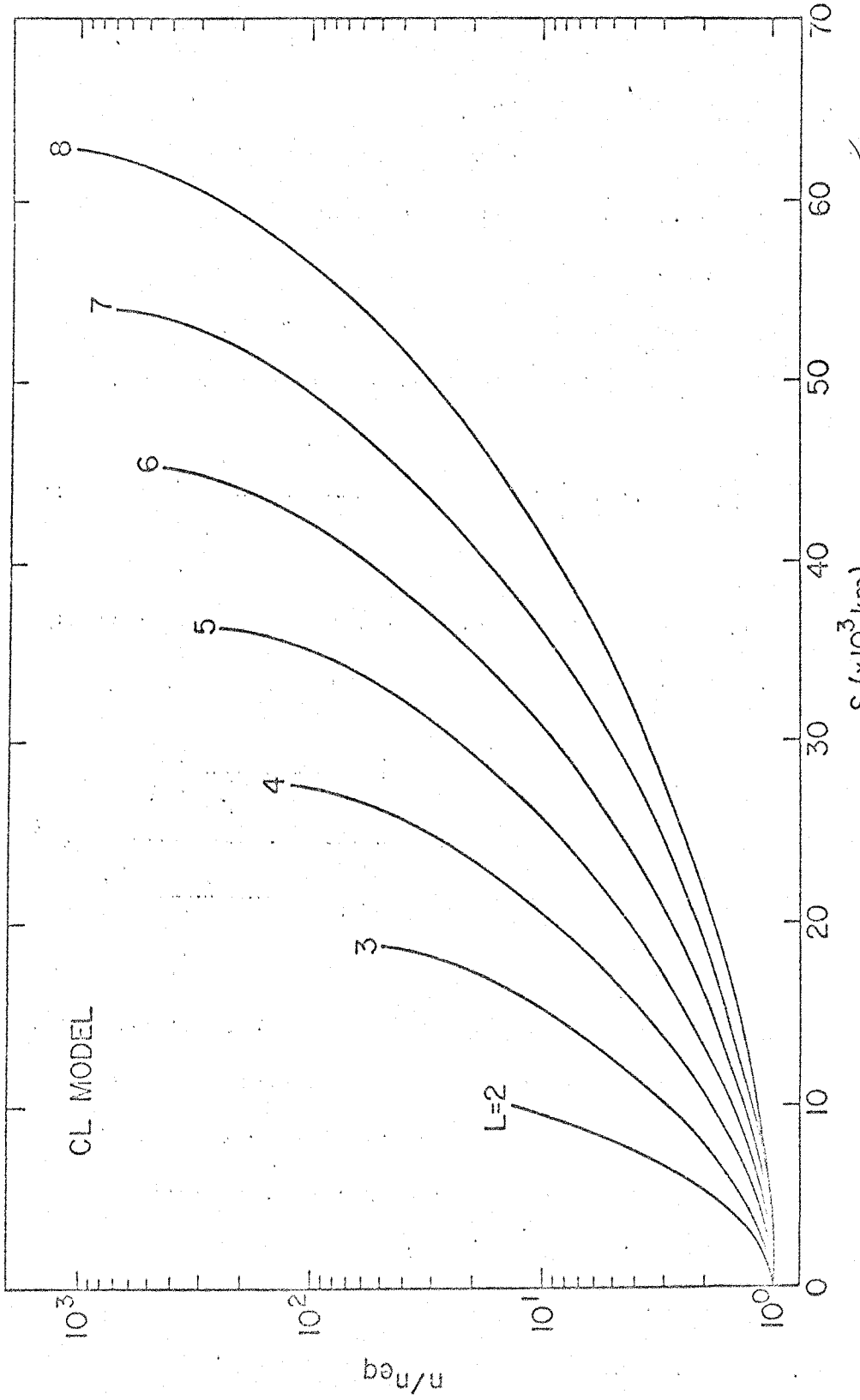

Fig. 4/12 (b) A plot of normalized electron concentration in a format similar to that of Fig. 4/12(a) but according to an idealized collisionless model.

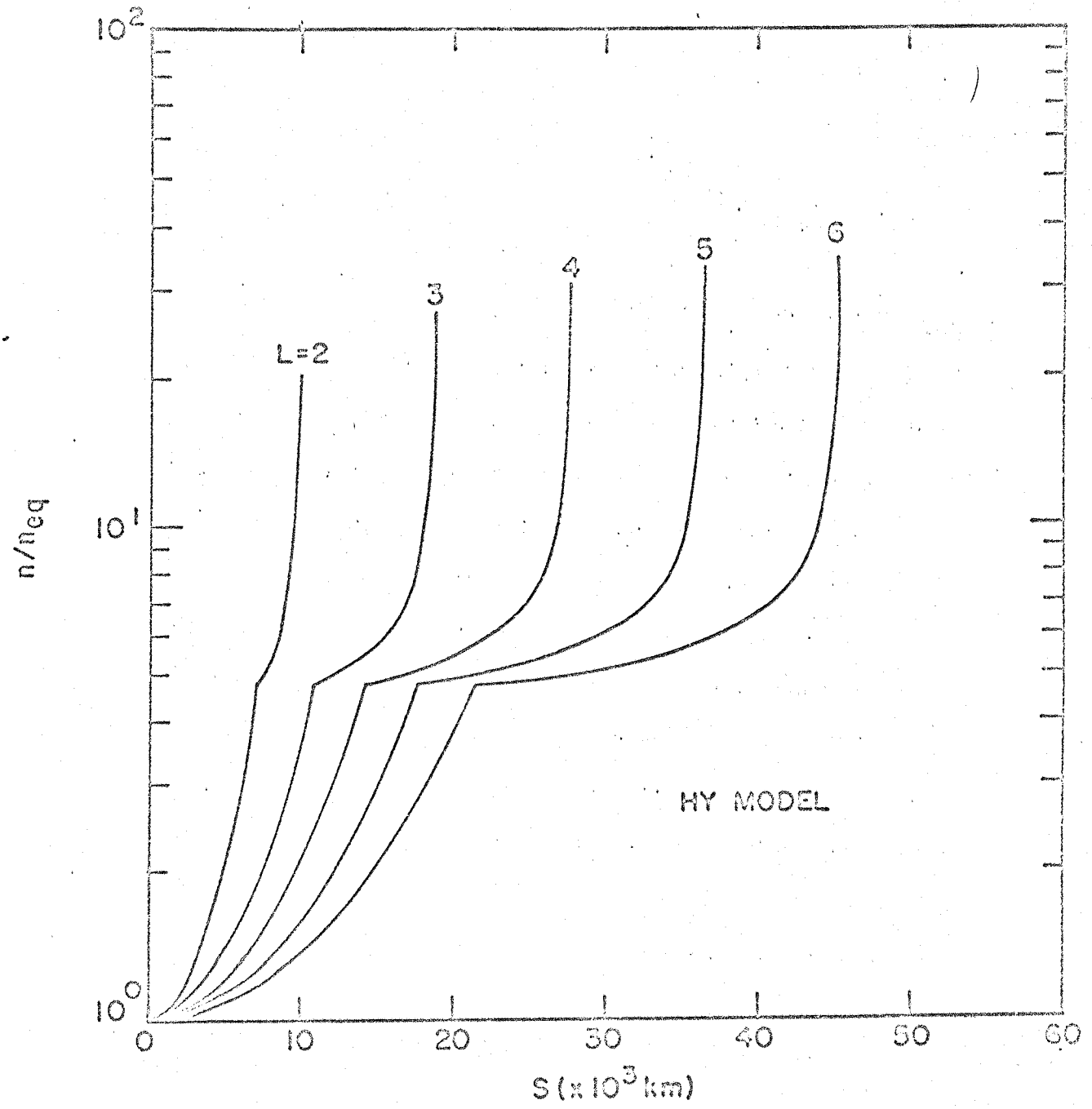

A plot of normalized electron concentration in a format similar to that of 4/12(a) but according to a hybrid model (see the text for details).

Fig. 4/12 (c)

(Rycroft and Alexander, 1969; Alexander, 1971). Using data from the Alouette I and Injun III satellites it has been shown that the electron density, hydrogen ion concentration and temperature at 900 km altitude may be represented by polynomials of the form:

$$P = p_o + p_1 G^2 + p_2 G^4 + p_3 G^6 \qquad 4.2/11$$

where G is the geomagnetic latitude.

The oxygen ion concentration is given by an exponential of the form:

$$Q = \exp(q_o G - q_1) \qquad 4.2/12$$

to which is added a portion of a sine curve below 15^o latitude to form an equatorial peak in the concentration. This is of the form:

$$q_3(\sin(q_4(G-15)/57.2957795))^2 \qquad 4.2/13$$

The helium ion concentration is obtained from the difference between unity and the sum of the oxygen and hydrogen ion concentrations.

The difference between the SD and WN models, which are taken to be the extremes for normal magnetospheric conditions, is in the value of the coefficients p_n and q_n, which are listed by Alexander (1971). Fig. 4/12 shows how the electron density in the magnetosphere varies according to the various models.

4.2.5 Model ducts and plasmapause

Included in the ray tracing program described by Alexander (1971), which has been used extensively in the course of this research are models of the plasmapause and magnetospheric ducts. The duct is represented by a field aligned enhancement of electron density, the cross section of which is a gaussian curve superimposed upon the normal electron density. The equation of the gaussian is given by:

$$I = E \exp(-0.5 \chi^2) \qquad 4.2/14$$

where E is the fractional enhancement of the duct at its centre

I is the fractional increase in electron density at any other point on the duct

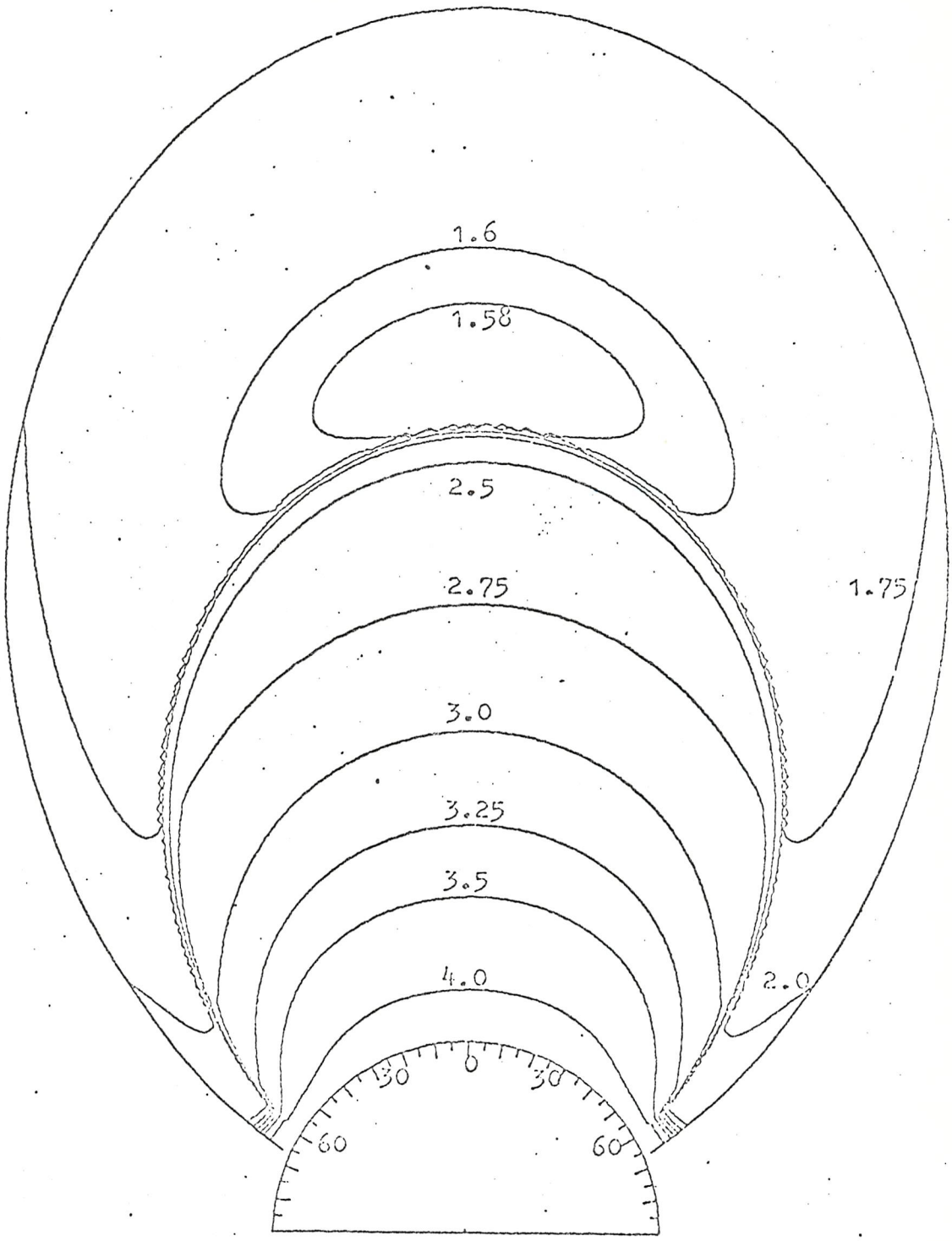

Winter Night Model

Contours of Log_{10} (electron density), plasmapause included.

Fig. 4/12 (d)

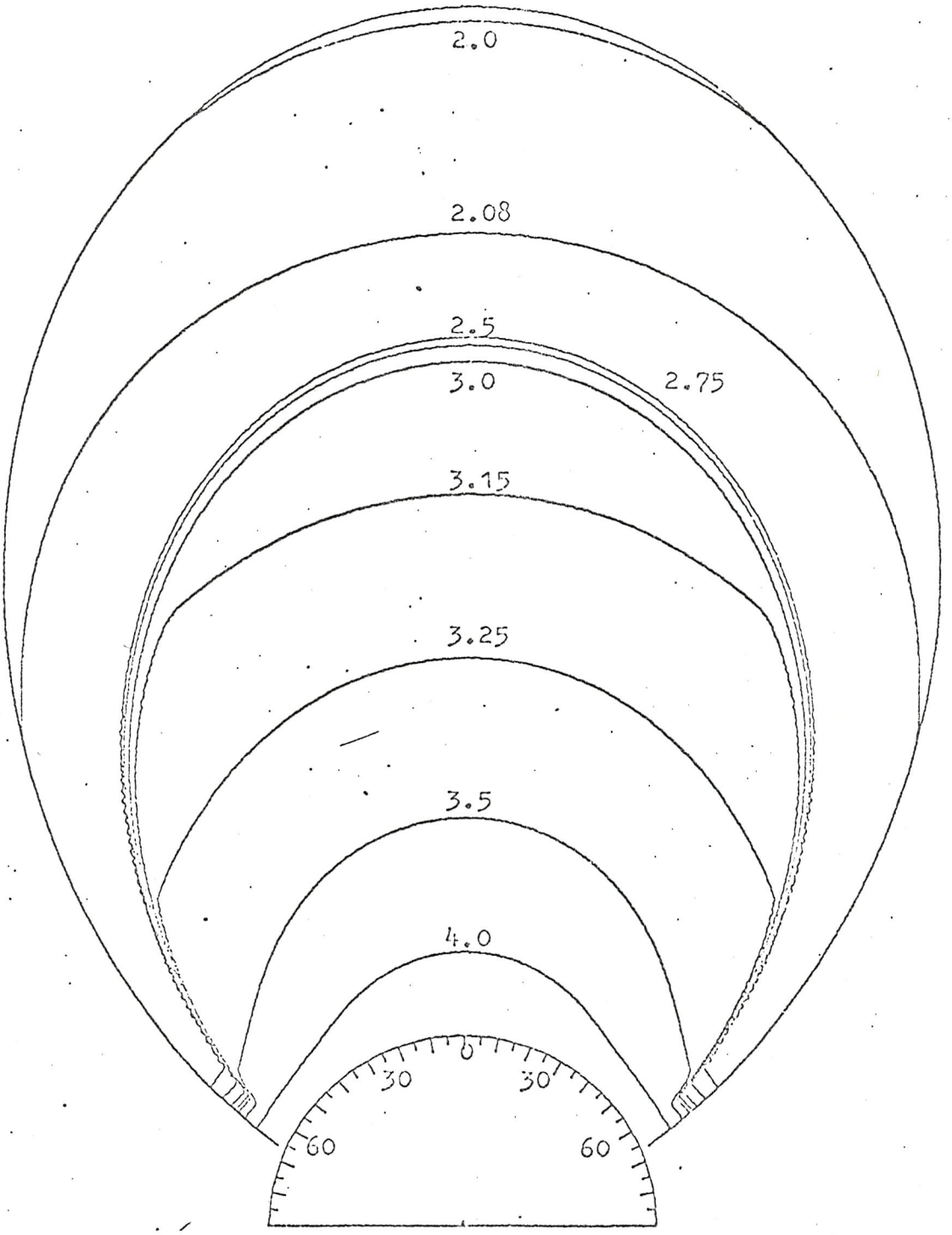

Summer Day Model

Contours of Log_{10} (electron density), plasmapause included

Fig. 4/12 (e)

and χ is given by

$$= \frac{\text{distance from duct centre}}{\text{duct width}}$$

The distance from the duct centre and the duct width are given in terms of latitude at the reference altitude. This ensures that the duct is field aligned and that the duct width varies as the distance between the field lines varies. As defined the duct width is the standard deviation of the gaussian shaped enhancement; a duct width of 30 km at the reference altitude ($\sim$180 km in the equatorial plane (as observed by Angerami (1966)) has been used throughout this research.

The model plasmapause is formed by smoothly decreasing the H^+ and He^+ concentrations at the base level by two orders of magnitude over an L value range of 0.3 in the region of the trough in the electron density; the position of this trough is related to the position of the plasmapause (Rycroft and Thomas, 1970). This results in a plasmapause in which the electron density falls by a factor of ten in the equatorial plane, while remaining the same at the base level This model of the plasmapause produces a more realistic result than would be obtained by reducing the electron density by a factor of ten at the base level since the latter does not allow for the gradual formation of the plasmapause as the altitude increases. The width of the model plasmapause in the equatorial plane is 0.3 R_E, which is a reasonable value at times when the plasmapause is at an L value of around 4. However there is reason to believe that the width of the plasmapause is less than this at disturbed times when the L value of the plasmapause decreases (Chappell, Harris and Sharp, 1970).

A more realistic model of the plasmapause has also been used in which the electron density in the equatorial plane decreases by a factor of 100 within a distance of 0.3 R_E, in better agreement with experimental observations (Carpenter, 1966). This is achieved by

squaring the smoothly varying function by which the H^+ and He^+ concentrations are multiplied at the base level resulting in a decrease in these parameters of four orders of magnitude.

4.3 Generation of VLF Emissions

Various mechanisms for the generation of VLF emissions have been postulated by a number of authors. A detailed review of the current theories has been presented by Rycroft (1972). In this section the fundamental concepts of these mechanisms are described; some of the refinements that have been suggested are also discussed.

All of the theories are based on a resonant interaction between VLF waves and fluxes of energetic charged particles in which energy is transferred from the particles to the waves. Following Brice (1964) the change in energy of a charged particle of charge q, moving a distance $\Delta\underline{s}$ at velocity $\underline{v}$ in time Δt in an electric field $\underline{E}$ and magnetic field $\underline{B}$ is given by:

$$\begin{aligned} \Delta W &= \underline{F} \cdot \Delta\underline{s} \\ &= q(\underline{E} + \underline{v} \wedge \underline{B}) \cdot \Delta\underline{s} \qquad 4.3/1 \\ &= q(\underline{E} + \underline{v} \wedge \underline{B}) \cdot \underline{v}\,\Delta t \\ &= q\,\underline{E} \cdot \underline{v}\,\Delta t \qquad 4.3/2 \end{aligned}$$

Thus, provided that $\underline{E}$ and $\underline{v}$ are in phase, there will be a net energy exchange between the particles and waves. The helical motion of a charged particle in a magnetic field may be described by two velocities, one parallel and one perpendicular to the magnetic field. If α is the pitch angle of the helix then $v_\perp = v \cos\alpha$ and $v_{//} = v \sin\alpha$. Thus there are two possible resonant conditions:

$$\begin{aligned} &\text{(i)} \quad \underline{E}_{//} \cdot \underline{v}_{//} = \text{constant} \quad \text{(longitudinal resonance)} \\ &\text{(ii)} \quad \underline{E}_\perp \cdot \underline{v}_\perp = \text{constant} \quad \text{(transverse resonance)} \end{aligned}$$

4.3/3

The above formulation is completely general and may apply to any charged particle under the influence of electric and magnetic fields. The remainder of this section will be concerned with the transvese resonance condition applied to electrons.

4.3.1 Transverse resonance

For transverse resonance the doppler shifted wave frequency seen by the electron should be equal in magnitude to the electron gyrofrequency and both should rotate about the geomagnetic field in the same sense. Since waves may only propagate in the whistler mode at frequencies less than the electron gyrofrequency, the waves and electrons must be travelling in opposite directions for this condition to be satisfied. In this case equation 4.3/3 becomes:

$$v_p = \frac{f_{B\,e} - f}{f} = - \gamma\, v_{\parallel} \cos\theta \qquad 4.3/4$$

where $\gamma = (1 - v_{\parallel}^2/c^2)^{-\frac{1}{2}}$

and θ is the angle between the wave normal and the magnetic field.

It is normally assumed that the electrons are non-relativistic (i.e. $\gamma = 1$). Thus writing $v_p = \omega/k$ and assuming longitudinal propagation (i.e. $\theta = 0$)

$$\omega_{B\,e} - \omega = - k\, v_{\parallel} \qquad 4.3/5$$

As a coherent collective effect this condition leads to the transverse resonance plasma instability. Fig. 4/13 shows the electron energies required for resonance along the L = 4 field line assuming a wave frequency of 5 kHz and longitudinal propagation (Brice, 1964). It may be seen that the energy required for resonance in the equatorial plane is around 10 keV, some two orders of magnitude less than that required at the foot of the field line. Since energetic electrons are generally more plentiful the lower their energy it is considered that resonance

is most likely to occur in the region of the equatorial plane (Helliwell, 1965).

Brice (1964) postulates a mechanism involving feedback between whistlers mode waves and electrons travelling in opposite directions. Doppler shifted cyclotron radiation from electrons travels back along the electron stream, phase bunching the incoming electrons and sustaining a coherent oscillation. By considering the energy transfer involved in the transverse resonance Brice (1964) has shown that the pitch angle of the electrons decreases. This decrease may be sufficient for the particles to be precipitated into the atmosphere and hence lost from the radiation belt. Thus the average longitudinal energy of the electrons remaining trapped becomes less than their average transverse energy, resulting in a pitch angle anisotropy.

One of the more complete theories of wave particle interaction in the magnetosphere is that due to Kennel and Petschek (1966), in which wave particle interactions are investigated, using the Maxwell-Vlasov equations for a plasma. It is shown that, since particles entering the loss cone are precipitated into the atmosphere, the steady state distribution of pitch angles must be anisotropic, and that since it is predominantly longitudinal energy that is lost, the anisotropy is of the appropriate sign for the transverse resonance instability. The subsequent growth rate of whistler mode waves is dependent upon the degree of anisotropy and the number of resonant particles. The generation of whistler mode radiation leads to pitch angle diffusion resulting in precipitation of particles into the atmosphere. For the pitch angle diffusion to be self sustaining the waves and particles that escape from the system must be replaced. Quasi-steady state conditions of continuous particle precipitation ("drizzle") may be established if the growth rate of the whistler mode energy is equal

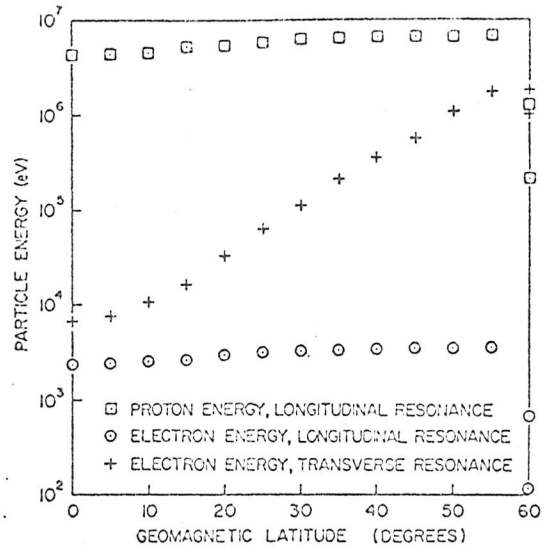

Particle energies required to satisfy the resonance conditions at different latitudes along a magnetic field line path.

Fig. 4/13

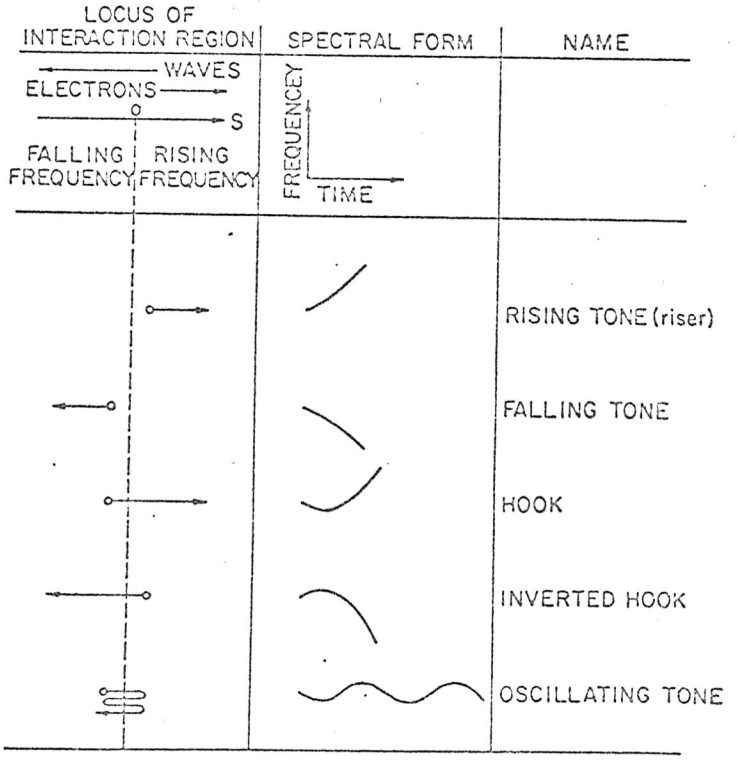

Classes of events and their explanation (HELLIWELL, 1967).

Fig. 4/14

to the rate at which the wave energy is lost by propagation away from the interaction region. Since this growth rate is proportional to the number of resonant electrons this requirement places an upper limit on the trapped electron flux; a large particle density gives rapid wave growth leading to rapid pitch angle diffusion and a subsequent loss of particles. Trapped particle fluxes predicted by this theory are found to be generally in agreement with satellite observations.

Another mechanism based on the transverse resonance instability is that due to Helliwell (1967). In his "consistent wave theory" the spatial variations of the electron gyrofrequency and doppler shifted wave frequency are required to be matched, enabling the wave to remain in resonance with the electron for a longer time. Unlike Brice's (1964) hypothesis, which considered a fixed interaction region, Helliwell's theory considers the movement of the interaction region. It is shown that the geomagnetic field gradient, and the feedback delay due to the finite wave and electron velocities, cause a characteristic rate of change of frequency, which depends on the initial frequency of instability and the position of the interaction region. Thus the spectral shapes of discrete VLF emissions may be explained in terms of the movement of the interaction region as shown in Fig. 4/14. It is found that the wave magnetic field is self-limiting, and that the limiting value B_w is independent of the particle flux. B_w is, however, found to be dependent on the energy spectrum of the electrons through a factor cot α, where α is the pitch angle of the electron; thus the limiting value of the wave magnetic field is dependent upon the anisotropy of the pitch angle distribution.

It has been shown (Kennel and Petschek, 1966; Rycroft, 1972) that for a given pitch angle anisotropy the electron energy, parallel to the earth's magnetic field, required for resonance, $W_{\parallel res}$, is proportional

to the magnetic energy per particle, $\frac{B^2}{2\mu_o N}$. Fig. 4/15 shows how $\frac{B^2}{2\mu_o N}$ varies with L value in the equatorial plane for (1) normal and (2) abnormal conditions with B decreased or N increased, or both. For curve 1) gyroresonance with high energy ($\sim$100 keV) electrons is possible and likely to take place at 2 kHz on or just outside the plasmapause. For curve 2) resonance with low energy ($\sim$10 keV) electrons is possible and likely to occur at $\sim$7 kHz just within the plasmasphere or at $\sim$3 kHz at more than 1 earth radius beyond the plasmapause (Rycroft, 1972). It may be seen that in both cases the energy required for resonance has a minimum just inside the plasmapause.

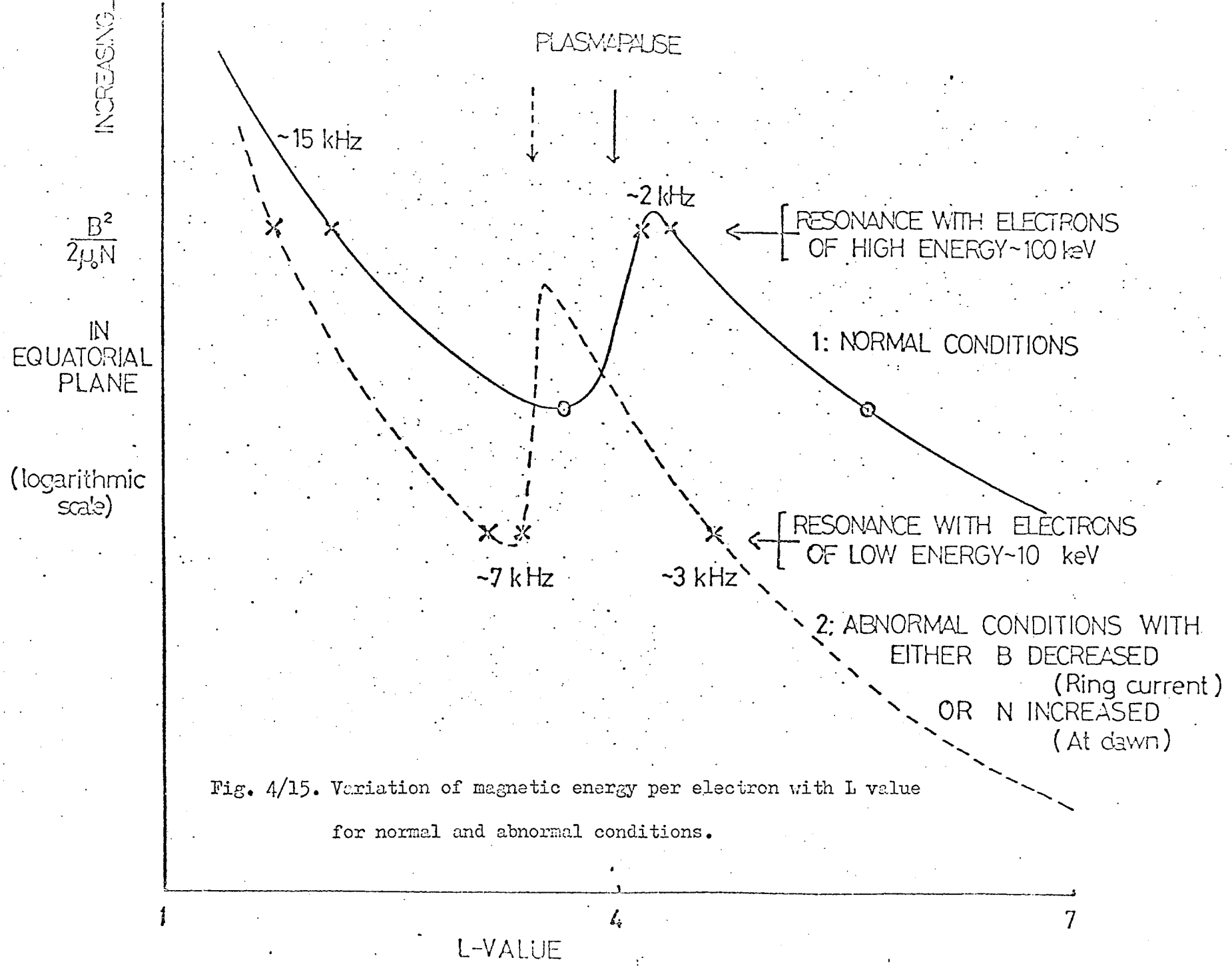

Fig. 4/15. Variation of magnetic energy per electron with L value for normal and abnormal conditions.

CHAPTER FIVE

Experimental Work

The majority of the work reported in this thesis is based on observations of natural VLF signals made during or shortly after the total solar eclipse of March 7th 1970 at a site close to St. John's, Newfoundland, Canada. The author has also made similar observations in Central Iceland during the period July - September 1969 as part of an investigation of the variation of VLF signals with latitude, to which reference has been made in section 1.4, and been involved in the running of the Southampton Radio Physics group's permanent station at Chilbolton, near Winchester. In all three cases the techniques used were the same. In this chapter the techniques employed to receive, record and analyse the VLF signals are described.

5.1 The VLF Receiving Equipment

5.1.1 The aerial

The VLF aerial, designed and built by Develco Inc. (Model 1002B), consists of a single turn loop of copper tubing forming a square of side 3 m. A single loop of insulated wire inserted in the copper tubing serves to calibrate the system. A known current flowing in this loop induces a signal in the aerial, enabling the entire receiving system to be calibrated, assuming a one to one coupling between the aerial and the calibration loop. A matching network and low-pass filter with cut off frequency 30 kHz are built onto the aerial and a preamplifier, contained in a separate sealed box is mounted on the structure of the aerial to minimise pickup in the low level signal. The circuit diagram of the aerial and preamplifier system is shown in Fig. 5/1. The signal from the preamplifier is fed to the receiver by a non-microphonic twin co-

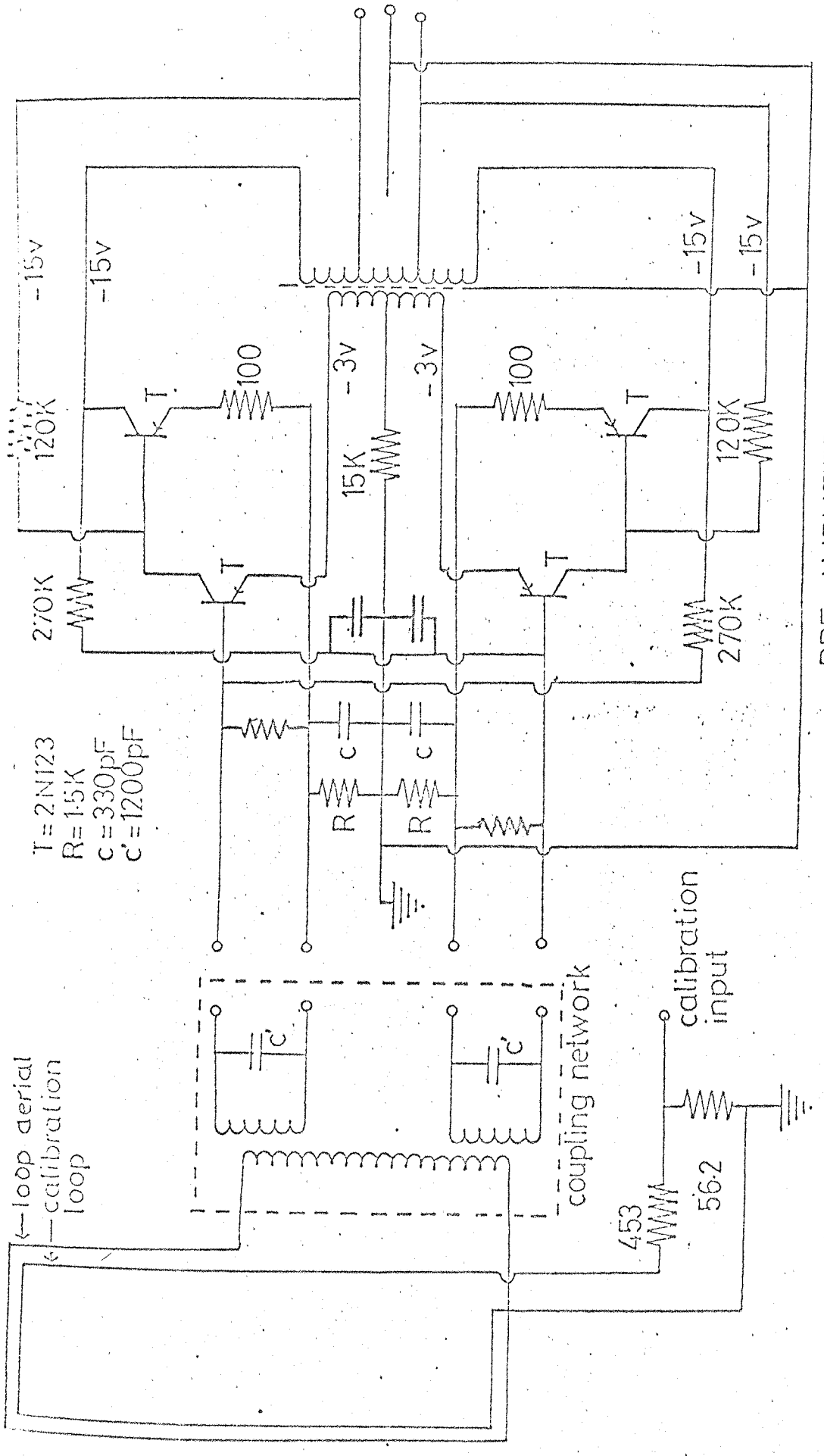

Fig. 5/1 CIRCUIT DIAGRAM OF AERIAL AND PRE-AMPLIFIER

axial cable, which also carries the d.c. power supply to the pre-amplifier.

The aerial is normally oriented so that its plane is in the magnetic East-West direction. Thus radiation propagating in the earth-ionosphere waveguide in the magnetic East-West direction is received preferentially. The e.m.f., ε, induced in a single loop by a magnetic flux, Φ, linking the loop is given by;

$$\varepsilon = - \frac{d\Phi}{dt} \qquad 5.1/1$$

Since the wavelength of the radiation is large compared to the dimensions of the loop the magnetic field of the wave may be considered uniform in the plane of the aerial. Thus

$$\Phi = A\,B\cos\Theta \qquad 5.1/2$$

where A is the area of the loop, B is the magnetic flux density of the wave and Θ is the angle between B and the normal to the plane of the loop. If the wave is considered to be travelling in free space then the magnetic flux density B is given by:

$$B = \mu_o H \qquad 5.1/3$$

where H is the wave's magnetic field strength.

The wave's electric field strength is given by:

$$E = \left(\frac{\mu_o}{\varepsilon_o}\right)^{\frac{1}{2}} H \quad \text{for the } TM_o \text{ mode.} \qquad 5.1/4$$

and hence E and B are related by the expression

$$E = (\mu_o \varepsilon_o)^{\frac{1}{2}} B$$

$$= cB \qquad 5.1/5$$

where c is the velocity of light in free space.

Hence $$\varepsilon = \mu_o A \cos\Theta \frac{dH}{dt} = \frac{A\cos\Theta}{c} \frac{dE}{dt} \qquad 5.1/6$$

5.1.2 The receiver

The VLF receiver, built to the design of Develco Inc., Model 2005,

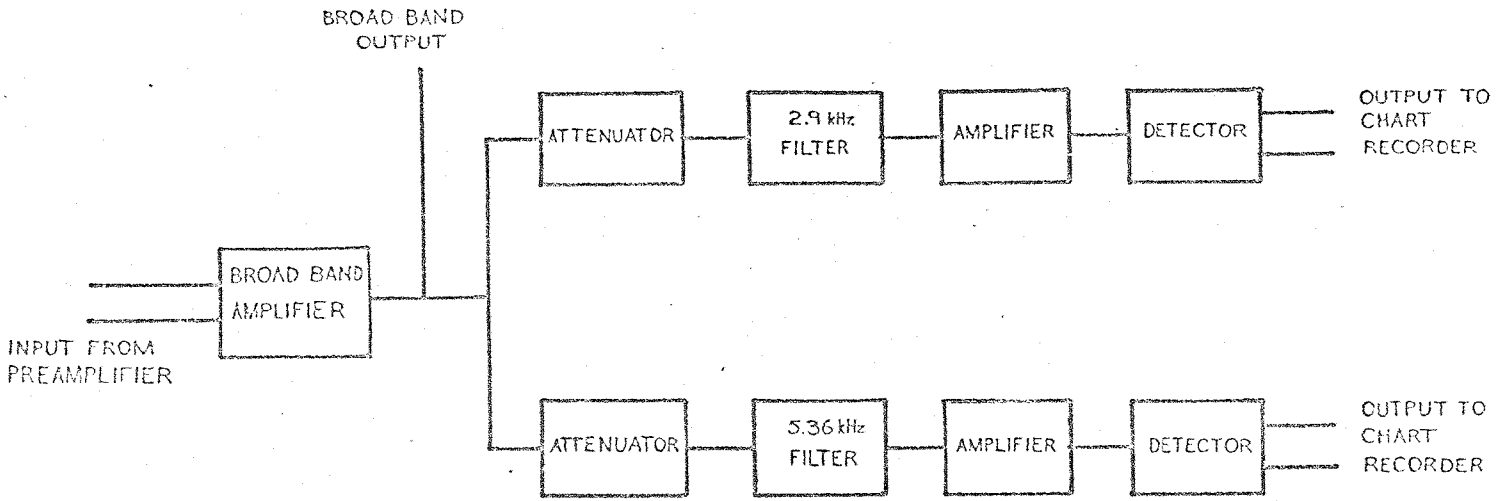

BLOCK DIAGRAM OF V.L.F. RECEIVER

Fig 5/2

is shown diagramatically in Fig. 5/2. The signal from the preamplifier is first amplified further by the differential input, broad band amplifier, which has a gain of 60 dB. The signal to be tape recorded is taken from the output of this amplifier. The frequency response of the aerial, preamplifier and main amplifier is shown in Fig. 5/3.

The receiver also incorporates two selective channels, by which the background signal level at two frequencies, 2.9 kHz and 5.36 kHz, may be monitored continuously using a paper chart recorder. Each channel comprises of a step attenuator, by which the signal may be reduced in steps of 10 dB up to a maximum of 70 dB, followed by a narrow pass band filter tuned to the appropriate frequency. The output from each filter is then amplified and passed through a dual time constant detector, whose function is to minimise the output due to impulsive signals from atmospherics. The d.c. output from the detector, which represents the background signal level at the channel frequency goes to a chart recorder. The frequency responses of the filters and amplifiers for the two channels is shown in Fig. 5/4.

5.1.3 Filters

Before the signal from the broad band output of the receiver may be tape recorded it is usually necessary to filter out unwanted, man-made signals. This is done using an L-C low pass filter, tuned to around 18 kHz in conjunction with a series of twin-T narrow band reject filters. The frequency to which these filters need to be tuned depends on the location of the receiving site. In Britain four twin-T filters are usually needed, tuned to 50 Hz and 150 Hz (to remove interference from a.c. mains), 16 kHz for the GBR transmissions from Rugby, and 200 kHz for the BBC radio 2 transmissions. The Omega transmissions at 10.2, 11.3, 12.5, 12.6 and 13.6 kHz are not filtered and may provide useful absolute timing information. The circuit diagram of the filter network used in Britain is shown

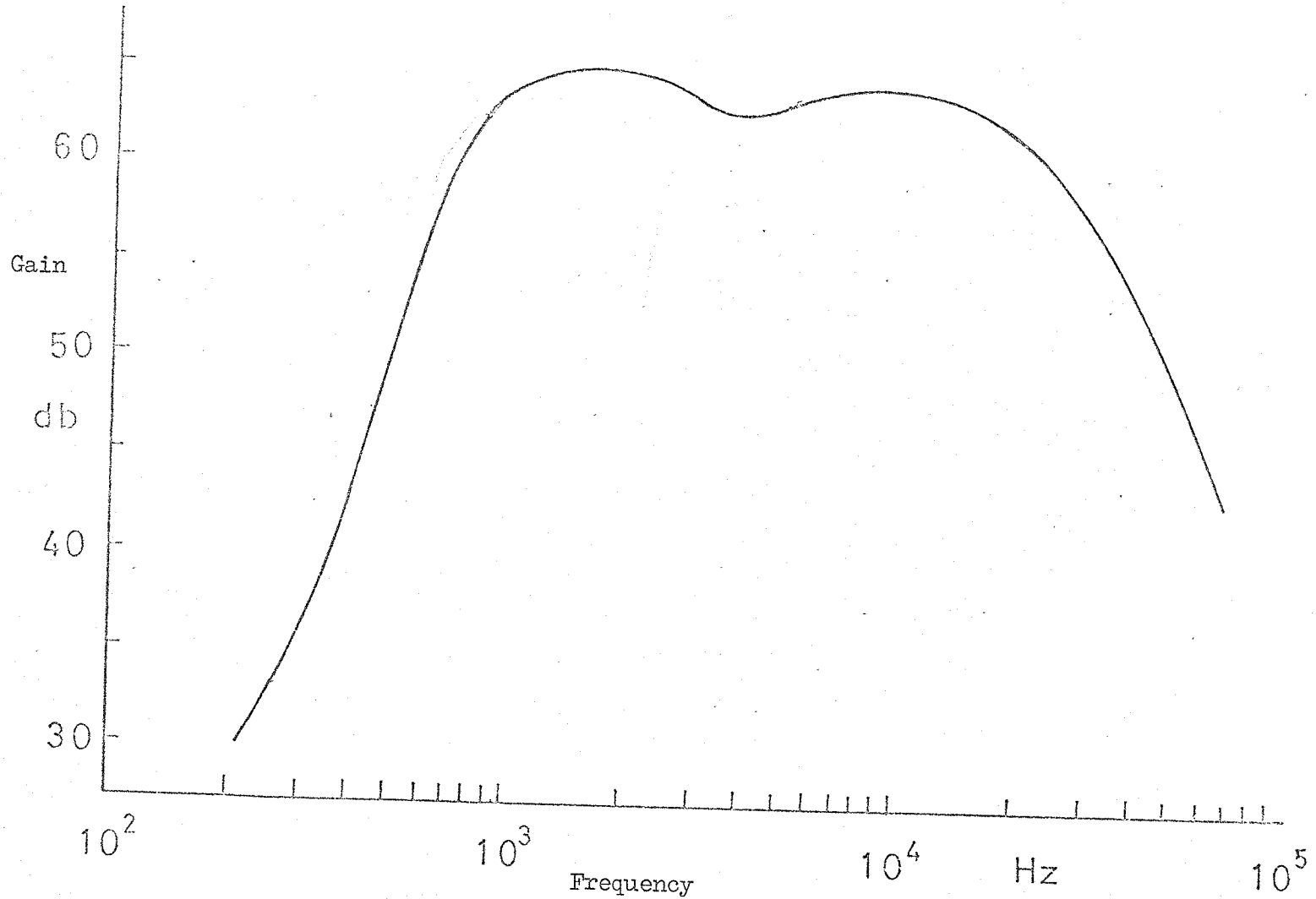

Fig. 5/3 . Frequency response of Develco receiver.

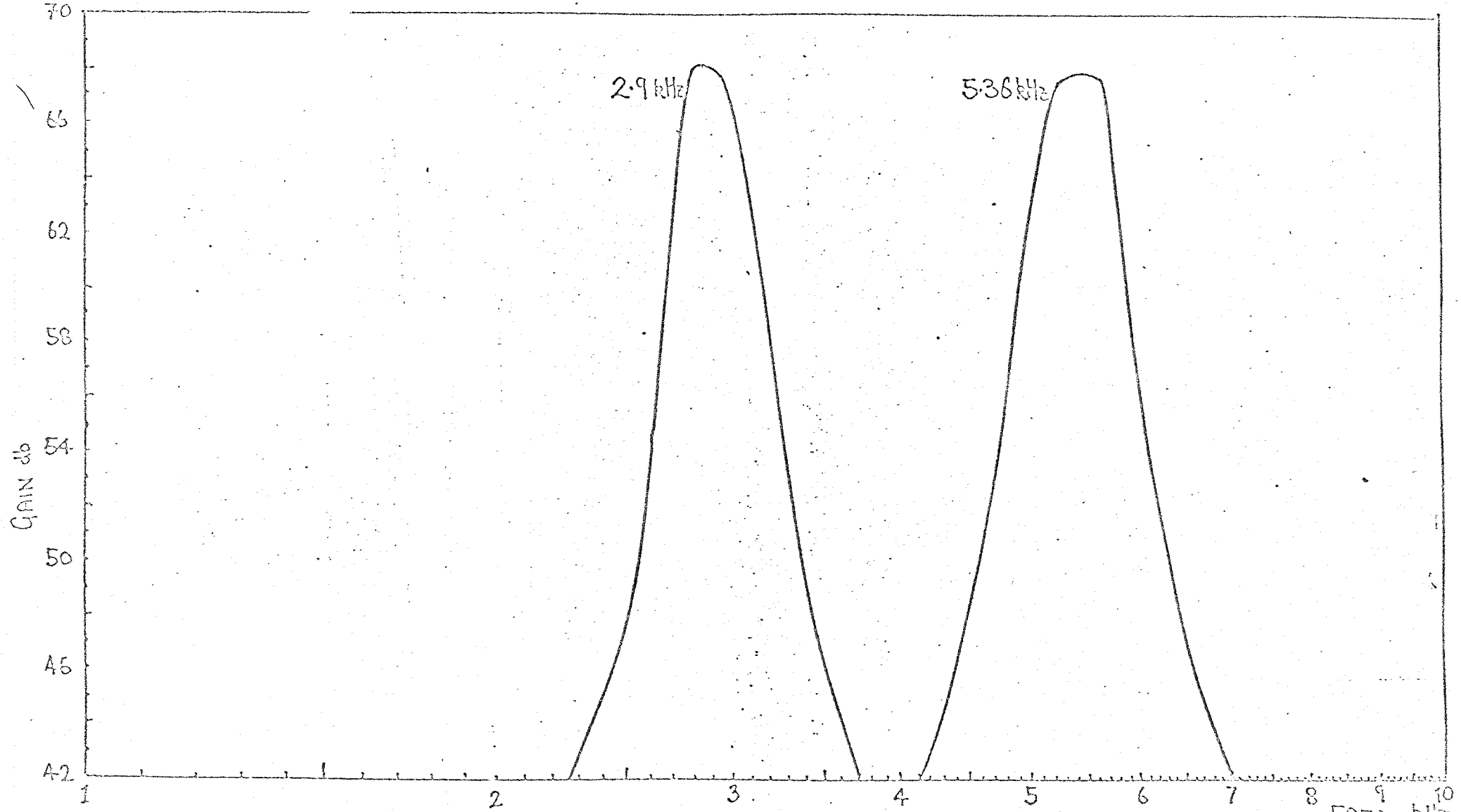

Fig. 5/4 Frequency response of selective channels in VLF receiver

in Fig. 5/5. The frequency response of the network is shown in Fig. 5/6.

When receiving at the site near St. John's, it was found necessary to include some extra filters as well as retuning the mains filters to 60 and 180 Hz. The additional filters were tuned to 17.8 kHz for the powerful NAA transmissions from Cutler, Maine, 100 kHz for Loran, and 112.6 kHz for a local navigational aid station, situated some 200 m from the aerial; even with this filter the equipment recorded a 2.8 kHz tone lasting 0.5s every 20s, which provided useful timing information. Since each filter also tends to attenuate all frequencies slightly it was found necessary to include an extra broad band amplifier after the filter network. A Levell, Type TA605, amplifier was used for this purpose.

In Central Iceland, a supremely quiet site some 100 km from the nearest habitation, the only filters found to be necessary were the low pass, GBR and sometimes the BBC radio 2 filters.

5.1.4 Recording

The broadband signal from the receiver is passed through the filter network described in the previous section and recorded on magnetic tape at a tape speed of 7.5 ips. The tape recorder used was a Lockheed model 417, four track recorder. In Britain the recordings were usually made using an Akai Model XV, at a tape speed of 3.75 ips.

The d.c. output from the two selective channels was recorded, using a three channel galvanometer-type paper chart recorder (Evershed and Vignoles, Model QT801), the paper chart being driven by a clockwork motor, usually at 2.5 cm h^{-1}, although at times the faster speed of 2.5 cm min^{-1} was used.

The operation of the dual-time constant detector has been investigated in detail by Adjepong (1972). The circuit is similar in design to the minimum reading circuit designed by Ellis (1959). It has a charging time constant of around 20 s and a discharge time constant of around 5 ms. Thus

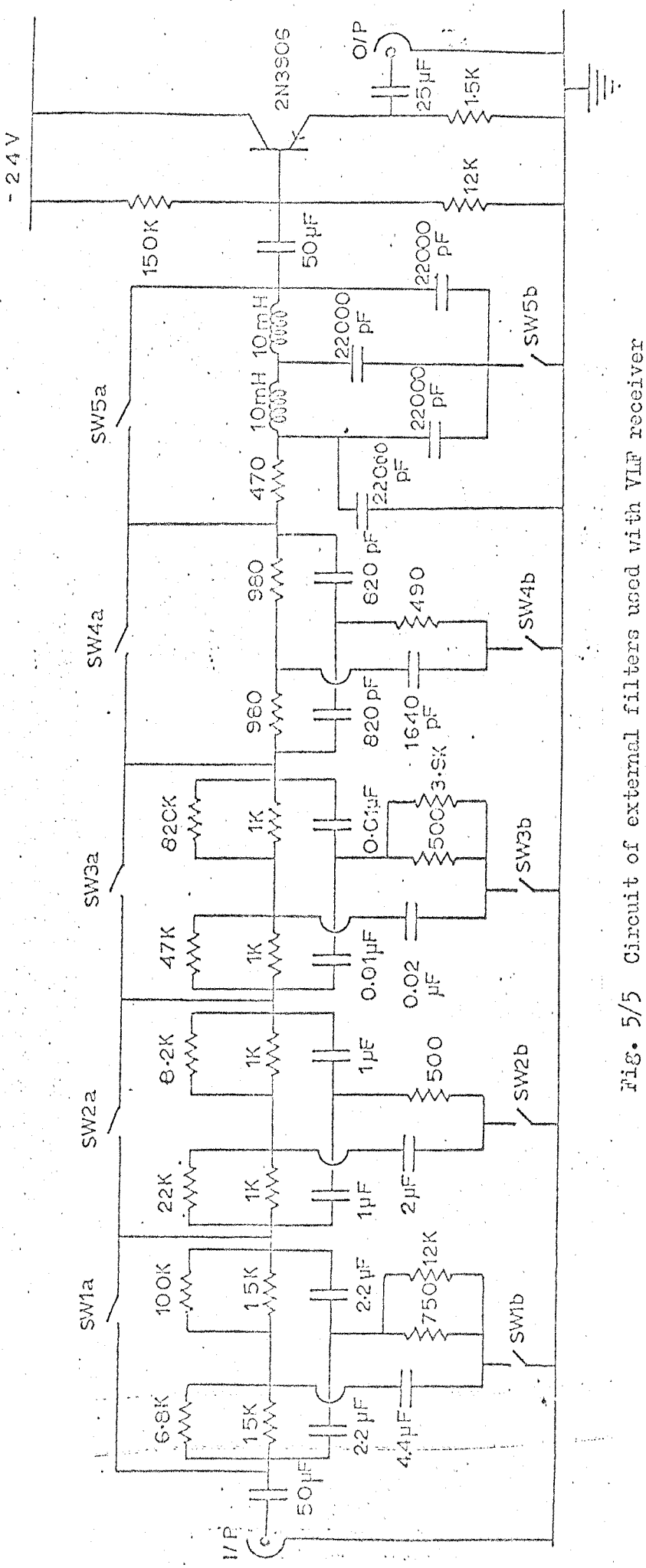

Fig. 5/5 Circuit of external filters used with VLF receiver

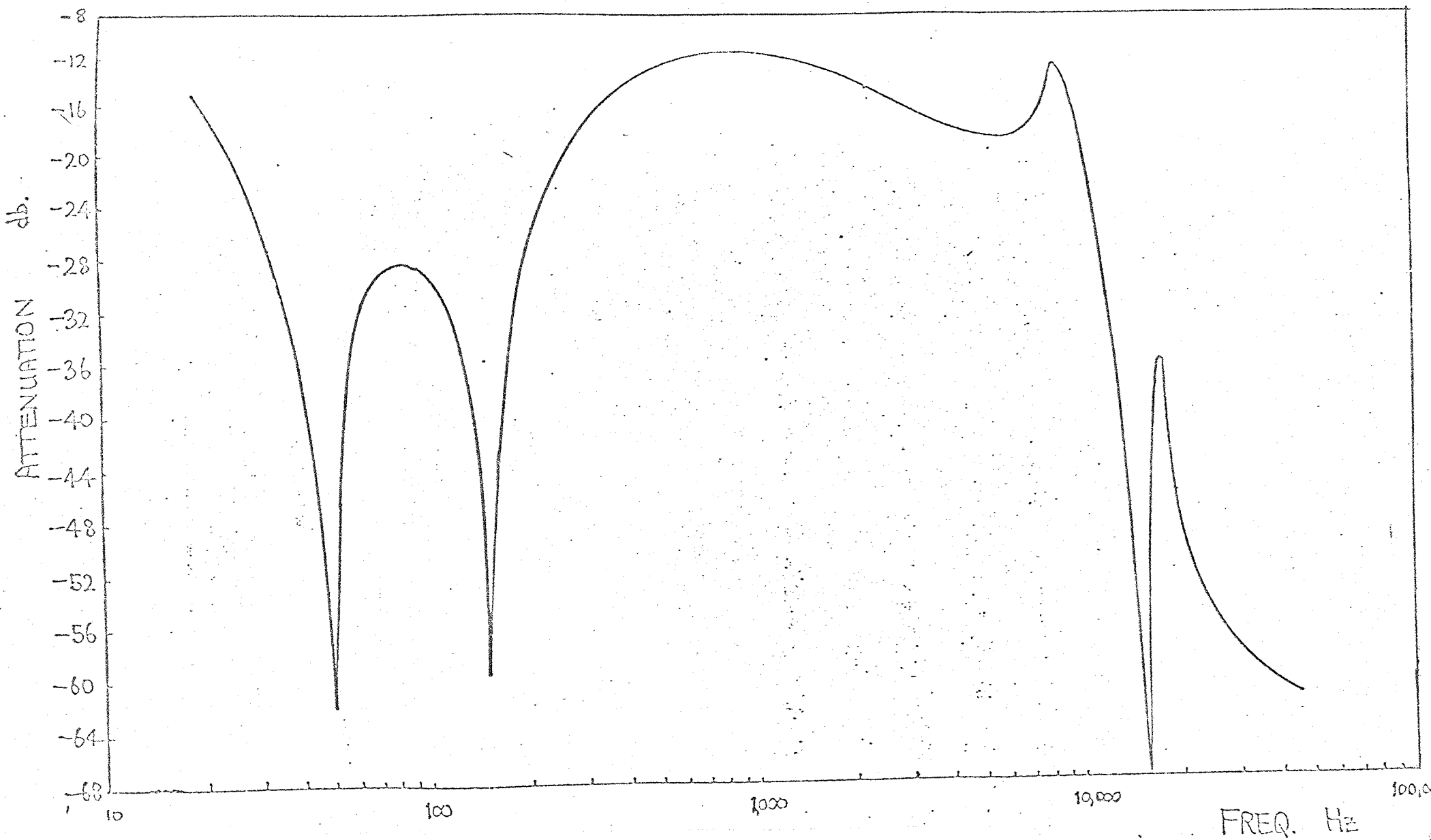

Fig. 5/6. Frequency response of external filters

it may provide a continuous monitoring of the background VLF signal level while remaining insensitive to impulsive signals such as atmospherics, which have a duration of a few milliseconds. It was found that the insensitivity of the detector to impulsive signals depends on their duration and rate of occurrence. If the impulsive signal is repeated very rapidly it tends to resemble white noise and may be integrated by the detector. It was found that the detector was insensitive for repetition rates below around 20 sec^{-1}; however Malan (1963) has shown that the repetition rate of atmospherics can be as high as 200 sec^{-1}.

The values of 2.9 and 5.36 kHz were chosen for the selective channels because the former is close to the centre of the chorus band at middle latitudes and the latter is within the hiss band at middle latitudes. Since both of these types of signals are non transient and may last for periods of an hour or more they are detected preferentially by the circuit and are displayed on the chart as a marked deviation from the normal diurnal trend.

5.1.5 The system as a whole

A block diagram of the entire VLF recording and receiving system is shown in Fig. 5/7. A single, integrated circuit amplifier and loudspeaker are included as shown for monitoring purposes. The system is designed to be operated at sites remote from the a.c. mains supply to minimise interference. The receiver, filters and audio amplifier are powered by 12 volt lead-acid accumulators and the tape recorders have their own rechargeable nickel-cadmium batteries.

5.2 Data Analysis

The methods of analysis of the transient VLF signals that are the subject of this thesis may be divided into two main categories. These are:

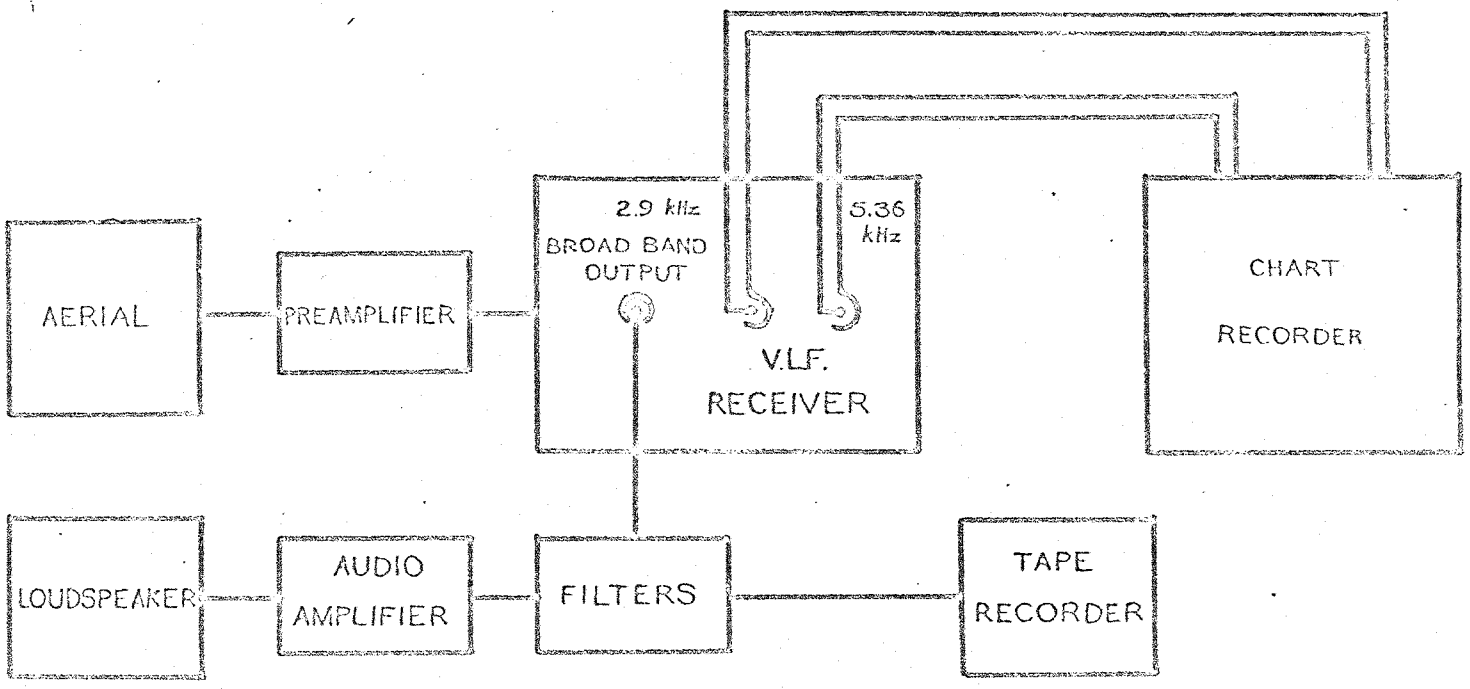

SCHEMATIC DIAGRAM OF V.L.F. EQUIPMENT

Fig. 5/7

(i) Analysis of the signal waveform.

This may be done in several ways. The waveform may be reproduced using a cathode ray oscilloscope, either with storage facilities or using a triggered camera; similarly the waveform may be reproduced using an ultra-violet light oscillograph. The waveform may also be transformed into digital form, using an analogue to digital converter, sampling at twice the maximum frequency of interest. The information may then be stored on punched paper tape or on magnetic disc or tape for analysis on a digital computer. All but the last of these techniques have been used to some extent in the course of this work.

(ii) The dynamic spectrum.

The dynamic spectrum is a frequency-time plane representation of the VLF signal. There are a number of machines that will produce dynamic spectrums but possibly the best known is the Kay Elemetrics Sonagraph. The dynamic spectrum produced by the sonagraph is known as a sonagram. The particular model that has been used extensively during this work is the 7030A 'Vibralyser', which is capable of producing spectra in the range 1 Hz - 16 kHz. Since this piece of equipment has been so extensively used there follows a short description of its operation.

First the frequency range of interest must be specified. There are eight ranges available from 1 Hz - 100 Hz to 160 Hz - 16 kHz. The machine also has the capability of expanding any portion of any range to cover the sonagram, if required. The frequency range chosen fixes the length of signal that may be analysed at one time. The frequency range is inversely proportional to the signal length such that using the usual 80 Hz to 8 kHz range the signal length is 2.4s. The signal to be analysed is recorded on a magnetic loop within the sonagraph. It is then reproduced continuously at a speed of 300 rpm, which is 12

times faster than the recording speed for the 8 kHz range. The signal is then passed through a low pass filter with a cut off frequency of 96 kHz (12 x 8). The output from this filter is mixed, in a balanced modulator, with a signal whose frequency varies between 200 kHz and 296 kHz as the stylus which traces out the sonagram moves from the bottom of its travel to the top. The output of the modulator, which consists of sums and differences of the oscillator frequency and heterodyned signal frequencies is then passed through a narrow pass band filter with a centre frequency of 200 kHz. The 200 kHz output of this filter, is amplified to a high voltage and fed to the stylus. This marks the sonagram paper, which revolves on a drum at the same speed as the magnetic loop, by passing a current through it to the metal drum. The sonagram paper is current sensitive; thus a three dimensional frequency-time-amplitude representation may be obtained. The fundamental dynamic range of the sonagram is 10 dB; however using the AGC circuit this may be improved to 40 dB if required.

Another machine somewhat similar to the Sonagraph is the Spectran. This analyses in real time unlike the sonagraph, and produces the spectrum as recorded by a bank of four hundred filters on 35 mm film. The Rayspan is useful for studying long sections of data but lacks the resolution necessary for the detailed frequency-time plane analysis required in this research.

5.3 Observations in Central Iceland

As stated in section 1.4 the work carried out in Central Iceland during the summer of 1969 formed part of an experiment to study the variation with latitude of VLF emissions. Accounts of these experiments have been given by Case et al (1970) and Reeve and Rycroft (1971). The equipment used was the VLF system as described in the previous sections

together with two flux gate magnetometers recording fluctuations in the vertical and horizontal (N-S) components of the earth's magnetic field on two channels of a chart recorder.

A recording schedule was established such that on certain pre-arranged days simultaneous recordings would be made in Iceland and at the other two stations, on South Uist in the Outer Hebrides and at Chilbolton near Winchester. Although many VLF emissions were recorded in Iceland during August and September none at all were received at the other two stations. In view of this and the many interesting observations made during and after the total solar eclipse of March 7th 1970, analysis of the data recorded in Iceland has been somewhat neglected to date. Some preliminary analysis has been made however. This will be discussed in the following paragraphs.

The geographic and geomagnetic coordinates of the three stations are shown in table 5.1. Chilbolton (L = 2.39) will be situated inside the plasmapause (L $\sim$ 4) under all but extremely disturbed conditions; South Uist (L = 3.38) will usually be inside but may sometimes be outside depending on magnetic activity and local time, while Jokulldalur (L = 6.17) will almost always be outside the plasmapause (Carpenter, 1966; Rycroft and Thomas, 1970). In view of the barrier-like nature of the plasmapause to VLF waves (Alexander, 1971) it is not altogether surprising that there should be a lack of correlation between the signals received at Jokulldalur and at the other two stations. Table 5.2 shows the three-hourly K_p indices for July, August and September 1969. Observations were started on July 30th and ended on September 5th. It may be seen that during this period magnetic activity was relatively low (max. K_p = 6) and although magnetic activity generally shows a 27 day period the activity towards the end of August did not compare with that on July 26 - 27 and September 28 - 30.

Station	Geographic Lat.	Long.	L value
Chilbolton	51.15°N	1.42°W	2.39
South Uist	57.35°N	7.27°W	3.38
Jokulldalur	64.72°N	18.07°W	6.17

Table 5.1 Coordinates of the three stations.

GEOMAGNETIC ACTIVITY INDICES

JULY 1969

DAY		K_p THREE-HOUR RANGE INDICES 1 2 3 4 5 6 7 8	SUM	C_i	C_p	A_p
1	D	2+ 2+ 5 2 3+ 2+ 4 3-	24	1.0	0.9	17
2		3 3- 1+ 1- 1- 0+ 0+ 1	10	0.2	0.3	6
3	Q	1- 1- 0+ 1 1- 1 1- 1+	6+	0.1	0.1	3
4	QQ	1- 0+ 0+ 1- 1- 0+ 0+ 1	4+	0.1	0.0	3
5	QQ	0+ 1- 0+ 1- 0+ 0+ 0 1	4-	0.1	0.0	2
6		1- 0+ 1- 1- 2- 2- 1 2	9-	0.3	0.1	4
7		1 2- 1- 1+ 2- 2+ 1+ 2-	12-	0.3	0.2	6
8		1 1 1 1- 1 1+ 2 2	10	0.1	0.2	5
9		3- 2 2 1 2- 2- 1+ 2-	14	0.4	0.3	7
10		2- 2+ 1- 2- 3- 1+ 1 2+	14-	0.5	0.3	7
11		2 1- 1 1- 1 1+ 3- 2-	11	0.3	0.2	6
12		3 2+ 3 1+ 2- 1+ 3- 4	19+	0.7	0.7	12
13	D	3- 3+ 3 3+ 2 2 4- 2+	22+	0.8	0.8	14
14	D	2+ 5- 2+ 2- 3+ 2 2 2	20+	0.8	0.7	13
15		1+ 1+ 2- 1+ 1+ 1- 1 2	11-	0.3	0.2	5
16		1+ 3 2- 3 2- 3 3 2-	18+	0.6	0.6	10
17	Q	1+ 1+ 1 1- 1 1 1 1-	8	0.1	0.1	4
18	Q	0 0+ 1 1+ 2 1- 1- 0+	6+	0.1	0.1	3
19	QQ	0+ 1- 1+ 0+ 0+ 0+ 0+ 0+	4	0.0	0.0	2
20	QQ	1- 1- 1- 1+ 1 1 1- 0+	6+	0.2	0.1	3
21		1+ 0+ 1- 0+ 1 2- 2- 2	9	0.3	0.2	4
22		2- 2- 2+ 1 2- 2+ 2- 3-	15	0.4	0.4	7
23		1 1- 0+ 1+ 0+ 2 3- 2	10+	0.3	0.2	5
24	Q	1+ 1- 1+ 0+ 1 1 1 1	8-	0.1	0.1	4
25	Q	1- 2- 1 1- 1- 1- 1 1+	8-	0.1	0.1	4
26	D	2- 2 1- 3+ 6- 3 2- 5-	23-	1.3	1.0	20
27	D	7 6+ 6 2+ 3 1+ 4- 1+	31	1.3	1.5	45
28		1+ 1 2 1- 0+ 1- 1- 1+	8	0.2	0.1	4
29	QQ	1- 0+ 0+ 0+ 0+ 0+ 1 0+	4-	0.1	0.0	2
30		2- 1- 1- 1+ 1+ 4 5- 3	17+	0.8	0.7	13
31		3- 1+ 1+ 1- 2- 1+ 1+ 2-	12	0.3	0.3	6
			MEAN	0.39	0.34	8

A preliminary storm sudden commencement occurred on July 26 at 1153 UT.

Table 5/2 (a)

GEOMAGNETIC ACTIVITY INDICES

AUGUST 1969

DAY		K_p THREE-HOUR RANGE INDICES 1	2	3	4	5	6	7	8	SUM	C_i	C_p	A_p
1	QQ	1-	1	0+	1-	1	1-	1-	1-	6-	0.1	0.1	3
2	Q	0+	0	0+	0+	2	2	2+	2+	10-	0.3	0.2	5
3	D	2	2	2-	3-	3-	3	4	4-	22-	0.9	0.8	14
4		4-	3+	2	3-	2+	3+	1+	3-	21+	0.8	0.7	13
5		2	3	2-	2	2+	1+	1	1-	14	0.4	0.4	7
6	Q	3-	2+	1+	1	1-	1-	1-	1-	10	0.2	0.2	5
7		2-	2	2-	2+	2	1	3-	3-	16	0.6	0.4	8
8		1+	1-	2	3+	3-	2	2-	3	17-	0.5	0.5	9
9		3	3+	2+	2-	3+	2+	2	2	20	0.6	0.6	11
10		2-	2+	2	3	2-	2-	0+	0	13-	0.2	0.3	6
11	QQ	0	1-	0+	1	1	1	1+	2-	7	0.2	0.1	4
12	D	4-	3+	3+	4	4	4	3+	2+	28	1.2	1.1	21
13		2-	2-	3-	3-	0+	1	1	2	13	0.4	0.3	7
14		1+	1+	3-	2+	1+	2-	1+	0	12	0.3	0.3	6
15	Q	0+	0	2-	0+	1+	2-	1+	2+	9	0.3	0.2	4
16	Q	0+	0	1-	1+	1-	1	1-	3-	7+	0.3	0.1	4
17		4-	2	2-	1	0+	1-	1+	1-	11+	0.4	0.3	6
18		2+	1+	1-	1	3+	3-	1-	1	13	0.4	0.4	7
19	D	3-	2+	2+	3-	2+	3	3	4-	22	1.0	0.7	13
20		2	2+	3-	1+	1+	1	1	2	14-	0.4	0.3	7
21		1+	2+	0+	1-	2-	2-	2	2-	12-	0.2	0.2	6
22		1+	0+	0+	1+	1+	2-	3-	1+	10+	0.3	0.2	5
23		3	3+	2+	3-	2+	2	2+	2	20	0.7	0.6	11
24		2	2-	1+	2+	2	1	2	2-	14	0.4	0.3	6
25	QQ	3-	1+	0+	0+	0+	0+	0	1-	6	0.1	0.1	4
26	D	1-	1+	2-	5	4-	2-	2-	4-	19+	0.9	0.8	15
27	D	4	6	3+	3+	2	2	2-	2	24+	1.3	1.1	21
28		3-	2	1	1-	2	1	2-	1-	12-	0.4	0.3	6
29	QQ	1	1-	1-	1	1+	2-	1-	0+	7+	0.2	0.1	4
30	QQ	0	1-	2-	1	2	1-	1+	1-	8	0.2	0.1	4
31	Q	1	0+	2	2-	1	1	1+	1+	10-	0.2	0.2	5
										MEAN	0.46	0.39	8

Table 5/2 (b)

GEOMAGNETIC ACTIVITY INDICES

SEPTEMBER 1969

DAY		K_p THREE-HOUR RANGE INDICES 1 2 3 4 5 6 7 8	SUM	C_i	C_p	A_p
1	QQ	1+ 2- 1- 0+ 0+ 0+ 0+ 0+	5+	0.1	0.1	3
2	QQ	0+ 1- 1- 0+ 0+ 0+ 0 0+	3	0.1	0.0	2
3	Q	1- 0+ 0+ 1 1 1 3- 1	8	0.2	0.2	4
4	Q	1 2- 1- 1 1 1- 2- 1	9-	0.2	0.1	4
5		0+ 0+ 1 2- 4 5- 4- 5-	20+	1.1	1.0	18
6	D	4+ 5- 4- 4 2 3- 1+ 3	26-	1.1	1.0	20
7		2+ 2- 3- 4- 2+ 2+ 3 4-	22-	0.9	0.7	13
8		3+ 5- 5 4 2 2- 1 1-	22+	0.9	1.0	19
9		2- 2+ 3- 3- 2+ 3 1 2+	18	0.7	0.5	10
10		4- 2+ 0+ 0+ 1+ 1+ 2+ 3-	14+	0.5	0.4	8
11		3+ 2+ 2+ 2+ 2- 1 2+ 1	16+	0.5	0.5	8
12	Q	2- 2+ 1+ 2 1- 1- 1- 0	9+	0.1	0.2	4
13	QQ	0 1- 1- 1+ 0+ 0+ 0+ 0+	4	0.0	0.0	2
14		1 1+ 0+ 1 1 3- 4 4	15+	0.7	0.6	11
15		5- 4 4- 2 3- 4- 3 2-	25+	1.2	1.0	19
16		3- 3+ 2- 1+ 1 1- 1- 2-	13	0.3	0.4	7
17		1- 0 0+ 3+ 3+ 3+ 4- 3-	17+	0.8	0.7	12
18	D	3- 3 3 3- 3 5- 4+ 3	26+	1.0	1.0	19
19		3 4- 2 2 2 1 1 2+	17	0.4	0.5	9
20		2 2- 3- 2+ 2 3+ 2- 1-	16+	0.4	0.5	8
21	Q	2- 2- 1+ 1+ 1- 1 1- 1+	10-	0.1	0.2	5
22	QQ	1 1 1+ 1- 0+ 0+ 0+ 0+	5+	0.1	0.1	3
23		0+ 0+ 0+ 1- 3 2 2+ 3+	12+	0.6	0.4	7
24	Q	1+ 2+ 1+ 3- 1- 1- 1- 1+	11	0.2	0.3	6
25		2 3+ 3 1+ 2 3- 1+ 2	18-	0.6	0.5	10
26	QQ	1+ 1- 1+ 2- 0+ 0+ 0+ 1	7	0.1	0.1	4
27		0 0+ 0+ 0 1 1 1+ 4+	8+	0.5	0.3	6
28	D	3- 4- 3 7 6+ 4+ 4- 5	36-	1.7	1.5	47
29	D	3 4+ 6- 6+ 6 6 6- 7	44	1.8	1.8	71
30	D	8 7 6+ 7- 6 4 5+ 3-	46	1.8	1.8	90
			MEAN	0.62	0.58	15

Preliminary sudden commencements (ssc) occurred in September 1969 at 05/1334UT, 14/1518UT, 27/2125UT and 29/0453UT.

Table 5/2 (c)

The main type of VLF emission recorded at Jokulldalur was that known as polar chorus or polar hiss (Helliwell, 1965). These emissions are confined to the frequency band of 500 Hz - 2 kHz. Fig. 5/8 (a) and (b) show dynamic spectra of polar chorus and hiss, the main difference being that the chorus is structured, consisting of rising tones, while the hiss is unstructured appearing as band limited thermal noise. The emissions showed no correlation with magnetic activity at the time of the recording, polar chorus being received on the most disturbed day, August 27th, as well as on September 1st, one of the quietest days. The emissions also appeared at all times during the day between 0700 LT and 2100 LT, with a possible peak of occurrence around local noon.

Since all these emissions were below 2 kHz no deflection was observed on either of the selective channels. However on a few occasions emissions in the dawn chorus range, 2 - 4 kHz (Helliwell, 1965), were received. Fig. 5/9 shows the chart record for August 17 - 18 showing the appearance of a burst of noise on the 2.9 kHz chart coinciding with the recording of dawn chorus. Fig. 5/10 shows a sonagram of the VLF signal during this period. It may be seen that although there is some energy in the band 2 - 4 kHz the strongest signal is in the polar chorus band. Fig. 5/11 shows sonagrams of chorus recorded at Jokulldalur, South Uist and Chilbolton at different times. It may be seen that although each sonagram has a different time and frequency scale there is a good deal of similarity between them suggesting that similar mechanisms produce the emissions at different latitudes. Since, according to the transverse resonance instability theory of emission generation (Brice, 1964) the triggering frequency of the emissions must be equal to the doppler shifted equatorial electron gyrofrequency, a lower frequency emission would be expected at higher latitudes where the equatorial electron gyrofrequency is less than at lower latitudes.

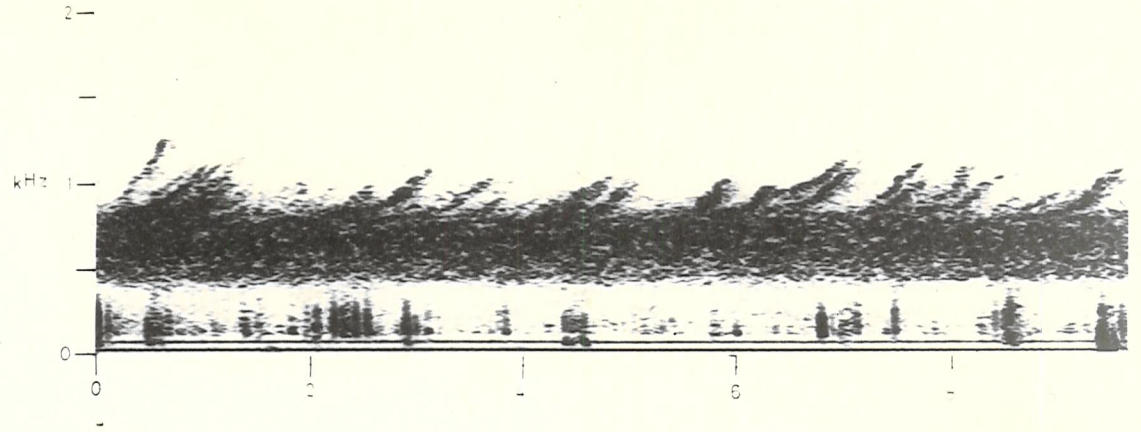

a) Polar Chorus.

Jokulldalur, Iceland. 18 August 1969. 1215 U.T.

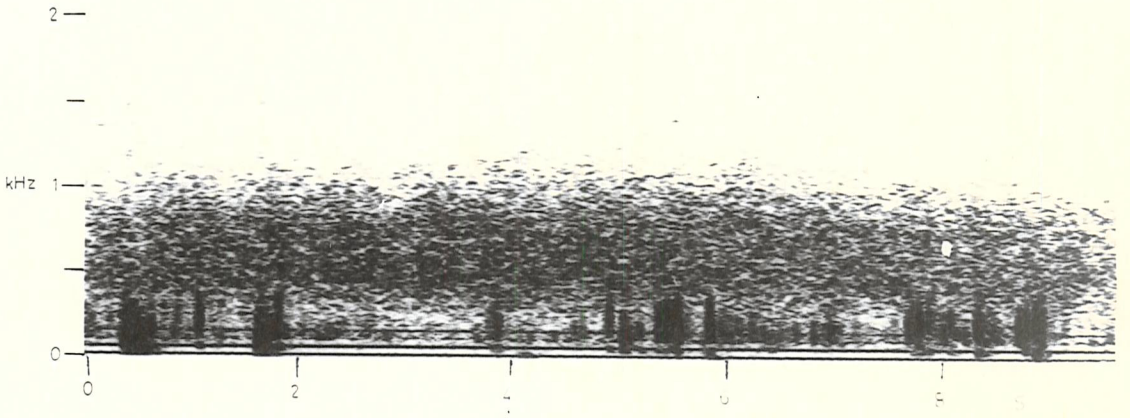

b) Polar Hiss.

Jokulldalur, Iceland. 20 August 1969. 1845 U.T.

Fig. 5/8

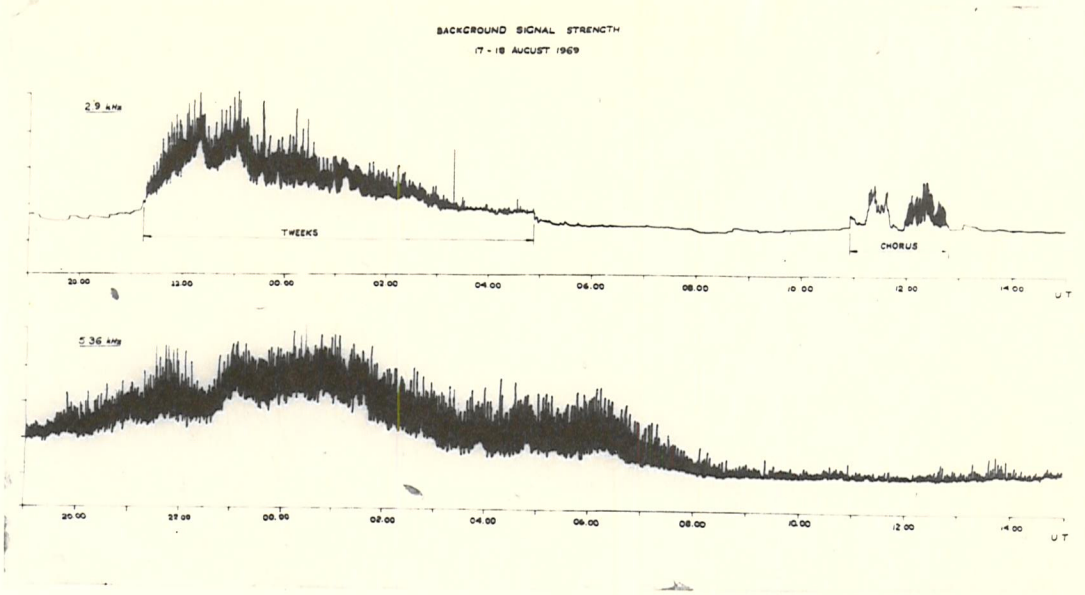

Fig 5/9 Background VLF signal strength at 2·9kHz and 5·3kHz recorded at Jokulldalur, Iceland, 17-18 August 1969.

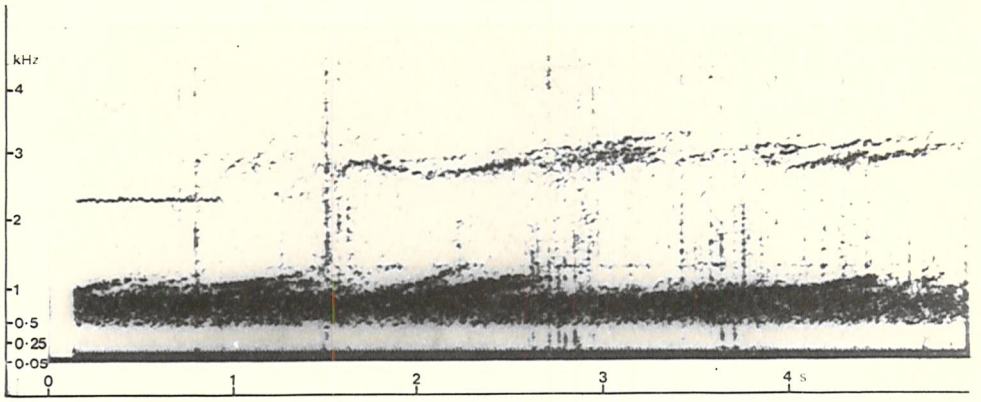

Fig 5/10 Sonagram of VLF waveform at 1215 U.T. 18 August 1969 recorded at Jokulldalur, Iceland.

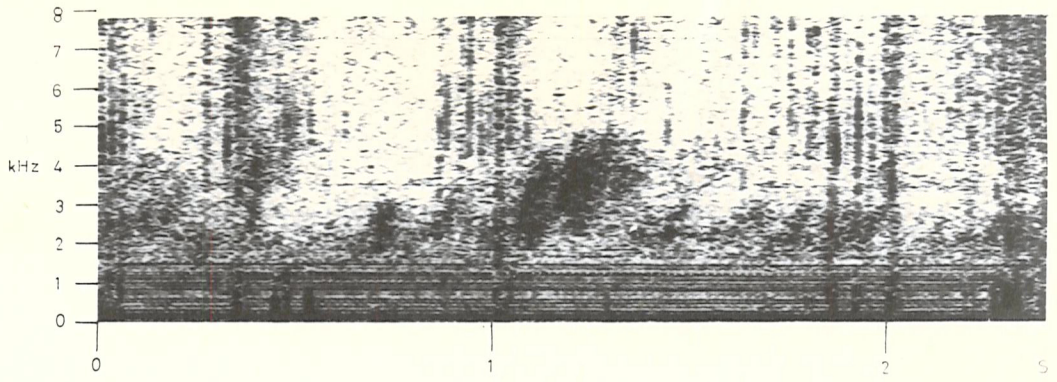

Chilbolton, Hampshire, England (L~2·4) 0330 U.T. 22 April 1970.

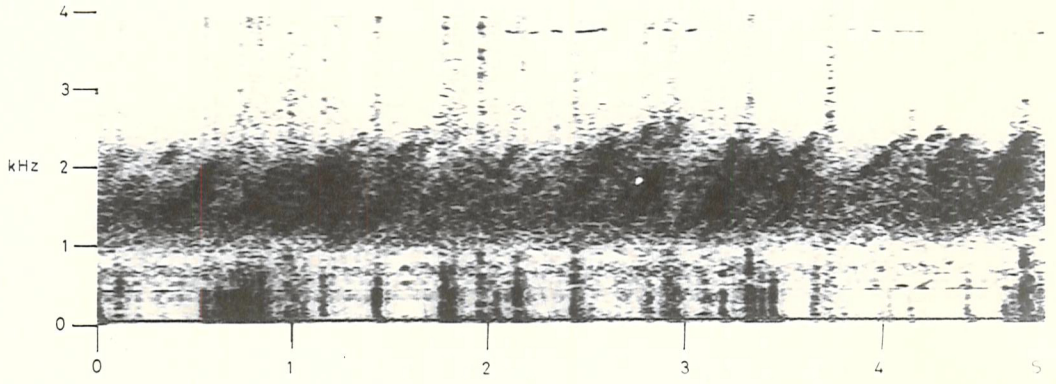

South Uist, Outer Hebrides, Scotland (L~3·4) 0650 U.T. 10 October 1969.

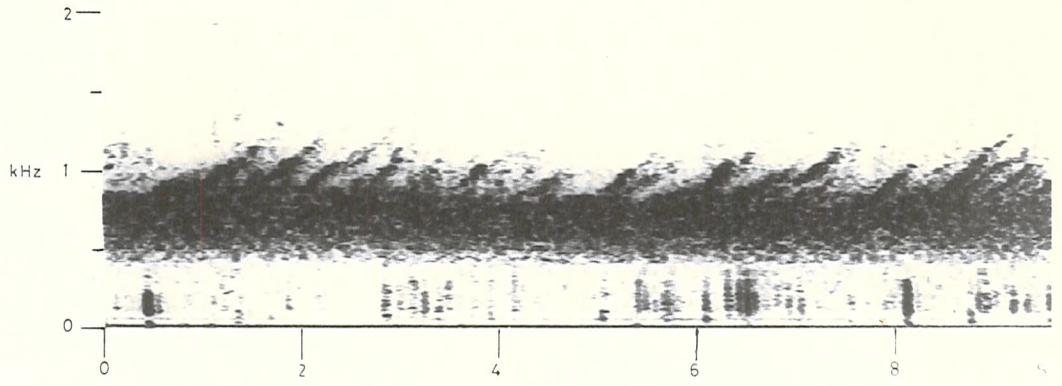

Jokulldalur, Iceland (L~6·2) 1215 U.T. 18 August 1969.

Fig 5/11 VLF CHORUS RECORDED AT VARIOUS LATITUDES.

This is in agreement with observed characteristics of the chorus emissions. In Fig. 5/12 sonagrams of some of the other emissions recorded at Jokulldalur are shown. It is hoped that further analysis of these data will be possible in the future.

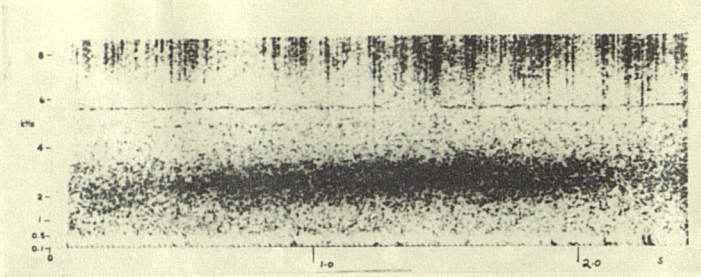

Unstructured Chorus, 0945 U.T.

27 August 1969.

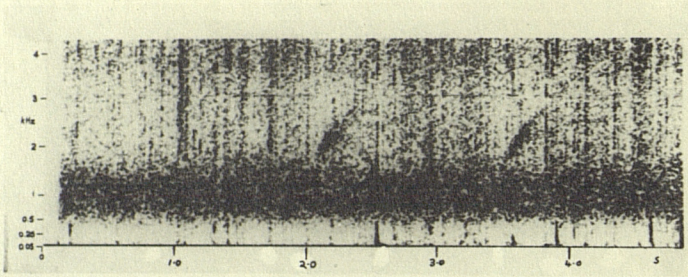

Hiss and risers, 1900 U.T.

20 August 1969.

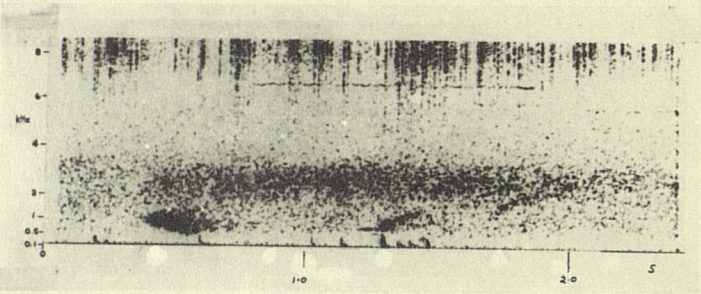

Chorus and emissions, 1145 U.T.

27 August 1969.

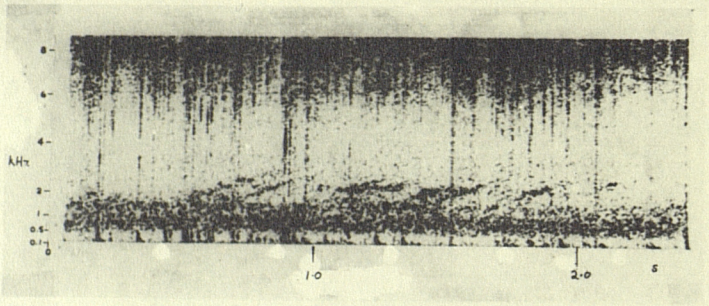

Hiss and risers, 1930 U.T.

20 August 1969.

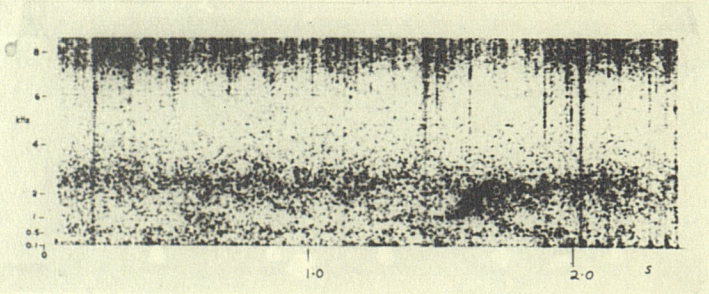

Hiss and emission, 1130 U.T.

27 August 1969.

Fig. 5/12 VLF emissions recieved at Jokulldalur, Iceland.

CHAPTER SIX

The Ionospheric D region during a solar eclipse as observed by natural VLF signals

6.1 Experimental Observations

Recordings of natural VLF signals in the band 0.5 kHz - 10 kHz were made by the author during the solar eclipse of March 7 1970 and on the preceding and following days at a site close to the STADAN station near St. John's, Newfoundland, Canada (geographic latitude $47^{\circ}44.9'$N, longitude $52^{\circ}43.4'$W, L = 3.46). The system used was that described in the previous chapter together with one flux-gate magnetometer recording fluctuations in the horizontal (N-S) component of the earth's magnetic field on the third channel of the chart recorder. Similar observations were also made by courtesy of Prof. M.G. Morgan, Dartmouth College, at Norwich, Vermont, U.S.A. (geographic coordinates $43^{\circ}45.0'$N, $72^{\circ}17.7'$W, L = 3.08) and by courtesy of Prof. T.R. Kaiser and Dr. K. Bullough, University of Sheffield, at Halley Bay, Antarctica, which is close to the magnetic conjugate of St. John's. The positions of the three stations and the path of totality of the eclipse at various altitudes are shown in Fig. 6/1. Near Newfoundland the path of the eclipse was approximately magnetic West-East. Since the aerial was mounted in the magnetic East-West plane it did not respond to signals propagating in the magnetic North-South direction. Therefore whistler mode signals propagating down field lines with their 'feet' in the eclipsed ionosphere were received preferentially since they would have to propagate in the magnetic East-West or West-East direction to the aerial.

Fig. 6/2 shows the chart record for the period 1500 UT March 7 to 0100 UT March 8 1970. The features of this record that are par-

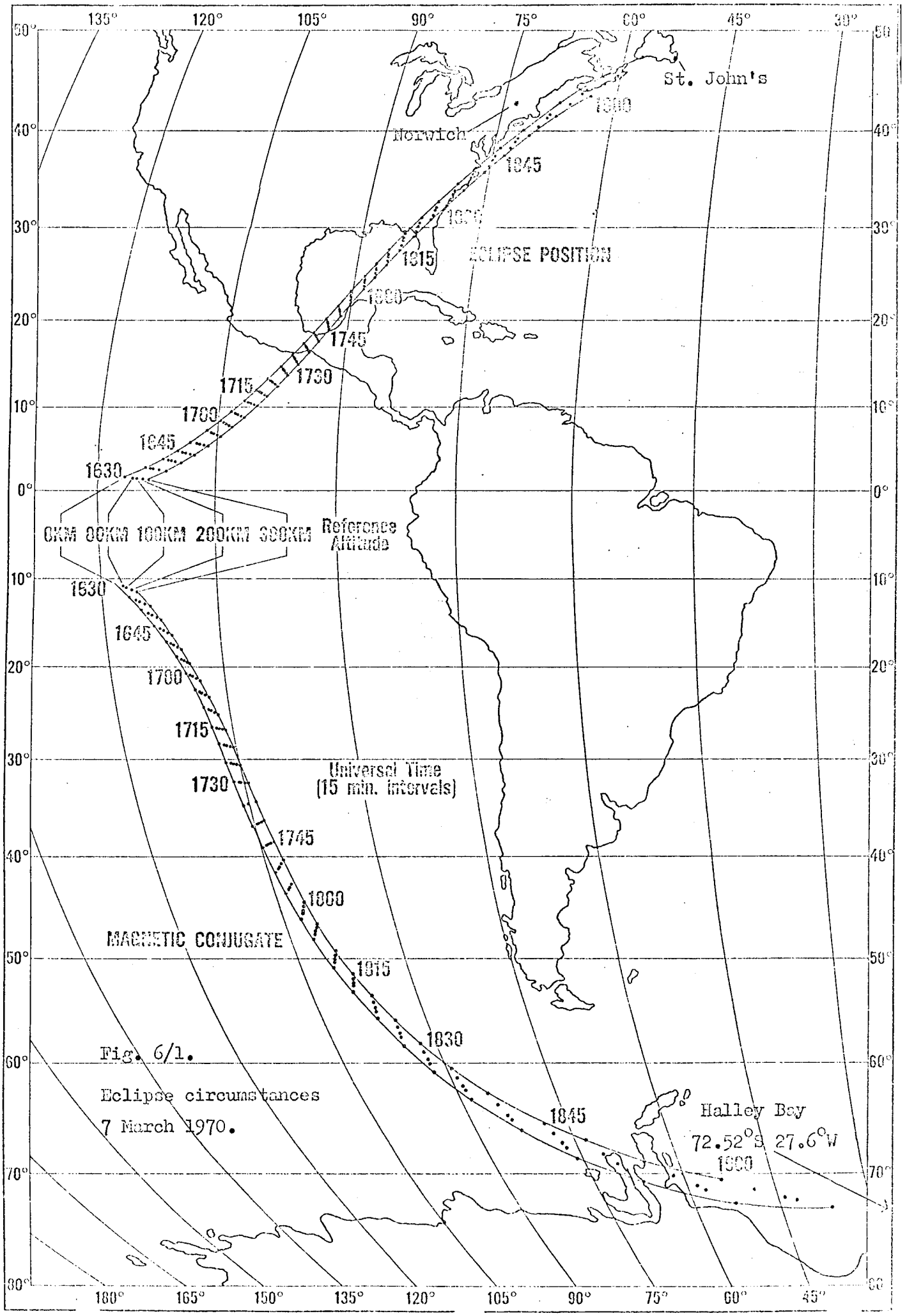

Fig. 6/1.

Eclipse circumstances
7 March 1970.

ticularly relevant to this chapter are the slight increases on both of the selective channels, with their maxima close to the time of eclipse maximum at the site. Some of the other features appearing on the record will be discussed in later chapters. A preliminary report of all VLF phenomena indicated on Fig. 6/2 has been presented by Rycroft and Reeve (1970). During the eclipse, which lasted from 1756:30 until 2009:08 UT at 80 km altitude above St. John's, with a maximum obscuration of 99.1% occurring at 1905:01 UT, two separate VLF phenomena were observed while aurally monitoring the signals. The first was that, throughout the eclipse, tweeks - that is sferics with sharp low frequency cut offs (Helliwell, 1965) - were occasionally audible. The second was a series of eighteen discrete risers (Helliwell, 1965), occurring within two minutes just before eclipse maximum at 80 km altitude. It is the tweeks that are the subject of this chapter; the risers will be discussed in the following chapter.

6.2 Analysis

6.2.1 Chart Records

Before proceeding to a detailed analysis of the tweeks the significance of the increase in the levels of the two selective channels will be discussed. The tweeks themselves could not be entirely responsible for these increases, although they may have contributed to them. Tweeks are essentially transient signals lasting a few milliseconds. Because of the effect of the dual time constant detector transient signals with a repetition rate less than 20 sec^{-1} would not be detected (Adjepong, 1972). In this particular case the occurrence of the tweeks was sporadic with periods of up to 30 seconds between events. It is clear, however, that very large transients produce spikes on the chart record as may be seen in Fig. 6/2 (upper trace) after 2200 UT. It is thus likely that the tweeks are responsible

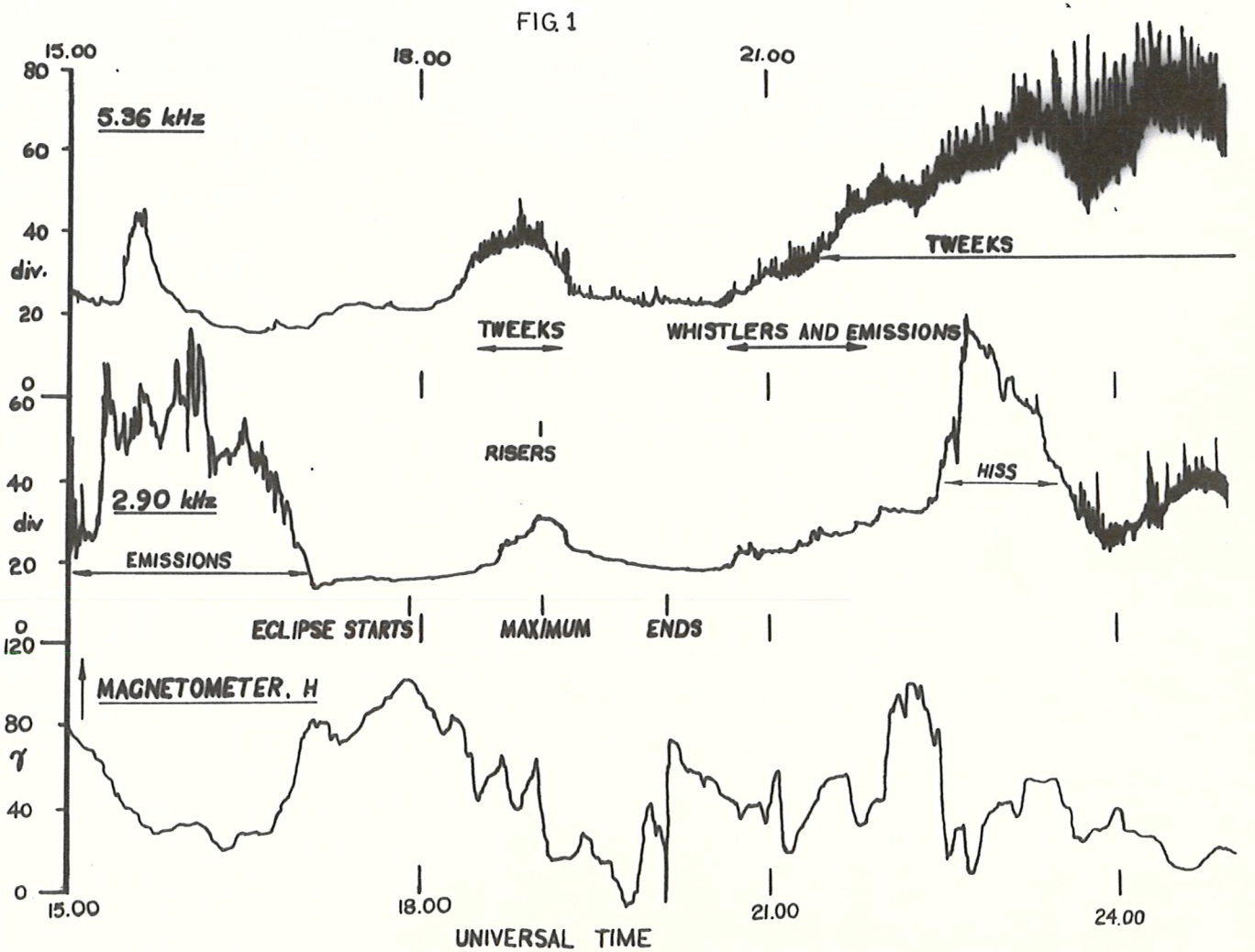

Fig. 6/2 Chart Record from St. John's, Newfoundland. 7 March 1970.

for the fine structure in the 5.36 kHz record around 1900 U.T.

Fig. 6/3 shows a typical chart record taken at South Uist at a similar L value to St. John's. It may be seen that, in the absence of VLF emissions there is a definite diurnal variation in the intensity at the two selected frequencies, the levels being around 10 db greater at night than during the day. This is in agreement with the results shown in Fig. 6/4, taken from Chapman et al. (1966). The reason for this difference is indicated in Fig. 6/5 (Deeks, 1966). At night the ionosphere is bounded by a sharp electron density gradient between 80 and 90 km, whereas during the day the boundary is less well defined. Hence at night the earth-ionosphere waveguide is closely approximated by a parallel side waveguide with perfectly reflecting boundaries, for which the absorption coefficient is low. During the day this approximation is not valid resulting in the higher attenuation coefficient.

The increase in the levels of the two selective channels may thus be interpreted in terms of the effect of the eclipse on the ionosphere. At quiet times the background VLF signal propagating in the waveguide mode is that due to remote lightning discharges which have a typical repetition rate (integrated around the world) of around 100 sec^{-1}, which is well above the threshold of the detector. Normally by day the attentuation for this type of signal is high (see Fig. 6/4). Under the effect of the total and partial eclipse the ionospheric D region electron density was modified so as to give less attenuation for these signals. Fig. 6/6 shows how the lower ionosphere is affected by a solar eclipse (Deeks, 1966). It may be seen that even at 80% obscuration the peak at around 62 km remains. It is only at 100% obscuration that it disappears leaving the sharp gradient at around 70 km.

The signals recorded at Norwich Vt. were replayed through the two selective channels to search for a similar effect. The maximum obscuration at 80 km above Norwich was 90.7% compared with 99.1% at

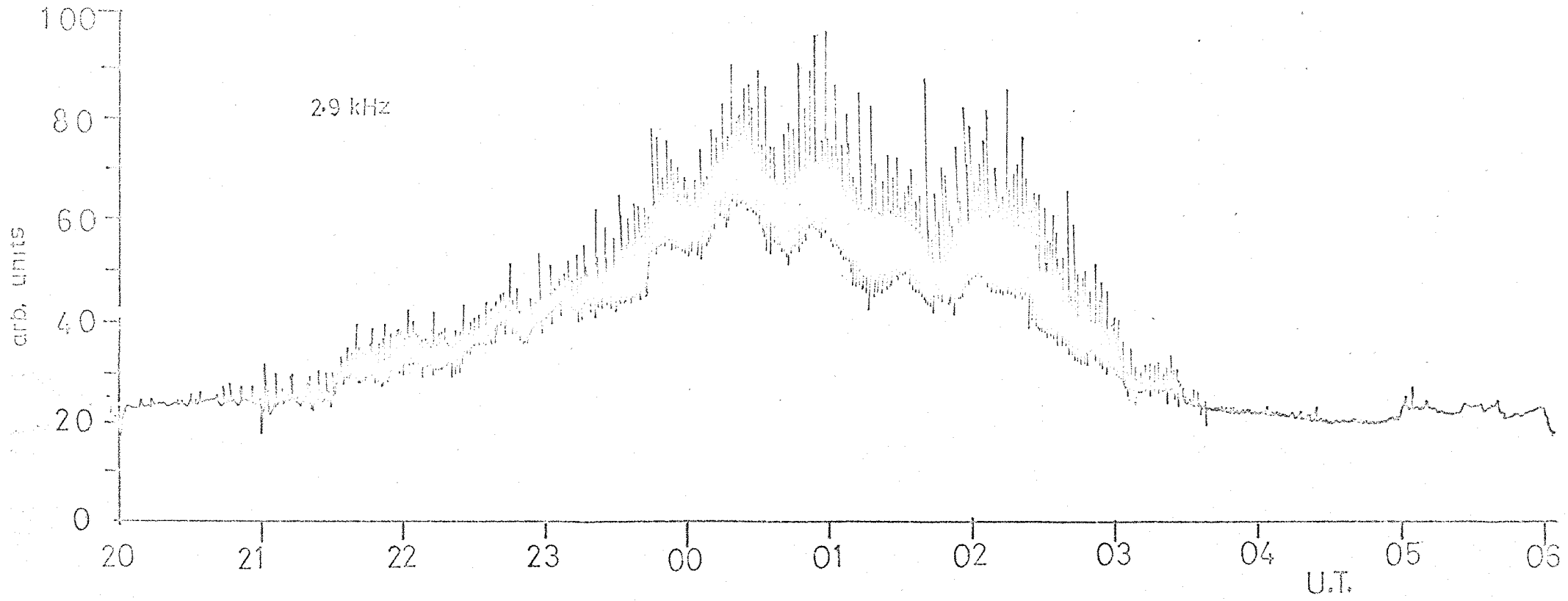

Fig. 6/3 Chart record from South Uist 3 - 4 July 1968 showing typical diurnal variation.

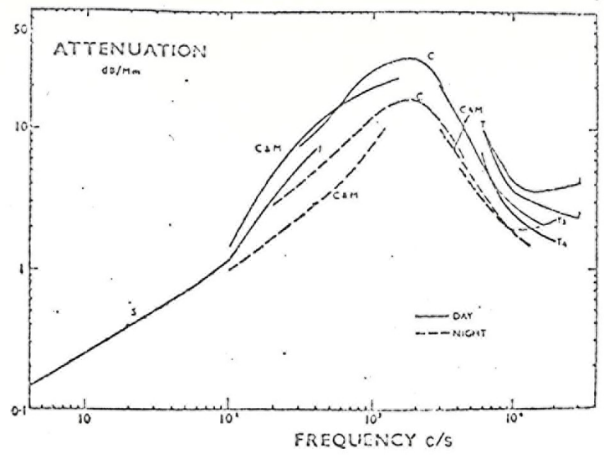

Variation of attenuation with frequency. S, from Schumann Resonances; C and M, Chapman and Macario; C, two-station observations; T, Taylor and Lange.

Fig. 6/4.

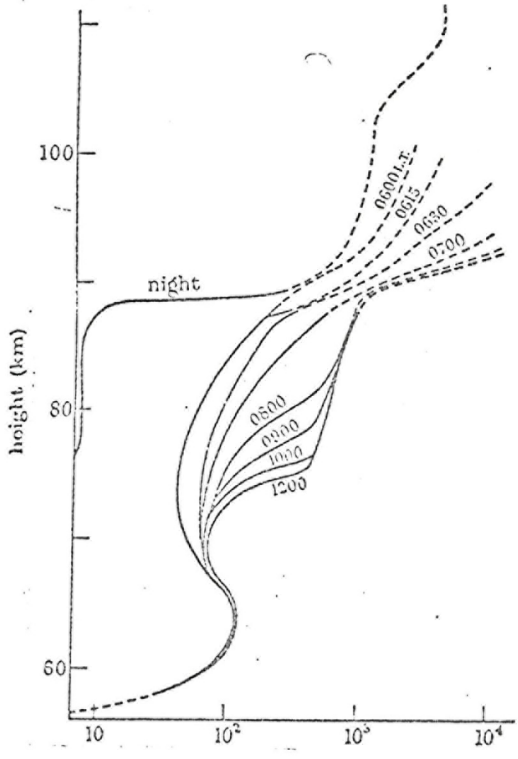

Fig. 6/5

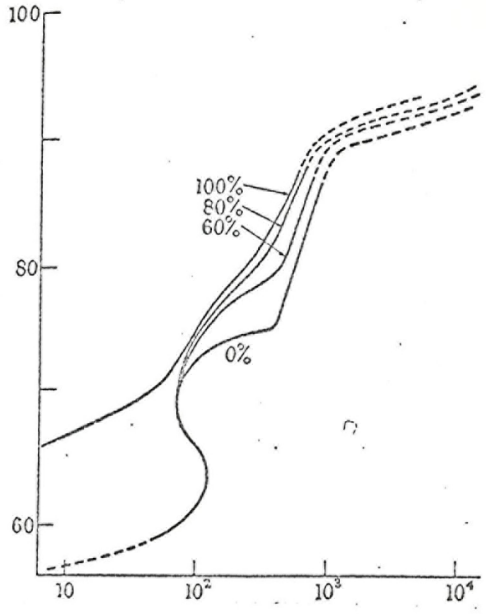

Fig. 6/6

electron concentration (cm^{-3})

Fig 6/5 The local-time variation of electron concentration at March equinox, sunspot minimum, at middle latitudes. The dashed parts of the curve are inserted to complete the calculations, but their precise form is not well determined.

Fig 6/6 The height distribution of electrons at different stages of a solar eclipse during mid-day, March equinox, sunspot minimum at middle latitudes. The figures on the curves represent the percentage obscuration of the solar disk. The dashed parts of the curve are inserted to complete the calculations, but their precise form is not well determined.

St. John's. Unfortunately due to interference on the tape it was impossible to determine whether the effect occurred or not. At the same time it was noted that no tweeks were audible on the Norwich records, over the period 1800 UT to 2000 UT.

6.2.2 Analysis of tweeks

Sonagrams have been made of all tweeks occurring between 1800 and 2000 UT on March 6 and 7. Sonagrams have also been made of some of the tweeks occurring between 2000 UT and 2400 UT on the two dates. Recordings were also made on March8 but because of the exceptional magnetic activity - a major magnetic storm occurred on March 8 with its sudden commencement at 1414 UT - these data have been excluded from this analysis. Fig. 6/7 shows spectrograms of tweeks typical of (a) the eclipsed period on March 7, (b) the corresponding period on March 6, (c) the post-sunset period on both days. It may be seen that the pre-sunset tweeks on March 6 were very weak compared with those on March 7 and that their cutoff frequency was much less well defined. The main differences between the eclipse time tweeks and post-sunset tweeks are: (i) the eclipse time tweeks are much less dispersed in the region of 3 kHz and (ii) the eclipse time tweeks retain some energy below their cutoff frequency. The significance of these differences will be considered later.

The lower cutoff frequency (f_c) of each tweek sonagrammed has been measured, provided that it was well enough defined for accurate measurement. To increase the accuracy of measurement the frequency scale of the sonagraph was chosen to be 40 Hz - 4 kHz and the scale expanding facility was employed so that only the range 1 - 3 kHz was displayed. The error in measurement is essentially equal to the bandwidth of the filter, in this case 22.5 Hz. Fig. 6/8 shows a sonagram of an eclipse time tweek using this scale. Systematic errors due to differences in the speed of the tape recorders when recording and

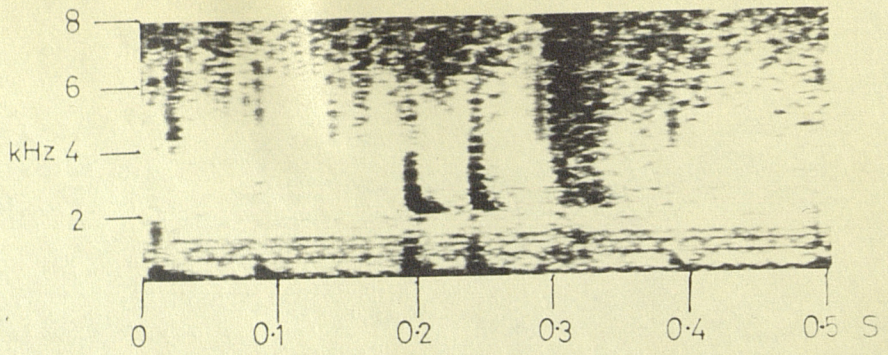

a) 1904 U.T. 7 March 1970.

Tweeks typical of eclipse period.

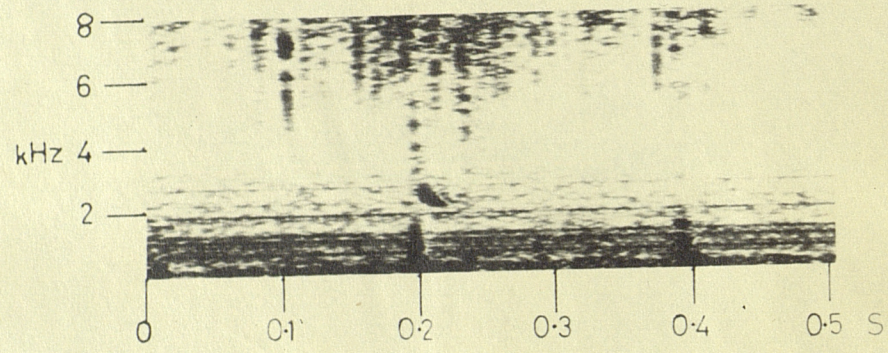

b) 1917 U.T. 6 March 1970.

Tweek during control period.

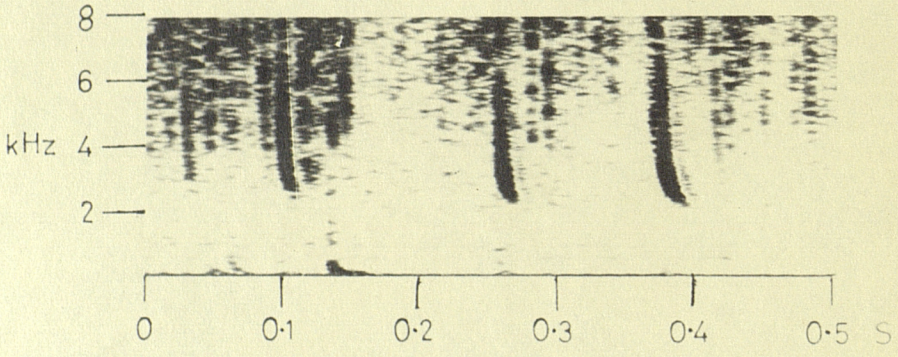

c) 2215 U.T. 7 March 1970.

Tweeks typical of normal post-sunset conditions.

Fig. 6/7

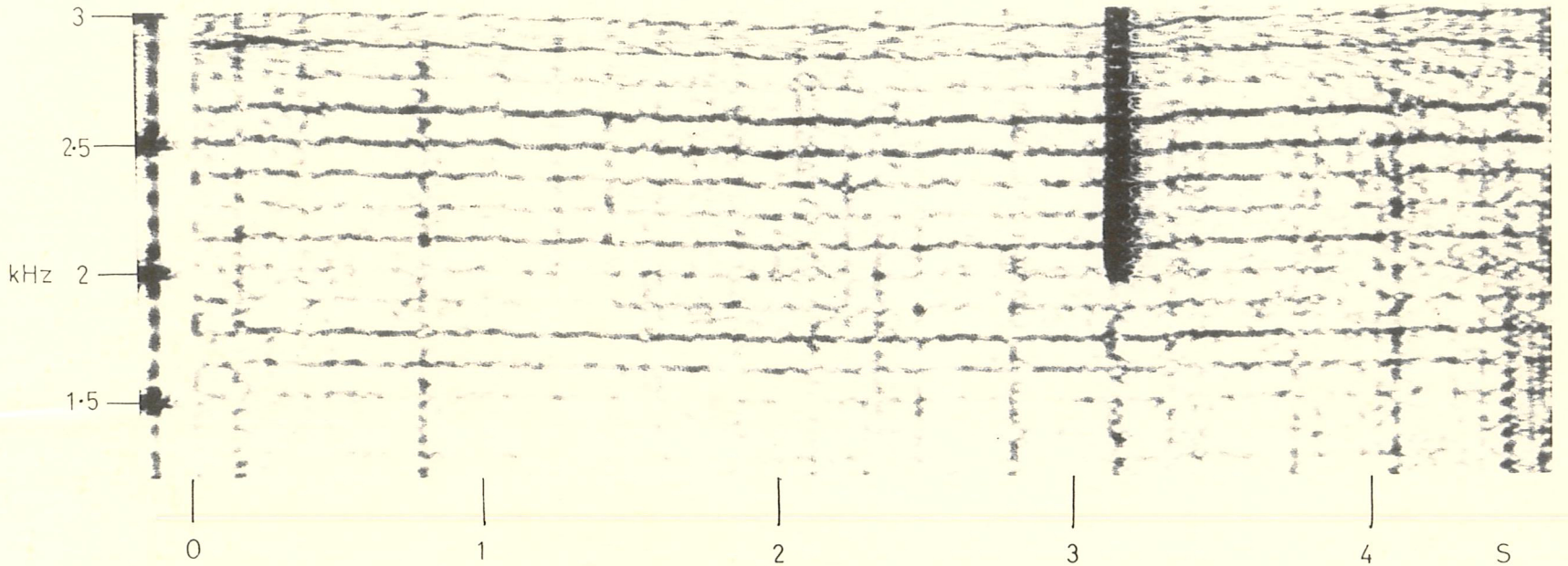

Spectrogram of VLF waveform received at 1901 U.T. 7 March 1970 at St.John's, Newfoundland.

Fig.6 Spectrogram of tweek using expanded scale.

replaying were eliminated by observing the time between the 2.8 kHz tones mentioned in section 5.1.3. These were known to have occurred at intervals of exactly 20 s. Hence the systematic error, if any, was determined and corrections to f_c were made. Fig. 6/9 (a) and (b) show how f_c varied with time betwee 1800 and 2400 UT on March 7 and 6 respectively. In Fig. 6/10 (a) the variation of f_c with Universal Time is shown for the period 1800 - 2000 UT, data from 16 March being shown as crosses, data from 7 March as dots. Fig. 6/10 (b) shows how solar obscuration at 80 km above St. John's varied with time. It may be seen that on 6 March only five tweeks were received in this period; all of these occurred after 1915 UT and were very weak compared with those on 7 March; their cutoff frequencies are apparently random. On March 7, however, around 60 tweeks were received during the eclipse period, many of which were exceptionally intense; their cutoff frequencies show a strong correlation with solar obscuration.

Least squares regression lines have been computed for the variation of f_c with time over the periods 1820 - 1900 and 1910 - 1950 when the variation of solar obscuration with time is approximately linear. These are shown as the solid lines in Fig. 6/10(a). For the sixteen points within the interval 1820 - 1900 UT the correlation coefficient (r) between the variables is -0.79, and the standard error in the gradient (Δm) is only $\pm$ 21% of m; for the 26 points in the interval 1910 - 1950 UT r = +0 68 and $\Delta m/m = \pm$ 22%. Since the probability of such a large magnitude of correlation coefficient arising by chance is less than 0.1% it is concluded that f_c may be considered to vary linearly with time over these two periods.

The time at which f_c reaches a minimum value has been investigated. One way of doing this is to extrapolate the lines shown in Fig 6/10(a) until they intersect at 1906:25 UT with a standard error of $\pm$ 4 min 00 sec. Another way is to compute best fit straight lines for all the points

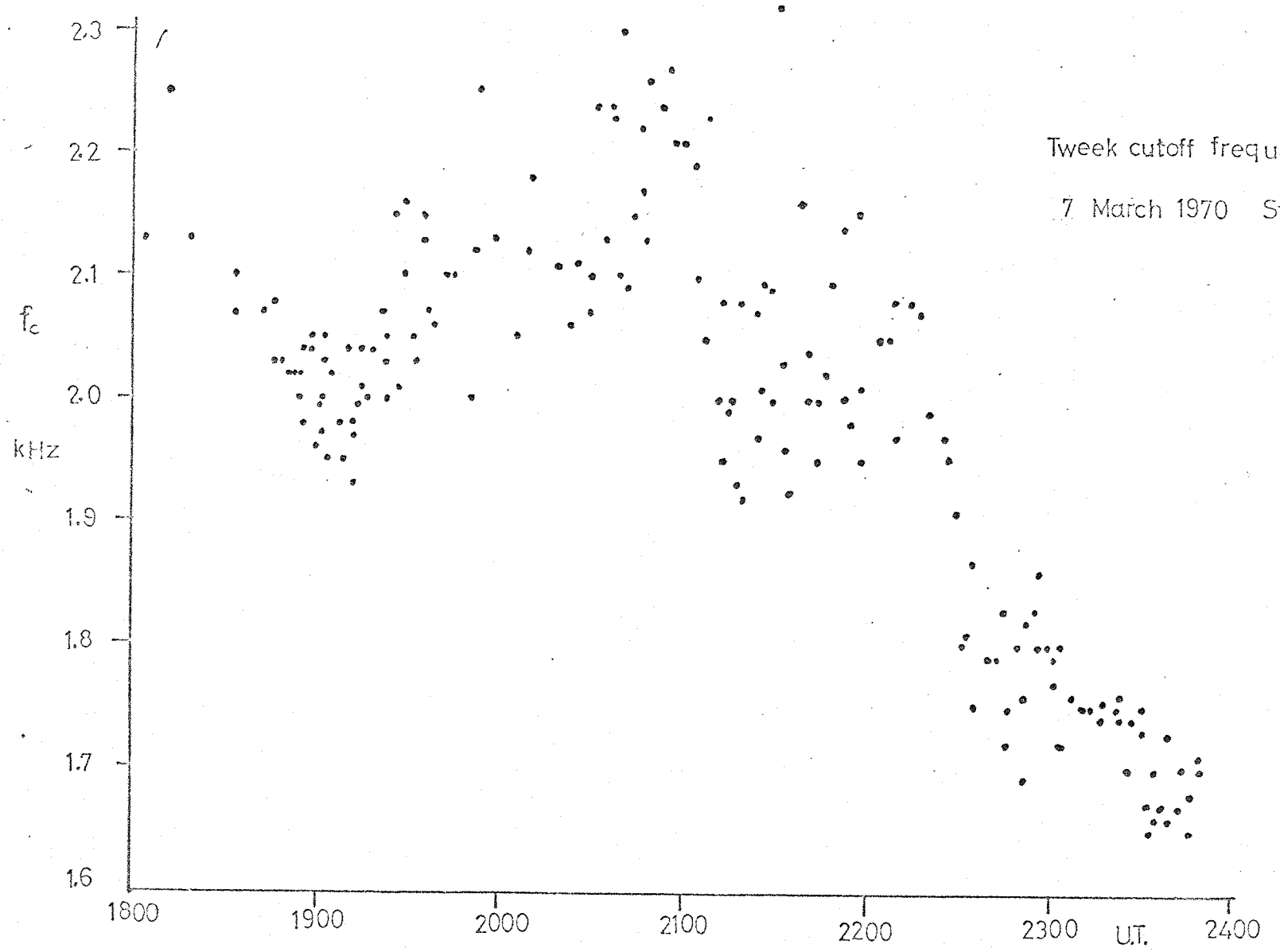

Fig. 6/9(a)

Tweek cutoff frequency vs time

7 March 1970 St. John's, Newfoundland

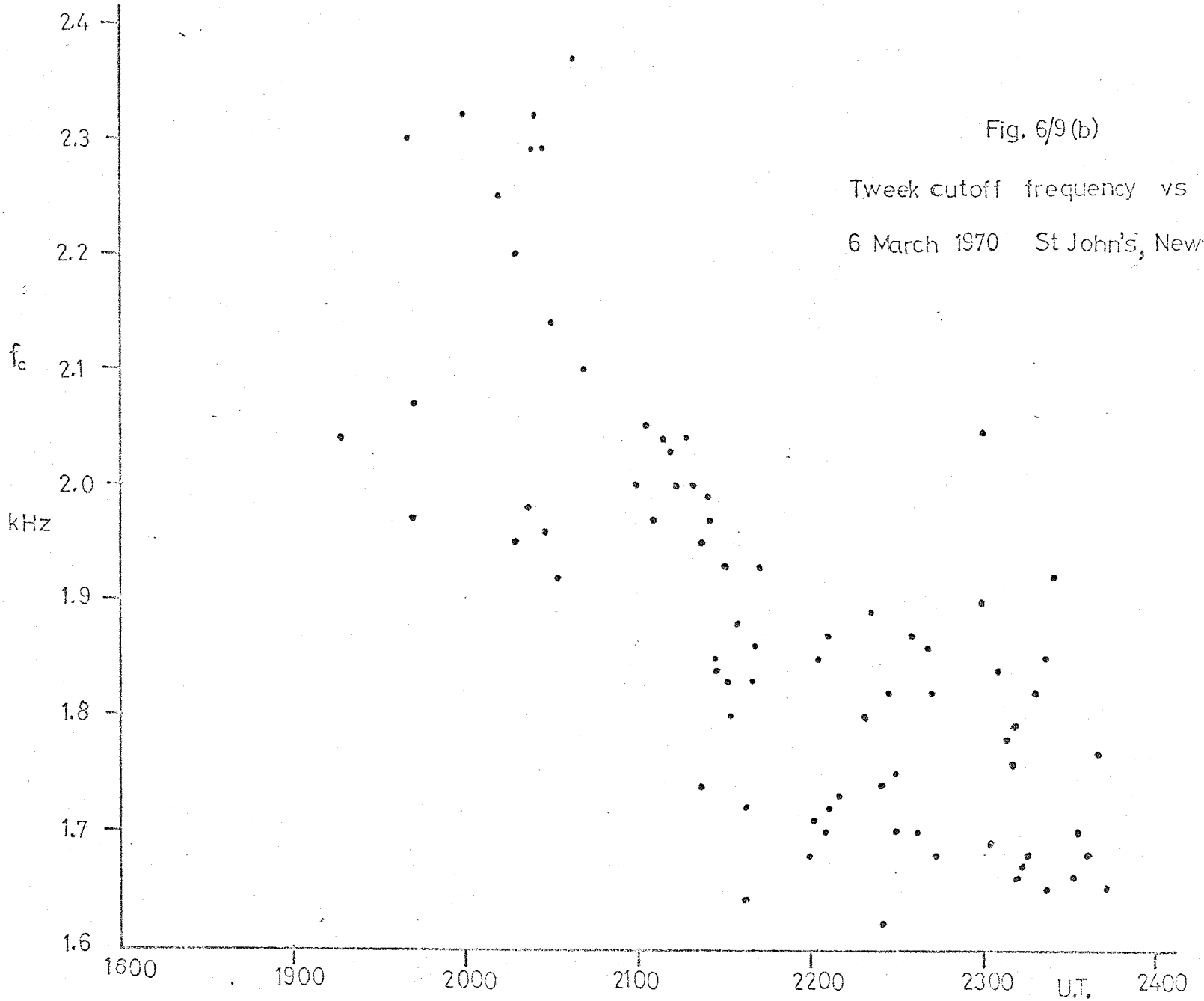

Fig. 6/9 (b)

Tweek cutoff frequency vs time

6 March 1970 St John's, Newfoundland

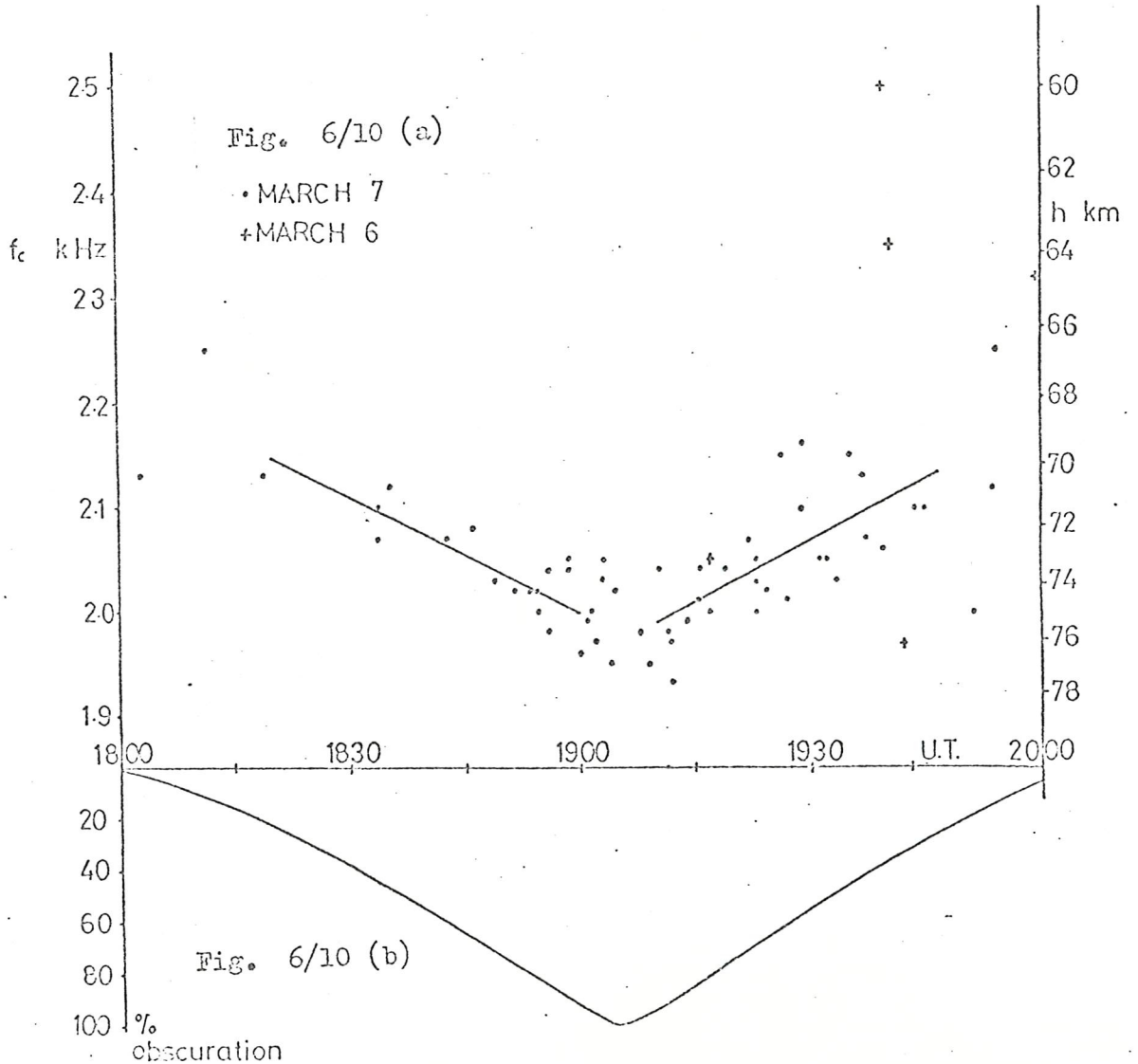

Variation of a) tweek cutoff frequency and b) solar obscuration during solar eclipse of 7 March 1970, St. John's, Newfoundland.

between 1820 and 1905 UT and between 1905 and 1950 UT. These lines are found to cross at 1906:10 UT ± 2 min 40 sec. The results of both these methods are prejudiced by the choice of 1905 UT as the time at which the data should be divided. Consequently best fit lines have been computed splitting the data at one minute intervals between 1900 and 1910 UT confirming a best estimate for the time at which f_c is minimum of 1906:10 UT ± 2 mins 40 sec.

6.2.3 Sferics observed at Norwich

It was mentioned in section 6.2.1 that no tweeks were audible on the recordings taken during the solar eclipse at Norwich, Vermont where the maximum obscuration at 80 km was 90.7% at 1846:39 UT. To confirm this sonagrams were made of the VLF waveform as recorded at Norwich at times corresponding to the reception of tweeks at St. John's. A number of these 'simultaneous sonagrams' are shown in Fig. 6/11. It is clear that in general the sferics are well correlated between the two stations but except for the 1900:50 UT sonagram there is no evidence of any tweeks occurring at Norwich Vt., in spite of the relatively high degree of solar obscuration. Indeed it seems that the sferics which appear as very intense tweeks at St. John's are in general very weak when received at Norwich, Vermont, 1600 km distant. The difference between the appearance of the sferics at the two sites will be discussed further in a later section.

6.3 Determination of the position of the storm centre responsible for the tweeks

Before any meaningful deductions could be made from the observations of tweeks during the eclipse it was necessary to determine the location of the thunderstorm responsible for generating them. Several factors indicated that the storm centre must be quite close, within less than 2000 km of St. John's. These were:

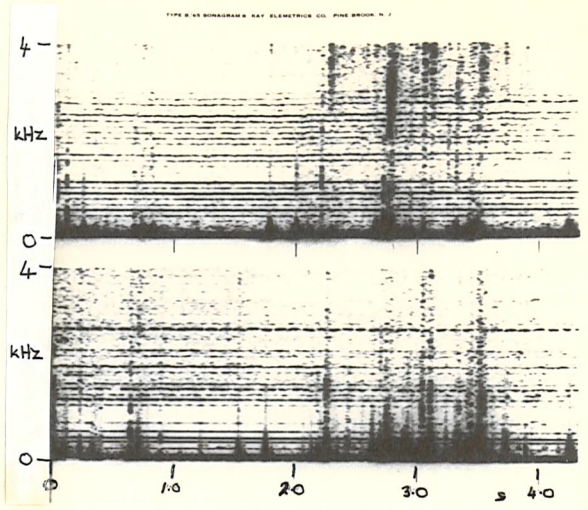

1802:45 U.T.

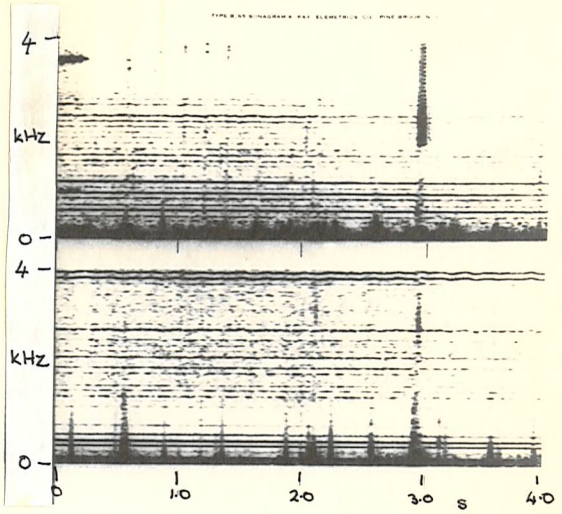

1900:50 U.T.

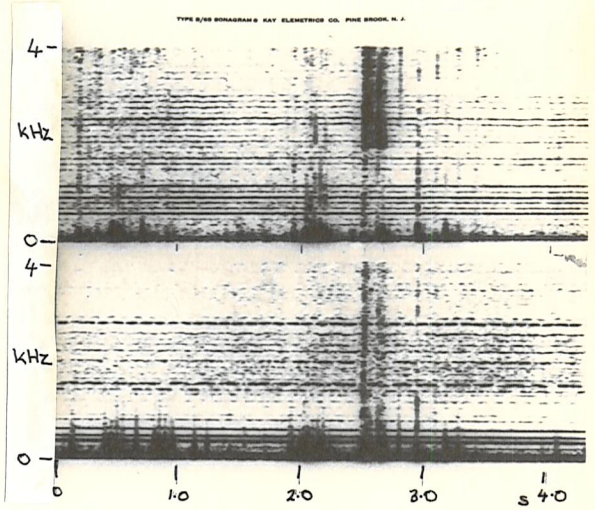

1911:16 U.T.

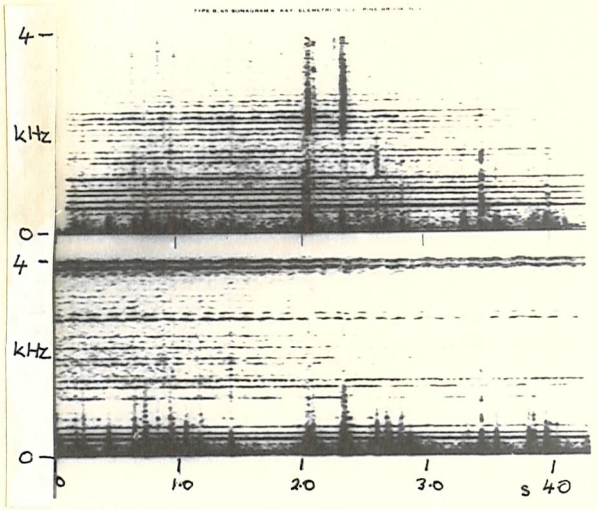

1953:36 U.T.

Fig. 6/11 Sonagrams of VLF waveform recorded simultaneously at St. John's, Newfoundland and Norwich, Vermont, USA, 7 March 1970

(Upper sonagram in each pair is from St. John's)

(i) For the eclipse to have any affect on the tweeks they must have been generated within the partially eclipsed region; for reference Fig. 6/12 shows the contours of obscuration at various times (Quiroz and Henry, 1972). If they had propagated any appreciable distance ($\lesssim$ a few hundred km) under a daytime ionosphere most of the energy below around 5 kHz would have been absorbed.

(ii) The intensity of the sferics as recorded at St. John's was very much greater than that at Norwich; it is therefore likely that the storm centre was considerably closer to St. John's than to Norwich.

(iii) The fact that the maximum levels on the two selective channels and the minimum value of f_c occurred close to eclipse maximum at St. John's suggests that the storm centre was close to St. John's.

(iv) The exceptional strength of the tweeks at St. John's relative to all the other signals received suggests that the sferics were generated close to St. John's.

(v) The low dispersion of the tweeks at frequencies just above the cut off frequency indicates a short propagation path (Helliwell, 1965).

Bearing these points in mind an attempt was made to locate the thunderstorm. The range of the lightning location equipment operated by the British Meteorological Office does not extend further than the mid Atlantic and neither the American nor the Canadian weather services were operating their equipment at the time. A search of weather charts revealed no reports of thunderstorms over North America and the North Atlantic on either 6 or 7 March. However a study of meteorolocial charts and cloud photographs of the region taken by satellites has, with the assistance of members, especially Messrs. Smith, Grey and Kirk, of the Meteorological Office, Bracknell, enabled an estimate tc be made of likely positions of thunderstorms.

Fig. 6/13 shows the surface chart for the North Atlantic region for 1800 UT, 7 March 1970 and Fig. 6/14 the 1749:13 UT photograph taken

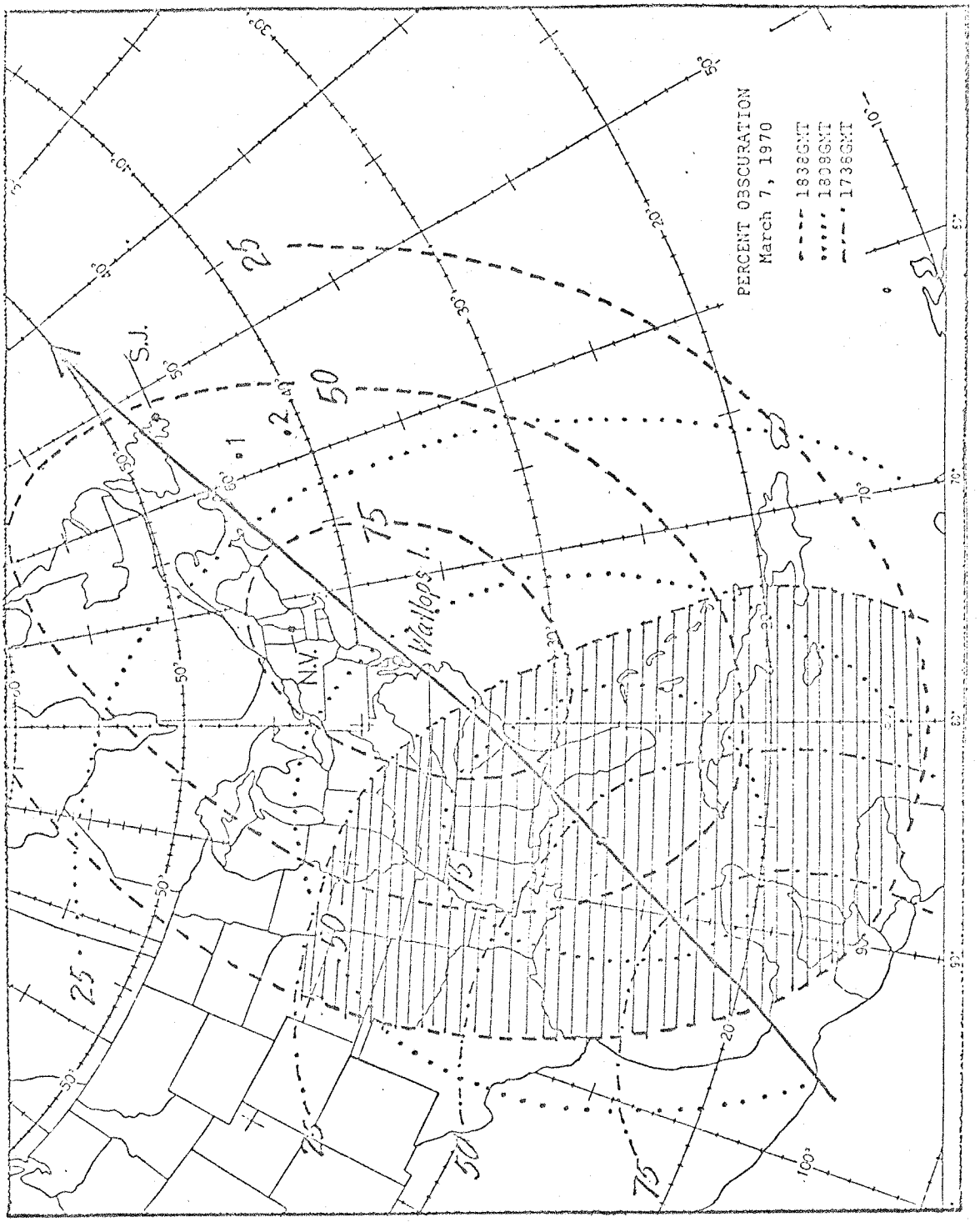

Fig. 6/12. Map showing contours of solar obscuration during eclipse and positions of St. John's(S.J.), Norwich(N.V.) and the two storm centres.

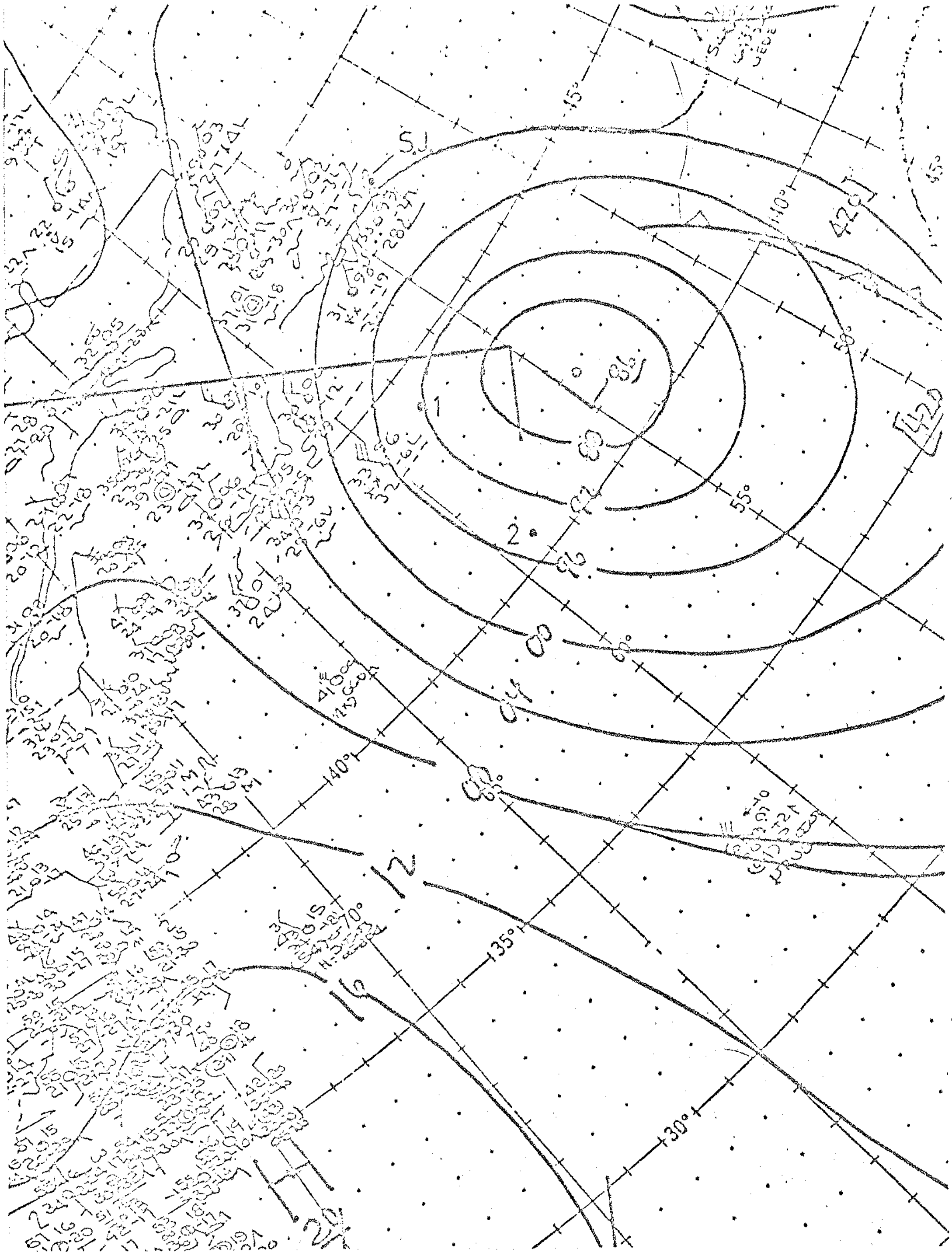

Fig. 6/13. Surface weather chart of N.W. Atlantic for 1800 U.T. March 7 1970 showing position of St. John's and the two storm centres.

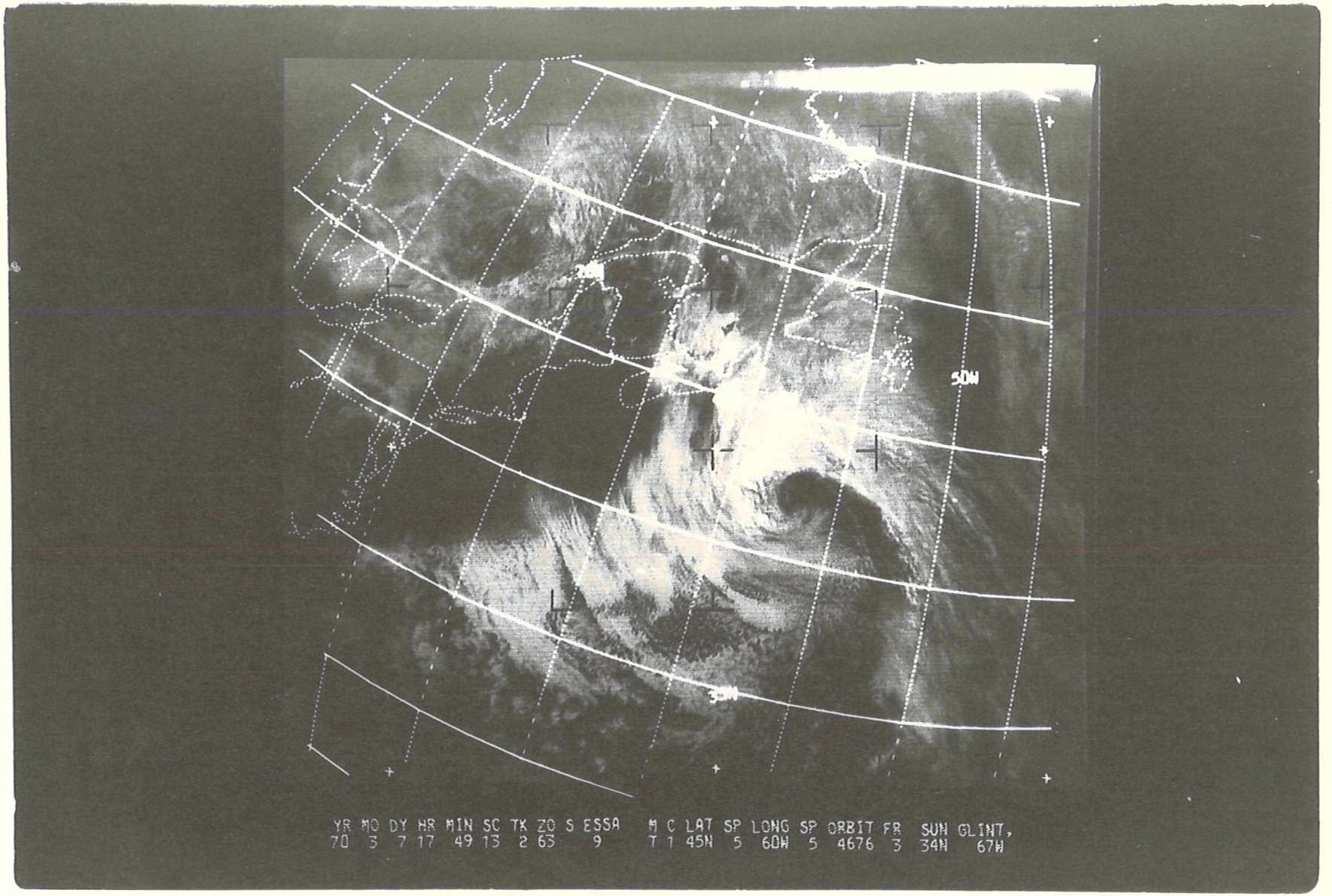

Fig. 6/14 Satellite photograph of N.E. Atlantic region 1749:13 U.T., 7 March 1970.

by the ESSA 9 weather satellite of the area including Newfoundland and the east coast of North America. The two most likely positions of thunderstorms are (E.J. Smith, private communication)

(i) around 44°N, 58°W, where the cloud shows signs of instability typical of thunderstorm conditions, and

(ii) along the trough between 41°N, 58°W and 40°N, 60°W, where instability in the cloud structure is also likely.

Further support is lent to these estimates by the fact that a sharp decrease in tweek cut off frequency occurred on March 7 at St. John's at around 2225 UT (see Fig. 6/9(b)), midway between sunset at the storm centres (2235 UT) and sunset at St. John's (2210 UT). The fact that both centres are located over the ocean explains why no reports of thunderstorms were found on the charts. Since the centre of the depression was found to move only 0.4°N, 0.5°W between 1800 UT and 2100 UT the storm centres will be considered stationary throughout the eclipse period. The storms centres will henceforth be referred to as numbers 1 and 2 as above and a mean position of 40.5°N, 59°W will be used for centre number 2.

Storm centre number 1 is 600 km from St. John's and 1150 km from Norwich; centre number 2 is 950 km from St. John's and 1150 km from Norwich. Thus centre number 1 would appear the more likely since it is in agreement with (ii) above that the storm centre should be considerably closer to St. John's than to Norwich. However centre number 2 may not be disregarded since other factors may have contributed to the difference in the observed intensity at the two stations. Radiation propagating in the waveguide mode over the sea tends to be less attenuated than over land since the sea is a better conductor. The paths from both centres to St. John's are exclusively over the sea while the paths to Norwich lie partly over land. This fact might contribute to an explanation of the difference between the spectrograms

of the same atmospherics as received at the two stations.

6.4 Interpretation of Results

6.4.1 Deduction of the height of the ionospheric reflecting surface

Considering the simplest model of the earth-ionosphere waveguide discussed in Chapter two, where the waveguide is assumed to consist of two perfectly conducting, flat parallel planes separated by a distance h, the cutoff frequency of the first order TM mode is given by equation 3.1/10:

$$f_c = c/2h$$

where c is the velocity of light in free space.

Thus if f_c is measured in kilohertz the apparent height of the ionospheric reflecting surface is given by the relation:

$$h = \frac{150}{f_c} \text{ km.} \qquad 6.4/1$$

Hence Figs. 6/9(b) and 6/10(a) also show how the apparent height of the ionospheric reflecting surface (h) varies during the eclipse. h is seen to increase from about 69 km soon after first contact to a maximum at around 76 km, returning to 69 km at the end of the eclipse. h again increases after sunset. The sharp increase in h at 2220 UT on March 7 corresponds to sunset close to the estimated storm centres, providing a further indication that the estimated position is reasonably accurate.

The suitability of this model of the earth-ionosphere waveguide, in view of the possibility that the height of the reflecting surface may change over the propagation path due to changes in solar obscuration, may be illustrated by studying the map in Fig. 6/12, which shows contours of obscuration as well as the positions of the storm centres and the two receiving sites. The difference in obscuration between the storm centres and St. John's at any given time is only of the order of 10 - 15% and

the difference in their respective times of eclipse maximum is around 5 - 10 mins. Thus the assumption that the height of the ionospheric reflecting surface does not change by a significant amount over the propagation path may be seen to be reasonable. One possible method of taking into account the change in the height of the reflecting surface would be to assume that the cutoff frequency was characteristic of the height of the reflector at a point halfway between the lightning flash and the receiver. In this case f_c would be dependent upon the distance of the lightning flash from the receiver. The relatively large spread of points in Fig. 6/10(a) could be explained on this theory if it is realised that lightning flashes may occur anywhere within one or two hundred kilometres of the estimated storm centres. The averaging of this effect by fitting straight lines to the points should then give a measure of the height of the ionospheric reflector at a point halfway between the centre of the thunderstorm area and the receiver. Eclipse maximum at 80 km above centre no. 1 occurs at 1859 UT; for centre no. 2 the corresponding time is 1857 UT. Since eclipse maximum at 80 km above the receiver was at 1905:01 the time of maximum halfway between the centres and the receiver may be taken to be 1902:30 UT $\pm$ 1 min. The best estimate for the time of minimum f_c was found, in section 6.2.2, to be 1906:10 $\pm$ 2 min 40 sec: Combining these random errors, it is therefore concluded that the response time of the D region is 1906:10 - 1902:30 = 3 min 40 sec $\pm$ 2 min 50 sec.

The waveguide mode conditions (equation 3.1/11) requires that the total phase change of the wave after reflection from both boundaries is $2n\pi$. Thus the apparent height of reflection derived from f_c is the phase height of reflection, h(f), (Budden, 1961), which is the height at which a perfect reflector would have to be placed to give the same phase change in the reflected wave. The phase change of a wave of frequency f on returning to the ground after reflection from the iono-

sphere is given by the phase integral (Budden, 1961):

$$\frac{4\pi}{\lambda}\int_{o}^{z_o} \mu \, dz = 2k\, h(f) \qquad 6.4/2$$

where z_o is the height at which the refractive index μ becomes zero. Fig. 6/15 shows the electron density profiles obtained during the eclipse by Belrose et al. (1972) at East Quoddy, Nova Scotia. The AAF 45 profile, obtained 6 minutes after totality, in the range of height 60 km < h < 90 km, has been approximated by

$$\log_{10} N_e = (h - 60)/10 \text{ (shown as a dotted line)}$$

where N_e is in units of cm^{-3}

and a collision frequency profile

$$\nu = 7 \times 10^4 \, p \qquad s^{-1}$$

where $\log_{10} p = (92.5 - h)/12.5$

and p is measured in millibars.

The true height of reflection, z_o, taken as the height at which the real and imaginary parts of the refractive index become equal, was found to be 75.3 km for a 2 kHz wave at normal incidence, at which height the electron density was around 50 cm^{-3}. Hence the phase height of reflection was found to be 73.2 km.

It is clear that, for the AAF 44 profile obtained at totality, where the electron density varies between 10 cm^{-3} and 100 cm^{-3} between 77 and 80 km, that the phase height and true height of reflection will be essentially the same, that is around 78 km. The latter profile shows the maximum eclipse effect in the D region; thus the agreement with the phase height deduced from f_c (76 $\pm$ 1 km at eclipse maximum) may be seen to be reasonably good.

To summarize, observations of the lower cut off frequency of tweeks during the eclipse yield the result that the phase height of reflection in the D region increases by 7 $\pm$ 1 km with a time lag of

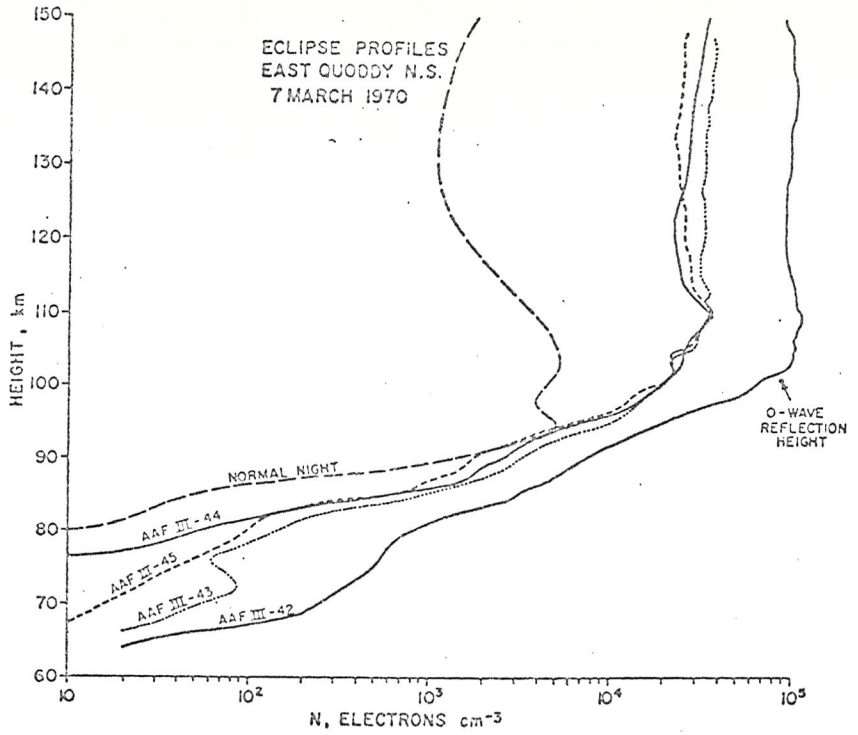

Composite electron density height profiles for the four rocket experiments

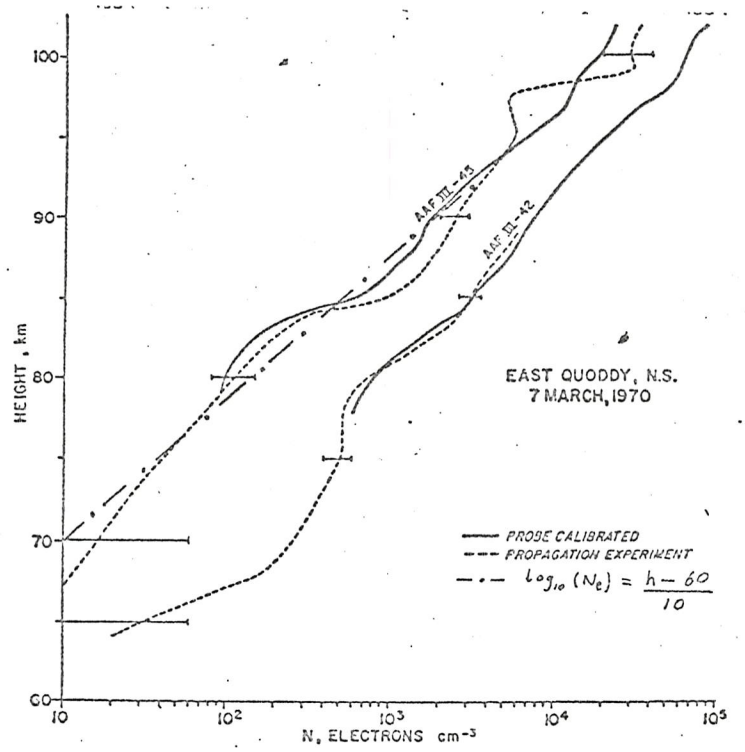

. The electron density height profiles as measured by the propagation experiment and by the probe calibrated by the propagation experiment, for full sun (AAF-III-42) and eclipsed sun (the results for AAF-III-45 are shown). The error bars apply to the propagation experiment.

Fig. 6/15. Electron density profiles obtained by Belrose et al(1972) during the solar eclipse of March 7 1970.

4 ± 3 minutes. This is in agreement with the observations of Sales (1967) who find a phase height change of 6 km with a time lag of six minutes using a VLF reflection experiment. Direct measurement of the electron density using rocket-borne experiments (e.g. Belrose, 1972) however, shows a time lag of only a few seconds.

Fig. 6/16 shows the electron density profiles obtained during the eclipse by Mechtly et al (1972) at Wallops Island, Virginia, U.S.A. It may be seen that the electron density gradients are steeper than those found by Belrose et al (1972). This is possibly due to there being extra sources of D region ionisation at the higher latitudes such as the precipitation of energetic charged particles, or to the use of different experimental techniques. The former is especially likely in view of the disturbed magnetic conditions.

The ionisation of nitric oxide by solar Lyman α (1216 Å) radiation is believed to be the predominant production mechanism in the D region producing a layer around 80 km. Smith (1972) has measured the flux of Lyman α at four times during the eclipse. It was found that at totality the Lyman α flux fell to 0.15% of that from the full sun. It was also found that at totality the background Lyman α flux fell from 1.37% of that from the full sun to 0.4% of it. The flux of 2 - 8 Å X-rays has also been measured during the eclipse by Accardo et al. (1972). Their calculations show that even at totality the ion production rate due to Lyman α was still four times greater than that due to 2 - 8 Å X-rays. Smith (1972) has shown that 60% (80 - 20%) of the Lyman α radiation is absorbed between 73 km and 86 km. Since during the eclipse this radiation almost entirely disappears, the electron density in this region decreases giving rise to the observed steep electron density gradients between 70 and 80 km. Comparison with results given by Mechtly and Smith (1968) shows that around 80 km eclipsed conditions are very similar to nighttime conditions.

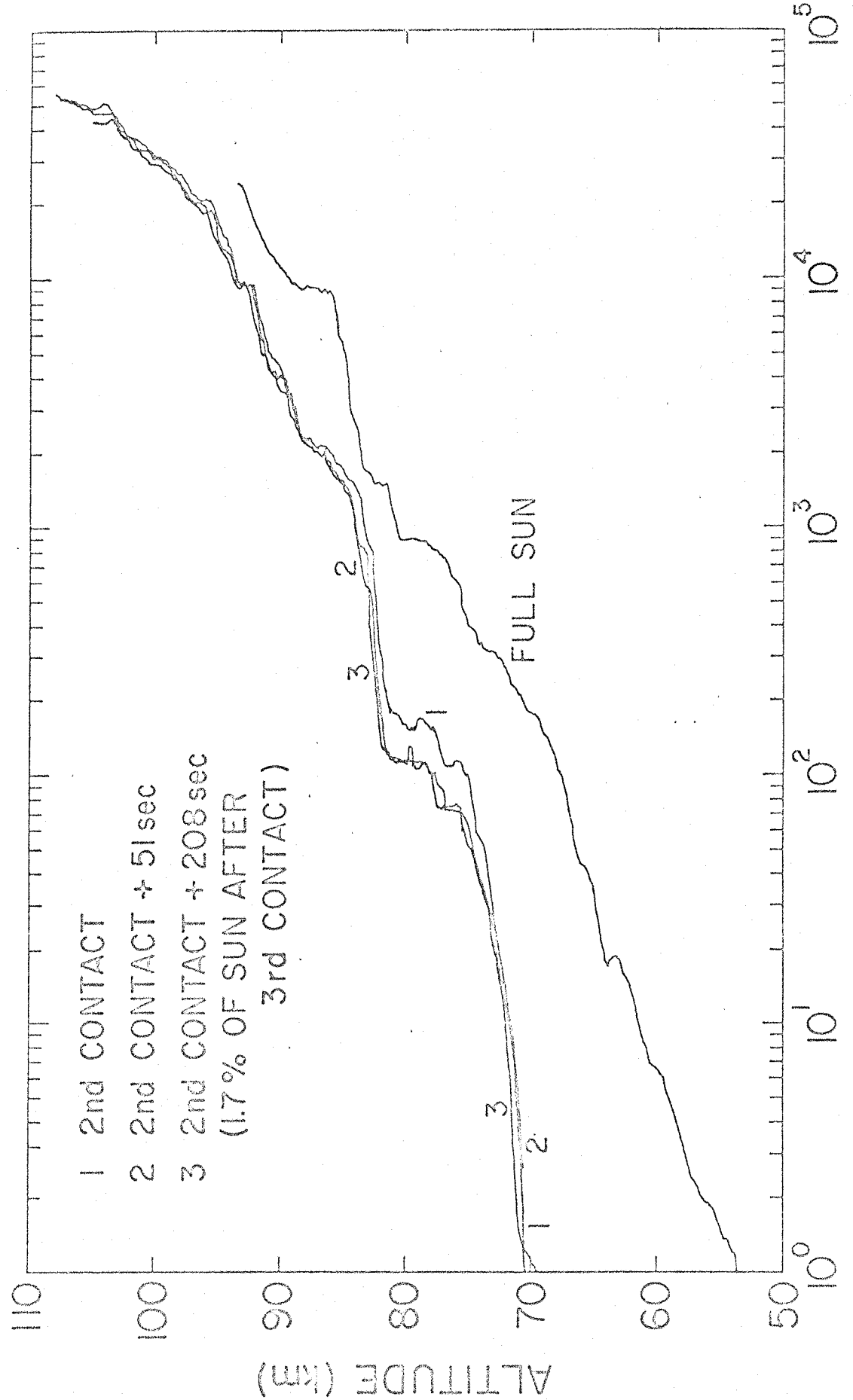

Fig. 6/16 Electron density profiles obtained by Mechtly et al. (1972)

6.4.2 Discussion of different effects at St. John's and Norwich

It is described in section 6.2.3 and illustrated in Fig. 6/11 that the sferics which appear as intense tweeks at St. John's are in general very weak, compared with other atmospherics and interfering signals, observed at Norwich, Vermont, with no sign of a tweek cutoff frequency except perhaps at 1900:50 UT. Several factors may have contributed to this effect:

(i) Both the estimated storm centres are further from Norwich than St. John's, centre no. 1 being about twice as far and no. 2 about 20% further. Assuming that the attenuation at around 2 kHz is 30 db/1000 km (Chapman et al., 1966) the relevant attenuations are: from centre no. 1 to St. John's 18 dB; from centre no. 1 to Norwich 35 dB; from centre no. 2 to St. John's 29 dB; from centre no. 2 to Norwich 35 dB. Thus a difference in intensity of between 6 and 17 dB would be expected.

(ii) The propagation paths from both centres to St. John's are in the magnetic SW-NE direction, while those to Norwich are in the E-W direction. Since the geomagnetic field causes the earth-ionosphere waveguide to be anisotropic, there is an extra attenuation of around 4 dB/1000 km for the propagation path to Norwich (Galejs, 1968). Thus the total difference in intensity between the two stations should be between 10 and 20 dB.

(iii) Since the sea is a better approximation to a flat perfect conductor than land the attenuation between the storm centres and St. John's, where the path lies totally over the sea, should again be less than that to Norwich where the path is partially over land.

(iv) The paths between the storm centres and St. John's are nearly parallel to the path of totality, whereas the paths to Norwich are transverse to it. This may affect the attenuation between the paths although the reason is not clear. It may also explain why the sferics observed at Norwich show no cutoff frequency in general. The one

sferic that shows some sign of a cutoff at Norwich occurs at 1900:50 UT, which could be interpreted as the time of eclipse maximum (plus a possible response time of around $6\frac{1}{2}$ mins) at the point halfway between the centre of the storm region and Norwich.

CHAPTER SEVEN

VLF emissions received close to eclipse totality

During the total solar eclipse of 7 March 1970 a number of VLF emissions known as risers (Helliwell, 1965) were received at St. John's, Newfoundland, and Norwich, Vermont, U.S.A. No emissions at all were recorded at Halley Bay, Antarctica, close to the magnetic conjugate of St. John's. It is suggested that these risers were typical of the prevailing magnetic conditions (K_p = 6-) but that under normal daytime ionospheric conditions they would have been reflected by or absorbed in the ionosphere, and hence not received at the ground. The modification of the ionospheric electron density distribution caused by the eclipse may have allowed the risers to penetrate the ionosphere and be received at the ground.

7.1 Observations

There are two main sequences of emissions that will be discussed in this chapter, although risers were recieved at other times during the eclipse. The earlier sequence, which will be referred to as sequence no. 1, was of risers received at both stations, simultaneously. Sequence no. 1 consists of one riser occurring at 1827:02 UT, three at around 1830:18, and five more between 1845:30 and 1848:06 UT. The second sequence, which will be called sequence no. 2, was received only at St. John's and consisted of eighteen intense risers occurring between 1901:29 and 1903:40 UT.

Apart from these two sequences around 30 risers were received at Norwich between 1800 and 1930 UT most of which were weak compared with those comprising the two sequences. At St. John's only three or four

other risers were received, between 1800 and 1930 UT, all of which were very much weaker than those in the two sequences, so weak in fact as to be barely audible and not to show up on a sonagram. The distribution in time of all the risers received at the two stations is shown in Fig. 7/1 .

7.2 Analysis of Risers

Sonagrams of risers typical of the two sequences are shown in Figs. 7/2 and 7/3. It may be seen that risers from the two sequences exhibit the same general characteristics with the exception of those received at 1847:51 and 52 UT, which show a more complex structure in the frequency-time plane than the others. The most striking difference between the two sequences is the much greater intensity of the risers of sequence no. 2.

The upper and lower frequency limits of the risers are shown in Fig. 7/4. It may be seen that the lower limit is generally less than the waveguide mode cut off frequency, indicating that the emissions did not propagate in the waveguide mode for a significant distance. Comparison with the magnetometer record at the St. John's site of the horizontal (North-South) component of the earth's magnetic field (H) shows that, with one exception, the risers in sequences 1 and 2, were received at times when H was rapidly decreasing. The electron energy required for resonance, which is proportional to $\frac{B^2}{2\mu_o N}$ (Rycroft, 1972) is therefore also decreasing, increasing the probability of resonance since electrons are generally more plentiful at lower energies.

The duration of the risers is generally small, the majority lasting less than 200 ms, many less than 100 ms. The initial slope (df/dt) of the risers is observed to be generally non-zero. This indicates that they were generated off the equatorial plane in the opposite hemisphere to the receiver (Helliwell, 1968).

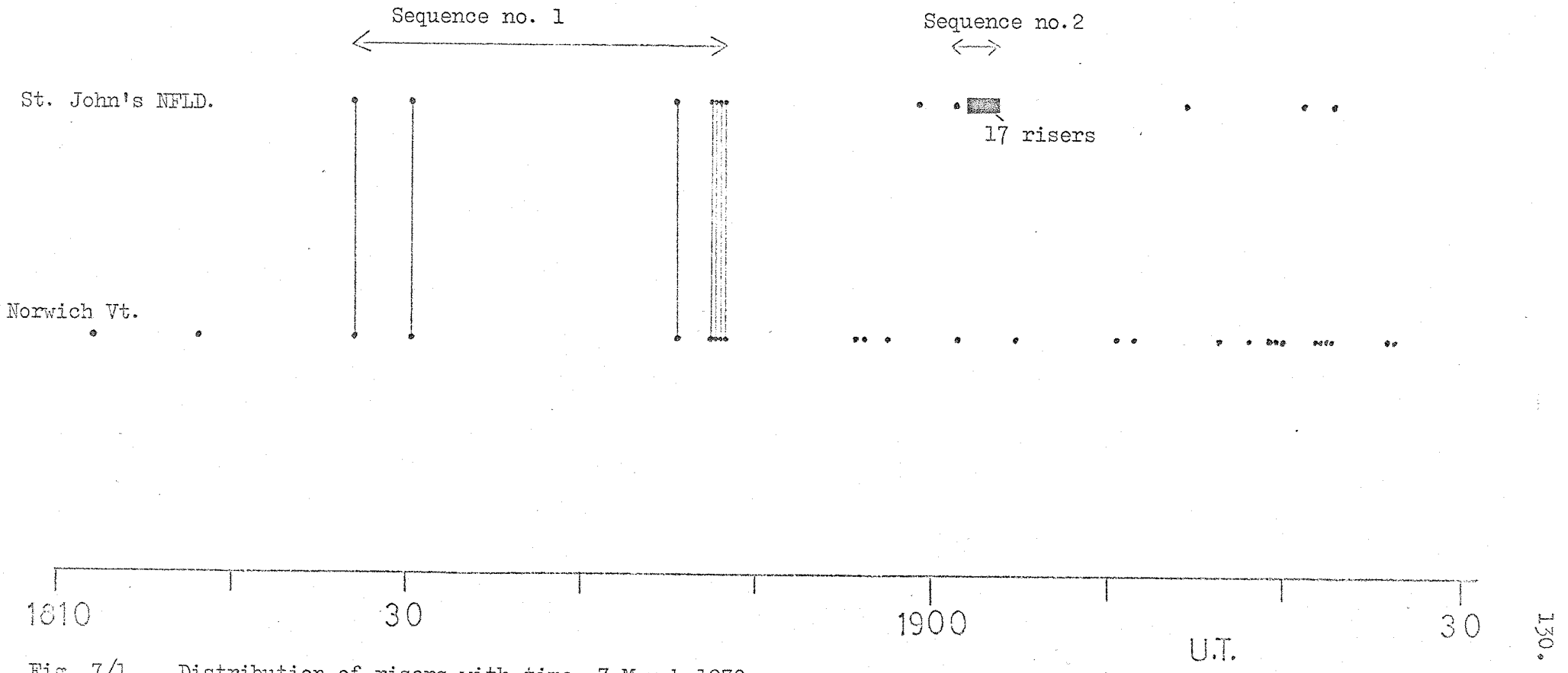

Fig. 7/1. Distribution of risers with time, 7 March 1970.

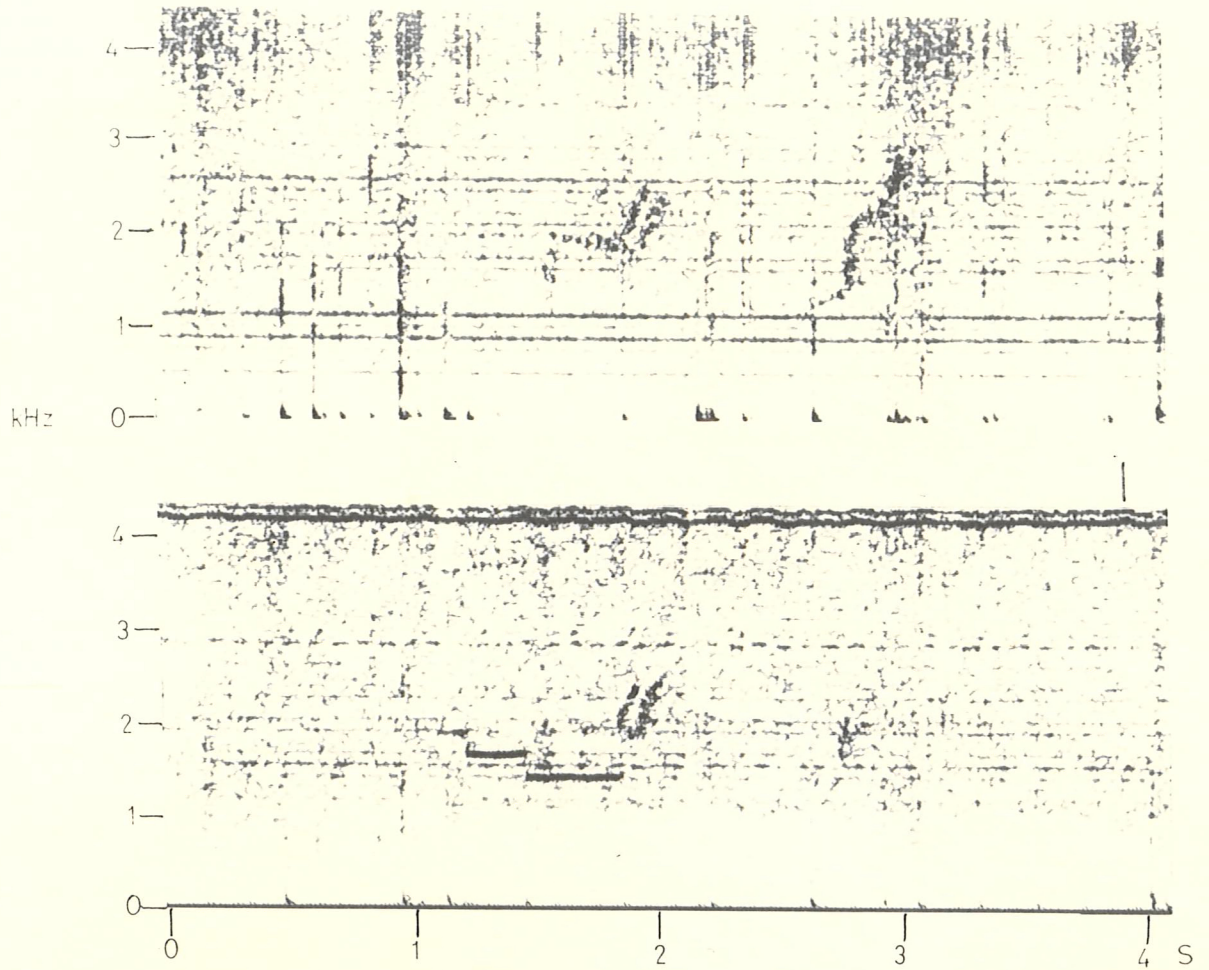

Fig. 7/2 Sonagrams of risers in sequence no.1 recorded simultaneously at St.John's, Newfoundland (upper sonagram) and Norwich, Vermont, U.S.A. at 1847:51 U.T. 7 March 1970.

(Tones on lower sonagram are time signals.)

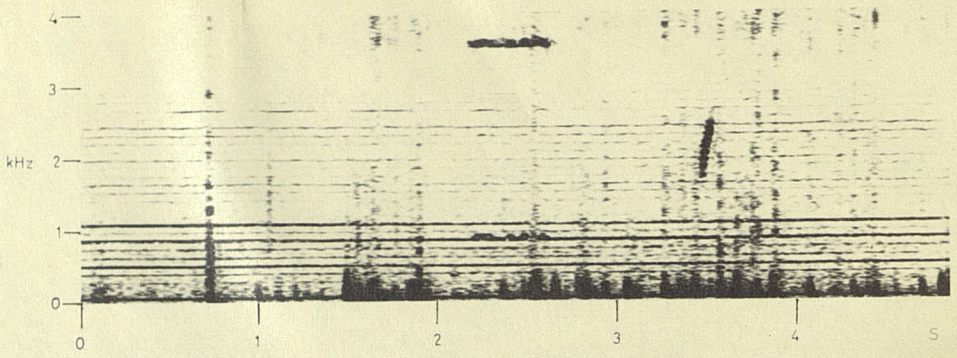

a) 1901:29 U.T.

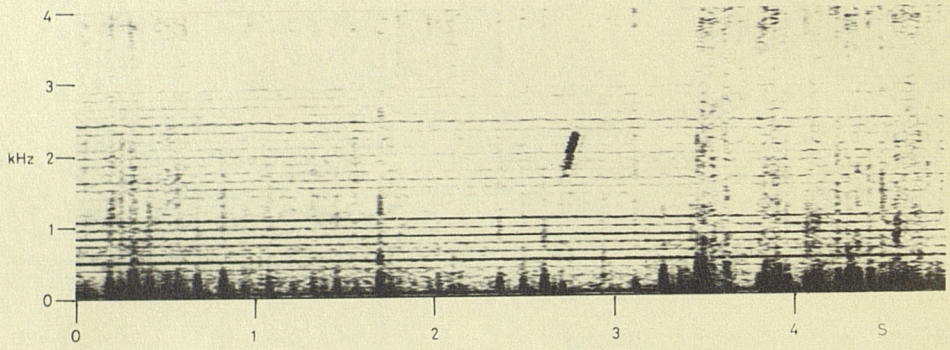

b) 1902:39 U.T.

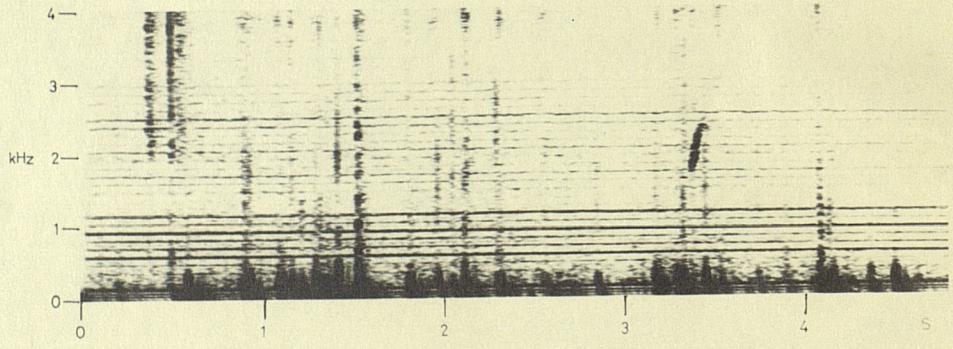

c) 1903:40 U.T.

Fig. 7/3 Risers from sequence no. 2. 7 March 1970. St. John's, Newfoundland

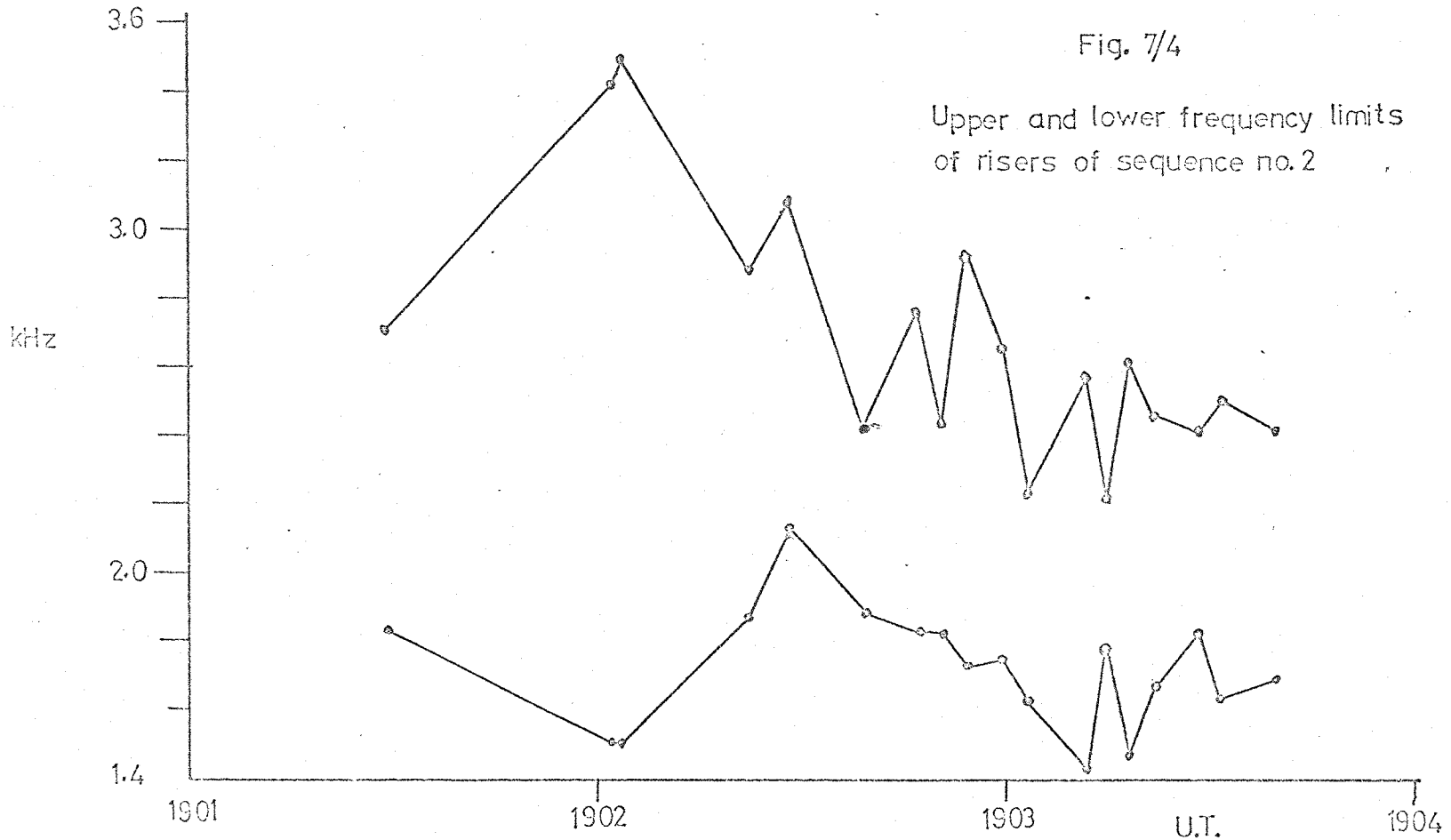

Fig. 7/4

Upper and lower frequency limits of risers of sequence no. 2

7.3 Interpretation of Results

The interpretation of the above characteristics must necessarily be of a qualitative nature; however it is thought that some useful conclusions may be drawn. It is likely that the risers were generated close to the equatorial plane by a transverse resonance plasma instability (Helliwell, 1968; Burtis, 1969), in which a whistler mode signal grows in intensity under conditions of enhanced magnetic activity. K_p was 6- for the period 1800 - 2100 UT, 7 March 1970. The possibility of their being triggered by unducted energy from lightning discharges will be discussed in Chapter Eleven. From the equatorial plane the risers must have propagated within field aligned ducts of enhanced electron density; otherwise they would have been magnetospherically reflected when the wave frequency became equal to the lower hybrid resonance frequency (Helliwell, 1965; Alexander, 1971). Upon emerging from the duct into the ionosphere the risers must have propagated to the receiver without spending a significant time in the waveguide mode, since they are observed to possess energy below the waveguide mode cut off frequency.

There are two possible explanations for the observation of emissions during the eclipse. Both require that the eclipse did not cause the generation of the emissions but merely modified the propagation characteristics in the ionosphere so as to allow the risers to be observed at the ground. Before discussing these mechanisms the effect of the eclipse on the ionosphere as a whole will be briefly reviewed.

The effect of the eclipse on the D region has been discussed in the previous chapter. It is found that at totality the electron density below around 75 km becomes very small (Mechtly et al, 1972; Belrose et al, 1972) falling by as much as three orders of magnitude ($10^3 cm^{-3}$ to 1 cm^{-3} at around 70 km). The phase height of reflection is found to increase by 6 km at totality (see Chapter Six or Sales, 1967), with a delay of

$\sim 4 \pm 3$ minutes between maximum obscuration and maximum phase height. However, direct observation of electron density using rocket borne experiments show much smaller response times, of the order of a few seconds (Mechtly et al, 1972; Belrose et al, 1972). The D region is the main absorbing layer for radio waves because of the high neutral density and hence high electron-neutral collision frequency. Ionospheric absorption measured using 3.5 MHz radio waves, was found to decrease during the eclipse by 15 dB (Kennedy and Scauble, 1970). This decrease is mainly attributable to the decrease in electron density in the D region.

The fractional decrease in electron density in the E region is found to be less than that in the D region, falling from $10^5 cm^{-3}$ to $3 \times 10^4 cm^{-3}$ at 110 km (Belrose et al, 1972). However in this region the electron density was found to be still decreasing 6 mins after third contact. Observations of electron density in the F region show that the electron density decreases by around 25 - 30% during the eclipse, with minimum electron density occurring up to 40 minutes after maximum obscuration (Flaherty et al, 1970; Thomas and Rycroft, 1970; Arendt et al, 1971).

The overall picture of the ionosphere during an eclipse is thus a large decrease in electron density with low response time in the D region below 80 km, the fractional decrease becoming smaller and the response time longer, with increasing altitude.

The first explanation for the observation of the risers during the eclipse concerns the decrease in absorption of the D region, due to the decreased electron density during the eclipse. Sequence no. 1, especially the latter part of this sequence, occurred close to eclipse maximum at 80 km above Norwich (1846:39 UT). However in view of the fact that these emissions were received with approximately equal in-

tensity at both stations it may be concluded that their exit point from the magnetosphere was closer to St. John's than Norwich. Sequence no. 2 was observed at St. John's only, around 3 mins before eclipse maximum at 80 km above that station, the risers being much more intense than those of sequence no. 1. Thus it is possible that the exit point from the magnetosphere was the same in both cases, the different effects being caused by the change in the eclipse circumstances. It is difficult to draw any conclusions from the observation of the risers not included in these two sequences, the majority of which were observed at Norwich (see Fig. 6/1).

The second explanation concerns the effect upon the propagation of VLF waves in the ionosphere caused by eclipse-induced horizontal gradients in electron density. When propagating through the magnetosphere in a field-aligned duct of enhanced electron density the wave normal and ray directions of the VLF wave are constrained to be close to the direction of the magnetic field, as described in section 4.2.3. On emerging from the duct, probably in the topside ionosphere below 1000 km, into a normal daytime ionosphere, the wave normal angle may become large and since the wave frequency of the risers was much less than the lower hybrid resonance frequency in the ionosphere the wave could be refracted in a similar way to a magnetospheric "reflection" (Alexander, 1971). Even if the wave were not reflected the combination of large wave normal angle and wave frequency much less than the lower hybrid resonance frequency would lead to a large value of the refractive index and hence great attenuation of the wave (Kimura, 1966). It is suggested that the eclipse-induced horizontal gradients in electron density in the E and F regions may act in a way somewhat analogous to a duct, preventing the risers from being either attenuated or reflected from the lower edge of the ionosphere by refracting the wave in such a way as to keep the

wave normal and ray directions close to the direction of the earth's magnetic field. It would therefore be expected that the ray would be deflected towards the region of greater electron density, that is away from the region of maximum eclipse effect.

Because of the large number of unknown quantities, e.g. the point of entry of the emission into the F region, the response time of the F region etc., it is impossible to say whether the observations of risers agree with the predictions of this theory. In all probability the observed effects are a combination of the effects of the two mechanisms discussed, as well as of the effect of the magnetic activity upon the generation of the emissions.

7.4 Further Work

Because of the unusual combination of circumstances leading to these observations it is unlikely that they will ever be repeated. However the use of a VLF goniometer, which mixes the signals induced in two orthogonal, vertical loop aerials in such a way as to be able to determine the direction of propagation, in the earth-ionosphere waveguide, of the signal received, would have greatly assisted the interpretation of these observations. It is proposed to make observations using goniometers at four spaced stations, during the total solar eclipse of 10 July 1972, in Eastern Canada.

CHAPTER EIGHT

Precursors to whistlers: previous work and experimental observations

One of the more intriguing VLF phenomena is the whistler precursor, a discrete VLF emission, usually a riser, which is observed before the whistler with which it appears to be associated. The first sonagrams of precursors were published by Dinger (1957). More recently precursors have been discussed by Helliwell (1965), Laaspere and Wang (1968) and Dowden (1972). Since frequency reference will be made to these three publications they will be abbreviated to H, LW, and D respectively.

Soon after the total solar eclipse of 7 March 1970 a series of around 40 whistler precursor pairs was received at St. John's, Newfoundland. This has led the author to consider the mechanism by which precursors are produced. In this chapter previous work on the subject of precursors is reviewed.

8.1 Observed Characteristics of Precursors

In the following discussion of the precursor it will be necessary to refer to a number of the more important observed properties of the precursor. In this section these properties are listed; for ease of reference they will be numbered and henceforth referred to by these numbers.

(1) Precursors have never been observed with a one hop whistler (H and LW).

(2) Echoing precursors show the same delay as their associated whistler, implying similar propagation paths (H and LW).

(3) The precursor appears to be spontaneously generated; no triggering signal is visible (H and LW).

(4) With reference to the schematic diagram in Fig. 8/1 the time delay between the causative sferic and the precursor at any frequency is always greater than the delay between the precursor and associated whistler at the same frequency (LW). More specifically, the time delay between the sferic and trigger point of the precursor (the point in the frequency-time domain at which the precursor begins) is greater than the delay between the trigger point and whistler at the same frequency (triggering frequency); this difference generally decreases with increasing triggering frequency (D).

(5) Simultaneous observations at spaced stations in the same hemisphere show differences in the relative intensities of the precursors and their associated whistlers, suggesting, contrary to property 2, different propagation paths (LW).

(6) The relative intensity of precursors and their associated whistler varies widely from event to event but in the majority of cases the intensity of the precursor is higher than that of the whistler in the same bandwidth. Sometimes the whistler is barely detectable and occasionally a sferic is followed by a riser which has all the ear-marks of a precursor but is accompanied by no whistler at all (LW).

(7) Most precursors occur under moderately disturbed conditions, K_p index around 3 (LW).

(8) Hiss bands are often present when precursors are observed (LW).

(9) The time delay between precursor and whistler tends to increase with increasing whistler dispersion (LW).

(10) A precursor often appears on a sonagram as a forward leaning letter S (see Fig. 8/1) but many variations are observed (LW). The initial slope of most precursors is small, indicating that they were generated close to the equatorial plane (Helliwell, 1967).

(11) The nose frequency (f_n) and minimum group delay (t_n) of around

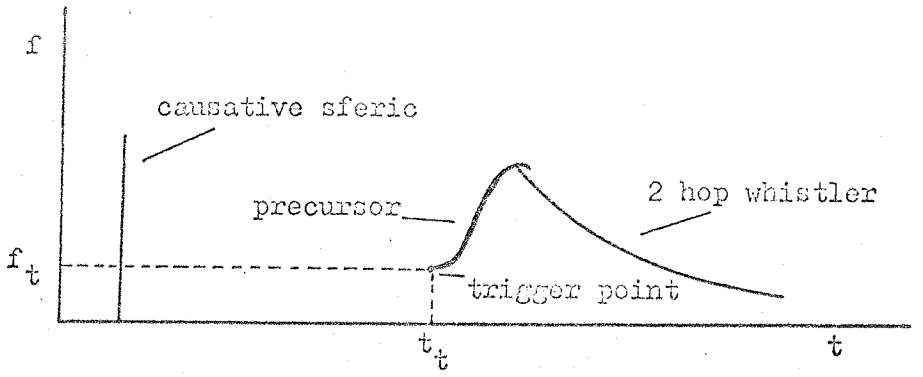

Fig. 8/1

Whistler - precursor pair, schematic

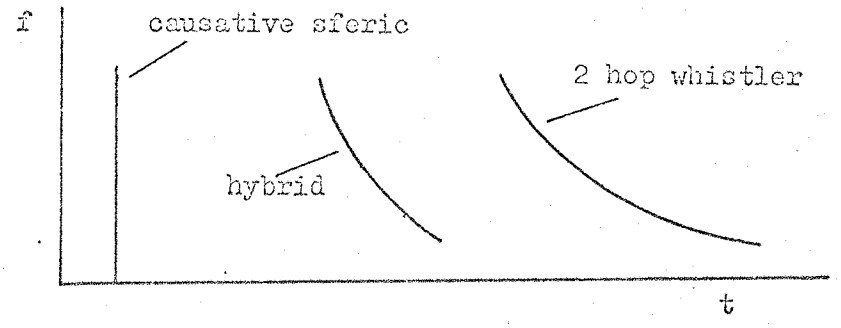

Fig. 8/2

Hybrid whistler, schematic

30 precursed whistlers have been measured (Dowden, 1972). Calculation of the 'scale' frequency (Dowden, 1962), obtained by dividing the square of the minimum plasma frequency (obtained from f_n and t_n) by the minimum electron gyrofrequency (from f_n) along the propagation path, indicates that the whistlers and precursors propagate within the plasmasphere, though perhaps just inside the plasmapause.

8.2 Theories of precursor generation

In section 1.3.2 two categories of VLF discrete emission were mentioned, the spontaneous and the triggered emission. Spontaneous emissions include risers, similar to those discussed in the previous chapter, hooks and falling tones (Helliwell, 1965). Sonagrams of spontaneous emissions have been shown in Fig. 1/4. Triggered emissions are those which emanate from other VLF signals. Emissions may be triggered by whistlers or other emissions (Helliwell, 1963; Brice, 1965), and also by man-made VLF signals such as morse-code transmissions (Helliwell et al., 1964). Sonagrams of triggered emissions are shown in Fig. 1/4.

Strictly speaking precursors belong to neither of these categories. Whereas no triggering signal is visible (property 3), they cannot be thought of as truly spontaneous emissions in view of their close association with a whistler. It is possible that an understanding of the process by which precursors are generated will provide a "missing link" between the two types of emission leading to a better overall understanding of the magnetospheric phenomena which case VLF emissions in general.

The generation mechanisms for both spontaneous and triggered emissions are thought to be similar, both relying on a wave-particle interaction involving the transverse resonance instability (Brice, 1964; Helliwell, 1967). This mechanism has been discussed in section 4.3.1.

In the case of a triggered emission it is the triggering signal which interacts with the resonant electrons to produce the emissions. In the case of spontaneous emissions there must be some stray VLF radiation to start the interaction off, possibly electron cyclotron radiation. Thereafter the mechanism is self-sustaining. The various theories of precursor generation attempt to explain how VLF energy from the same source as the precursed whistler could trigger an emission, which is observed before the associated two-hop whistler.

The most complete theory of precursor generation to date has been presented by Dowden (1972). This mechanism involves the hybrid whistler (Helliwell, 1965). A hybrid whistler is one whose dispersion is characteristic of a one hop whistler but which is observed in the same hemisphere as its causative sferic. Energy from the sferic is thought to propagate under the ionosphere into the opposite hemisphere and then in the whistler mode back to the original hemisphere, being received as a one hop whistler with an extra time delay of around 30 ms due to its propagation under the ionosphere. Thus a one-hop whistler from the same sferic may be observed at two conjugate points. The hybrid whistler is illustrated in Fig. 8/2. It may be seen that if the hybrid whistler in some way triggers an emission close to the equatorial plane that emission will appear as a precursor to the ordinary two-hop whistler. Laaspere and Wang (1968) reported an apparent objection to this theory in that among the several hundred precursor events they had studied not a single case of a one-hop hybrid whistler preceding the precursor had been detected (property 3). It was also noted that the precursors tended to occur too late to be accounted for by the hybrid whistler theory. It would also be expected that the trigger point of the precursor should be approximately half way in time between the sferic and two-hop whistler, slightly offset towards the whistler to allow for the propagation time under

the ionosphere (in partial agreement with observed property 4).

Dowden (1972) has reported one apparent exception to property 3, a one-hop hybrid whistler extending down to within 500 Hz of the precursor trigger frequency. He postulates a mechanism based on the hybrid whistler overcoming the objections of Laaspere and Wang (1968) as follows:

(i) The nonobservance of the one-hop hybrid is attributed to the weakness of the hybrid signal.

(ii) According to Helliwell's (1967) theory of VLF discrete emissions a weak triggering signal leads to a triggering delay Δt, which depends on the initial stability of the plasma. For a plasma on the brink of instability the delay could be very short; the maximum is taken as the time required for the electrons to go through the complete unbunched, fully phase-bunched, fully debunched cycle. The halfway point, the resonance time, when the electrons are fully phase-bunched is taken as a likely intermediate value. It is shown that the delay time normalised with respect to the minimum one hop group delay, the nose time delay, is given by

$$\frac{\Delta t}{t_n} = K_1 \, (1 + 2\Lambda)(1 - \Lambda)^{-1}\Lambda^{-2/3} \qquad 8.2/1$$

where Λ is the normalised frequency $f/f_{B\,e\,min}$, and K_1 has a maximum value of 0.02 corresponding to the interaction time and an intermediate value of 0.01 corresponding to the resonance time.

A frequency offset Δf is also predicted by Helliwell's consistent wave theory, whereby the initial frequency of the triggered signal differs from the frequency of triggering signal by an amount Δf. Dowden (1972) shows that this may vary between zero and a maximum value of

$$\Delta f = \frac{4.5\, f_{B\,e}\, L^2}{R_m^{\,2}} \qquad 8.2/2$$

length of the interaction region (Helliwell, 1967)
where L is the ~~L value of the propagation path~~ and R_m is the geocentric distance to the field line at the equatorial plane. An intermediate value is taken to be one quarter of this. In terms of normalised frequency this is represented by the relation:

$$\Delta\Lambda = K_2(1-\Lambda)\Lambda^{-1/3} \qquad 8.2/3$$

where K_2 has a maximum value of 0.014 and an intermediate value of 0.0035. The trigger locus curves for the combined effects of trigger delay and frequency offset are shown in Fig. 8/3, curve A representing the zero effect, that is the unaffected hybrid whistler trace, D the maximum effect, and E the intermediate effect. It may be seen that there is good agreement between the observed trigger points (shown as circles) and the predicted curves.

However there are still a number of reasons to doubt the validity of the hybrid whistler theory of precursor generation. The first is concerned with the hybrid whistler itself. The above theory assumes that the hybrid first propagates under the ionosphere entering the magnetosphere in the opposite hemisphere to the causative sferic. It would appear just as likely, if not more so, that the hybrid enters the magnetosphere in the same hemisphere as the sferic and, after propagating through the magnetosphere, travels back to the initial hemisphere under the ionosphere. In the latter case the hybrid would show the same dispersion and delay as in the former. However the latter case could not explain the precursor.

The second objection is concerned with statistical studies of precursors. Out of the many hundreds of precursor events examined by various authors, mainly Laaspere and Wang (1968), who report that precursors are 'fairly common' at the Whistlers East network of stations, only one observation of an associated hybrid whistler has been reported (Dowden, 1972). If the hybrid is, in fact, res-

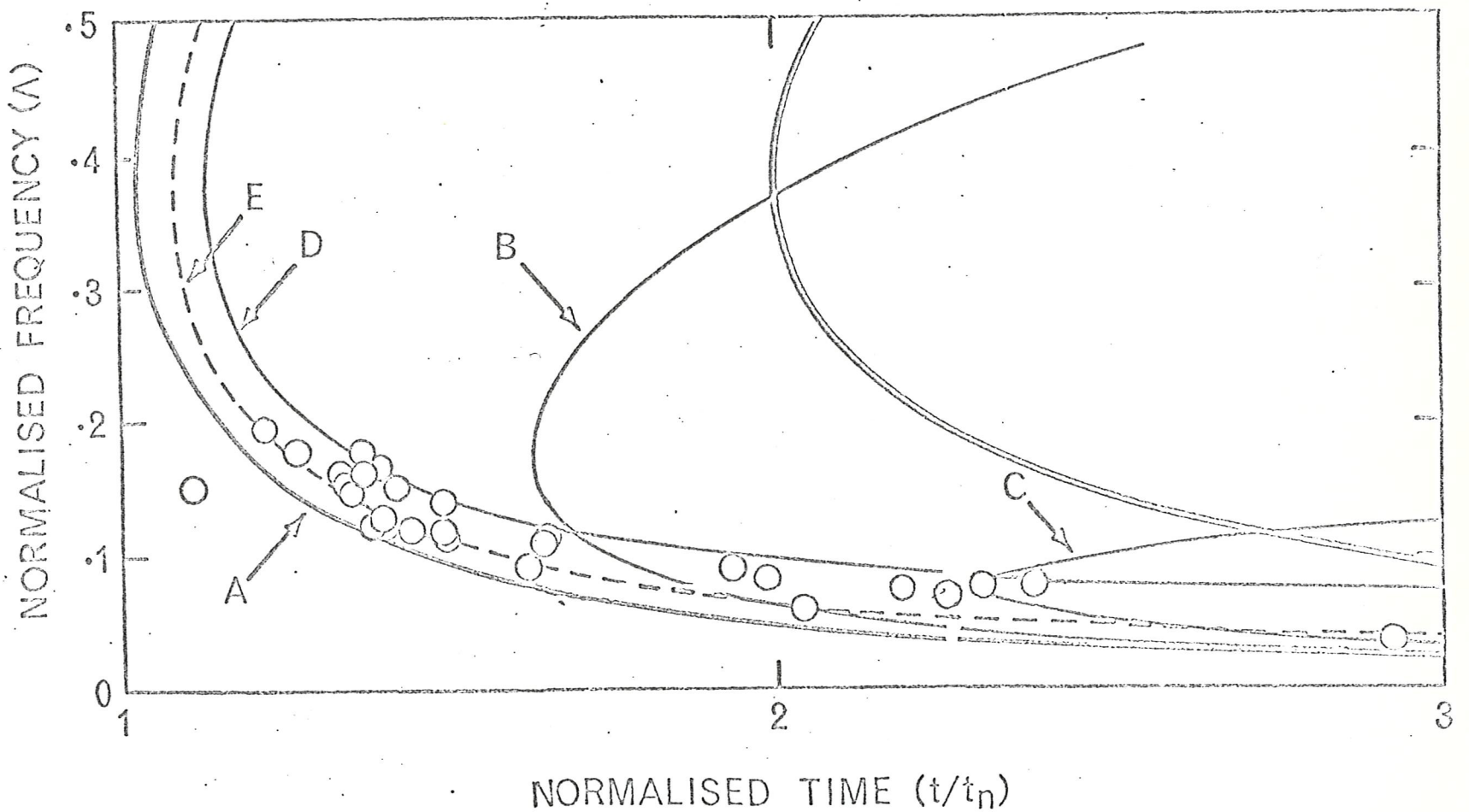

Fig. 8/3 Experimental and theoretical precursor trigger loci obtained by Dowden(1972).

ponsible for triggering the precursor it would be reasonable to expect a greater rate of coincidence than this.

Thirdly, the hybrid theory depends to a large extent on the time delay and frequency shift as predicted by the consistent wave theory of Helliwell (1967). The detailed mechanism of the wave-particle interaction is by no means well understood and so the quantitative results of this theory are open to doubt. In addition, observations of emissions definitely known to be triggered by signals show that while emissions triggered by Morse code dashes show a time delay of $\sim$140 ms and frequency shift of $\sim$300 Hz (Helliwell et al., 1964; Helliwell, 1965) those triggered by whistlers appear to branch off the whistler with neither time delay nor frequency shift (Helliwell, 1963). It is possible that these different effects might be caused by the difference in the triggering signals, the one being at a constant frequency, the other consisting of a changing frequency. In this case the precursor triggered by the hybrid would be expected to show no delay or frequency shift.

Several other mechanisms have been suggested for the generation of precursors, all of which are subject to serious objections.

(i) Longitudinal Resonance

It was suggested by Helliwell (1965) that an electron stream, modified by longitudinal resonance by the one-hop whistler might become unstable to transverse resonance and radiate an emission back along the path. This mechanism has been considered by Dowden (1972), who concludes that it is not clear how longitudinal phase bunching can induce a transverse instability, which requries helical phase bunching. It is also shown that the electron energy required for transverse resonance at a typical frequency is at least two orders of magnitude greater than that required for longitudinal resonance.

(ii) Electron Bounce

Cornwall and Schulz (1970) have shown that two particles having the same three adiabatic invariants recover their initial gyrophase relationship after each bounce period, and hence a reversed relationship after a half period. Dowden (1972) considers a mechanism in which electrons are phase bunched by transverse resonance with the one-hop whistler, but for some reason do not radiate. These electrons will become phase bunched again, in the reverse direction after half a bounce period, and could conceivably radiate an emission back along the path, which would be observed with an apparent trigger delay corresponding to half the electron bounce period. The predicted locus of trigger points is shown as curve B in Fig. 8/3, which clearly does not fit the observations.

(iii) Magnetospherically Reflected Whistler

Dowden (1972) also considers a mechanism in which unducted energy from the same sferic which produces the precursed two-hop whistler is magnetospherically reflected somewhat beyond the equator and triggers an emission on the way back. The predicted trigger locus is shown as curve C in Fig. 8/3. However it will be shown in the following chapter that this mechanism, with a number of important refinements, can explain the observed properties of precursors.

CHAPTER NINE

Experimental Observations of Whistler-Precursors Pairs

9.1

During the period 2030 - 2200 UT on March 7 1970 a series of around 120 two-hop whistlers was received at the station near St. John's, Newfoundland. Of these 40 were accompanied by precursors. In the same period a number of risers were also received; these were of a similar spectral shape to the precursors and have since been identified as precursors to unobserved two hop whistlers. No whistlers or emissions were received at Norwich, Vermont, U.S.A., or Halley Bay, Antarctica, during this period.

The precursors recorded in the sequence fell mainly under the following four headings:

(a) Single component precursors (Fig. 9/1(a));

(b) precursors containing a small ($\lesssim 4$) number of discrete components (Fig. 9/1(b));

(c) multicomponent precursors (Fig. 9/1(c));

(d) diffuse precursors (Fig. 9/1(d)).

Apart from the diffuse precursors, which appeared at the end of the sequence, there was no apparent order in the appearance of the various types. The spectral shapes of most of the precursors was the forward leaning letter S shape with near zero initial slope, reported to be the most common by Laaspere and Wang (1968). However some showed a definitely non-zero initial slope (Fig. 9/1(a)).

Fig. 9/2 shows sonagrams of some apparently spontaneously triggered risers received in the same period as the precursors. It has been

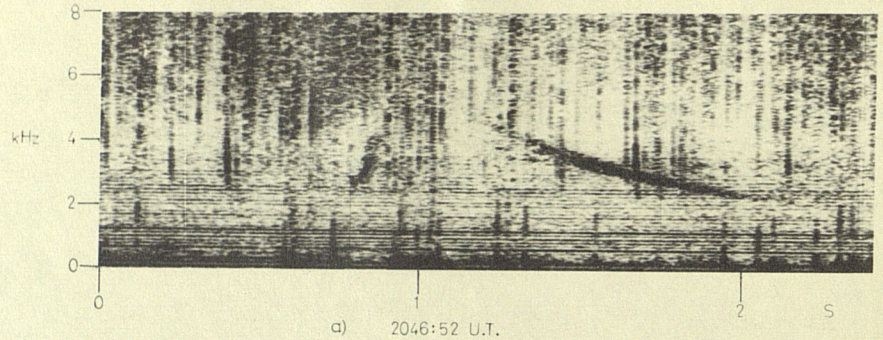

a) 2046:52 U.T.

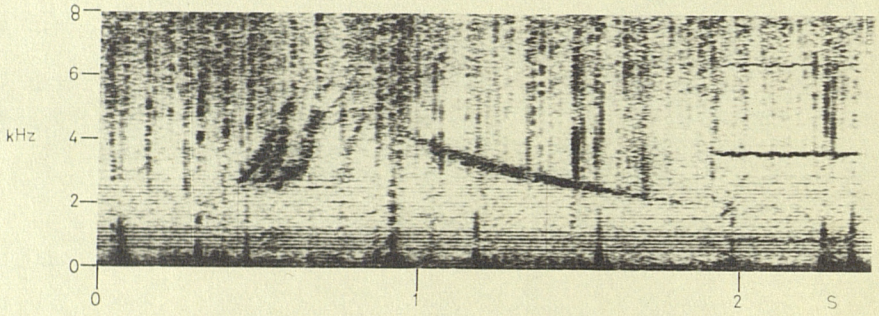

b) 2045:45 U.T.

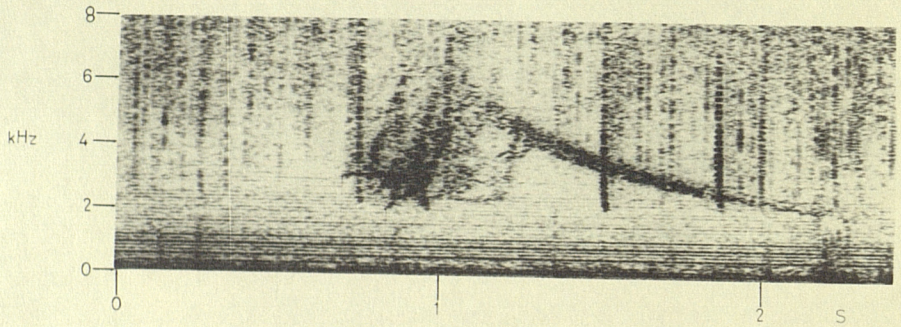

c) 2106:09 U.T.

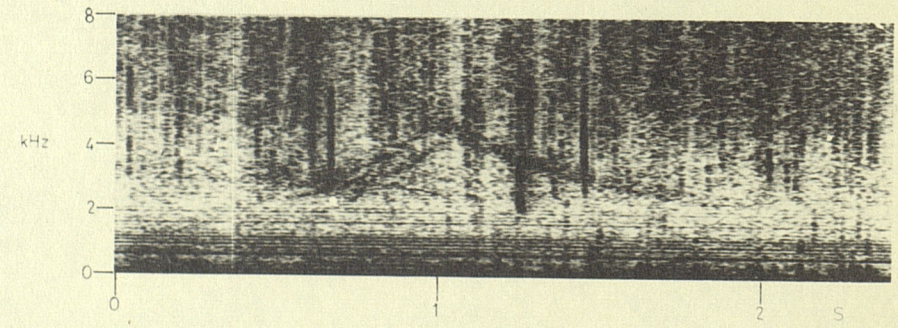

d) 2133:32 U.T.

Fig. 9/1 Sonagrams of Precursors recorded on 7 March 1970 at St. John's, Newfoundland.

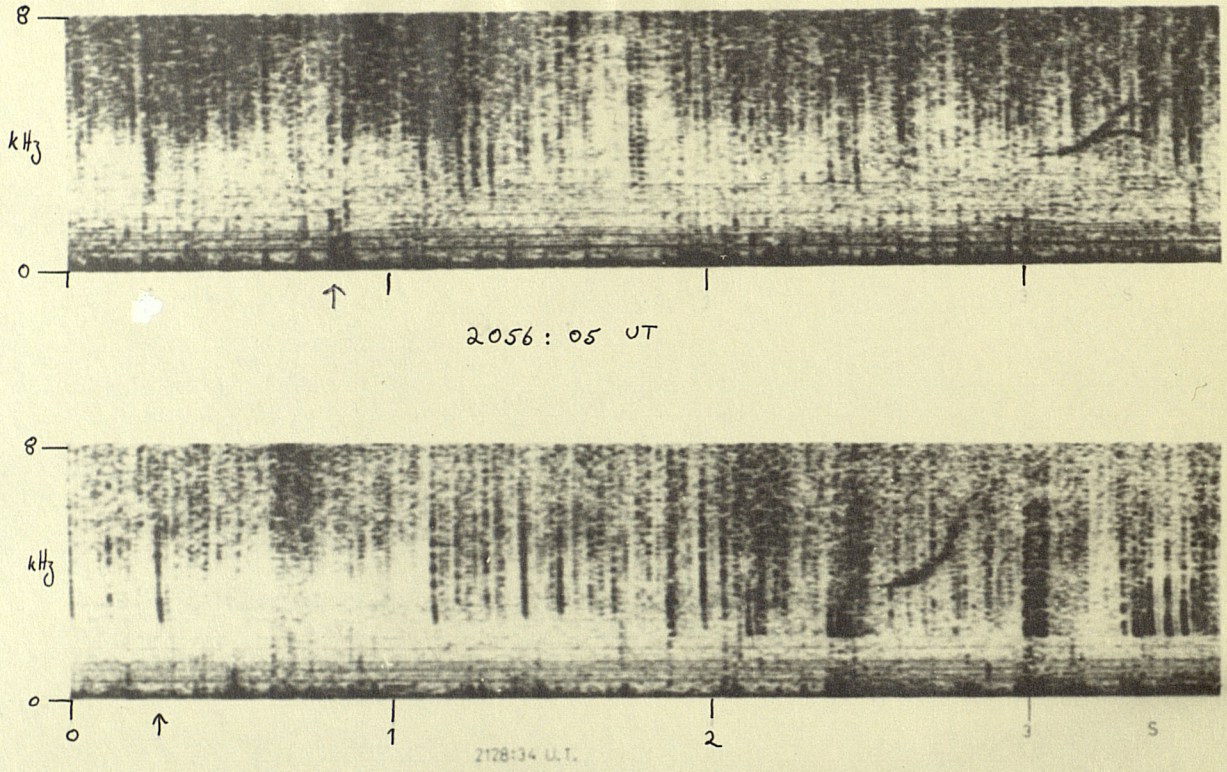

Fig.9/2 Apparently spontaneous emissions identified as precursers to unobserved whistlers.

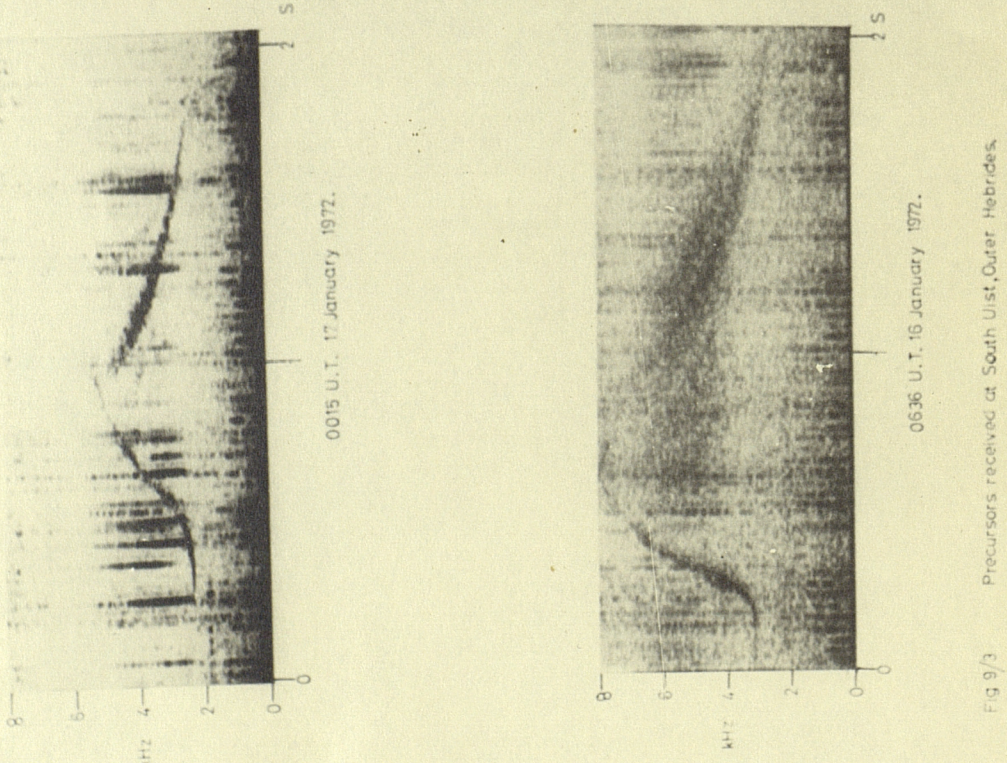

Fig 9/3 Precursors received at South Uist, Outer Hebrides.

possible to identify these as precursors to unobserved two hop whistlers. The causative sferic in each case is labelled by an arrow.

Precursors have also been received at the station on South Uist, Outer Hebrides. Fig. 9/3 shows sonagrams of two whistler-precursor pairs received on 16 and 17 January 1972.

Sonagrams of unprecursed whistlers received in the same period as the precursors at St. John's are shown in Fig. 9/4. The differences between these and the precursed whistlers will be discussed in a later section.

9.2 Analysis of Whistler-Precursor Pairs

9.2.1 Determination of causative sferic

In order to calculate the L value of the duct along which a whistler has propagated it is necessary to determine its nose frequency, that is the frequency showing the minimum group delay. Since the upper cut off frequency of all the observed precursed whistlers was well below the nose frequency, a method for determining the nose frequency of a non-nose whistler, based on that discussed by Dowden and Allcock (1971) has been used. This method requires the time of the causative sferic to be known accurately.

The first method used to determine the time of the causative sferic was the Eckersley (1935) method. Using an artitary time origin a best fit straight line is computed of t against $f^{-\frac{1}{2}}$ for the leading edge of the whistler, measured from the sonagram. The slope of this line gives the dispersion, D, of the whistler, and the intercept on the y-axis the time of the causative sferic since, with reference to Fig. 9/5,

$$t + t_s = D f^{-\frac{1}{2}} \quad \text{(see section 1.3.1)}$$

in the low frequency limit. The values of dispersion computed by

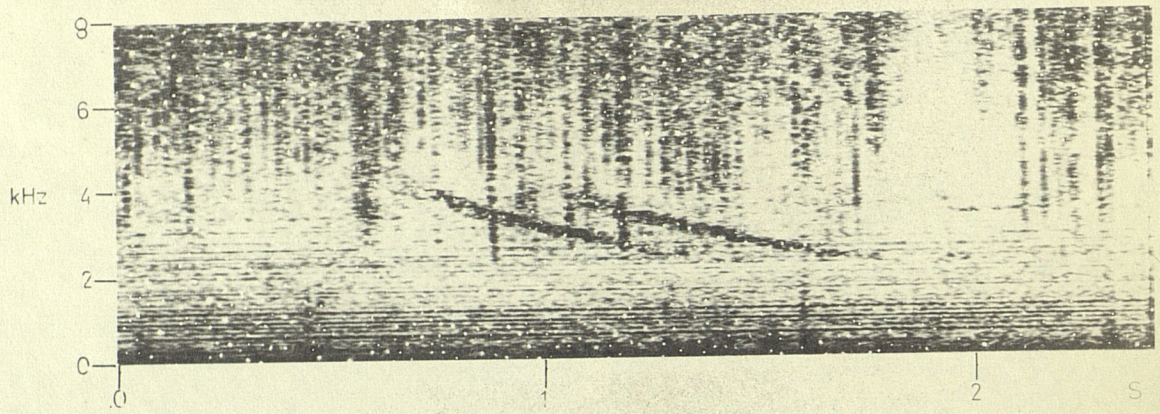

2049:26 U.T.

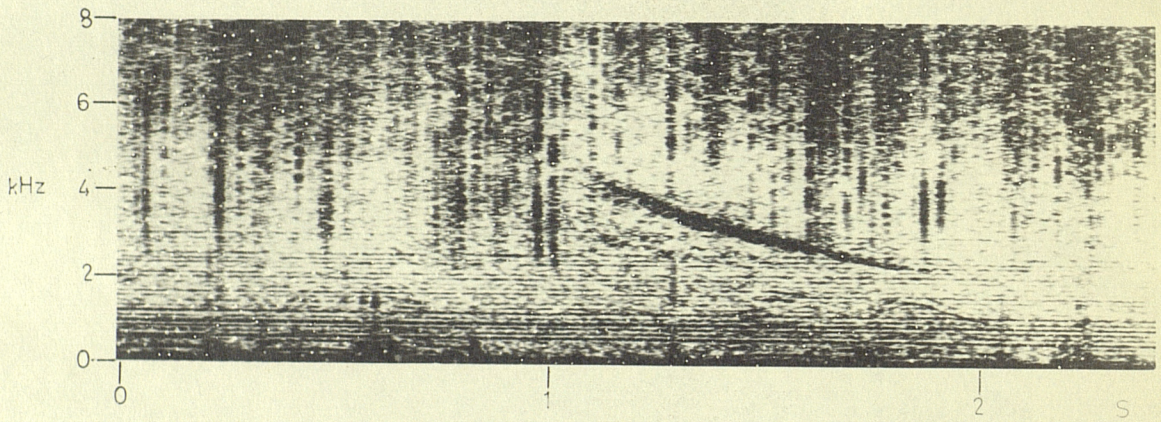

2051:08 U.T.

Fig. 9/4 Unprecursed whistlers received at St.John's, Newfoundland. 7 March 1970.

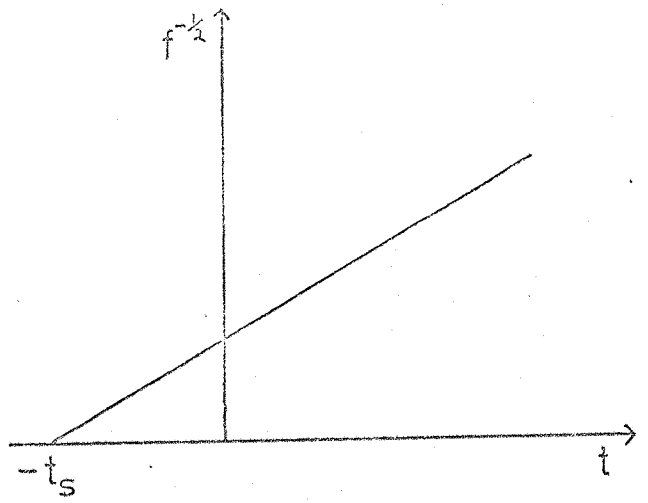

Fig. 9/5. Eckersley Method

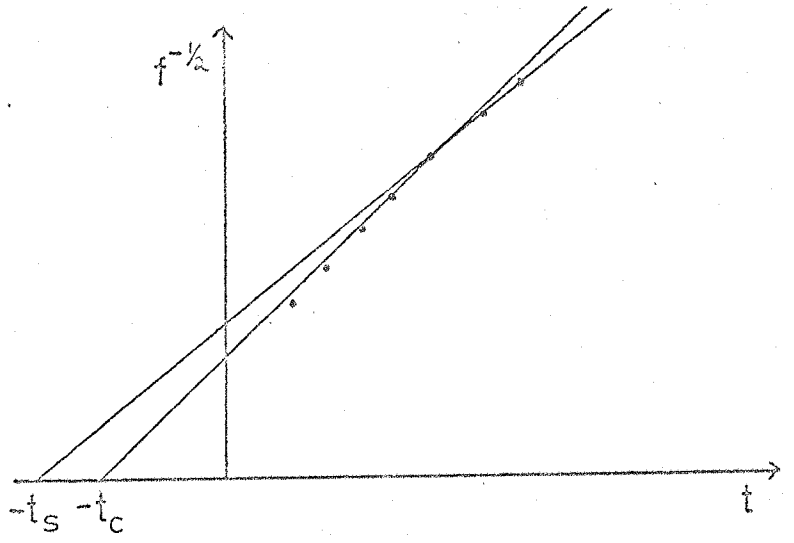

Fig. 9/6. Deviation from Eckersley law; best fit straight line to points gives an estimated sferic time t_c which is later than the true sferic time t_s.

this method were typical of two-hop whistlers, in agreement with property 1. The causative sferic must therefore have occurred in the same hemisphere as the receiver, and probably not more than a few hundred kilometers from it. It should therefore show up as a strong vertical line on the sonagram. However the sferic times obtained by the Eckersley method did not generally correspond to a strong sferic on the sonagram, although there was always a strong sferic around 0.2 s earlier than this time. It is known that the Eckersley law applies only in the low frequency limit and that the deviation from this law is such as to predict a sferic time that is too late (e.g. Helliwell, 1968). This deviation is illustrated in Fig. 9/6. All the precursed whistlers had a low frequency cut off above 2 kHz; this suggests that the low frequency cut off is too high for accurate Eckersley analysis and that the strong sferics mentioned above are those responsible for the whistler-precursor pairs.

The second method used was that devised by Rycroft and Mathur (1972). Dowden and Allcock (1971) have shown that for a whistler

$$Q(f) = D^{-1} = (t\, f^{\frac{1}{2}})^{-1} \propto f \qquad 9.2/1$$

where t is measured from the causative sferic. When Q is plotted against f it has been shown that the intercept on the frequency axis, f_o, is equal to $(3.09 \pm 0.04) f_n$. The minimum group delay, t_n, may then be calculated from the relationship

$$t_n = -(2.09 \frac{dQ}{df} f_n^{3/2})^{-1} \qquad 9.2/2$$

This method obviously does not apply in the low frequency limit, where the Eckersley law applies and D is constant, contradicting equation 9.2/1.

If the time of the causative sferic is known the nose frequency may be calculated by plotting Q against f and extrapolating to find the intercept (Dowden-Allcock method). In the Rycroft-Mathur method, Q

is calculated using many different time origins. In each case a straight line is computed for Q against f using the method of least squares. For the case in which the chosen time origin corresponds to the time of the causative sferic the points should fit a straight line with minimum error. However when this method was applied to the precursed whistlers no minimum in the error was found. The error decreased as the time origin was moved to an earlier time. The reason for this failure is that the upper cut off frequency of the whistlers was never greater than 5 kHz, well below the nose frequency. Thus the data available for analysis was in the band 2 - 5 kHz. Although it has been shown that at the higher end of this range the data deviate from the Eckersley law, the Rycroft-Mathur method also fails because data are available only over a small range of frequencies.

The problem of determining the causative sferic has been resolved in the following way. In a number of cases the results of the Eckersley analysis indicated that, the sferic occurred 0.1 - 0.2 s after a particularly energetic sferic, which was the only one of its kind within around $\pm$ 0.5 s (e.g. Fig. 9/7). In all these cases, the group delay at a frequency of 3.5 kHz was measured and found to lie in the range 2.97 $\pm$ 0.04 s. An investigation of each of the cases where the result of the Eckersley analysis had left some ambiguity it was found that there was a strong sferic within the above range. In a few ($\sim$ 6) cases there was more than one sferic in the range. However, since it is unlikely that any method would be able to resolve these they were left as ambiguous cases.

9.2.2 Determination of whistler propagation path

Having established the time of the causative sferic it is possible to compute the nose frequency using the standard Dowden-Allcock method described in the previous section. Assuming propagation along a dipole field aligned duct the L value of the duct may be calcu-

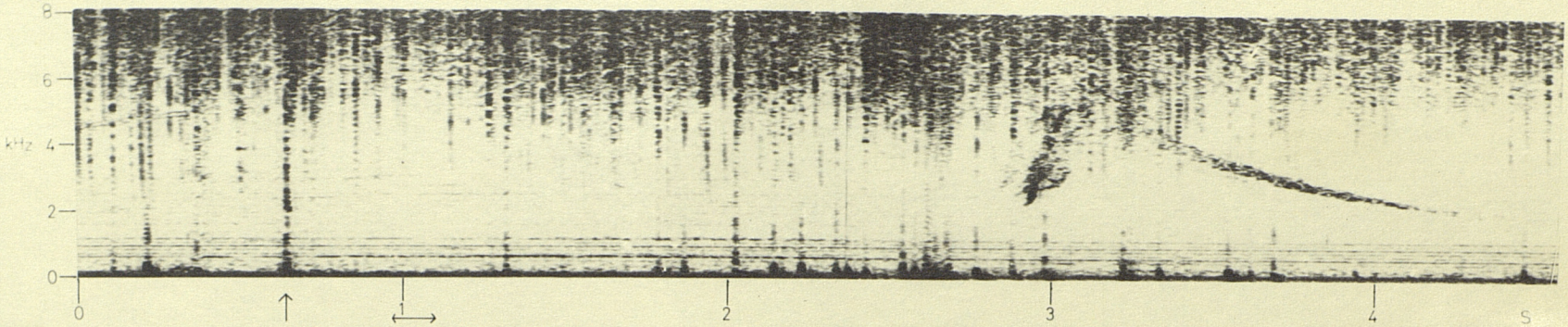

Fig. 9/7 2043:13 U.T. 7 March 1970. St. John's, Newfoundland.

Sonogram of Precursor where result of Eckersley analysis was unambiguous. (Causative sferic shown by vertical arrow: result of Eckersley analysis shown by horizontal arrow.)

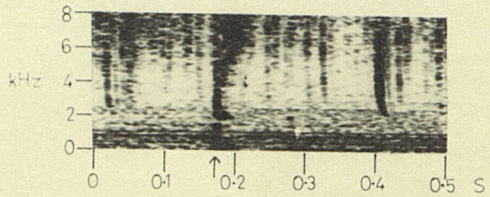

Fig. 9/8 Typical Causative tweek for whistler-precursor pair.
2106:08 U.T. 7 March 1970. St. John's, Newfoundland.

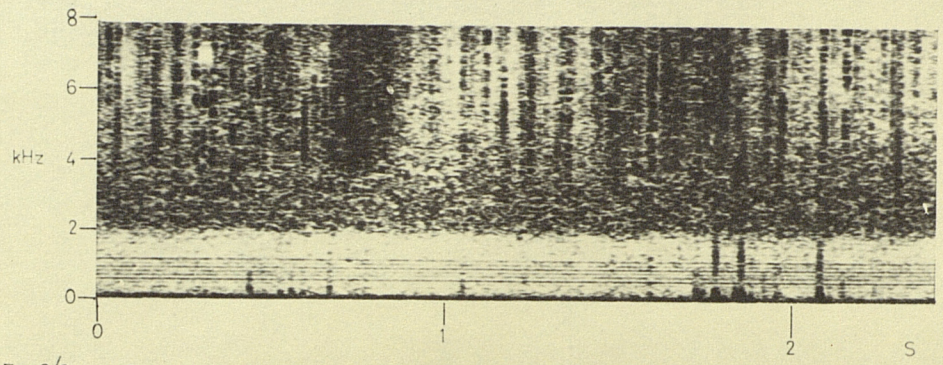

Fig. 9/9 Sonogram of VLF waveform, at 2240 U.T. 7 March 1970. St. John's, Newfoundland, showing band of hiss.

lated using the relationship

$$L = \left(\frac{325.6}{f_n}\right)^{1/3} \qquad 9.2/3$$

where f_n is measured in kHz.

In order to reduce error in extrapolation of the Q vs f relationship it is necessary to include data over as wide a range of frequencies as possible. For this reason the whistlers chosen for this analysis were those extending to the highest frequencies. Best fit straight lines of Q against f were computed using the method of least squares and extrapolated to find f_o and hence f_n. The calculated nose frequencies and corresponding L values for the whistlers analysed are shown in table 9/1. Also included in table 9/1 are the results of a similar analysis of one of the precursed whistlers received at South Uist.

It may be seen that the calculated L values for the whistlers received at St. John's are very nearly the same. Because of this result and the other similarities observed in the dispersion and group delay of all the whistlers in this sequence, it is concluded that the propagation path is in each case the same. The discrepancies in the calculated values of f_n and hence L are attributed to the errors incurred in the Dowden-Allcock analysis due to the large extrapolation necessitated by the narrow range of frequencies available for analysis. It is concluded that the nose frequency of the precursed whistlers received at St. John's was 11.4 $\pm$ 0.4 kHz and the L value of the propagation path was 3.06 $\pm$ 0.04. The precursed whistler received at South Uist extended up to a frequency which was much closer to the nose frequency; hence there was a much smaller error in the computed nose frequency.

9.2.3 Identification of thunderstorm generating whistler-precursor pairs

The sferics identified as being responsible for generating the whistler precursor pairs at St. John's show many characteristics in

Station	Date	Time(UT)	f_n(kHz)	L value
St. John's	7 March 1970	2043:13	10.51	3.14
" "	" " "	2052:22	11.28	3.07
" "	" " "	2056:05	11.45	3.05
" "	" " "	2100:02	11.87	3.01
" "	" " "	2106:09	11.76	3.02
" "	" " "	2116:25	10.96	3.10
" "	" " "	2118:05	11.74	3.02
" "	" " "	2119:55	11.32	3.07
South Uist	17 Jan. 1972	0015:18	7.55	3.59

Table 9.1 Results of Dowden-Allcock analysis to determine the nose frequency of the precursed whistlers.

common with the tweeks received during the eclipse some two hours earlier (see Chapter 5). All are observed as tweeks with a cut off frequency around 1.8 - 1.9 kHz. In all cases some energy is retained below this cut off frequency and all show less dispersion in the range 2 - 3 kHz than do other tweeks received in the same period (see Fig. 9/8). It is therefore concluded that these sferics were generated at the same storm centre as those received during the eclipse (see section 5.3). The probable positions of the storm centres at 2100 UT are: centre number 1: 44.4°N, 57.5°W corresponding to an L value of 3.20 at an altitude of 300 km; centre number 2: between 41.4°N 57.5°W and 40.4°N 59.5°W corresponding to an L value of 2.84 - 2.77 at 300 km.

9.2.4 Differences between precursed and unprecursed whistlers

A number of the unprecursed whistlers received at St. John's at the same time as those with precursors have been analysed in the same way. No systematic differences were found in their dispersion, group delay or nose frequency; their causative sferics appeared to come from the same source. Two differences were apparent, however. The unprecursed whistlers tended to be less intense and to have their upper cut off frequency at a lower value. It is therefore suggested that the wave-particle interaction responsible for generating the precursor close to the equatorial plane also acts to amplify the whistler, which passes through the interaction region shortly after the resonant interaction has taken place. It is also observed that the frequency band to which the precursors and precursed whistlers are confined is the same as that for the band of VLF hiss (see Fig. 9/9) received at St. John's between 2230 and 2330 UT, shortly after the precursors and whistlers ceased. This suggests that electrons with energies suitable for resonant amplification of whistler mode energy in this band only were available at this L value at this time. This subject will be discussed at greater length in the following chapter.

9.2.5 Precursor trigger points

The precursor trigger point, as defined by Dowden (1972), is the point in the frequency-time plane at which the precursor has its origin. The trigger point coordinates of each of the observed precursors have been measured, except in those cases where the trigger point was not well enough defined for accurate measurement. In cases of multicomponent precursors each well defined trigger point has been included. Fig. 9/10 shows trigger frequency, f_t, normalised to the minimum gyrofrequency of the whistler propagation path, $f_{B\ e\ min}$, plotted against trigger time, t_t, normalised to t_n. The minimum gyrofrequency is related to the whistler nose frequency by:

$$f_n = 0.37\ f_{B\ e\ min} \qquad \text{(Angerami, 1966)} \qquad 9.2/4$$

The solid lines shown in the figure are the extreme limits predicted by Dowden's (1972) theory of precursor generation (curves A and D in Fig. 8/6).

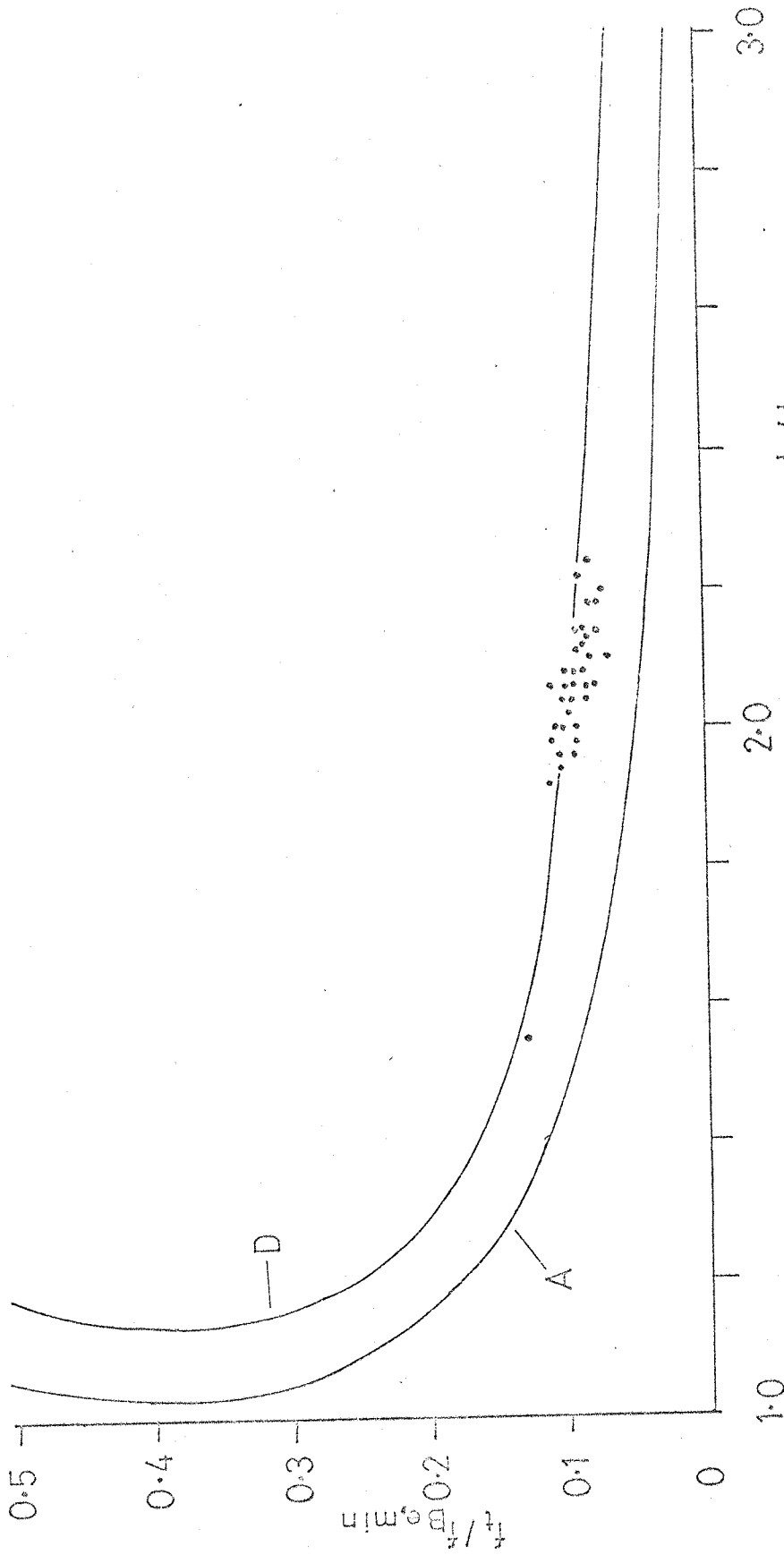

Fig. 9/10. Trigger points of the precursors received at St. John's and South Uist.
Curves A and D correspond to curves A and D in fig. 8/3.

CHAPTER TEN

New theoretical models of precursor generation

The reception of the series of precursors discussed in the previous chapter has led the author to consider the mechanism by which precursors are generated. Although the theory of Dowden (1972) leads to good agreement with the experimental data it is open to some objections which have been discussed in Chapter Eight. An attempt is made here to formulate a new mechanism involving only well established properties of the magnetosphere.

10.1 Transverse Resonance

It is assumed that the precursor is generated by a wave particle interaction involving the transverse resonance instability (Brice, 1964; Helliwell, 1967), which has been discussed in Chapter Three. Since the initial slope $(\frac{df}{dt})$ of the precursor in the frequency-time plane is observed to be typically close to zero it is concluded that the interaction region is close to the equatorial plane. Before proceeding to consider the new models of precursor generation some factors affecting the possibility of transverse resonance will be discussed. Fig. 10/1 illustrates the general case of a circularly polarised wave crossing the equatorial plane, where the angle between the wave vector $\underline{k}$ and the earth's magnetic field $\underline{B}$ is θ. The electric vector $\underline{E}$ may be resolved into a linearly polarised component parallel to the magnetic field and an elliptically polarised component perpendicular to it. The ray direction of the wave makes an angle β with the geomagnetic field. An electron spiralling along the field line has a velocity $v_{//}$ parallel to the field and a velocity $v_{\perp}$ perpendicular to it. There are three factors affecting the transverse resonant instability which

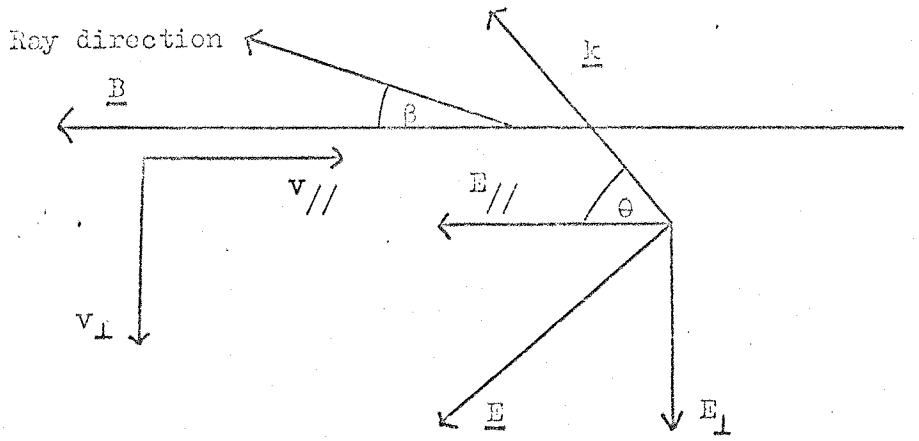

Fig 10/1 Waves and particles crossing equatorial plane

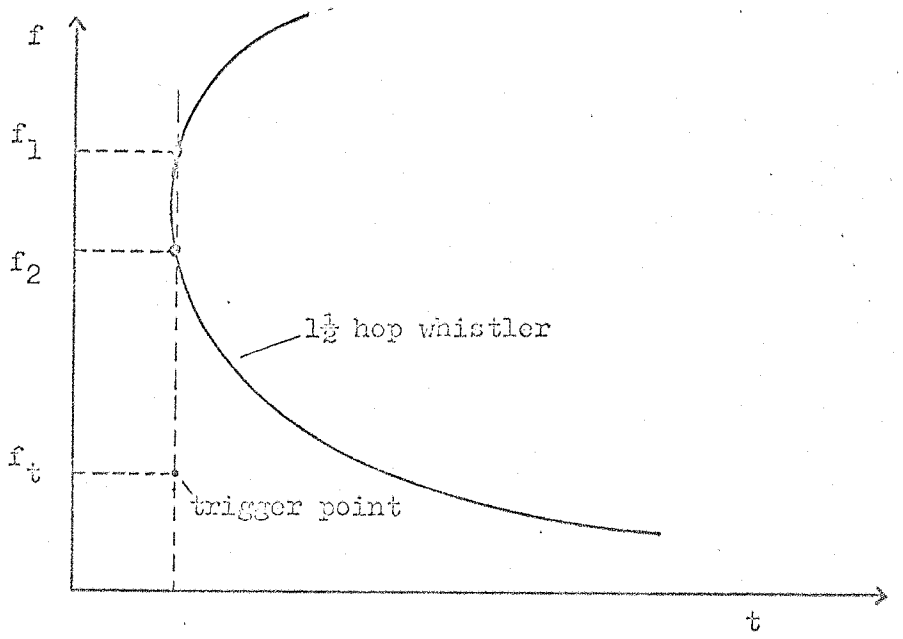

Fig. 10/2 ' Beating Model '

are dependent on Θ and β. These are:

i) The electron energy required to satisfy the transverse resonance condition which is given by

$$W_{\parallel \ res} \alpha \qquad v_{\parallel}^2 = \left[\frac{v_p(f - f_{Be})}{f \cos \Theta} \right]^2 \qquad 10.1/1$$

where v_p is the wave phase velocity, for non-relativistic electrons. Thus the electron energy required for resonance increases with Θ. Since there are progressively less electrons available at higher energies the probability of resonance decreases as Θ increases, especially for $\Theta > \pi/3$.

ii) The condition for transverse resonance is given by

$$\underline{E}_{\perp} \cdot \underline{v}_{\perp} = \text{constant} \qquad 10.1/2$$

Since $\underline{v}_{\perp}$ describes a circle about the magnetic field this condition may only be truly satisfied if $\underline{E}_{\perp}$ is circularly polarised. When $\Theta \neq 0$, $\underline{E}_{\perp}$ is elliptically polarised, and may be resolved into a circularly polarised component of magnitude $E \cos \Theta$ and a linearly polarised component which varies as $E(1 - \cos \Theta) \sin 2\pi ft$ in a direction mutually perpendicular to $\underline{k}$ and $\underline{B}$. Although the linearly polarised component may contribute to the resonant interaction it does not satisfy equation 10.1/2 since the scalar product varies between 0 and a maximum value. Thus as Θ increases the magnitude of the component of $\underline{E}$ that is effective in the interaction decreases, reducing the probability of occurrence of the interaction.

iii) The exchange in energy between electrons and waves in the interaction is given by

$$\Delta W = q \, \underline{E} . \underline{v} \Delta t \qquad 10.1/3 \ (4.3/2)$$

Hence the longer the particles and waves are in resonance the greater will be the energy interchange. Since the interaction involves the collective effect of waves upon a stream of electrons this time may

be maximised if the waves and particles are travelling parallel to one another (although in opposite directions), that is if $\beta = 0$ and hence $\Theta = 0$. Otherwise the waves and particles will only be in resonance for as long as it takes for the waves to traverse a few gyro radii, say three r_{Be}, of the electrons. This time, t, is given by

$$t = \frac{3\, r_{Be}}{v_p \sin\beta} \qquad 10.1/4$$

For an electron energy of 100 keV in the equatorial plane at an L value of around 3 this places an upper limit on t of 1 ms for $\beta = \pi/6$, corresponding to 3 cycles of a 3 kHz wave. This is much smaller than the bunching time, of the order of 0.1 s, predicted by Helliwell (1967) for the occurrence of a particle-wave interaction.

These three factors combine to make resonance between electrons and waves whose wave vectors are field aligned much more probable than with waves whose wave vectors are at a large angle to the earth's magnetic field.

The basic problem to be solved in formulating a model for the generation of precursors is how energy at the correct frequency, and from the same lightning discharge as that which causes the two hop whistler, can propagate to the equatorial plane arriving at the correct time and with the correct characteristics to trigger the observed precursor.

10.2 First model: 'beating'

One way of ensuring that the ray direction and wave vector of the triggering signal make small angles with the earth's magnetic field is for the triggering signal to be ducted (see section 4.2/3). The first new model considered, which involves ducted energy, is illustrated in Fig. 10/2 which shows a 1½ hop whistler as viewed in the equatorial plane. It is suggested that two frequencies f_1 and f_2,

which have the same group delay, interact to give a beat frequency $f_1 - f_2 = f_t$, which triggers the observed precursor. The trigger time predicted by this mechanism is thus

$$t_t = 0.75\ t(f_1) + 0.25\ t(f_t) \qquad 10.2/1$$

where $t(f)$ is the observed two hop group delay of the precursed whistler. Since the precursed whistlers do not generally show a nose frequency it is necessary to compute f_1, f_2, and $t(f_1)$ using the Dowden-Allcock law. f_1 and f_2 are found by solving the simultaneous equations

$$f_1 - f_2 = f_t$$

$$t(f_1) = t(f_2) \qquad 10.2/2$$

where $t(f)$ is obtained from the Dowden-Allcock law:

$$Q(f) = (t\ f^{\frac{1}{2}})^{-1} = j\ f + k, \text{ where } j \text{ and } k \text{ are constants,}$$

giving $$t(f) = \left[(jf + k)(f^{\frac{1}{2}}) \right]^{-1} \qquad 10.2/3$$

f_2 is thus given by the solution of the quadratic

$$a\ f_2^2 + b\ f_2 + c = 0 \quad \text{where} \quad \left.\begin{aligned} a &= 3\ j^2\ f_t \\ b &= 3\ j^2\ f_t^2 + 4\ j\ k\ f_t \\ c &= j^2\ f_t^3 + 2\ j\ k\ f_t^2 + k^2 f_t \end{aligned}\right\} 10.2/4$$

Hence $t(f_2)$ may be calculated using 10.2/3.

Using data from precursed whistlers from St. John's and South Uist values of j and k have been found by computing least squares regression lines of $Q(f)$ against f in each case. Hence f_2 and $t(f_2)$ were found using equations 10.2/3 and 10.2/4. The trigger frequency f_t and the two hop delay at the trigger frequency $t(f_t)$ were measured directly from the sonagrams and hence the predicted value of t_t was calculated using 10.2/1. It was found that in each case the trigger

times predicted by this model are significantly later (by around 0.2 s) than the observed values. Further investigations into the feasability of 'beating' between the two frequency components of the same whistler have not, therefore, been pursued.

10.3 Second model: triggering by unducted energy

In the absence of a convincing model involving triggering by ducted energy it was decided to investigate the possibility of precursors being triggered by unducted energy from the same causative sferic as the precursed two hop whistler. This investigation has been carried out using the VLF ray tracing computer programe developed by Alexander (1971), which has been discussed briefly in Chapter Four. The magnetospheric models used were the summer days (SD) and winter night (WN) diffusive equilibrium models described in section 4.2.4.

It has been shown in section 10.1 that it is unlikely that energy arriving at the equatorial plane with angles between the wave vector and magnetic field and ray direction and magnetic field that are not small will be able to trigger a precursor by transverse resonance. Therefore an unducted path must be found where the wave arrives at the equatorial plane with these angles close to zero. To search for such paths by starting rays in the ionosphere is obviously a very lengthy process because of the large number of combinations of possible starting parameters. The method employed has been to launch rays in the equatorial plane at various L values, with wave normal angles equal to (π + required wave normal angles). The ray paths are traced in reverse to find under what circumstances the rays return to the ionosphere in the correct hemisphere. This method has been successfully used by Alexander (1971) to find the possible unducted paths to a satellite Alexander (1971) also showed that the path

obtained by tracing in reverse does not differ significantly from that obtained when the ray is started off at 300 km altitude, the lowest altitude for which the ray tracing program is valid. In all figures of ray paths presented here the ray direction shown will be the forward direction regardless of whether the ray was traced in the reverse or forward direction.

Fig. 10/3 shows a typical ray path for a wave started off in the equatorial plane with $\Theta = \pi$ (and hence $\beta = \pi$) and where no model plasmapause nor duct has been included (see section 4.2.5). It is found that in all cases the ray undergoes at least two magnetospheric reflections. However, to arrive at the equatorial plane travelling in the correct direction to trigger a precursor to the two hop whistler the number of magnetospheric reflections must be odd. The time delay involved in undergoing three magnetospheric reflections is obviously too long to be able to account for the observed trigger time. It is therefore concluded that an unducted path that could be responsible for triggering a precursor must contain only one magnetospheric reflection. The simple model illustrated in Fig. 10/3 cannot therefore explain the appearance of the precursor.

Ray tracing results presented by Alexander (1971) show that rays impinging upon the model plasmapause from within are refracted back into the plasmasphere. It is possible, therefore, that if a ray started off in the ionosphere encounters the plasmapause at some stage along its path after its first magnetospheric reflection the path might be modified so as to allow the ray to propagate to the equatorial plane, arriving with its wave vector field aligned. A set of rays has been traced in reverse starting from the equatorial plane with $\Theta = \pi$, with the centre of the plasmapause, rather than being set at a particular L value, taking on a number of different L values. It is

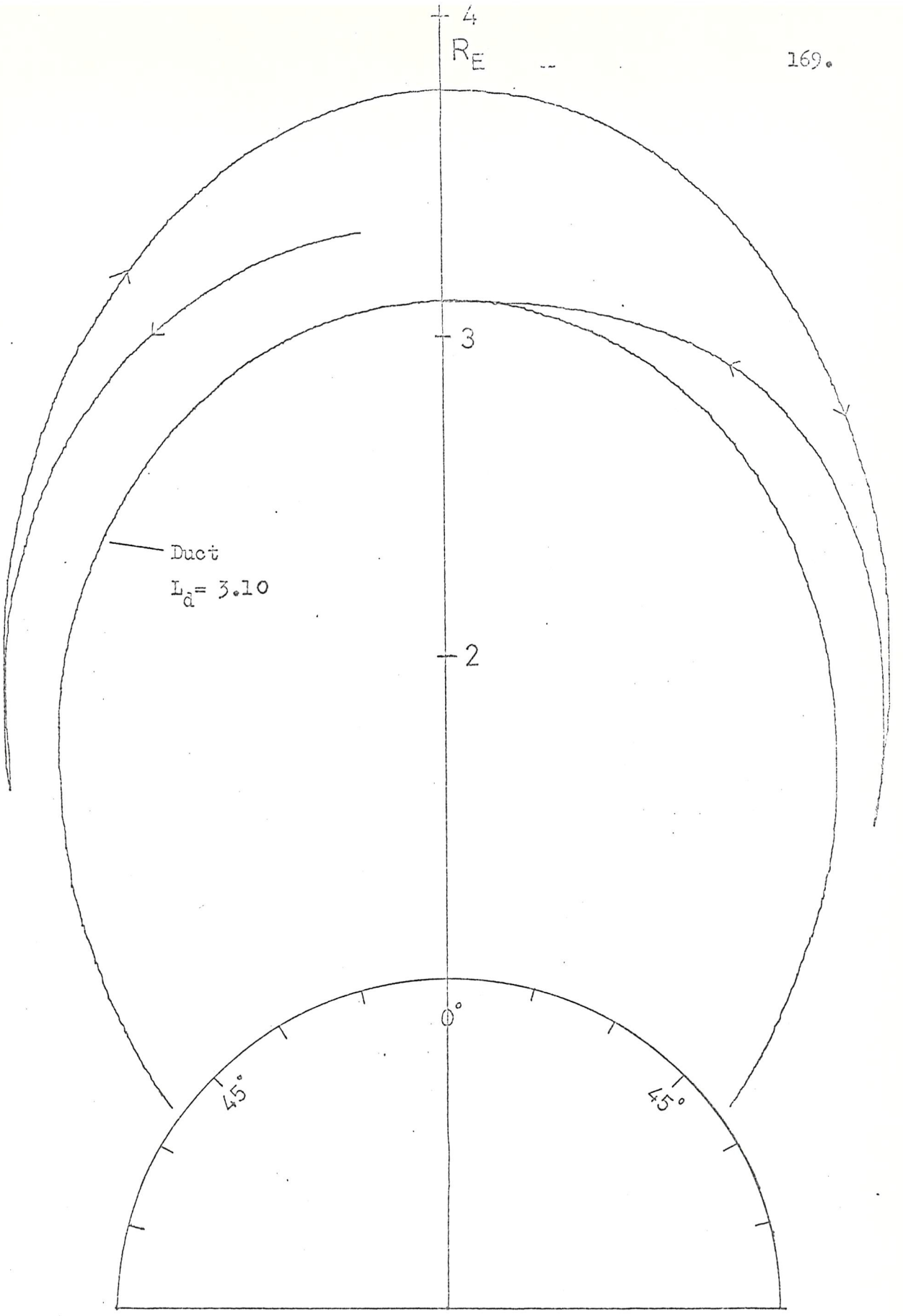

Fig. 10/3. Ray diagram illustrating unducted model with no plasmapause included.

found that certain plasmapause positions give rise to ray paths of the type shown in Fig. 10/4 where a ray launched from the ionosphere is, after one magnetospheric reflection, refracted by the plasmapause and arrives at the equatorial plane with $\Theta = 0$. This model appears to fulfil all the general conditions required for the generation of precursors. The model has, therefore, been investigated in detail, by means of the ray tracing program, the results being presented in the following section.

10.4 Ray Tracing Results

10.4.1 Winter night model

Using the method of reverse ray tracing throughout, paths of the type shown in Fig. 10/4 have been found for rays with frequencies between 1 and 4 kHz arriving with $\Theta = 0$ in the equatorial plane at L values between 3 and 3.9. The L value at which the ray arrives in the equatorial plane is the L value of the duct (L_d) in which the precursor is triggered. It is assumed that L_d is the same as or very close to the L value of the duct in which the precursed two hop whistler propagates. Fig. 10/5 shows how L_p, the position of the centre of the plasmapause required for such ray paths varies with L_d for 3 kHz rays. It may be seen that at the lower values of L_d a suitable path is available for a relatively wide range of plasmapause positions, this range becoming progressively narrower with increasing L_d. Similar results are obtained at other frequencies. The plasmapause region covers the range $L_p \pm 0.15$. Therefore all points on Fig. 10/5 which lie below the line $L_p = L_d + 0.15$ (shown as a dotted line) correspond to a predicted overlap between the duct and plasmapause regions. However in the model plasmapause the electron density falls by only a factor of 10 in an L value range of 0.3, which is considerably less steep than is often observed (Carpenter, 1966). When a more realistic model of the plasmapause is used in which the electron density falls by a factor of 100 in an L value range of 0.3 the predicted values of L_p are as shown in Fig. 10/6. It may be seen

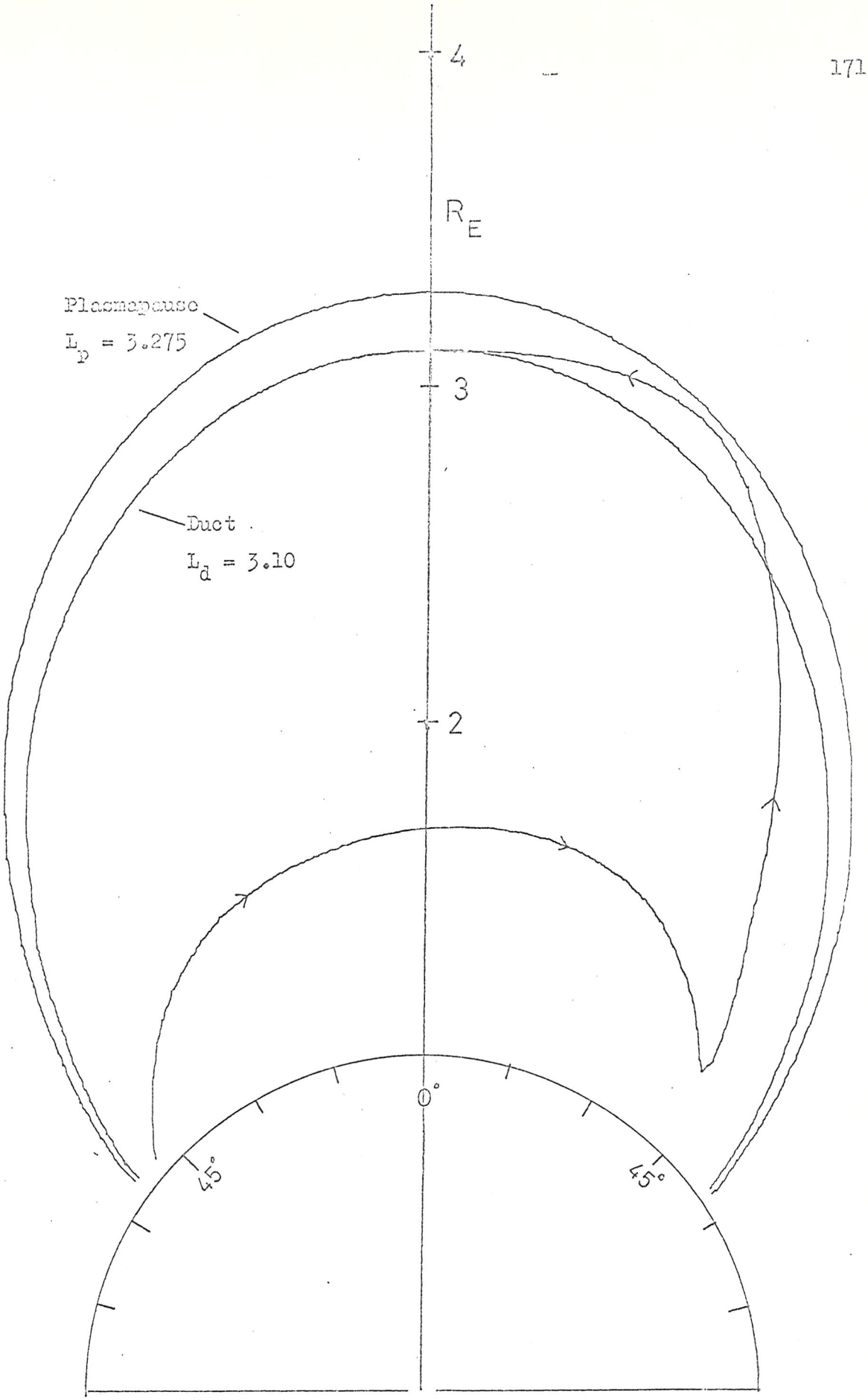

Fig. 10/4. Ray diagram illustrating unducted model with plasmapause included.

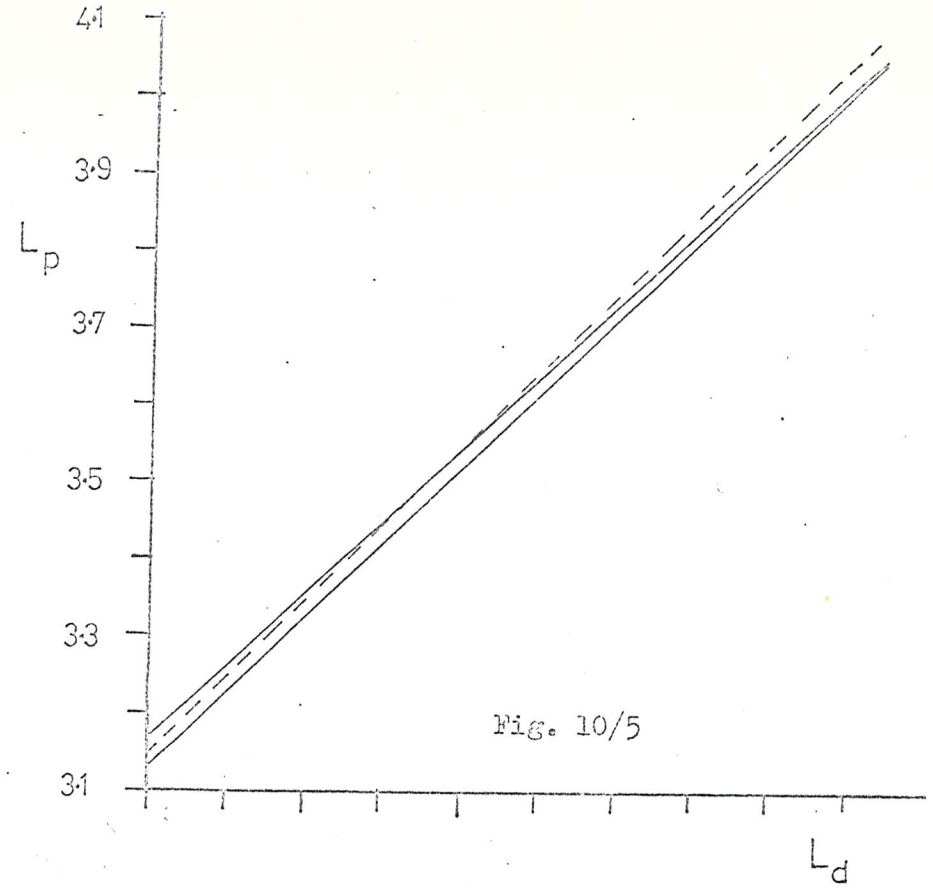

Fig. 10/5

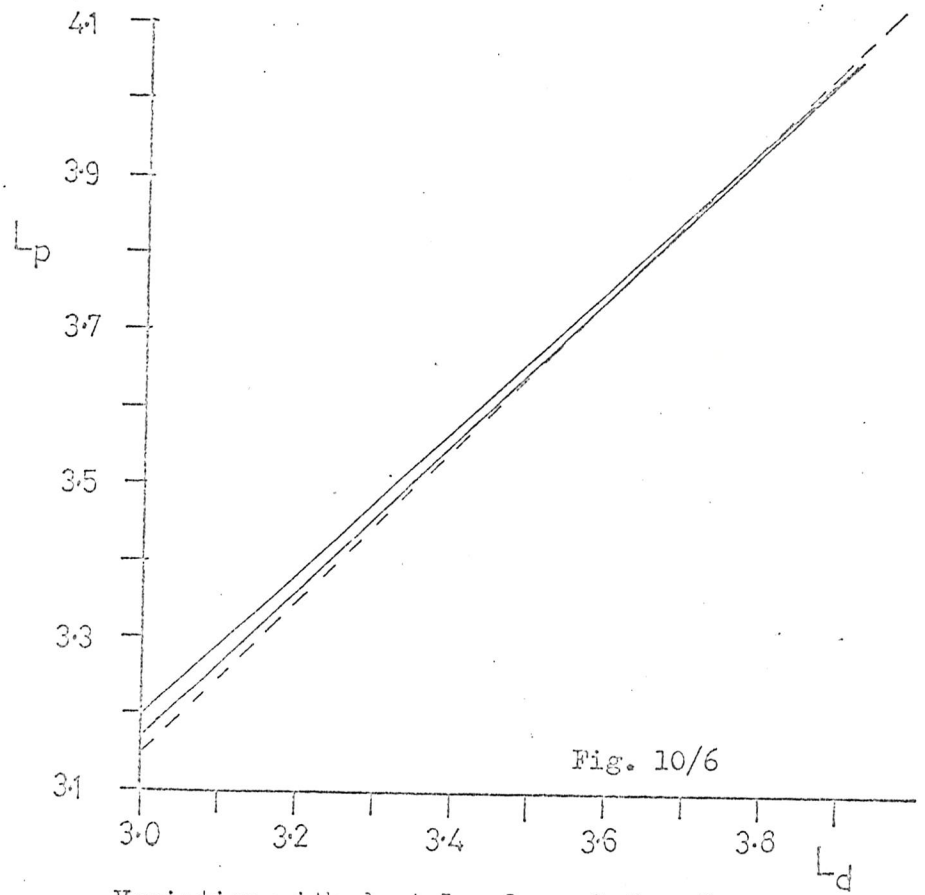

Fig. 10/6

Variation with duct L value of the plasmapause position required for the unducted model of precursor triggering using the Winter Night model. Fig. 10/5 - using Alexander's(1971) plasmapause model. Fig. 10/6 - using steeper plasmapause model.

(Dotted line represents the inner edge of the plasmapause)

that here no overlap between plasmapause and duct is predicted except at the highest latitudes, where precursors are seldom observed. It is found that the inclusion of the sharper plasmapause model does not significantly alter either the ray path or the propagation time to the equatorial plane; its only effect is to increase the predicted value of L_p by around 0.2.

The predicted starting values of geomagnetic latitude or L value (L_i) and wave normal angle with respect to the vertical (V_i), (that is the values of these parameters with which the ray traced in reverse arrives at 300 km), are plotted against L_p in Fig. 10/7 (a) and (b) for a 3 kHz wave arriving in the equatorial plane at $L_d = 3.1$. Energy starting from a predicted initial L value (L_i) that differs greatly from the duct L value (L_d) is unlikely to produce a whistler precursor pair since part of the energy must become ducted to produce the whistler. This energy may however trigger a precursor which may be received without its two hop whistler as an apparently spontaneously generated emission. This possibility is discussed further in the following chapter.

The predicted initial wave normal angles with the vertical (V_i) may be seen to vary between around 15° to values greater than 60°. It may be shown (e.g. Helliwell, 1965) that for waves propagating upwards through a horizontally stratified ionosphere the wave normal angle with respect to the vertical decreases as long as the refractive index increases since, by Snell's law,

$$\mu_1 \sin V_1 = \mu_2 \sin V_2 \qquad 10.4/1$$

and if $\mu_2 > \mu_1$, then $V_2 < V_1$. If μ_1 is taken as 1, for the earth-ionosphere waveguide, and μ_2 as 10, a typical value for the ionosphere, then eq. 10.4/1 gives a maximum value for V_2 of around 6°. However the electron density in the ionosphere increases only as far as the peak in the F2 region which is typically around 300 km. If the peak were

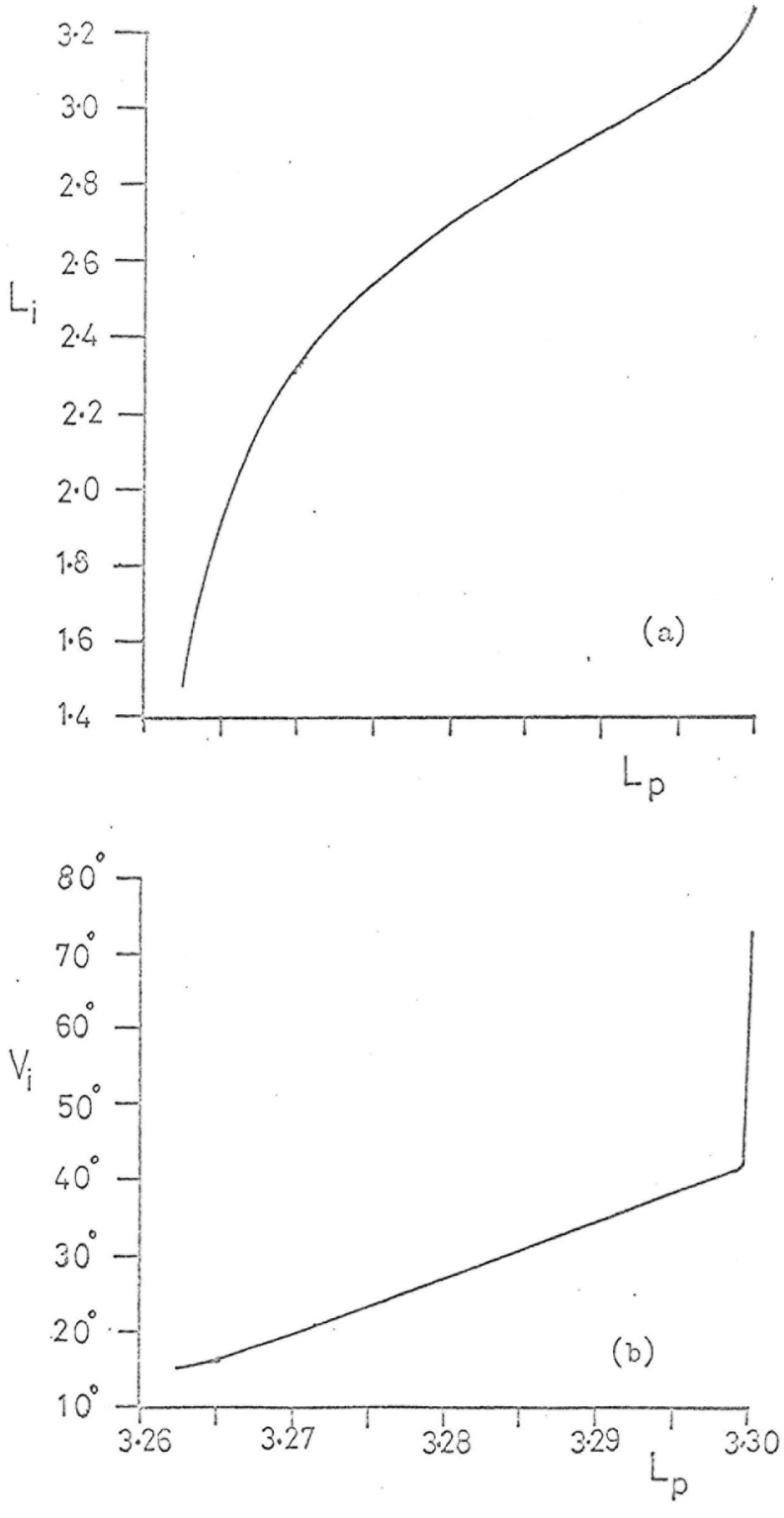

Fig. 10/7. Variation with plasmapause position of a) initial L value and b) initial wave normal angle predicted by the unducted model of precursor triggering using the Winter Night model.

lower than this, say around 250 km, then wave normal angles with the vertical up to around 15° might be expected at 300 km. Horizontal gradients in ionospheric electron density will also cause changes in the wave normal angle (Helliwell, 1965). Significant horizontal gradients may be found at sunrise and sunset times, and also during solar eclipses. Similar gradients may be found at other times, especially at middle latitudes (Helliwell, 1965). It is concluded that if horizontal gradients or some other type of discontinuity exist in the ionosphere and/or the F2 region peak lies below 300 km then wave normal angles in excess of 15° with the vertical are not unlikely at 300 km altitude. It is difficult to put an upper limit on possible values of V_i but a value of around 40° is suggested. This argument is supported by the fact that the precursors received at St. John's occurred between 30 and 90 minutes after the solar eclipse had ended, when it would be reasonable to expect that horizontal gradients still persisted in the F region, the response time of which is of the order of one hour.

The trigger time (t_t) of the precursor predicted by this mechanism is given by

$$t_t(f_t) = t_u(f_t) + t_{\frac{1}{2}}(f_t) \qquad 10.4/1$$

where t_u is the unducted propagation time to the equatorial plane and $t_{\frac{1}{2}}$ is the half-hop ducted propagation time from the equatorial plane back to ground level. $t_{\frac{1}{2}}$ has been computed using the model duct given by Alexander (1971) in which the duct is represented by a gaussian shaped enhancement superimposed on the background electron density profile (see section 4.2.5). $t_{\frac{1}{2}}$ is a function of the duct enhancement, a greater duct enhancement giving a long ducted propagation time. Values of t_t have been computed using duct enhancements of 10% and 40%, these values being taken to represent the extremes of likely duct

enhancements (Angerami, 1970). Following Dowden (1972) f_t and t_t have been normalised to the minimum electron gyrofrequency of the ducted propagation path, $f_{B\ e\ min}(L_d)$, and the minimum group delay, t_n, respectively as in Fig. 8/3. This has the advantage of allowing data from all whistler precursor pairs regardless of the L value of their propagation path, to be presented on one graph. A graph normalised trigger frequency vs normalised trigger time is referred to as the trigger locus. The nose frequency, f_n is given by

$$f_n = 0.37\ f_{Be\ min} \qquad \text{(Angerami, 1966)} \qquad 10.4/2$$

where $f_{Be\ min}(L) = \frac{880}{L^3}$ kHz (Helliwell, 1965)

In each case t_t has been normalised to a value of t_n computed using the same duct enhancement. The travel time between 300 km and 100 km has been estimated in each case by assuming that it was equal to twice the travel time between 300 km and 400 km, a reasonable assumption in view of the approximate symmetry of the electron density profile about 300 km. Since it is found that the ratio $\frac{t_t}{t_n}$ is not significantly (i.e. $< 1\%$) altered by its inclusion, this correction factor has been omitted throughout the results presented here.

The predicted loci of trigger points for the two duct enhancements are shown in Fig. 10/8(a) and (b). The experimental points shown in Fig.s 8/3 and 9/10 are shown as dots. It may be seen that there is reasonably good agreement between the predicted curves and the experimental data and that slightly better agreement is obtained with the higher duct enhancement. The trigger locus may be thought of as being made up of a family of curves, one for each value of the triggering frequency, f_t. Similarly it may be thought of as being made up of a family of curves for each value of L_d. Figs. 10/9(a) and (b) show these two families of curves within the trigger locus shown in Fig. 10/8(a). The wedge shape of the curves in Fig. 10/9(a) arises from the same reason as the wedge shape

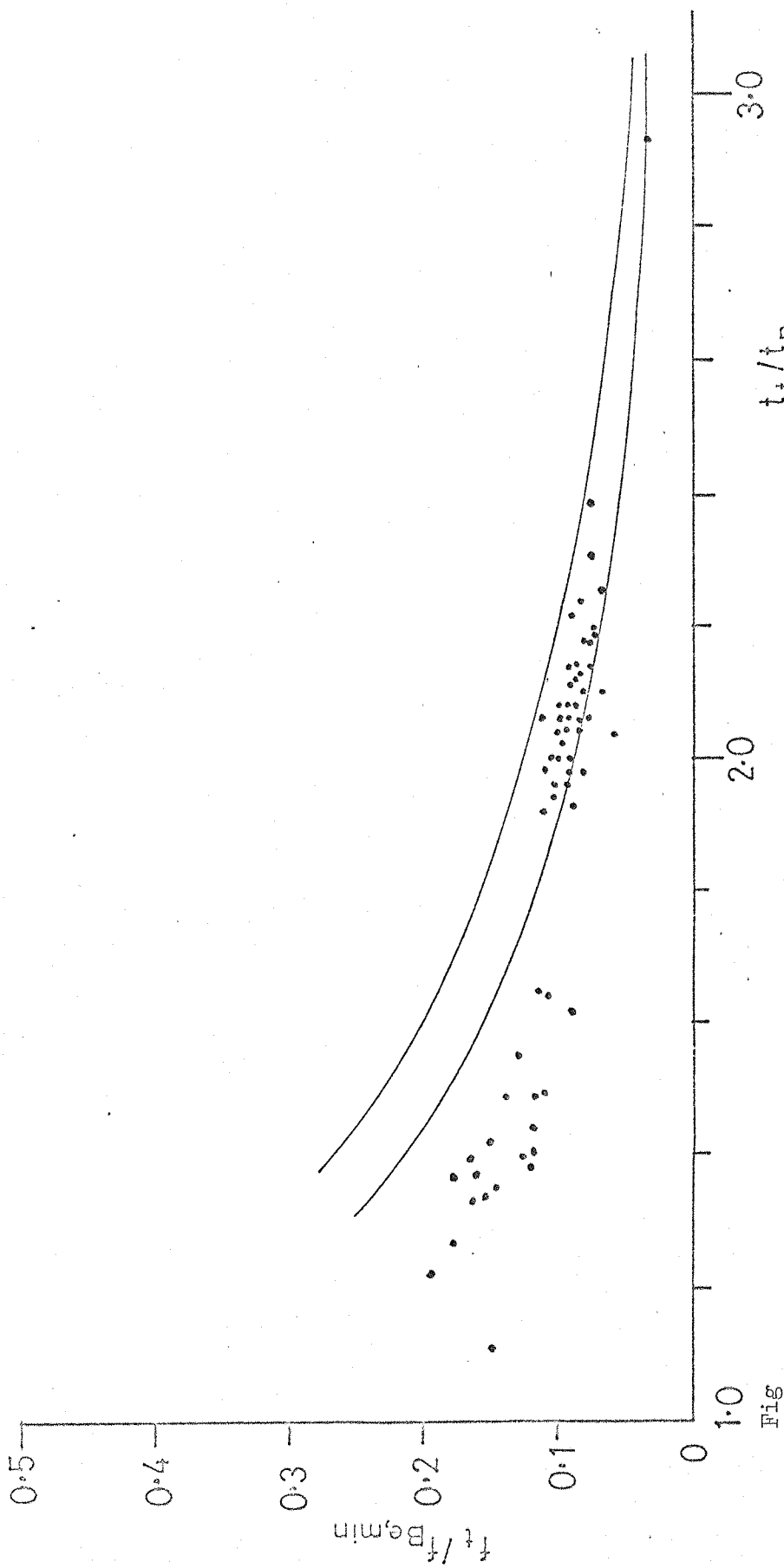

Fig. 10/8(a) Trigger locus predicted by the unducted model using the Winter Night model with a duct enhancement of 10%.

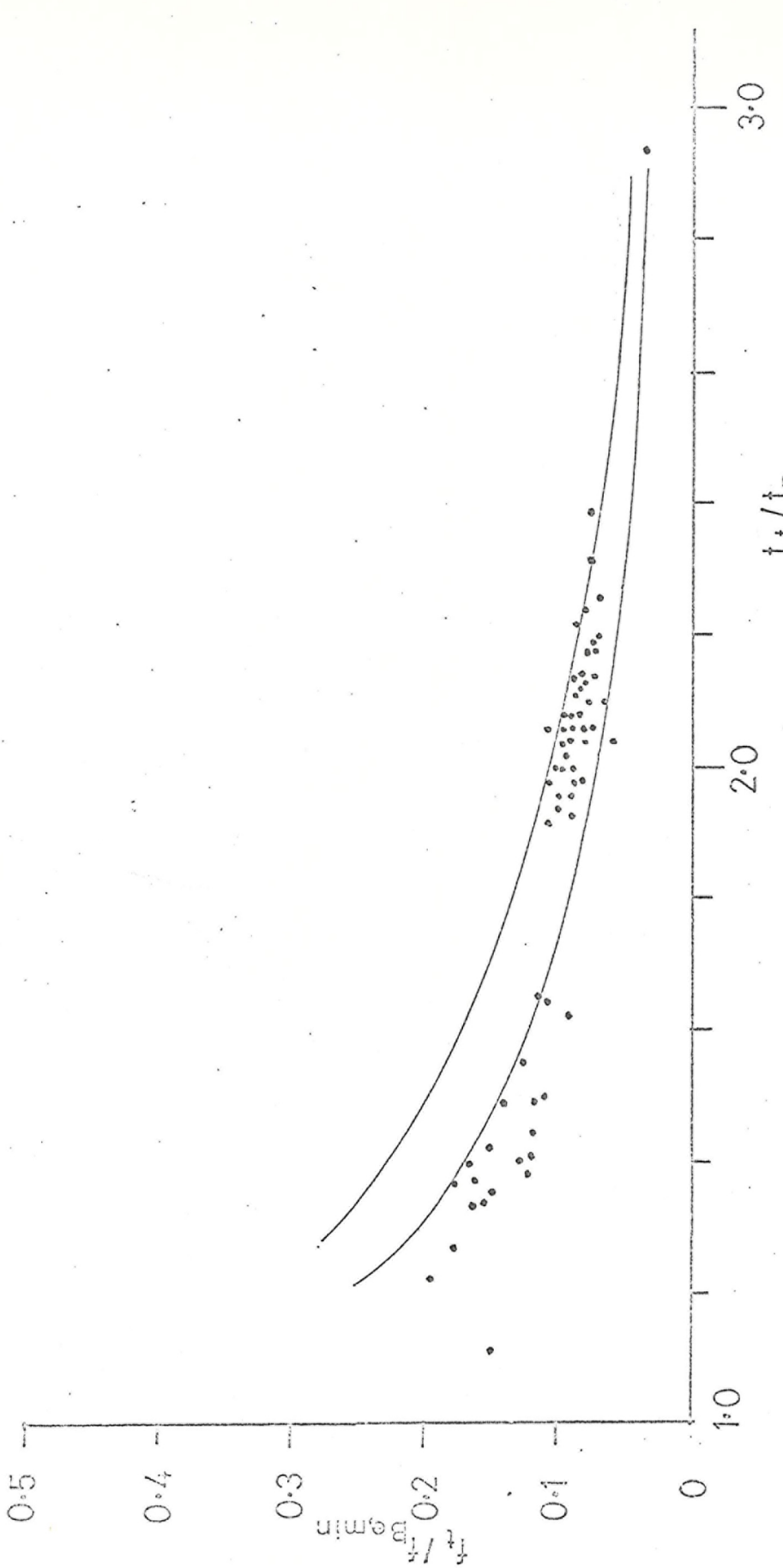

Fig. 10/8(b) Trigger locus predicted by the unducted model using the Winter Night model with a duct enhancement of 40%.

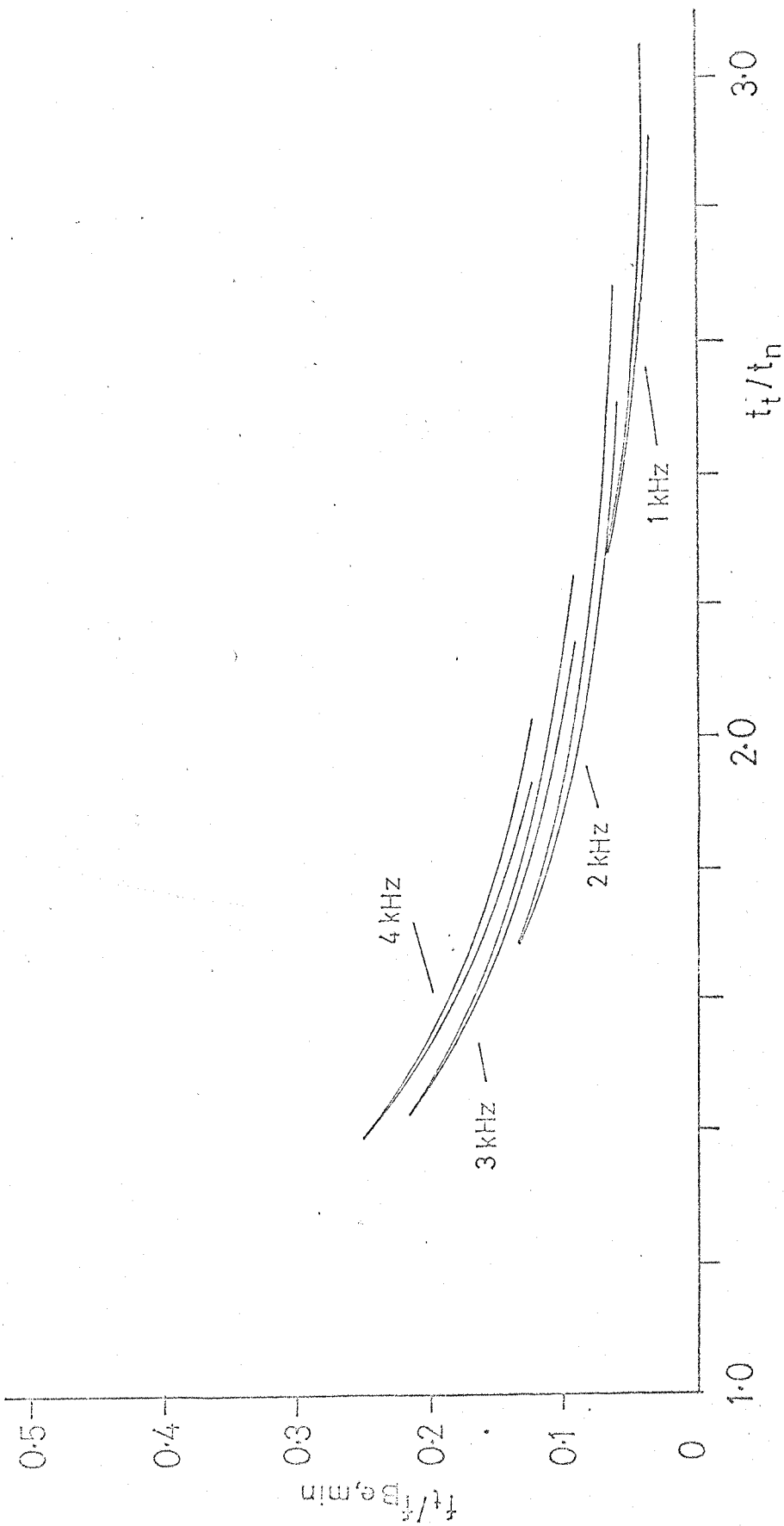

Fig. 10/9(a) Individual trigger loci for different values of f_t within the trigger locus shown in fig. 10/8(a).

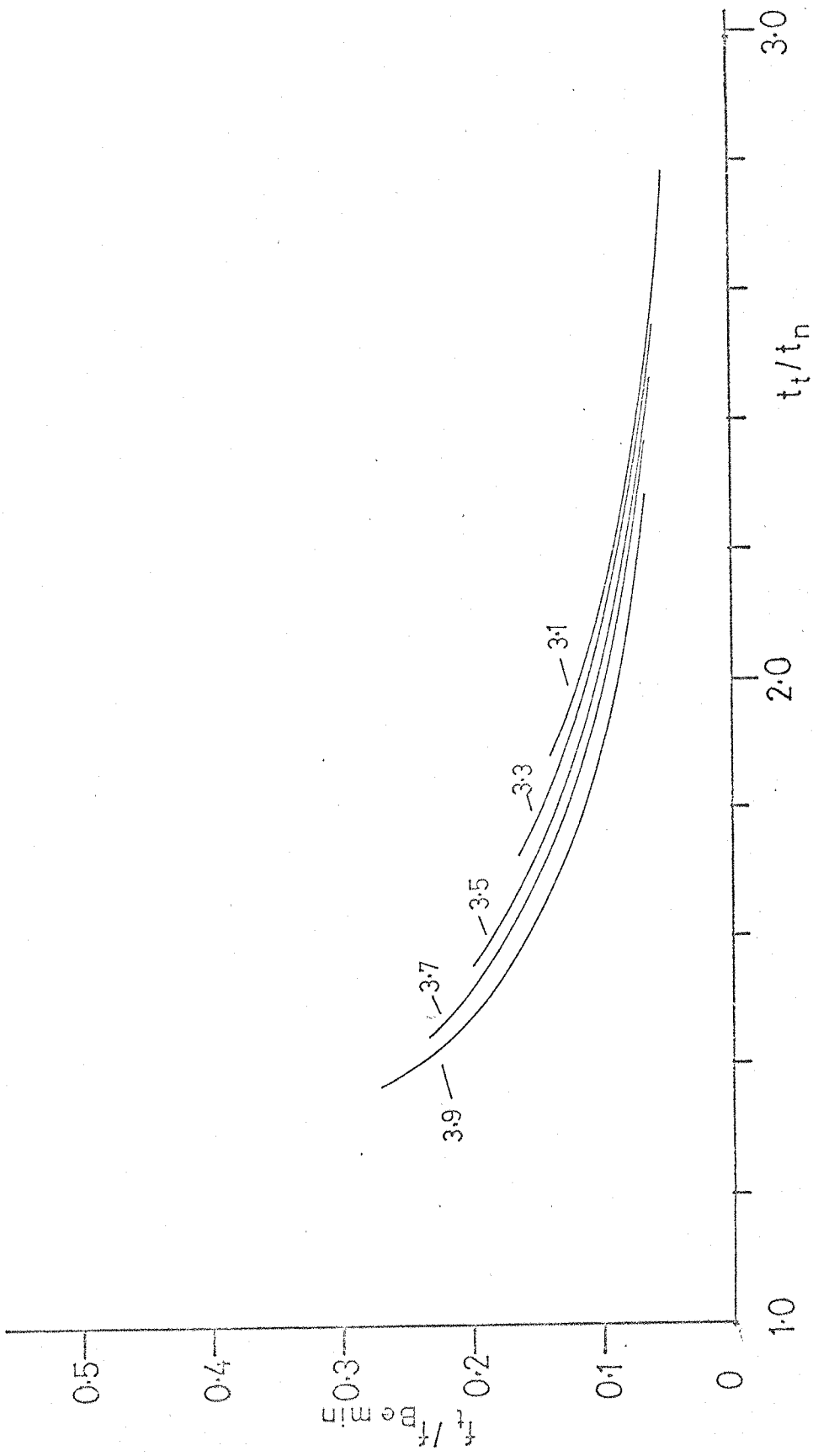

Fig. 10/9(b). Individual trigger loci for different values of L_d within the trigger locus shown in fig.10/8(a).

in Fig. 10/5, that is that at the lower values of L_d a wider range of L_p values gives a suitable path than at the higher values, giving a wider range of unducted travel times to the equatorial plane.

10.4.2 Summer day model

The ray tracing computations described in the previous section have also been carried out using the summer day model of the magnetosphere. The steeper plasmapause model has been used throughout. It was found that for a given duct L value, L_d, the range of plasmapause positions that resulted in a suitable unducted ray path was much smaller for this model. Fig. 10/10 shows how L_p varies with L_d for a 3 kHz wave traced through the summer day model (cf. Fig. 10/5).

Fig. 10/11 (a) and (b) show the predicted starting parameters L_i and V_i plotted against L_p for a 3 kHz wave arriving at the equatorial plane at an L value of 3.1 (cf. Fig. 10/7). It may be seen that although the predicted ranges of L_i and V_i are similar to those for the winter night model the detailed shapes of the curves are different. It is felt that no great significance should be placed on these differences, especially in view of the fact that if the northern hemisphere section of the path is in summer then the southern hemisphere will be in winter.

Fig. 10/12 (a) and (b) show the loci of trigger points predicted by ray tracing through the summer day model for duct enhancements of 10% and 40% respectively (cf. Fig. 10/8). The individual curves for each value of trigger frequency are shown in Fig. 10/13 (a) and (b). It may be seen that again the agreement with experiment is reasonably good and that better agreement is obtained using the higher duct enhancement. From Fig. 10/13 (b) it may be seen that using the summer day model with a 40% duct enhancement the agreement between theory and experiment is excellent at trigger frequencies below 3 kHz.

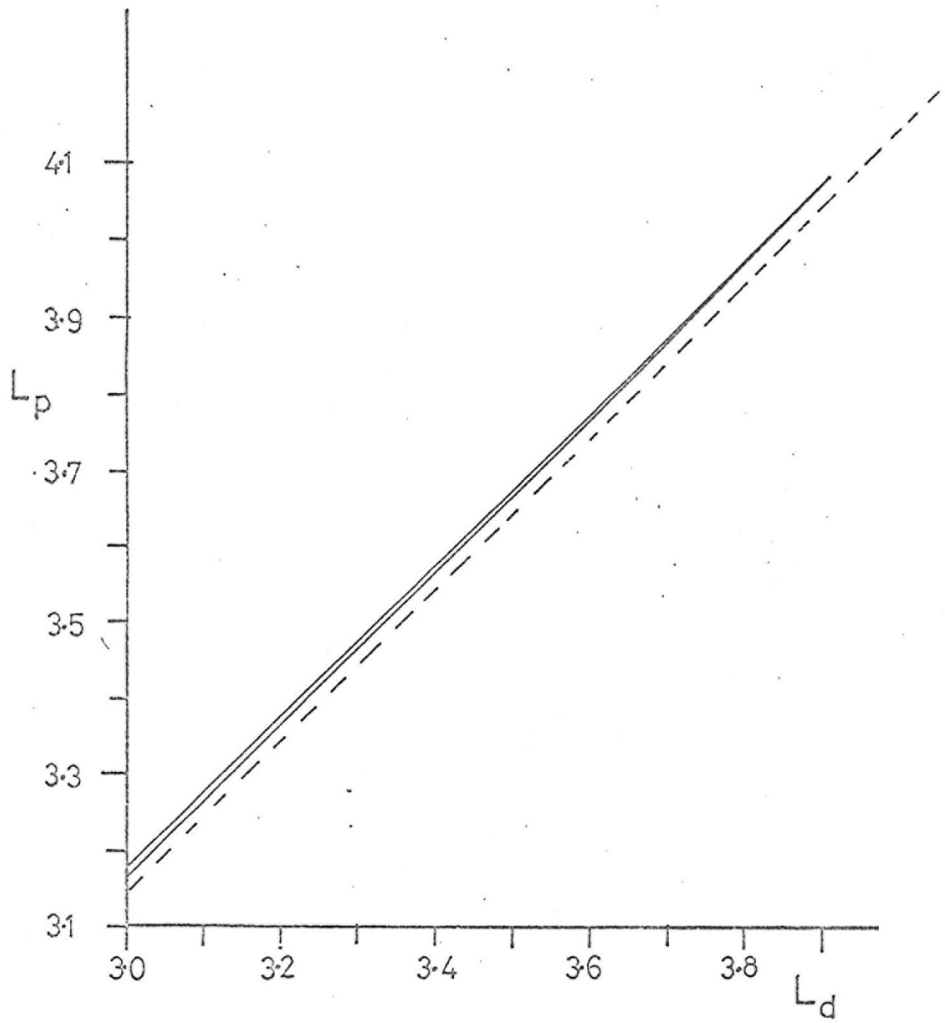

Fig. 10/10. Variation with duct L value of the plasmapause position required for the unducted model of precursor triggering using the Summer Day model. (Dotted line represents the inner boundary of the plasmapause region).

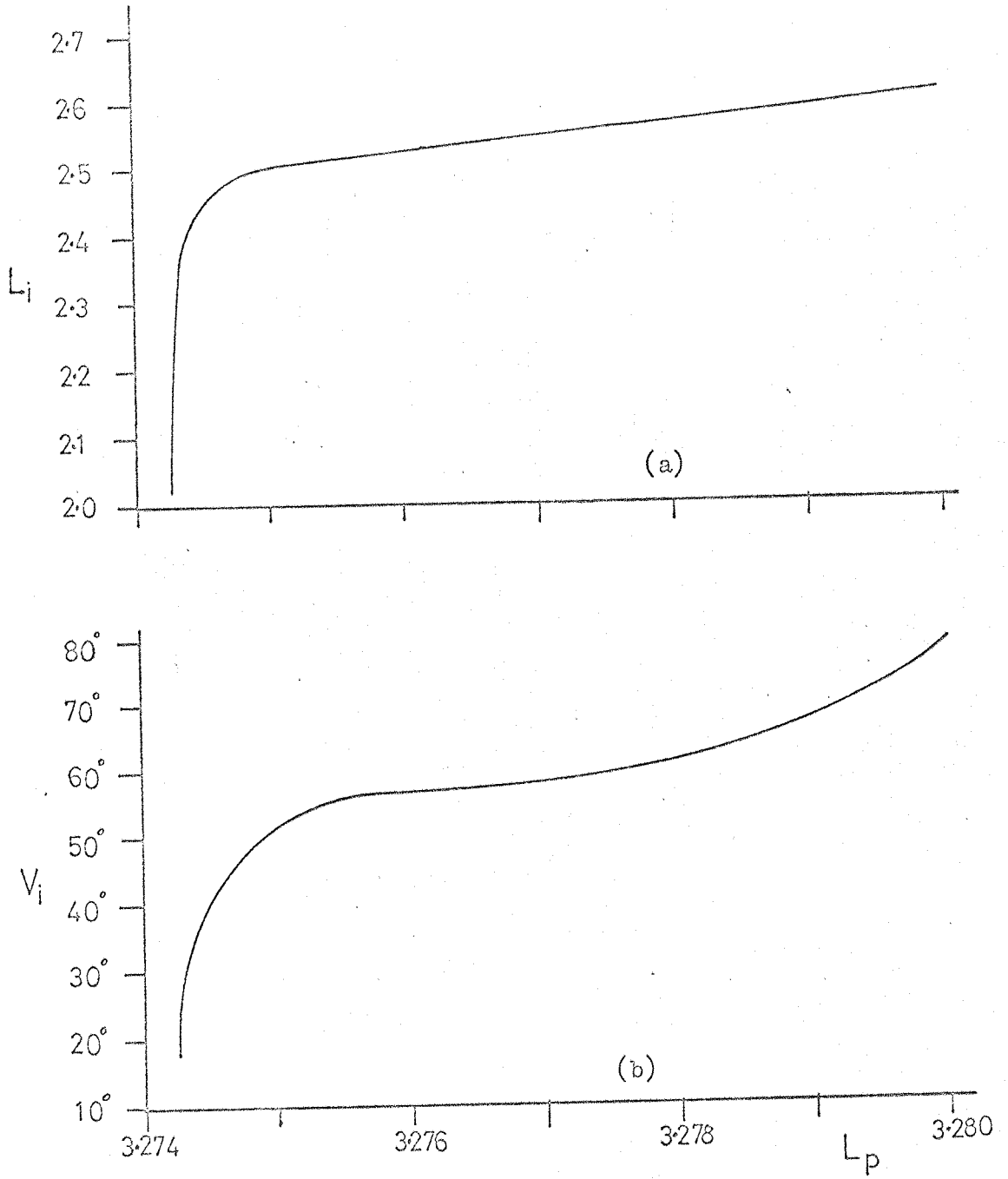

Fig. 10/11 Variation with plasmapause position of a) initial L value and b) initial wave normal angle predicted by the unducted model of precursor triggering using the Summer Day model.

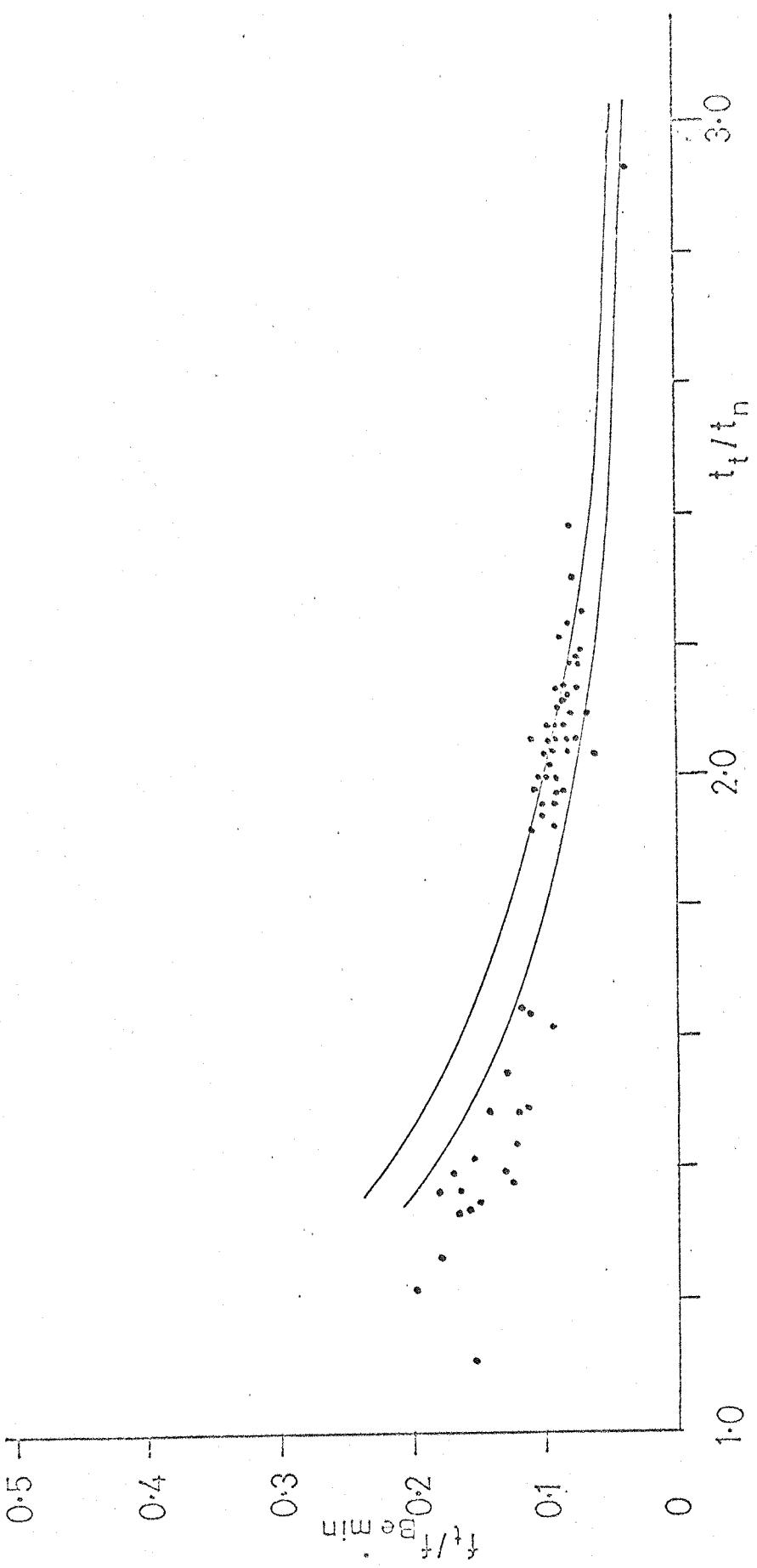

Fig 10/12(a) Trigger locus predicted by the unducted model using the Summer Day model with a duct enhancement of 10%.

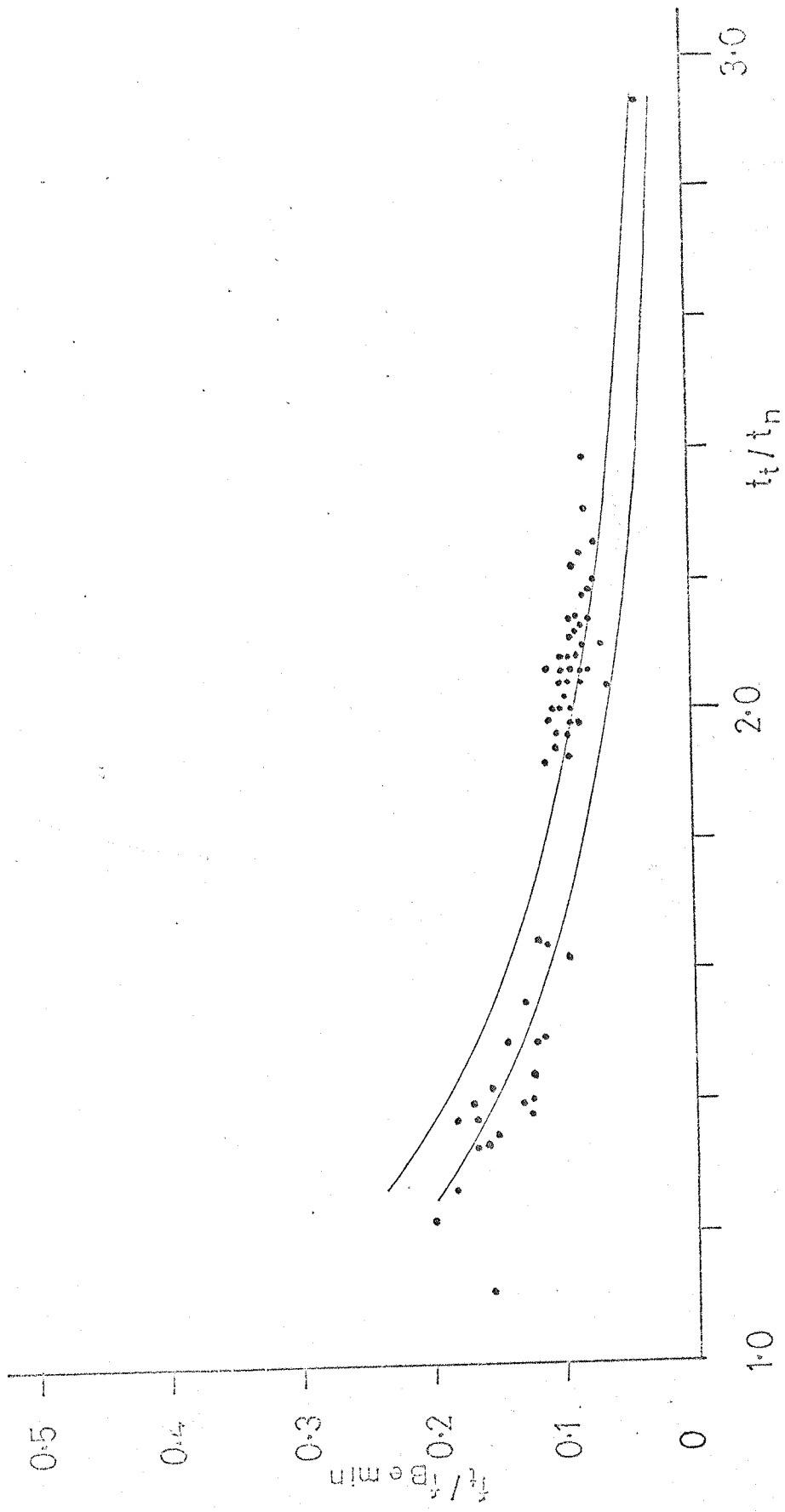

Fig. 10/12(b). Trigger locus predicted by the unducted model using the Summer Day model with a duct enhancement of 40%.

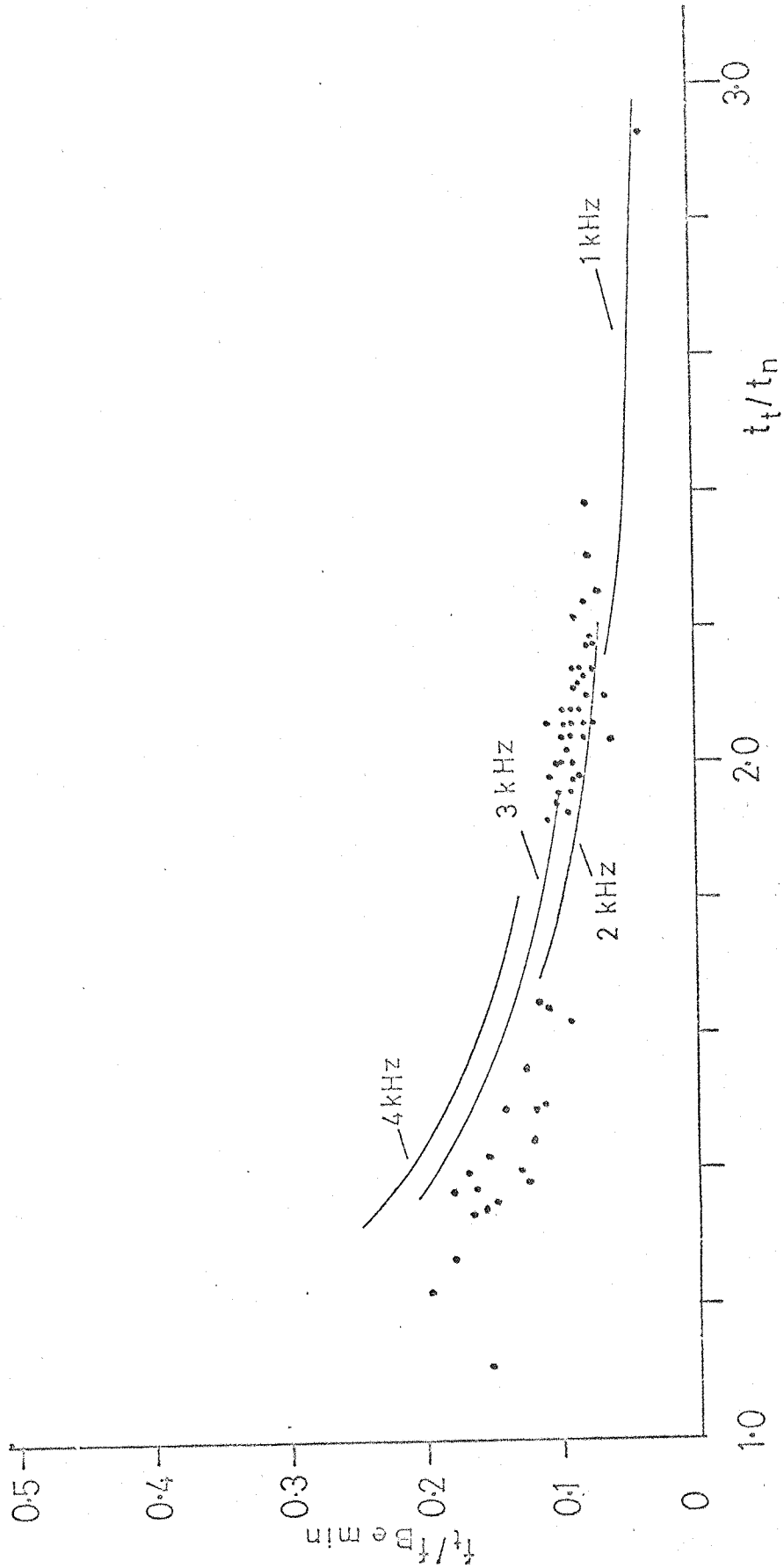

Fig. 10/13(a) Individual trigger loci for different values of f_t within the trigger locus shown in fig. 10/12(a).

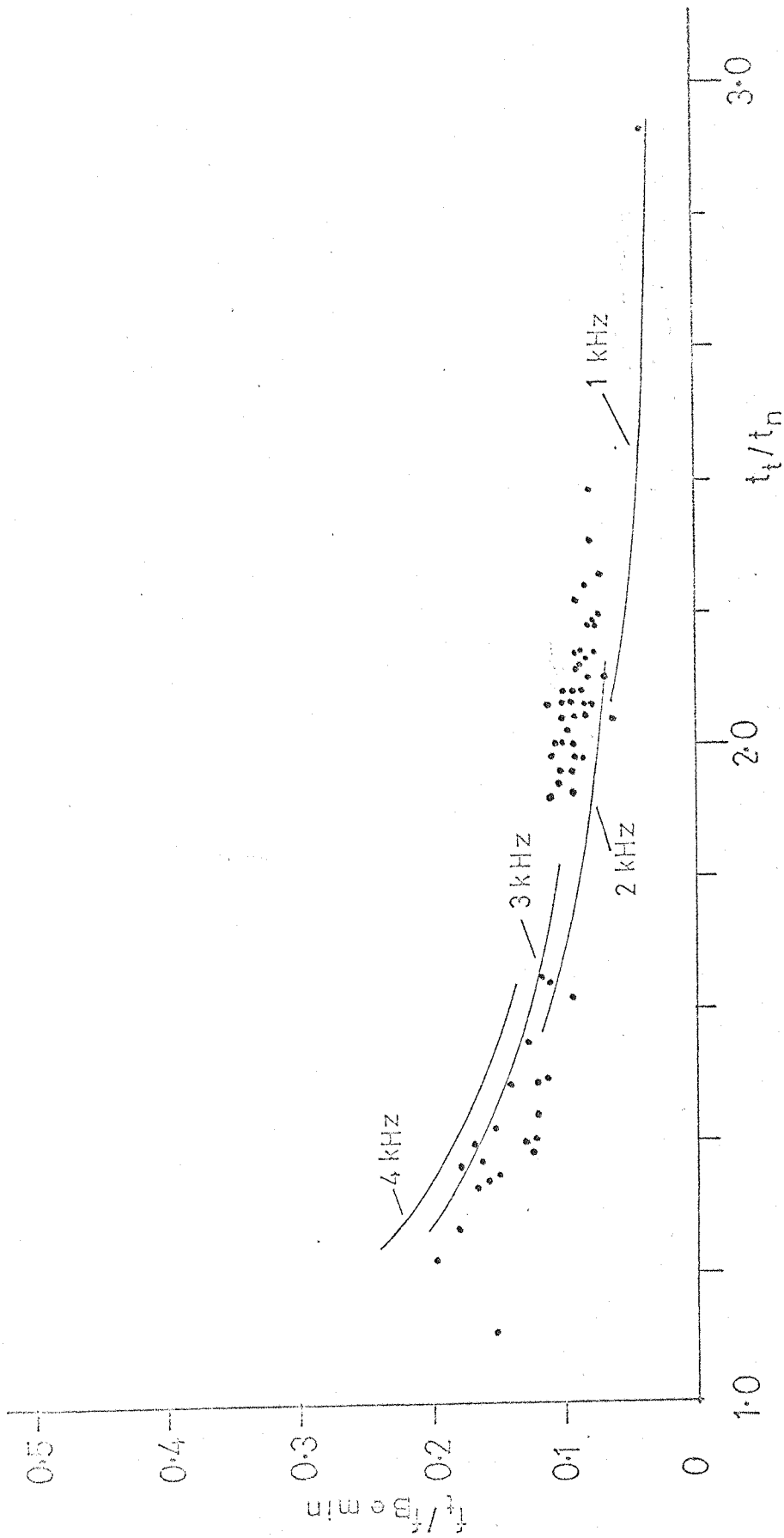

Fig. 10/13(b) Individual trigger loci for different values of f_t within the trigger locus shown in fig. 10/12(b).

10.5 Discussion of Ray Tracing Results

The most important results to emerge from the ray tracings carried out to test the unducted model of precursor triggering are those which are independent of the magnetospheric model used. It would be unreasonable to believe that either model described the typical magnetospheric plasma distribution since they were intended to represent the extremes of possible conditions. The model-independent results are as follows:

i) For all duct L values between 3.0 and 3.9, which was the whole range tested, and for all trigger frequencies between 1 and 4 kHz there is a range of plasmapause positions for which a ray, traced in reverse from the equatorial plane at L value L_d with $\theta = \pi$, arrives at 300 km altitude after first refracting off the inner edge of the plasmapause and undergoing one magnetospheric reflection. The favourable plasmapause positions are such that the duct is situated just inside the plasmapause.

ii) The predicted initial L value (L_i) and wave normal angle with respect to the vertical (V_i) both increase with L_p. L_i typically ranges from a value less than 2 up to L_d, while the range of V_i is generally between 10° and 80°. It has been shown that under certain ionospheric conditions, such as the presence of horizontal electron density gradients, wave normal angles of up to around 40° with the vertical might reasonably be expected. In all cases the predicted deviation of V_i from the vertical is towards the earth's magnetic field which, over the range of interest is at an angle of between 16° and 24° to the vertical at 300 km altitude. Thus the horizontal gradients that would give the appropriate wave normal angles for the unducted path to the equatorial plane would also increase the probability of part of the energy being ducted since waves with field aligned wave normals are most likely to become trapped in a field

aligned duct (Alexander, 1971). The horizontal electron density gradients reported by Helliwell (1965) to occur at middle latitudes are directed towards the equator and therefore tend to deviate the wave normal towards the earth's magnetic field.

iii) The agreement between the predicted loci of precursor trigger points and the experimentally observed data is generally good.

In order to obtain the maximum probability of generating a whistler precursor pair L_i should be as close to L_d as possible and V_i should have as small a value as possible. However it may be seen that both these conditions may not be fulfilled simultaneously (see Figs. 10/7, 10/11 and ii) above); they must be optimised with respect to each other. This will generally require an initial wave normal angle of around 25^o with the vertical at 300 km, necessitating some special ionospheric conditions such as those discussed earlier in this chapter. This condition places a restriction on the probability of precursor generation. Other conditions restricting the probability of precursor generation are as follows:

i) A duct must exist just inside the plasmapause.

ii) Energetic electrons of the correct energy must be present within this duct. Kennel and Petschek (1966), Rycroft (1972) and Thorne (1972) have shown that the factor $B^2/2\mu_o N$, which is proportional to the critical electron energy required for resonance for a given critical pitch angle anisotropy, has a minimum just inside the plasmapause (see Fig. 10/14). It may be seen that electrons with the correct energy for resonance at this minimum may also resonate some distance beyond the plasmapause; thus it would be expected that electrons with this energy convecting inward from the magnetospheric tail would resonate beyond the plasmapause and be precipitated into the atmosphere in the vicinity of the auroral zone. For electrons of this energy to be present just inside

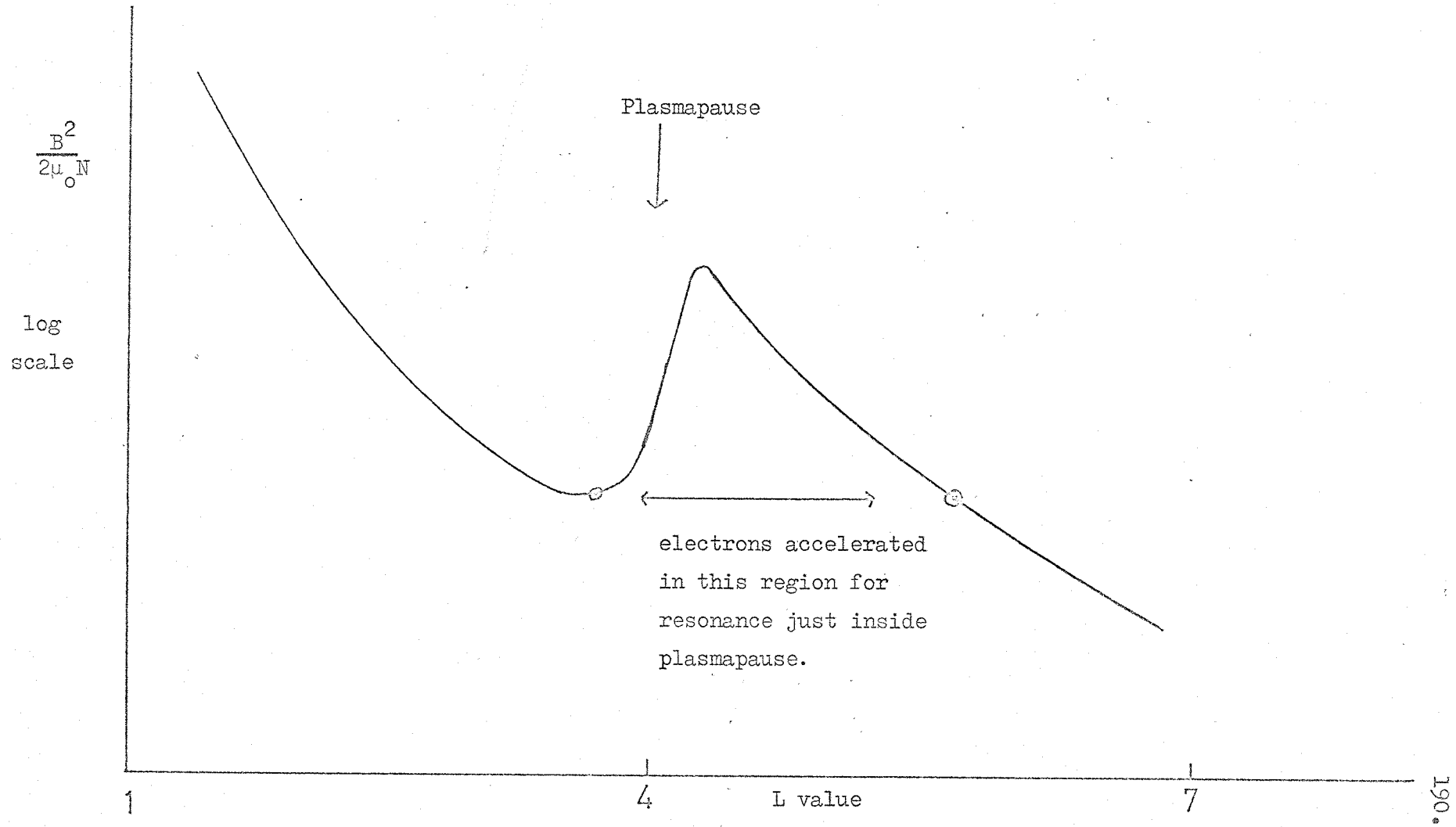

Fig. 10/14 Variation of magnetic energy per electron with L value.

the plasmapause they must be accelerated in the region where the critical energy graph has its maximum and convect inward. It may be seen that the probability of resonance with these newly accelerated electrons is greatest just inside the plasmapause since the energy required for resonance is a minimum. The probability of resonance is further increased if the plasmapause should move to a slightly higher L value. Electrons whose energy was previously too low for gyroresonance now become able to resonate, increasing the probability of resonance.

iii) A thunderstorm must be suitably located so that part of the energy from the lightning discharges may propagate in a ducted mode and part in an appropriate unducted mode. This condition will generally require the storm centre to be located at a slightly lower L value than L_d.

iv) The special ionospheric conditions mentioned previously to allow wave normal angles of around 25° with the vertical at 300 km altitude should exist.

These four conditions, which must be satisfied simultaneously, undoubtedly place a severe restriction upon the probability of receiving a whistler precursor pair. However since precursors are observed to be very much rarer than whistlers this should not detract from the plausibility of the model. On the contrary a model that did not predict a low probability of precursor generation would be less plausible since precursors would then be expected to be as common as whistlers.

Fig. 10/15 shows the ray path of a ray started off at 300 km with the computed initial parameters L_i and V_i; a duct has been placed at L_d and the plasmapause at L_p. The duct enhancement is 10% and the duct half width at 300 km altitude is 30 km corresponding to

Fig. 10/15

RAY TRACING, THROUGH SD MODEL, OF UNDUCTED 3kHz WAVES ILLUSTRATING PRECURSOR TRIGGERING IN INTERACTION REGION

(Direction of wave normal is shown every 0.25 s.)

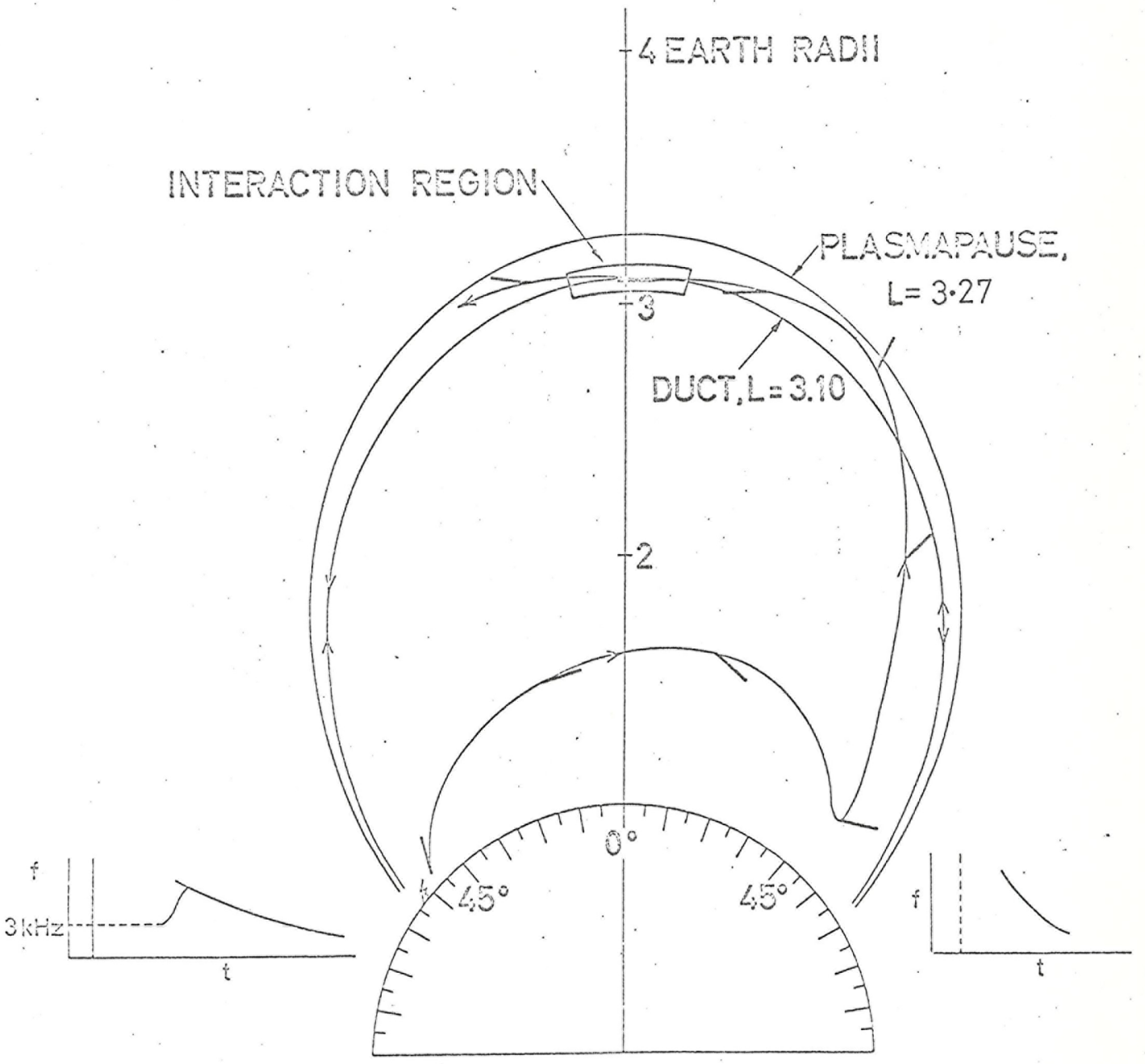

a half width in the equatorial plane of ~190 km. For the ray path shown the parameters are f = 3 kHz, L_i = 2.32, V_i = 30°, L_d = 3.10, L_p = 3.27; the magnetospheric model used was the summer day model. An almost identical path at the same frequency is obtained using the winter night model with L_i = 2.32, V_i = 20°, L_d = 3.10, L_p = 3.27. The ray enters the duct at a latitude of -5.5° and leaves it at +4.5°, spending 0.27 s in the duct during which time its ray direction is very closely field aligned ($\lesssim 5^\circ$) and its wavenormal is everywhere within 25° of the magnetic field direction. It is possible to compute ray paths for which the ray remains in a narrower duct for a longer time than this. However 0.27 s is well in excess of the bunching time of 0.1 s calculated by Helliwell (1967).

It is possible that a number of similar ray paths starting off with slightly different L_i or V_i contribute to the interaction allowing resonance to occur over a wider region. Similarly in the case of triggering by ducted waves there is probably not one unique ray path through the duct at a given frequency but a number of similar paths.

Fig. 10/16 shows the effect of varying the initial latitude of the ray leaving all other parameters unchanged. In the set of rays shown the range of initial latitudes is 2°. It may be seen that in each case the ray is directed into the duct close to the equatorial plane giving a concentration of energy preferentially in that region. Thus energy from one lightning discharge entering the ionosphere over a range of latitudes may contribute to the triggering of a precursor. A similar result is obtained when the initial wave normal angle is varied over a range of 4° (See Fig. 10/17). An appropriate combination of these two effects could give an increased concentration of energy in the equatorial plane resulting in a sort of focussing effect.

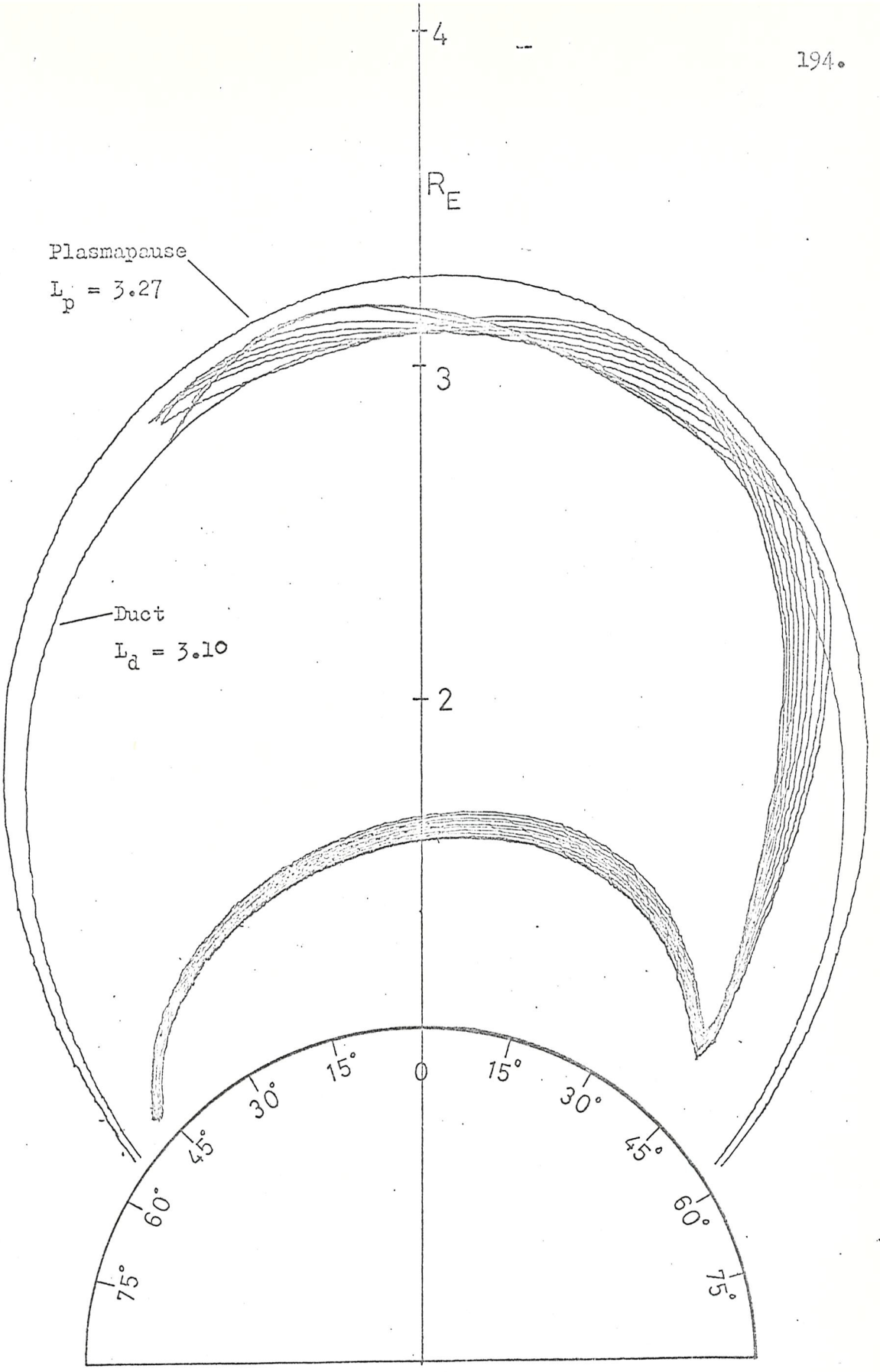

Fig. 10/16. A set of 3 kHz rays with equal initial wave normal angles whose initial latitudes range over 2° showing energy directed preferentially to the equatorial plane at L value L_d.

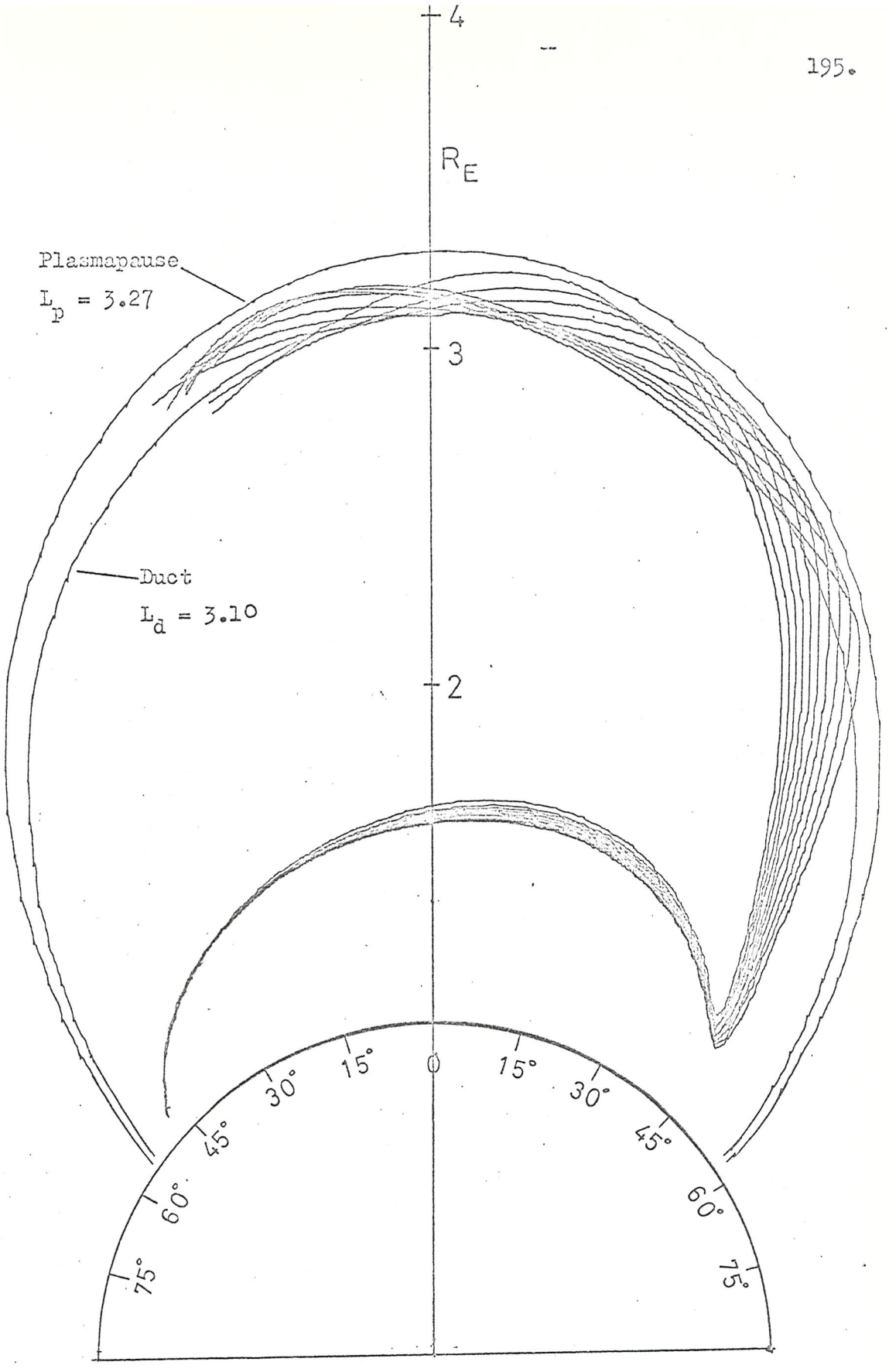

Fig. 10/17. A set of 3 kHz rays with equal initial latitudes whose initial wave normal angles range over 4° showing energy directed preferentially to the equatorial plane at L value L_d.

10.6 Comparison with Dowden's Hybrid Whistler Model

Dowden's (1972) hybrid whistler model of precursor generation has been discussed in Chapter Eight, where some objections to it have been noted. In this section Dowden's model is compared with the unducted model with reference to some of the observed properties of precursors listed in section 8.1.

Both models predict the most important property, that is that precursors to one hop whistlers are not observed (property 1); both models predict trigger loci that agree well with the observations; both models allow that the precursor need not be triggered in the same duct as that in which the two hop whistler is propagating, thus allowing agreement with both apparently contradictory properties 2 and 5.

There are some properties that may be explained by the unducted model but not by the hybrid model. Of these the most obvious is the observation that precursors have propagated just inside the plasmapause (property 11), which is a basic property of the unducted model. The appearance of multiple component precursors such as that shown in Fig. 10/18, in which two trigger points at different frequencies appear at approximately the same time, with $\Delta t \sim 5$ ms, may be explained by the unducted model in the following way. With reference to Fig. 10/19 the lightning flash radiates a wide range of frequencies over a wide distance range. Because of the high refractive index of the ionosphere the wave normal angle in the ionosphere will be virtually independent of its value in the earth-ionosphere waveguide. A ray path such as path 1 will lead to the wave being trapped in the duct, giving rise to the two hop whistler. Since the unducted paths are frequency dependent any given entry point into the ionosphere will in generall allow only one frequency to arrive in the equatorial

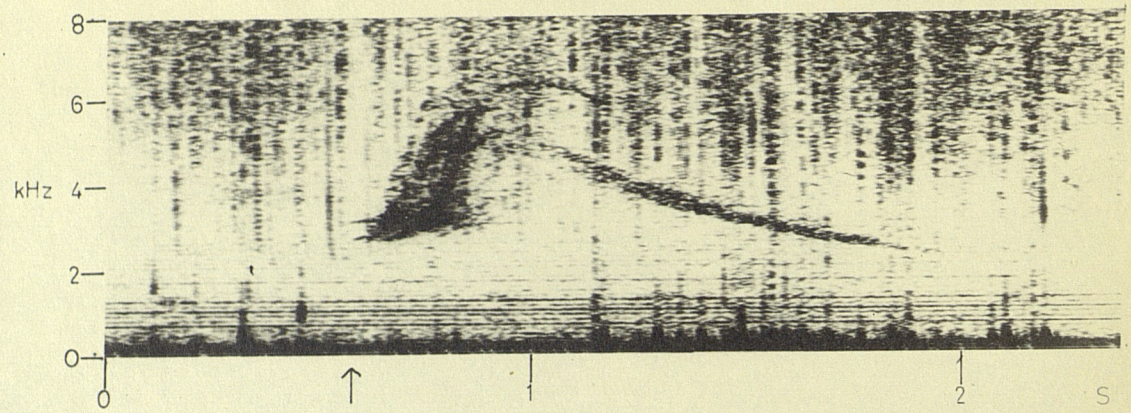

2052:12 U.T.

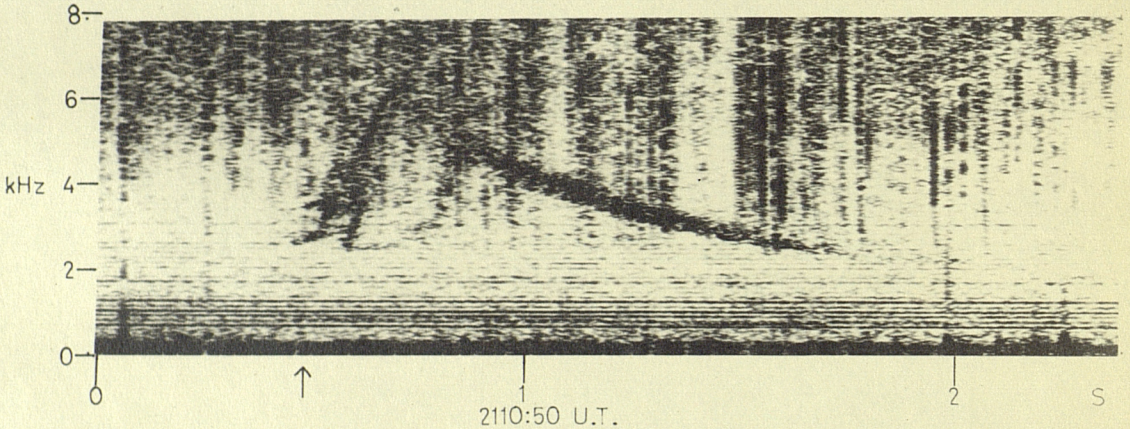

2110:50 U.T.

Fig. 10/18 Precursors showing two trigger points with equal trigger times but different trigger frequency. St.John's, Newfoundland, 7 March 1970.

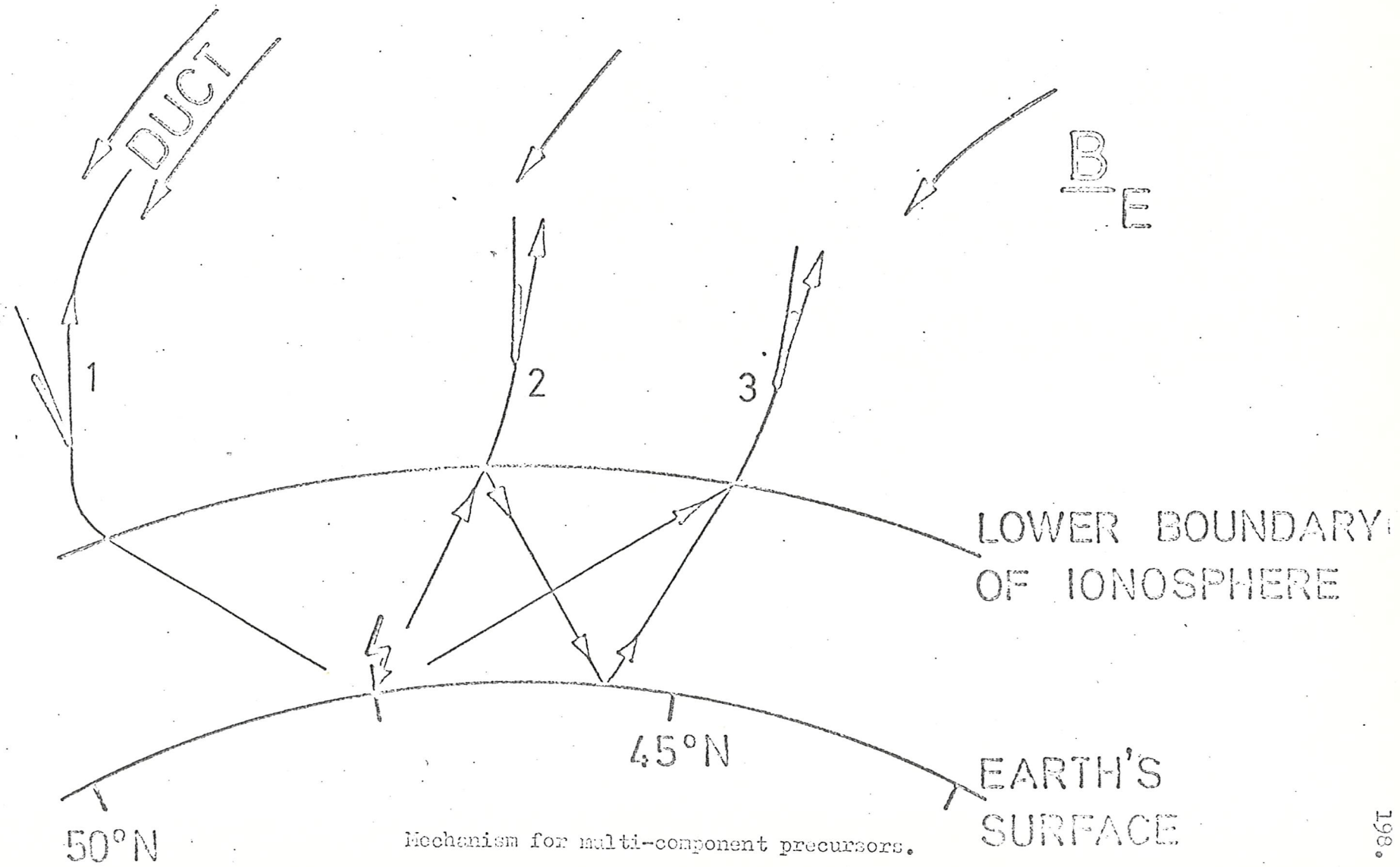

Mechanism for multi-component precursors.

Fig. 10/19.

plane with its wave normal field aligned. If paths 2 and 3 are the correct paths for frequencies f_1 and f_2 where $f_1 > f_2$ then their propagation times to the equatorial plane may be equal since the longer propagation path at f_1 may be cancelled out by the greater group velocity at the higher frequency This effect could not be explained by the hybrid model since in general only one trigger point would be expected.

The observation that precursors occur under moderately disturbed magnetic conditions (property 2) may be explained by the unducted model in terms of the inward motion of the plasmapause with increasing magnetic activity (Carpenter 1966). The average plasmapause position at times of low magnetic activity is around 4 0 corresponding to a duct L value of around 3.85. At such high latitudes the whistler rate is low resulting in a very low probability of precursor generation. At more distrubed times the plasmapause may move to L values of 3.5 or lower corresponding to a duct L value of around 3.3 Here the whistler rate is considerably greater; thus a higher probability of precursor generation would be expected. A study of precursed whistler L values and plasmapause positions should show a positive correlation. However, because of the uncertainties in estimating the plasmapause position the data available to the author are not sufficient for an accurate statistical analysis. In the events studied, however, there was no instance of the predicted plasmapause position (Rycroft and Thomas, 1970) being unreasonable for the magnetic conditions and local time. For the precursors received at St. John's the L value of the whistler duct was found to be around 3.1. For the prevailing magnetic conditions (K_p = 6-) and local time 1700-1830 the predicted plasmapause position of around 3.25 is not unreasonable. For the precursor received at

South Uist the predicted plasmapause position is around L = 3.8, a not unreasonable value at 0015 LT and $K_p = 4_{o}$. For the two precursors presented by Laaspere and Wang (1968) (their Fig. 1) the predicted plasmapause L values are around 3.45 and 3.65; again not unreasonable for local times around noon and K_p indices of 4- and 3o respectively.

CHAPTER ELEVEN

Discussion and conclusions

11.1 Extensions and implications of the unducted model

It has been shown in the previous chapter how the unducted model may explain the appearance of precursors to whistlers. However since a number of special conditions must be fulfilled in order to obtain a reasonable probability of receiving a whistler-precursor pair (see section 10.5) this mechanism may be thought of as a special case of a more general process in which unducted radiation from lightning discharges may resonate with energetic electrons just inside the plasmapause. It may be seen from Figs. 10/7 and 10/11 that the initial wave normal angle with the vertical required by the unducted model decreases with decreasing initial latitude. For example, a 2 kHz wave starting at 300 km from as low an L value as 1.5, and with the plasmapause at L = 3.27, requires an initial wave normal angle of only 6° with the vertical in order to arrive in the equatorial plane at L = 3.1 with its wave normal field aligned. There is no reason to believe that this is a special case; in general it is found that there are unducted paths with initial L values between 1 and 2 and initial wave normal angles with the vertical less than 10° that satisfy the conditions that $\Theta = 0$ in the equatorial plane at any L value in the range tested provided that it is just inside the plasmapause. Because of the low initial wave normal angles these paths do not require any special ionospheric conditions; hence there appears to be no reason why they should not occur commonly. Such paths would be unlikely to produce whistler precursor pairs since even if there happened to be a duct in the correct place it is improbable that

energy from one lightning discharge would become ducted at an L value greater than 3 as well as propagating along an unducted path with an initial L value around 1.5. However since the thunderstorm rate is higher at low latitudes it is probable that energy from these lightning discharges will arrive in the equatorial plane with their wave normals field aligned. It was shown in section 10.5 that there is a relatively high probability of electrons unstable to transverse resonance being present just inside the plasmapause. Thus the probability of a resonant interaction taking place in this region appears to be high. If a suitably placed duct should exist then ducted radiation may be triggered. Such radiation, if received at the ground would appear as apparently spontaneously generated emissions. Such emissions are frequently observed especially at disturbed times (Helliwell, 1965).

In this context the unducted path shown in Fig. 11/1 should be mentioned, which also results in energy arriving in the equatorial plane with its wave normal field aligned; in this case, however, the energy originates in the opposite hemisphere to the observer and is not magnetospherically reflected before refracting off the plasmapause. The plasmapause L value required for such a path is marginally smaller than that required for the magnetospherically reflected path to the same equatorial L value. For this type of path however the initial wave normal angle with the vertical increases with decreasing initial L value. Hence in the presence of a suitably placed duct VLF emissions may be triggered by unducted energy from the opposite hemisphere to that in which they are observed.

The risers received close to eclipse totality at St. John's (see Chapter 7) have been studied to search for evidence that they were triggered by unducted energy from lightning discharges. Their trigger frequency was around 1.5 kHz giving a predicted trigger time of around 3 s assuming that they had propagated along the same duct

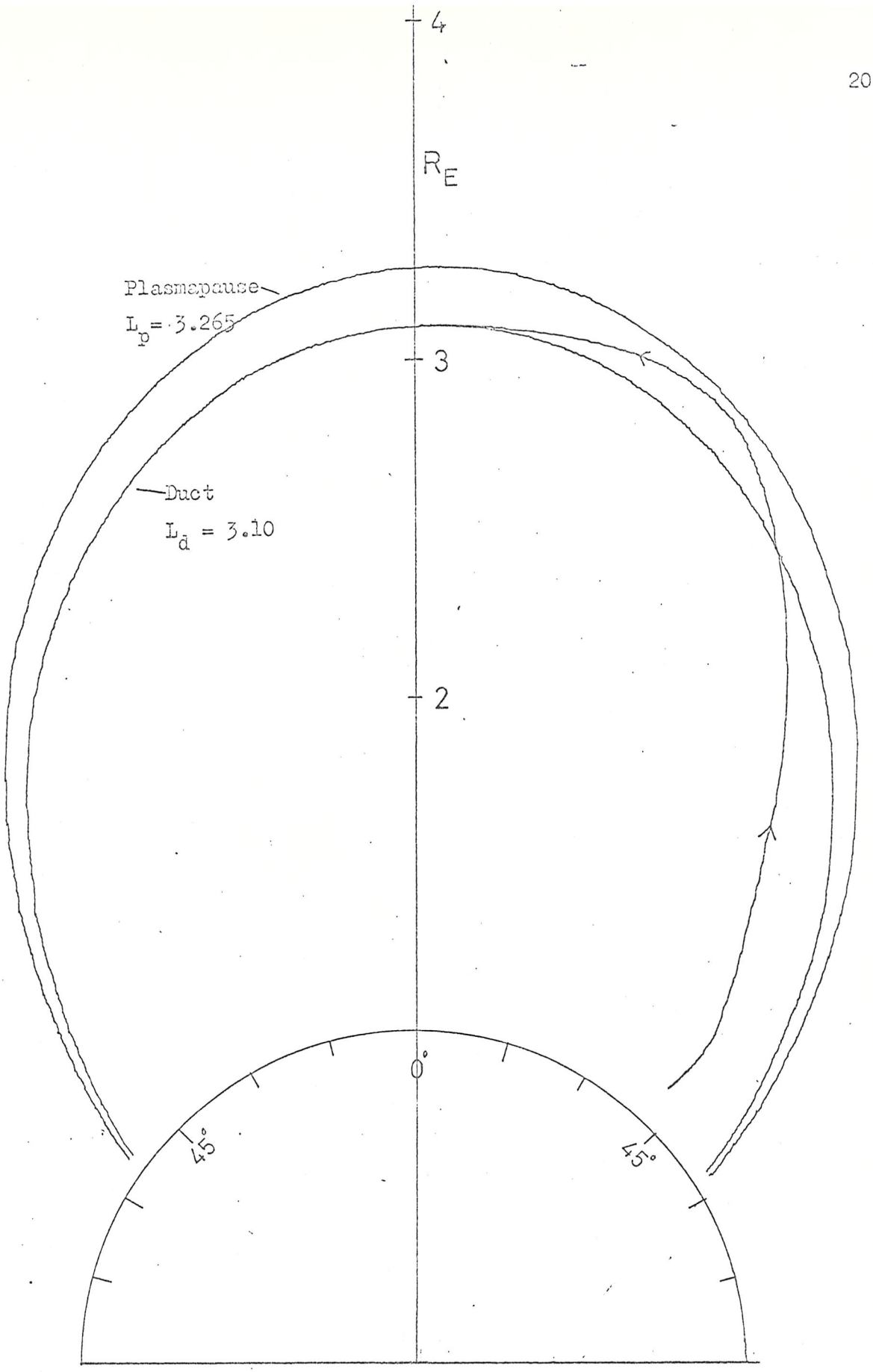

Fig. 11/1. Ray diagram illustrating unducted path to the equatorial plane not involving a magnetospheric reflection.

as the precursor. Since the risers occurred only 90 minutes before the precursors this is not an unreasonable assumption. In some cases (5 out of 18) an energetic sferic was found at approximately the right time, within around 0.2 s (see Fig. 7/3) but in general there was none. If the risers had been triggered by energy from sferics in the opposite hemisphere none would be expected because of the high attenuation of the earth-ionosphere waveguide at very low frequencies.

Even in the absence of a suitably placed duct the resonant interaction may take place; any energy so triggered would propagate in an unducted mode and should not therefore be received at the ground. Whether a duct exists or not the effect of the wave particle interaction upon the electrons is to reduce their pitch angle so that some are precipitated into the atmosphere. Since it has been shown that there is high probability of resonance occurring just inside the plasmapause an enhanced precipitation of energetic electrons should be observed at an L value just inside the plasmapause.

11.2. Suggestions for further work

There are a number of points raised by the unducted model which require further investigation. A statistical study of the L value of the precursed whistler duct against plasmapause should be carried out to investigate whether the relationship between them agrees with the predictions of the model. Also observations of precursors may provide another method of determining the position of the plasmapause since if the L value of the whistler duct may be found (from its nose frequency) then the plasmapause position is fixed within limits of around 0.01 in L value, according to the unducted model.

Further experiments to test whether enhanced precipitation of energetic electrons occurs at an L value just inside the plasmapause would help to verify the model as would evidence from satellite data of an increase in the intensity of unducted VLF radiation at L values just within the plasmasphere, in the equatorial plane.

Experiments to test whether apparently spontaneous emissions were in fact triggered by unducted energy from lightning discharges would be difficult to carry out since the L value of the duct along which they had propagated would need to be determined before any conclusions could be drawn. For emissions, unlike whistlers there is no easy method of doing this. The VLF goniometer receiver, which gives information about the direction from which the received signal has propagated could be usefully employed in this context. Analysis of signals from two or more spaced stations should allow the point of exit of the signals from the ionosphere to be determined by triangulation and hence the L value of the duct could be deduced. Having done this the plasmapause position could be estimated, from the K_p index and local time, if it were not known either from direct observation by satellite or by ground based observation of 'knee' whistlers. Thunderstorm data would show whether there was activity at a suitable latitude and hence the model could be tested. A statistical study of the latitude of reception of spontaneous emissions and plasmapause position would also serve to investigate whether such emissions were received preferentially at L values just inside the plasmapause.

Conclusions

A correlation is found between the cutoff frequency of tweeks and solar obscuration during a solar eclipse. The phase height of reflection in the D region is found to increase by 7 ± 1 km at totality with a time lag of 4 ± 3 min. These results are in agreement with

previous results obtained by observation of man-made VLF signals reflected from the D region. The reception of VLF emissions close to eclipse totality is attributed to the eclipse induced modification to the ionospheric electron density distribution allowing the emissions to propagate to the ground whereas under normal daytime conditions they would have been reflected by or absorbed in the lower ionosphere.

Analysis of whistler-precursor pairs received soon after the solar eclipse shows that the L value of their propagation path was 3.06 ± 0.04 and that the minimum group delay was 1.05 ± 0.02 s. The locus of precursor trigger points obtained from these precursors and others received at South Uist is found to be in reasonable agreement with the theory of Dowden (1972). However because of some doubts as to the validity of this theory some alternative mechanisms of precursor triggering have been considered. It is found that an unducted path in which energy from a lightning discharge is first magnetospherically reflected and then refracted from the inner edge of the plasmapause results in the energy arriving in the equatorial plane with the correct wave normal angle to be able to trigger a precursor. It is found that the trigger loci predicted by this mechanism agree reasonably well with the observed data. Because of the relatively large initial wave normal angles predicted by this mechanism it is concluded that some special ionospheric conditions such as horizontal electron density gradients must exist in order to give reasonable probability of precursor generation. It is found that the unducted model may explain most of the observed properties of the precursor. In particular it explains the observation of multiple component precursors having trigger points with different trigger frequencies but approximately equal trigger times and also the observation that precursed whistlers have propagated just inside the plasmapause, neither of which are explained by Dowden's theory.

It is also found that paths similar to those thought to be responsible for precursor triggering exist starting from L values too low to be able to give rise to a whistler-precursor pair. Energy propagating along these paths does not require any special ionospheric conditions in order to be able to take part in a transverse resonance interaction in the equatorial plane. Furthermore, it is found that rays starting with a range of initial latitudes and wave normal angles are directed preferentially to the equatorial plane giving a sort of focussing effect. It is concluded that such paths may trigger apparently spontaneous emissions and may give rise to an enhanced precipitation of energetic electrons at L values just inside the plasmapause.

References

Accardo C.A., Smith L.G. and Pintal G.A. Rocket observations of solar X rays during the eclipse of 7 March 1970. J. Atmos. Terr. Phys. 34, 613 (1972).

Adjepong, S.K. Analyses of time series representing the intensity of VLF chorus and other related geophysical phenomena. Ph.D. Thesis. University of Southampton (1972).

Aikin, A.C. Theoretical models of the lower ionosphere. Ground-based Radio Wave Propagation Studies of the Lower Ionosphere. Conference Proceedings, Ottawa, Canada (1967).

Alexander, P.D. Computation of ray paths for very low frequency radio waves propagating through the magnetospheric plasma. Ph.D. Thesis, University of Southampton (1971).

Angerami, J.J. A whistler study of the distribution of thermal electrons in the magnetosphere, Tech. Report No. 3412-7, Stanford University, May 1966.

Angerami, J.J. Whistler duct properties deduced from VLF observations made with the OGO 3 satellite near the magnetic equator. J. Geophys. Res., 75, 6115 (1970).

Angerami, J.J. and J.O. Thomas. The distribution of ions and electrons in the earth's exosphere, Rept. SEL-63-110, Stanford University, December 1963.

Angerami, J.J. and J.O. Thomas. The distribution of ions and electrons in the earth's exosphere. J. Geophys. Res. 69, 4537-60 (1964).

Angerami, J.J. and D.L. Carpenter. Whistler studies of the plasmapause in the magnetosphere - 2; electron density and total tube content near the knee in magnetospheric ionization. J. Geophys. Res. 71, 711-25 (1966).

Barkhausen, H. Zwei mit Hilfe der neuen Verstarke entdeckte Erscheinungen. Physik Zeitschrift, 20, 401 (1919).

Barkhausen, H. Whistling tones from the earth. Proc. IRE, 18, 7, 1155 (1930).

Barron, D.W. and K.G. Budden. The numerical solution of differential equations governing the reflexion of long radio waves from the ionosphere. III, Proc. Roy. Soc. (London) A249, 387-401 (1960).

Bøerth, C.A. Rocket measurements of nitric oxide in the Upper Atmosphere. Space Res., 5, 767 (1965).

Bauer, S.J. and J.E. Jackson. Rocket measurements of the electron density distribution in the topside ionosphere. J. Geophys. Res., 67, 1675-1677 (1962).

Belrose, J.S., D.B. Ross and A.G. McNamara. Ionization changes in the lower ionosphere during the solar eclipse of 7 March 1970. J. Atmos. Terr. Phys., 34, 627 (1972).

Belrose, J.S., M.J. Burke, T.N.R. Coyne and J.E. Reed. D-region measurements using the Differential Absorption Differential Phase Partial Reflection Experiments. To be published in Journal of Geophysical Research, September 1, 1972.

Bowhill, S.A. Ionospheric effects in solar eclipses. Solar eclipses and the ionosphere. Plenum Press (1970).

Bowhill, S.A. and L.G. Smith. Rocket observations of the lowest ionosphere at sunrise and sunset. Space Res., 6, 511 (1966).

Brice, N. Fundamentals of very low frequency emission generation mechanisms. J. Geophys. Res., 69, 4515 (1964).

Brice, N. Generation of very low frequency hydromagnetic emissions. Nature, 206, 283 (1965).

Budden, K.G. The waveguide mode theory of wave propagation. Logos Press (1961).

Burtis, W.J. Magnetic radiation observed by the OGO-1 and OGO-3 broadband VLF receivers. Tech. Rep. 3438-1, Radioscience Laboratory, Stanford University, SU-SEL-69-019 (1969).

Burton, E.T. Submarine cable interference. Nature, 126 (3167), 55 (1930).

Burton, E.T. and E.M. Boardman. Effects of solar eclipse on audio frequency atmospherics. Nature, 131, 81 (1933a).

Burton, E.T. and E.M. Boardman. Audio frequency atmospherics. Proc. IRE, 21 (10), 1476 (1933b).

Carpenter, D.L. New experimental evidence of the effect of magnetic storms on the magnetosphere. J. Geophys. Res., 67, 135 (1962).

Carpenter, D.L. Whistler evidence of a knee in the magnetosphere. J. Geophys. Res., 68, 1675 (1963).

Carpenter, D.L. Whistler studies of the plasmapause in the magnetosphere 1. Temporal variations in the position of the knee and some evidence on plasma motions near the knee. J. Geophys. Res., 71, 693 (1966).

Case, D.J., J.S. Leach, G. Price, C.D. Reeve, W.J. Salter and M. Whale. Report of the University of Southampton Expedition to Iceland 1969, University of Southampton (1970).

Chapman, F.W., D.L. Jones, J.D.W. Todd and R.A. Challinor. Observations on the propagation constant of the earth-ionosphere waveguide in the frequency band 8 c/s to 16 k c/s. Radio Sci. 1 (New Series), 1273 (1966).

Chappell, C.R., K.K. Harris and G.W. Sharp. A study of the influence of magnetic activity on the location of the plasmapause as measured by OGO-5. J. Geophys. Res., 75, 50 (1970).

Cornwall, J.M. and M. Schulz. Adiabatic preservation of gyrophase coherence in the earth's field. J. Geophys. Res., 75, 4339, (1970).

Crain, C.M. Electron Ionization and loss processes and rates. Ground based radio wave propagation studies of the lower ionosphere. Conference Proceedings. Ottawa, Canada (1967).

Deeks, D.G. D-region electron distributions in middle latitudes deduced from the reflexion of long radio waves. Proc. Roy. Soc. (London), A291, 413 (1966).

Dowden, R.L. and G. McK. Allcock. Determination of the nose frequency of non-nose whistlers. J. Atmos. Terr. Phys. 33, 1125 (1971).

Dowden, R.L. Scale frequency of the exosphere. Nature 195, 984 (1962).

Dowden, R.L. Trigger delay in whistler precursors. J. Geophys. Res., 77, 695 (1972).

Eckersley, T.L. Note on musical atmospheric disturbances. Phil. Mag., 49 (5), 1250 (1925).

Eckersley, T.L. Letter to the Editor. Nature, 122 (3081), 768 (1928).

Eckersley, T.L. An investigation of short waves. J. Inst. Elec. Engrs., 67, 992 (1929).

Eckersley, T.L. Musical atmospherics. Nature, 135, 104 (1935).

Ellis, G.R.A. A receiver for observation of VLF noise from the outer atmosphere. Proc. IRE, 48, 1650 (1960).

Fejer, J.A. The interaction of pulsed radio waves in the ionosphere. J. Atmos. Terr. Phys., 7, 322 (1955).

Flaherty, B.J., H.R. Cho and K.C. Yeh. Response of the F-region ionosphere to a solar eclipse. Nature (Lond.), 226, 1121 (1970).

Fuchs, J. Discussion. A report to the National Academy of Sciences - National Research Council. National Academy of Sciences-National Research Council Pub. 581, 105 (1938).

Galejs, J. ELF and VLF waves below an inhomogeneous anisotropic ionosphere. Radio Sci., 68D, 693 (1964a).

Galejs, J. Propagation of VLF waves below a curved and stratified

anisotropic ionosphere. J. Geophys. Res., 69, 3639 (1964b).

Galejs, J. On the terrestrial propagation of ELF and VLF waves in the presence of a radial magnetic ~~fluid~~ field. Radio Sci., 69D, 705 (1965).

Galejs, J. Propagation of VLF waves below an anisotropic stratified ionosphere with a transverse static magnetic field. Radio Sci., 2 (New Series) 557 (1967).

Galejs, J. Propagation of ELF and VLF waves below an anisotropic ionosphere with a dipping static magnetic field. J. Geophys. Res., 73, 339 (1968a).

Galejs, J. Propagation of ELF and VLF waves below a generally anisotropic ionosphere. Radio Sci., 3 (New Series), 781 (1968b).

Gardner, F.F. and J.L. Pawsey. Study of the ionospheric D-region using partial reflections. J. Atmos. Terr. Phys., 3, 321 (1953).

Gibbons, J.J. and R.J. Nertney. A method for obtaining the wave solutions of ionospherically reflected long waves including all variables and their height variation. J. Geophys. Res., 57, 355 (1952).

Gordon, W.E. Incoherent scattering of radio waves by free electrons with applications to space exploration by radar. Proc. IRE, 46, 1824 (1958).

Haselgrove, J. Ray theory and a new method for ray tracing. Report of the Physical Society Conference on Physics of the Ionosphere (1954).

Helliwell, R.A. Whistler triggered periodic emissions. J. Geophys. Res., 68, 5387 (1963).

Helliwell, R.A. Whistlers and related ionospheric phenomena. Stanford University Press, Stanford, California (1965).

Helliwell, R.A. A theory of discrete VLF emissions from the magnetosphere, J. Geophys. Res., 72, 4773 (1967).

Helliwell, R.A. Whistlers and VLF emissions. Physics of the Magnetosphere. Edit. by R.L. Carovillano, J.F. McClay and H.R. Radoski. Reidel Pub. Co. (1968).

Helliwell, R.A., J.H. ~~Carey~~ Crary, J.H. Pope and R.L. Smith. The nose whistler - a new high latitude phenomenon. J. Geophys. Res. 61, 139 (1956).

Helliwell, R.A., J. Katsufrakis, M. Trimpi and N. Brice. Artificially stimulated VLF radiation from the ionosphere. J. Geophys. Res., 69, 2391 (1964).

Kane, J.A. D-region electron density measurements during the solar eclipse of 20 May 1966. Solar Eclipses and the Ionosphere. Edit. by M. Anastassiades. Plenum Press (1970).

Keneshea, T.J. Theoretical variations of minor constituents during an eclipse. Proceedings of Conference on Meteorological and Chemical Factors in D-region Aeronomy. Urbana, Illinois (1968).

Kennedy, J.R. and T.J. Schauble. Preliminary results of a radio absorption study at 3.5 MHz. Nature (Lond.), 226, 1116 (1970).

Kennel C.F. and H.E. Petschek. Limit on Stably Trapped particle fluxes. J. Geophys. Res. 71, 1 (1966).

Kimura, I. Effect of ions on whistler-mode ray tracing. Radio Sci. 1, 269 (1966).

Laaspere, T. and G.Y. Wang. Whistler Precursors, Radio Sci., 8, 213, (1968).

Langmuir, I. and H. Mott-Smith. The theory of collectors in gaseous discharges. Phys. Rev. 28, 727 (1926).

Little, C.G. and H. Leinbach. Some measurements of high latitude ionospheric absorption using extraterrestrial radio waves. Proc. IRE, 46, 334 (1958).

Malan, D.J. Physics of Lightning. The English Universities Press, London (1963).

Mathur, A. and M.J. Rycroft. Electron density profiles deduced from plasmapause whistlers observed in the U.K. J. Geophys. Res. 77, 1982 (1972).

Matsushita, S. and W.H. Campbell. Physics of Geomagnetic Phenomena II. Academic Press, New York (1967).

McIlwain, C.E. Coordinates for mapping the distribution of magnetically trapped particles. J. Geophys. Res., 66, 3681 (1961).

Mechtly, E.A. and L.G. Smith. Growth of the D-region at sunrise. J. Atmos. Terr. Phys., 30, 363 (1968).

Mechtly, E.A., K. Seino and L.G. Smith. Lower ionosphere electron densities measured during the solar eclipse of 12 November 1966. Radio Sci., 4, 371 (1969).

Mechtly, E.A., C.F. Sechrist, Jr., and L.G. Smith. Electron loss coefficients for the D-region of the ionosphere from rocket measurements during the eclipses of March 1970 and November 1966. J. Atmos. Terr. Phys. 34, 641 (1972).

Narcisi, R.S. and A.D. Bailey. Mass spectrometer measurements of positive ions at altitudes from 64-112 km. J. Geophys. Res., 70, 3687 (1965).

Nicolet, M. Ionospheric processes and nitric oxide. J. Geophys. Res., 70, 691 (1965).

Northrup, T.G. and E. Teller. Stability of the adiabatic motion of charged particles in the earth's magnetic field. Phys. Rev., 117, 215 (1960).

Park, C.G. Methods of determining electron concentrations in the magnetosphere from nose whistlers. Tech. Report No. 3451-1, Radioscience Laboratory, Stanford University 1972.

Pitteway, M.L.V. The numerical calculation of wave fields, reflection coefficients, and polarizations for long radio waves in the lower ionosphere, I. Phil. Trans. Roy. Soc. London A257,

219 (1965).

Poeverlein, H. Strahlwege von Radiowellen in der Ionosphäre. Sitz. Bayerischen Akad. Wiss. (1), 175, (1948).

Preece, W.H. Earth currents. Nature, 49, 554 (1894).

Quiroz, R.S. and R.M. Henry. Cooling near the stratopause and perturbation of the meridianal flow during a solar eclipse. Paper presented at COSPAR, Seattle (1971). (To be published in J. Atmos. Sci.).

Rao, M.K., S.C. Mageemdar and S.N. Mitra. Investigation of ionospheric absorption at Delhi. J. Atmos. Terr. Phys., 24, 245 (1962).

Ratcliffe, J.A. The Magneto-Ionic theory and its applications to the ionosphere. Cambridge Univ. Press (1959).

Reeve, C.D. and M.J. Rycroft. Expedition to Iceland. Physics Bulletin, 22, 145 (1971).

Rishbeth, H. and O.K. Garriott. Introduction to Ionospheric Physics. Academic Press (1969).

Reid, G.C. A study of the enhanced ionization produced by solar protons during a polar cap absorption event. J. Geophys. Res., 66, 4071 (1961).

Reid, G.C. Physical processes in the D- region of the ionosphere. Rev. Geophys., 2, 311 (1964).

Rycroft, M.J. Resonances of the Earth-Ionosphere cavity observed at Cambridge, England. Radio Sci., 68D, 1071 (1965).

Rycroft, M.J. VLF emissions in the magnetosphere. To be published in Radio Sci. (1972).

Rycroft, M.J. and P.D. Alexander. Model hydrogen and helium concentrations in the plasmasphere. Presented at the 12th Plenary Meeting of COSPAR, Prague, 1969.

Rycroft, M.J. and C.D. Reeve. VLF radio signals observed in Newfoundland during the solar eclipse of 7 March 1970. Nature (Lond.), 226,

1126, (1970).

Rycroft, M.J. and J.O. Thomas. The magnetospheric plasmapause and the electron density trough at the Alouette I orbit. Planet. Space Sci., 18, 65 (1970).

Rycroft, M.J. and A. Mathur. The determination of the minimum group delay of a non-nose whistler. Submitted for publication to J. Atmos. Terr. Phys. (1972).

Sagredo, J.L. VLF goniometer observations at Halley Bay, Antarctica, and the effect of the ring current on whistler propagation in the magnetosphere. Ph.D. Thesis, University of Sheffield (1971).

Sales, G.S. D-region solar eclipse effects. Ground based radio wave propagation studies of the lower ionosphere. Conference Proceedings, Ottawa, Canada (1967).

Sechrist, C.F., Jr., Interpretation of pre-sunrise electron densities and negative ions in the D-region. J. Atmos. Terr. Phys., 30, 371 (1968).

Seddon, J.C. Propagation measurements in the ionosphere with the aid of rockets. J. Geophys. Res., 58, 323 (1953).

Sen, H.K. and A.A. Wyller. Generalization of the Appleton-Hartree magneto-ionic formulas. J. Geophys. Res., 65, 3931 (1960).

Schumann, W.O. Uber die strahlunglosen eigenschwingungen einer leitenden kugel, die von einer Luftschicht und einer Ionosphärenhulle ungeben ist. Z. Naturforschg., 7A, 149 (1952).

Smith, L.G., C.A. Accardo, L.H. Weeks and P.J. Mckinnon. Measurements in the ionosphere during the solar eclipse of 20 July 1963. J. Atmos. Terr. Phys. 27, 803 (1965).

Smith, L.G. Ionization by Lyman α in the E-region at sunrise. J. Atmos. Terr. Phys., 28, 1195 (1966).

Smith, L.G. Rocket observations of solar UV radiation during the

eclipse of 7 March 1970. J. Atmos. Terr. Phys. 34, 601 (1972).

Smith, R.L., R.A. Helliwell and I. Yabroff. A theory of trapping of whistlers in field aligned columns of enhanced ionization. J. Geophys. Res., 65, 815 (1960).

Smith, R.L. and D.L. Carpenter. Extension of nose whistler analysis. J. Geophys. Res., 66, 2582 (1961).

Smith, R.L. and J.J. Angerami. Magnetospheric properties deduced from OGO-1 observations of ducted and non-ducted whistlers. J. Geophys. Res. 73, 7 (1968).

Storey, L.R.O. An investigation of whistling atmospherics. Phil. Trans. Roy. Soc. (London), A246, 113 (1953).

Storey, L.R.O. Tables of functions in interpreting the dispersion curves of whistlers. RPL Project Rept. No. 23-4-2, Defence Res. Telecommunications. Estab., Ottawa, Canada (1957a).

Storey, L.R.O. A method for interpreting the dispersion curves of whistlers. Con. J. Phys. 35, 1107 (1957b).

Storey, L.R.O. and J.C. Cerisier. An interpretation of the noise bands observed near the lower hybrid resonance frequency by artificial satellites. (GRI Report GRI/TP/79) C.R. Acad. Sci., Paris, 226, 525 (1968).

Swider, W. On the production of ionization by H Lyman alpha. Ground-based radio wave propagation studies of the lower ionosphere. Conference Proceedings, Ottawa, Canada (1967).

Thomas, J.O. and M.J. Rycroft. Recent ionospheric E and F region measurements during solar eclipse, and their interpretation. Solar Eclipses and the Ionosphere. Edit. by M. Anastassiades. Plenum Press (1970).

Thorne, R.M. The importance of wave-particle interactions in the magnetosphere. To be published in J. Geophys. Res.

Vette, J.I. Summary of particle populations in the magnetosphere. Particles and Fields in the Magnetosphere. Ed. B.M. McCormac. D. Reidel Pub. Co. (1970).

Wait, J.R. The mode theory of VLF ionospheric propagation for finite ground conductivity. Proc. IRE, 45, 760 (1957).

Wait, J.R. Terrestrial propagation of VLF radio waves. J. Res. NBS, 64D, (Radio Prop.), 153 (1960).

Wait, J.R. Electromagnetic waves in stratified media, Pergamon Press (1962).

Wait, J.R. Influence of the lower ionosphere on propagation of VLF radio waves to great distances. J. Res. NBS, 67D, (Radio Prop.), 375, 1963).

Wait, J.R. and K. Spies. Influence of earth curvature and terrestrial magnetic field on VLF propagation. J. Geophys. Res., 65, 2325 (1960).

Wait, J.R. and L.C. Walters. Reflection of VLF waves from an inhomogeneous ionosphere. Pt. 1. Experimentally varying isotropic model. J. Res. NBS, 67D, (Radio Prop.), 3, 361 (1963).

Wait, J.R. and L.C. Walters. Reflection of electromagnetic waves from a lossy magnetoplasma. Radio Sci. J. Res. NBS 68D, 95 (1964).

Whitten, R.C. and I.G. Poppoff. Fundamentals of Aeronomy. Wiley. (1971).